

Design and Synthesis of Novel Rh(II)-containing Polymer Catalysts. Organometallic Gold(III) Catalysis in Organic Synthesis

Vladimir Levchenko



Master's Thesis, Department of Chemistry

UNIVERSITETET I OSLO

14.05.2016

© Vladimir Levchenko

2016

Design and Synthesis of Novel Rh(II)-containing Polymer Catalysts. Organometallic Gold(III)
Catalysis in Organic Synthesis

Vladimir Levchenko

<http://www.duo.uio.no/>

Trykk: Reprosentralen, Universitetet i Oslo

II

Acknowledgments

The work done for this master's degree has been carried out in the Department of Chemistry, at the University of Oslo, under the supervision of Associate Professor Tore Bonge-Hansen and Professor Mats Tilset.

First of all, I want to express my sincere gratitude to my supervisors – Tore Bonge-Hansen and Mats Tilset. Tore, thank you for teaching me a tremendous amount of chemistry and for being a constant source of encouragement through the course of this study. I admire your patience – you have always had time for me, regardless if it was at night, a weekend or a holiday. Thank you for giving me this project, for believing in me, and for always listening whether it was about chemistry or not. Mats, it was an honor for me to be your student. Besides your great personality, I admire your professionalism. I gained strength, courage, and confidence after each discussion with you. Thanks to you, I was a part of the greatest team, with the most talented and intelligent people within the whole department.

Enormous thanks goes to the “Golden Girls” - Marte Sofie Holmsen and Franziska Stefanie Ihlefeldt. Marte, thank you for the fruitful discussions, proof reading, and willingness to help me anytime and anywhere. Franziska, I admire your writing and communication skills. Girls, this work would have been shaped differently if it had not been for your valuable time, which I appreciate very much. Both of you are the most important contributors to an inspiring and social working environment which I enjoyed a lot!

The next thanks goes to Sigurd Øien-Ødegaard for the X-ray analysis and characterization of my samples. I would like to thank Carl H. Gørbitz for the general introduction to the X-ray analysis as well as Frode Rise and Dirk Petersen for the NMR facilities and help when I needed it. Also, thanks to Evgeniy Redekop and Michaela Salajkova, for the BET and TEM/SEM-EDX analysis.

I tip my hat to Knut Hylland, Martin Hennem, and the guys from the 2nd floor – Eirik, Jakob, Kim and Håkon. I would like to thank CEO of the Reactive Metal Particles AS, Eirik Ruud, for giving me the opportunity to work part-time during my masters.

In the end I want to thank my friends and family. Mother and Father, I cannot thank you enough for your never failing encouragements and uplifting words during the difficult times. Thank you, my adorable girlfriend, Julia, for believing in me and constantly supporting me.

Oslo, May 2016

Vladimir Levchenko

Abstract

The preparation of heterogeneous polymer catalysts is of a special interest since they allow easy separation of the catalyst from the reaction medium. The heterogeneous polymer catalysts can also be recycled, which is attractive for expensive catalysts as rhodium(II) tetraacetate, $\text{Rh}_2(\text{OAc})_4$.

This work demonstrates the synthesis and characterization of four new analogues of $\text{Rh}_2(\text{OAc})_4$. The four achiral rhodium(II) carboxylates were successfully immobilized to form six different polymer catalysts. The six novel polymer catalysts were investigated in cyclopropanation reaction and compared to $\text{Rh}_2(\text{OAc})_4$.

The interest of cyclometalated gold(III) complexes continues to grow. The synthetic methods for preparing them have successfully been developed in the group of Mats Tilset. Despite the developed synthesis of cyclometalated gold(III) complexes, the catalytic activity of them remains undiscovered.

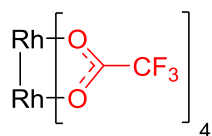
The second project of this thesis aims to investigate the catalytic activity of cyclometalated gold(III) complexes in various synthetic transformations. In addition, the detailed study of the formal insertion of various alkynes to the cyclometalated gold(III) complex $\text{Au}(\text{tpy})(\text{OAc}^{\text{F}})_2$ was performed.

Abbreviations

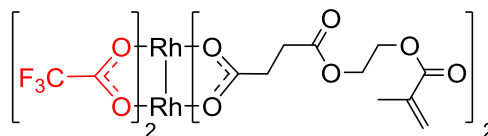
4VBA	4-vinylbezoic acid
AIBN	2,2-Azo <i>bisisobutyronitrile</i>
BET	Brunauer-Emmett-Teller adsorption method
d	doublet
DBU	1,8-diazabicycloundec-7-ene
DCC	<i>N,N'</i> -dicyclohexylcarbodiimide
dd	double doublet
<i>de</i>	diastereomeric excess
DFT	density functional theory
DMAP	4-dimethylaminopyridine
DMF	<i>N,N</i> -Dimethylformamid
EDG	electron donating group
EDX	energy-dispersive X-ray spectroscopy
<i>ee</i>	enantiomeric excess
EDA	ethyl diazoacetate
EI	electron ionisation
ESI	electrospray ionisation
<i>et al.</i>	<i>et alii</i>
EWG	electron withdrawing group
FTIR	fourier transform infrared spectroscopy
HPLC	high performance liquid chromatography
<i>J</i>	coupling constant
m	multiplet
m/z	mass-to-charge ratio
MCES	mono-2-(Methacryloyloxy) ethyl succinate

MCR	multicomponent reaction
MEPP	(2 <i>S</i> ,4 <i>R</i>)-4-((4-(2-(methacryloyloxy)ethoxy)-4-oxobutanoyl)oxy)-1-(phenylsulfonyl)pyrrolidine-2-carboxylate
min	minutes
MS	mass spectrometry
NMR	nuclear magnetic resonance spectroscopy
OAc	acetate group
OAc ^F	trifluoroacetate group
p-ABSA	4-acetamidobenzenesulfonyl azide
pol(I)	immobilized rhodium(II) carboxylate, Generation I
pol(II)	immobilized rhodium(II) carboxylate, Generation II
pol(PM)	immobilized rhodium(II) carboxylate by post-modification strategy
ppm	part per billion
PS	poly(styrene)
PVA	poly(vinyl alcohol)
q	quartet
r.t.	room temperature
rpm	rounds per minute
s	singlet
SEM	scanning electron microscopy
TEM	transmission electron microscopy
TFA	trifluoroacetic acid
TLC	thin layer chromatography
TON	turn over number
tpy	2-(<i>p</i> -tolyl)pyridine
XAS	X-ray absorption spectroscopy
δ	chemical shift (NMR)

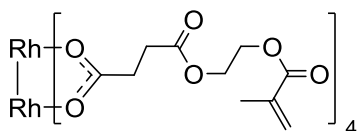
Overview of key compounds



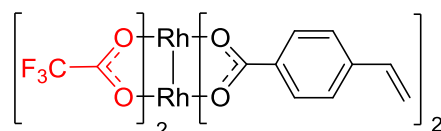
7 Rh₂(OAc^F)₄



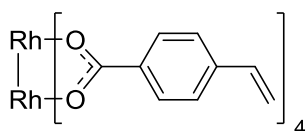
78* Rh₂(MCES)₂(OAc^F)₂



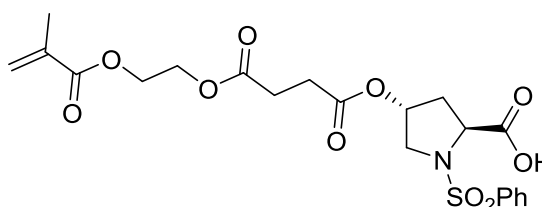
74* Rh₂(MCES)₄



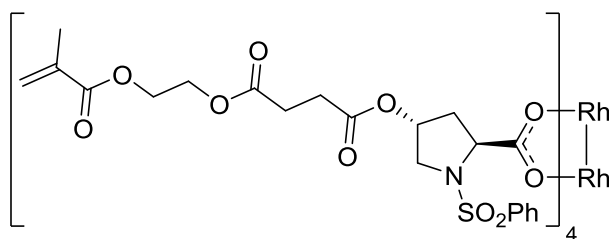
77* Rh₂(4VBA)₂(OAc^F)₂



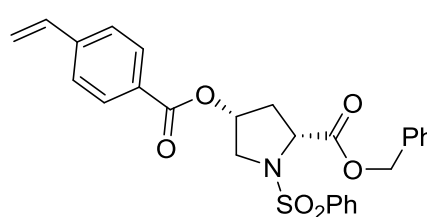
75* Rh₂(4VBA)₄



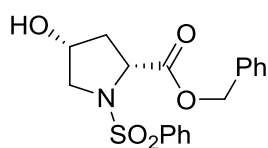
99*



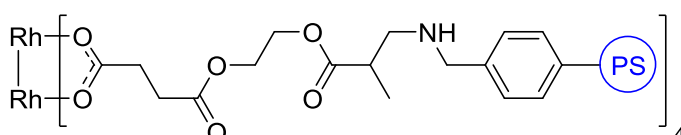
102* Rh₂(MEPP)₄



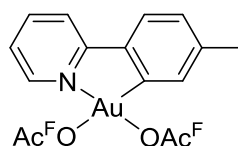
108*



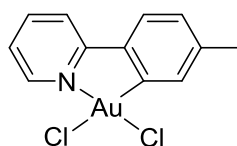
107*



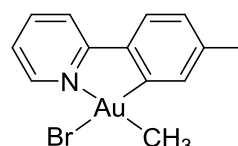
94* pol(PM)-Rh₂(MCES)₄



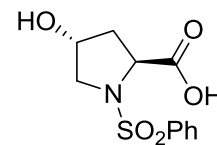
136



135

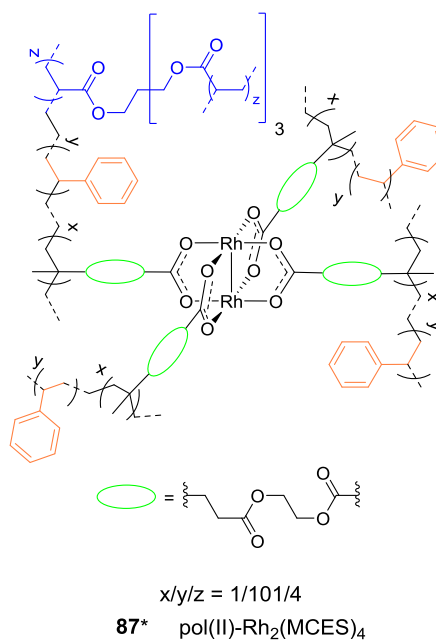
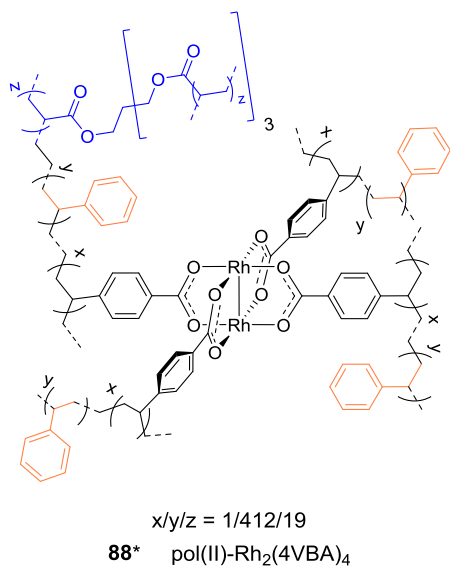
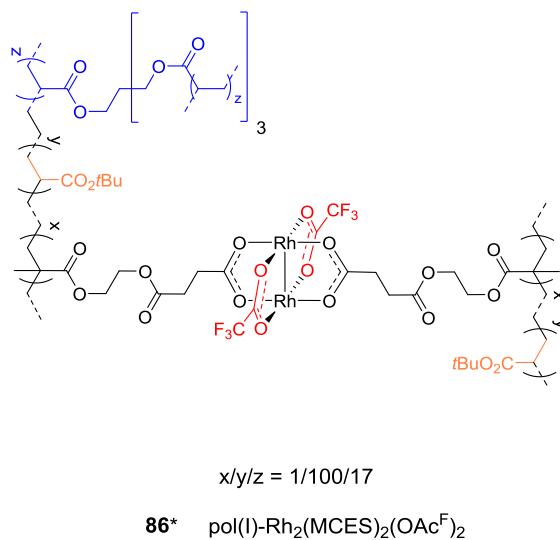
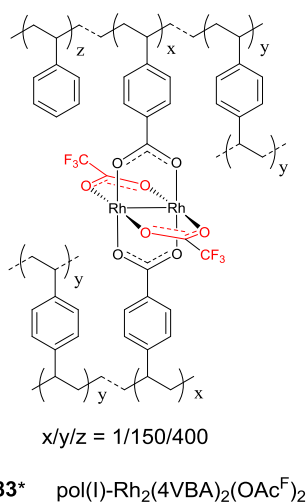
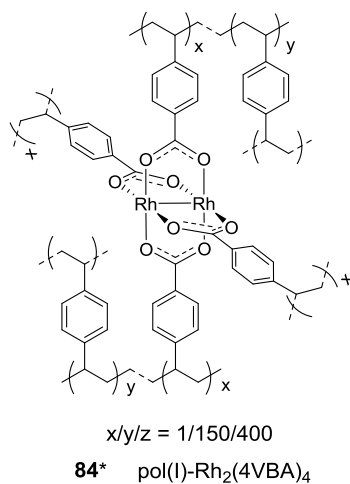
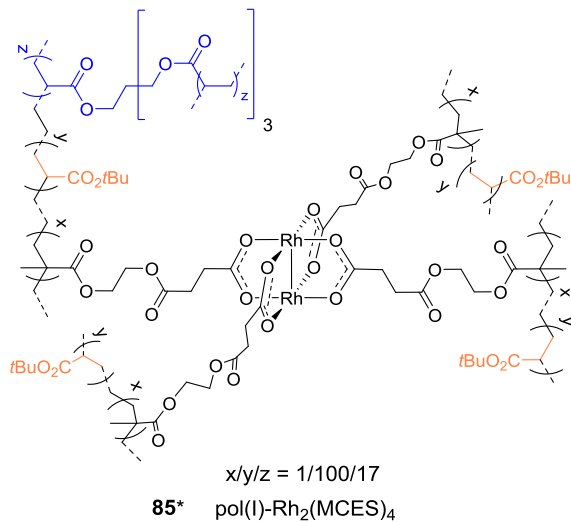


137



100*

* = new compounds



* = new compounds

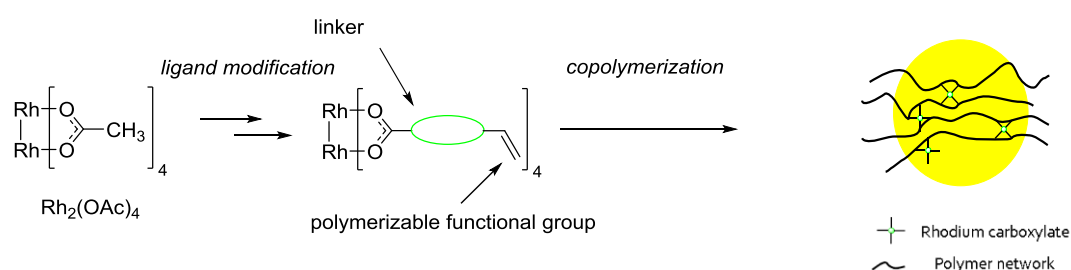
X

Description and aim of the project

This project consists of two independent parts: organometallic rhodium(II) catalysis in the group of Tore Bonge-Hansen, as a supervisor, and organometallic gold(III) catalysis in the group of Mats Tilset as a supervisor.

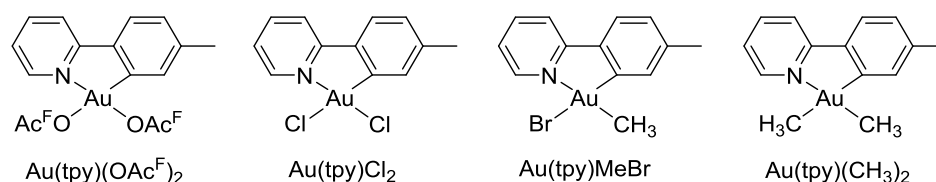
Rhodium(II) tetraacetate, $\text{Rh}_2(\text{OAc})_4$, has found wide applications in organic transformations as a homogeneous catalyst. It catalyses numerous carbene-transfer reactions that lead to the synthesis of building blocks and natural products. The aim of this project was to synthesize novel rhodium(II)-monomeric catalysts and immobilize them into heterogeneous, more efficient, reusable and robust polymer catalysts.

The dependence of the polymer structure on the catalytic activity of the immobilized rhodium(II) carboxylates was investigated. The catalytic performance of the polymer catalysts was studied in carbene-transfer reactions.



In case of succeeding with the synthesis of the immobilized achiral analogues of $\text{Rh}_2(\text{OAc})_4$, the synthesis of the chiral analogues of $\text{Rh}_2(\text{OAc})_4$ would be performed in a similar manner.

The second part of the thesis focused on the investigation of catalytic activity of cyclometalated gold(III) complexes in various organic transformations. The cyclometalated gold(III) complexes possess ligands with different abilities to dissociate, thus, one major goal was to investigate the effect of the leaving group with respect to the catalytic activity.



In addition, the reactivity of $\text{Au}(\text{tpy})(\text{OAc}^{\text{F}})_2$ towards a wide variety of different alkynes was investigated.

Table of contents

Acknowledgments	III
Abstract	V
Abbreviations	VII
Overview of key compounds	IX
Description and aim of the project	XI
Introduction	1
1 Introduction to the rhodium project	2
1.1 Rhodium carbenoids: history and development	2
1.1.1 Rhodium paddle-wheel complexes	3
1.1.2 Formation of rhodium(II) carbenoids.....	4
1.1.3 History of rhodium(II) carboxylates in carbene-transfer reactions	5
1.2 Rhodium(II) carbenoids and their reactivity.....	9
1.3 Heterogenization of rhodium(II) carboxylates.....	13
1.3.1 Covalent bonded rhodium(II) carboxylates	14
1.3.2 Axially coordinated rhodium(II) carboxylates.....	16
1.4 Polymerization as bottom-up approach.....	19
2 Results and discussion – rhodium project	23
2.1 Development of novel achiral rhodium(II) carboxylates	23
2.1.1 Synthesis of $\text{Rh}_2(\text{OAc}^{\text{F}})_4$	24
2.1.2 Synthesis of tetrasubstituted rhodium(II) carboxylates: $\text{Rh}_2(\text{MCES})_4$ (74) and $\text{Rh}_2(4\text{VBA})_4$ (75)	25
2.1.3 Synthesis of disubstituted rhodium(II) carboxylates: $\text{Rh}_2(\text{MCES})_2(\text{OAc}^{\text{F}})_2$ (78) and $\text{Rh}_2(4\text{VBA})_2(\text{OAc}^{\text{F}})_2$ (77)	28
2.2 Heterogenization by polymerization. Bottom-up in action.....	30
2.2.1 Polymerization	30
2.2.2 Synthesis of polymer catalysts – Generation I.....	31
2.2.3 Characterization of polymer catalysts – Generation I	33
2.2.4 Synthesis of polymer catalysts – Generation II	37
2.2.5 Characterization of polymer catalysts – Generation II.....	38
2.3 Catalytic performance of novel heterogenized rhodium(II) catalysts	42
2.3.1 Heterogenization by post-modification strategy.....	46
2.3.2 Polymer catalysts performance in C-H insertion reaction	47

3	Synthesis of novel chiral rhodium(II) carboxylates	49
4	Introduction to the gold project	54
4.1	General introduction and historical aspects	54
4.2	Gold(I) catalysis in carbene-transfer reactions	55
4.3	Nucleophilic addition to π -systems	56
4.3.1	Coordination to alkenes and alkynes	56
4.3.2	Coordination to other π -systems	57
4.4	Gold(III)-catalyzed C-H activation reactions and gold(III) cyclometalated complexes .	58
4.5	Tandem Au(I) and Au(III) system	63
4.5.1	Multicomponent reactions	64
5	Results and discussion – gold project	67
5.1	Cyclopropanation reaction	67
5.2	Multicomponent reactions	70
5.3	Alkyne insertion	73
5.3.1	Phenyl propargyl ether (175)	73
5.3.2	Phenyl acetylene (174)	78
5.3.3	Conclusions regarding the alkyne insertion	82
5.4	Gold-catalyzed ethynylation of arenes.....	83
6	Conclusions and Future Prospects	85
7	Experimental Section	87
	General.....	87
7.1	Experimental section for the rhodium project.....	88
7.1.1	Synthesis of $\text{Rh}_2(\text{OAc}^{\text{F}})_4$ (rhodium(II) trifluoroacetate), ¹⁴ 7.....	88
7.1.2	Synthesis of $\text{Rh}_2(\text{MCES})_2(\text{OAc}^{\text{F}})_2$, 78.....	89
7.1.3	Synthesis of $\text{Rh}_2(4\text{VBA})_2(\text{OAc}^{\text{F}})_2$, 77.....	91
7.1.4	Synthesis of $\text{Rh}_2(4\text{VBA})_4$ (Rhodium(II) tetra-4-vinylbenzoate), 75.....	93
7.1.5	Synthesis of $\text{Rh}_2(\text{MCES})_4$ (Rhodium(II) tetra-4-(2-(methacryloyloxy)ethoxy)-4-oxobutanoate), 74.....	95
7.1.6	Synthesis of $\text{pol(I)-Rh}_2(4\text{VBA})_4$, 84.....	97
7.1.7	Synthesis of $\text{pol(I)-Rh}_2(4\text{VBA})_2(\text{OAc}^{\text{F}})_2$, 83.....	98
7.1.8	Synthesis of $\text{pol(I)-Rh}_2(\text{MCES})_4$, 85.....	99
7.1.9	Synthesis of $\text{pol(I)-Rh}_2(\text{MCES})_2(\text{OAc}^{\text{F}})_2$, 86.....	100
7.1.10	Synthesis of $\text{pol(II)-Rh}_2(4\text{VBA})_4$, 88.....	103
7.1.11	Synthesis of $\text{pol(II)-Rh}_2(\text{MCES})_4$, 87.....	104

7.1.12	General procedure for intermolecular cyclopropanation of styrene with EDA, catalyzed by rhodium(II) tetraacetate (5)	106
7.1.13	General procedure for intermolecular cyclopropanation of styrene with EDA, catalyzed by heterogenized Rh-containing polymers.	108
7.1.14	Synthesis of Methyl 2-diazo-2-phenylacetate, ¹³⁸ 189.....	109
7.1.15	Synthesis of Methyl 2-(4-chlorophenyl)-2-diazoacetate, ⁴⁴ 95.....	110
7.1.16	Synthesis of (2 <i>S</i> ,4 <i>R</i>)-4-hydroxy-1-(phenylsulphonyl)pyrrolidine-2-carboxylic acid, 100	111
7.1.17	Synthesis of (2 <i>S</i> ,4 <i>R</i>)-4-((4-(2-(methacryloyloxy)ethoxy)-4-oxobutanoyl)oxy)-1-(phenylsulfonyl)pyrrolidine-2-carboxylic acid, 99.....	113
7.1.18	Synthesis of Rh ₂ (MEPP) ₄ , 102.....	115
7.1.19	Synthesis of benzyl (2 <i>R</i> ,4 <i>R</i>)-4-hydroxy-1-(phenylsulfonyl)pyrrolidine-2-carboxylate, 107	117
7.1.20	Synthesis of benzyl (2 <i>R</i> ,4 <i>R</i>)-1-(phenylsulfonyl)-4-((4-vinylbenzoyl)oxy)pyrrolidine-2-carboxylate, 108.....	119
7.1.21	Heterogenization of Rh ₂ (MCES) ₄ by post-modification approach – Synthesis of pol(PM)-Rh ₂ (MCES) ₄ , 94.....	121
7.1.22	Attempt at synthesis of (2 <i>R</i> ,4 <i>R</i>)-1-(phenylsulfonyl)-4-((4-vinylbenzoyl)oxy)pyrrolidine-2-carboxylic acid, 103.....	121
7.2	Experimental section for the gold project	122
7.2.1	Synthesis of Au(tpy)(OAc ^F) ₂ , ¹²³ 136.....	122
7.2.2	Synthesis of Au(tpy)Cl ₂ , ¹⁴⁰ 135	123
7.2.3	Synthesis of Au(tpy)BrMe, ¹²³ 137.....	124
7.2.4	Synthesis of ethyl cyclohepta-2,4,6-triene-1-carboxylate, ¹³⁶ 172.....	125
7.2.5	Synthesis of 3-phenyl-1-(piperidin-1-yl)indolizine, ^{141,142} 167.....	126
7.2.6	Synthesis of 1-(1,3-diphenylpro-2-yn-1-yl)piperidine, 164.....	127
7.2.7	Cyclopropanation reaction utilizing Au(tpy)(OAc ^F) ₂ as a catalyst.....	128
7.2.8	General procedure for A ³ coupling for synthesis of propargylamine 164	128
7.2.9	General procedure for A ³ coupling for synthesis of indolizine 167	128
7.2.10	Procedure for gold(III)-catalyzed ethynylation reaction ¹²⁹	128
7.2.11	NMR experiment – reaction of Au(tpy)(OAc ^F) ₂ with phenylacetylene (174)	129
7.2.12	NMR experiment – reaction of Au(tpy)(OAc ^F) ₂ with phenyl propargyl ether (175)	129
	Appendix	130
	Bibliography	151

Introduction

Gold and rhodium are considered to be noble metals. Discovered in 1803 by William Wollaston, rhodium was considered to be a precious metal. Its rare occurrence in nature and poor chemical activity limited applications more than 100 years. Unlike rhodium, gold has been known since the earliest of time. Its value and unusual stability has made it to be an outstanding metal that was always associated with power, money and beauty.

During the last 100 years rhodium and gold have evolved from the noble, royal metals to valuable organometallic compounds. Both rhodium and gold organometallic compounds have proven to be extremely useful catalysts in numerous synthetic transformations, with unique selectivity.¹ The growing number of publications for gold and rhodium catalysis depicts their applicability and great forthcoming potential.

The following master project consists of two parts where the chemistry of organometallic rhodium(II) and gold(III) compounds will be presented. The two parts are independent and yet related to each other, since they belong to the same field of chemistry – organometallic.

A short introduction to transient rhodium carbenes, organometallic rhodium(II) catalysts, their synthesis and structure, as well as properties, will be presented. In addition, methods of heterogenization of rhodium(II) complexes will be described, along with applications in organic synthesis.

The second part of the introduction is dedicated to the homogeneous catalysis of gold(I) and gold(III) species. The variety of transformations catalysed by organometallic gold catalysts will be presented. Furthermore, achievements of the organometallic gold(III) complexes in our group will be discussed.

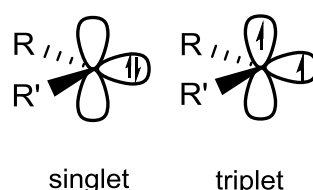
For a better reading flow, the chapters about rhodium and gold chemistry are presented separately. While in the first part, the focus lies on analysis concerning rhodium complexes, the second part will give a better insight into catalysis utilizing gold complexes.

1 Introduction to the rhodium project

In this section, a literature overview of existing rhodium(II) carboxylates will be given. The structure, synthesis and catalytic activity of the rhodium(II) carboxylates will be presented. In the end, state of the art techniques and strategies for the immobilization of the rhodium(II) carboxylates will be discussed.

1.1 Rhodium carbenoids: history and development

Carbenes are highly reactive molecules containing divalent carbon atoms and two unshared electrons. Depending on the arrangement of these two electrons, there are singlet and triplet carbenes (Figure 1).² The stability, as well as the lifetime, of singlet and triplet carbenes depends on the steric and electronic environment around the carbon atom.^{3,4}



R, R' = CO₂R, alkyl, aryl, CN, COR, etc.

Figure 1: Electronic arrangements in carbenes.²

Over the past 50 years, various substrates have been used to generate carbenes.^{5,6} Due to the high reactivity of carbenes, the selectivity in chemical reactions and efficient transfer to the substrate have been an issue to consider.⁷ The most used and versatile method for synthesis of carbenes is decomposition of diazo compounds, where the formation of N₂ drives the reaction.⁸

Diazo compounds are inherently unstable.⁹ Their stability increases with stabilization of the negative charge *via* mesomeric effect, achieved by introduction of electron-withdrawing groups, which are able to delocalize the charge (Figure 2).¹⁰

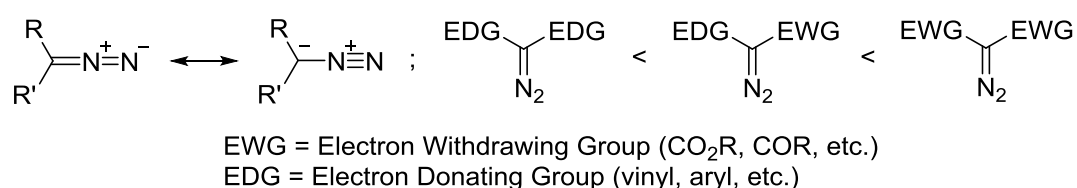


Figure 2: Resonance structures and stability of diazo compounds.¹⁰

Diazo compounds are found to be toxic and potentially explosive.¹¹ Therefore, great care is recommended while handling diazo compounds.

The generation of carbenes from diazo compounds can be triggered under photochemical, thermal or transition metal-catalyzed conditions.¹² The latter has emerged as a powerful and versatile tool to generate transient metal-carbenes, as a result of the development and design of new and more convoluted transition-metal complexes. Initially, the first used transition metal known to decompose a diazo compound was Cu and its complexes.¹³ Later, other metals were successfully employed, such as Ru, Mo and Pd.¹⁴

The next sections will provide an overview of the structures and reactivity of rhodium(II) carboxylates with diazo compounds, followed by a detailed discussion of the literature precedent for the reactions relevant to this project.

1.1.1 Rhodium paddle-wheel complexes

Since 1973 rhodium(II) carboxylates have been playing a prominent role in metal-carbene transformations.¹⁵ Rhodium(II) carboxylates are air-stable, colored and easy to handle. Rhodium(II) complexes possess a paddlewheel structure, with 4 ligands around the dirhodium bridge (Figure 3).¹⁶ A rhodium atom, as a part of a paddlewheel complex, has only one vacant coordination site where carbenoid formation occurs.¹⁷ As depicted by Drago and co-workers, the ligands on the dirhodium bridge play a crucial role in the donor-acceptor capability of the rhodium atoms.^{18,19}

Varying the ligands, it becomes feasible to control the electron density on the rhodium atoms: electron-withdrawing ligands make them more electrophilic, electron-donating – less electrophilic. This statement was proven in the group of Doyle, where it was reported that $\text{Rh}_2(\text{OAc}^{\text{F}})_4$, unlike $\text{Rh}_2(\text{OAc})_4$, can coordinate olefins to its axial positions.²⁰

Rhodium(II) complexes are inclined to have coordinated molecules in axial positions (Figure 3). The nature of the coordinated molecules can vary. This coordination is due to σ -lone pair donation from the coordinated molecule, and a π -back-donation from the Rh atom, which plays a much more significant role than it was originally believed.²¹

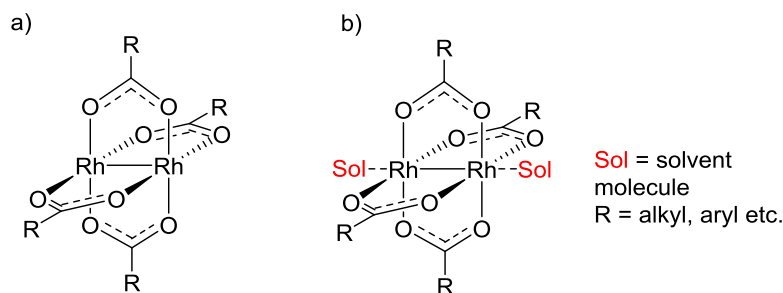
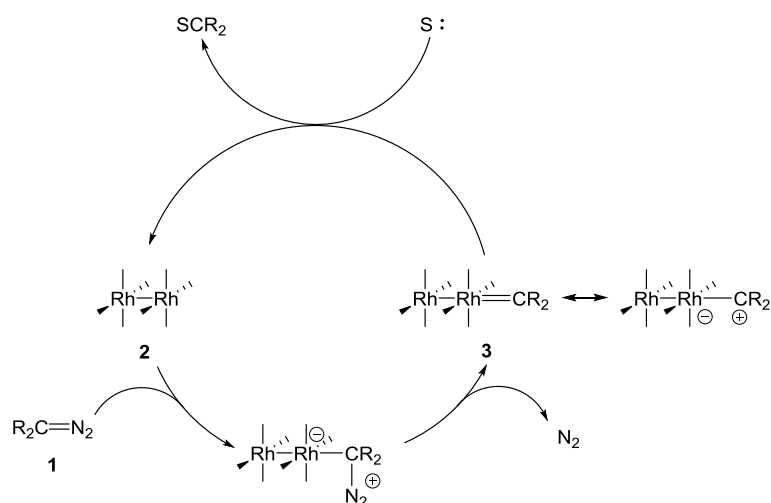


Figure 3: Paddle-wheel structure of rhodium(II) complexes: a) with no axial coordination; b) with axially coordinated solvent molecules.

Therefore, it is highly likely to observe additional signals in the NMR spectra of rhodium(II) complexes, which belong to the coordinated solvent molecules – THF, acetone, EtOAc, methanol, etc.¹⁶

1.1.2 Formation of rhodium(II) carbenoids

Yates and co-workers predicted the generation of transient electrophilic metal carbenes in reactions between diazo compounds **1** and rhodium(II) complexes **2**, which act as an electrophile.²² After coordination to the metal complex, the diazo compound liberates N_2 and the carbene moiety in the rhodium(II)-carbenoid **3** becomes electrophilic. In the end of catalytic cycle, the rhodium(II) carbenoid **3** transfers its carbene group onto electron-rich substrates (Scheme 1).

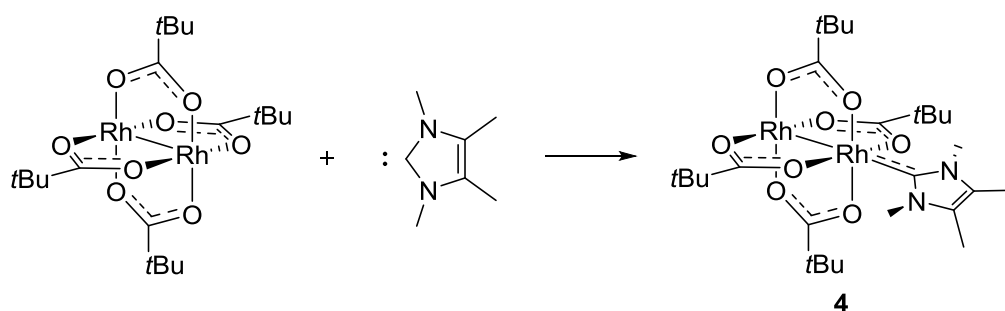


Scheme 1: Formation of rhodium(II) carbenoid in carbene-transfer reactions. Ligands are omitted for clarity.²²

The two catalytic sites of rhodium, for example in $Rh_2(OAc)_4$, are identical, so that the rhodium(II) carbenoid can be formed with equal probability on both sites. Introducing more

bulky ligands, it becomes possible to force the formation of the carbenoid on one or the other side of the Rh-Rh bridge, which leads to increased selectivity.²³

In 2011, Snyder *et al.* isolated and characterized wine-red crystals of rhodium(II)-carbene complex **4** (Scheme 2).²⁴ The structure of complex **4** is consistent with DFT calculations and X-ray structure, which both provide valuable information about the rhodium(II)-carbene complex.



Scheme 2: The first isolated rhodium(II) carbenoid.²⁴

The newly formed Rh-C bond appeared to be slightly longer than calculated.²⁵ This occurrence is a so-called “half-double” bond, which includes lone pair donation of the C-atom and π -back-donation at the Rh-atom to the carbon *p*-orbital. The Rh-Rh bond length is shorter in the carbene-complex, which indicates the increase of the electronic density on the Rh-Rh bridge.²⁵

Recently, Furstner *et al.* provided a detailed study of the constitution and conformation of rhodium(II) carbenoids that confirms and refines computational data.²⁶ The main conclusion of their work was the importance of stereoelectronic rather than steric effect, which is a major selectivity determining factor.

1.1.3 History of rhodium(II) carboxylates in carbene-transfer reactions

Since the first introduction of rhodium(II) tetraacetate (**5**) in 1973 by Teyssie,¹⁵ it has established a versatile class of complexes for carbene-transfer reactions (Figure 4).²⁷ Its effectivity in decomposition of diazo compounds that results in rhodium(II) carbenoid formation made it a widely-used catalyst, despite the high price of a metallic rhodium – 23 \$ for 1 g.²⁸

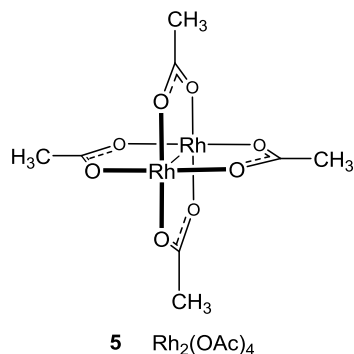
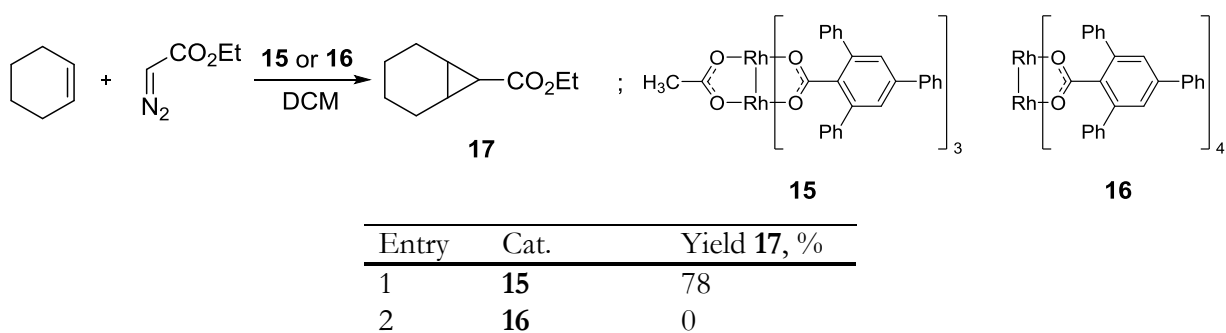


Figure 4: Paddle-wheel structure of rhodium(II) tetraacetate (**5**).^{15,27}

Rh₂(OAc)₄ (**5**) has found wide applications in cyclopropanation and C-H insertion reactions.^{29,1} By substituting the acetates in **5** with other carboxylic groups, it is feasible to control the steric availability of the rhodium active site, which leads to a higher selectivity of the rhodium catalyst to the substrates in the carbene-transfer reactions.³⁰

Nowadays, numerous rhodium(II) carboxylates with enhanced selectivity have been synthesized and studied (Figure 5).^{29,31,32} It is clear from Figure 5 that the scope of synthesized rhodium(II) carboxylates became diverse: fluorinated carboxylates **6**, **7** together with non-crowded **8-10**, and crowded carboxylates **11-14** have been widely used in the carbene transfer.²⁹

Varying the degree of substitution, it is also viable to alter the accessibility of the rhodium active site.³³ Metz *et al.* demonstrated that sterically hindered dirhodium(II) triphenylbenzoate **15** possesses a high catalytic activity, whereas the dirhodium(II) triphenylbenzoate **16** shows no catalytic activity and degrades under the reaction conditions (Scheme 3).^{32,33}



Scheme 3: Dependence of the steric factors on the yield of the reaction.^{32,33}

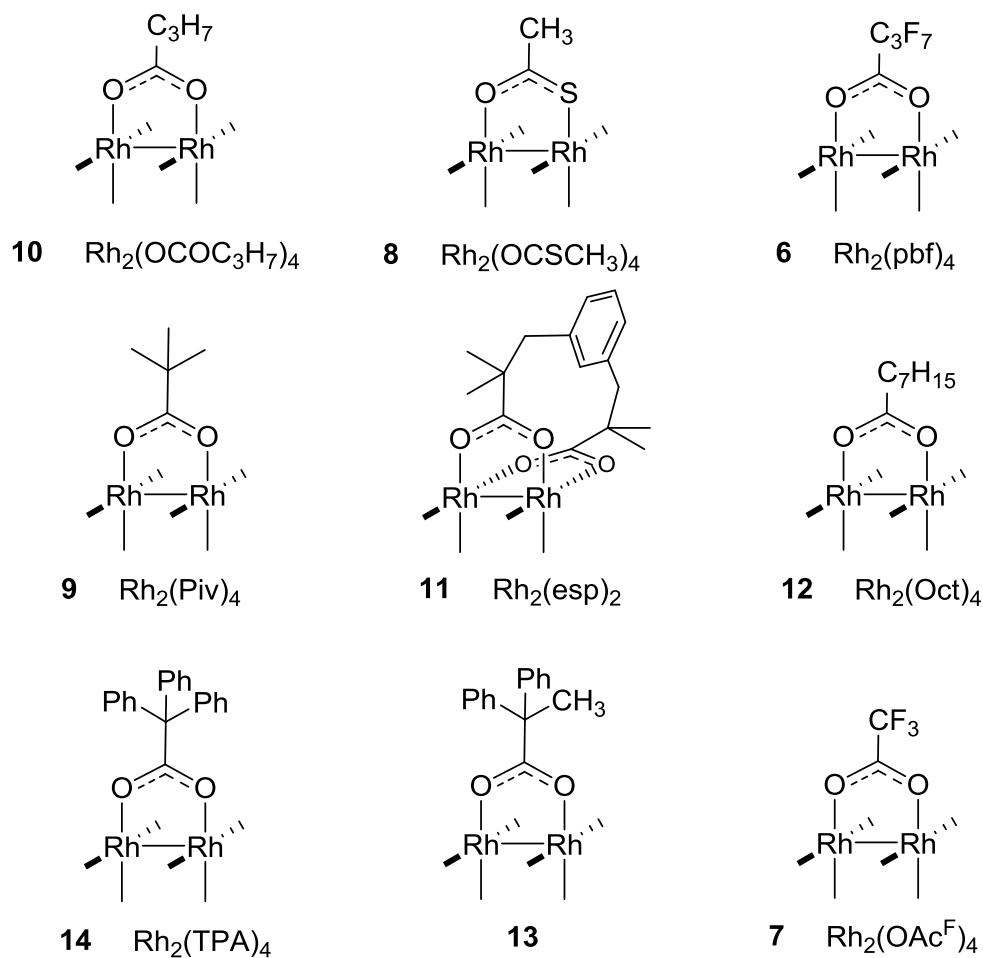


Figure 5: Known achiral rhodium(II) carboxylates. Only one ligand is shown for clarity.^{29,31,32}

Based on the previous discussions in this chapter, an attempt to expand the class of the existing rhodium(II) catalysts was one of many objectives of this project.

Starting from 1990, numerous chiral ligands were introduced in the form of carboxylates (Figure 6).^{23,34,35} Their evolution resulted in an explicit study on the influence of the ligands on rhodium catalysts and provided a powerful instrument in catalyst design.^{36,37}

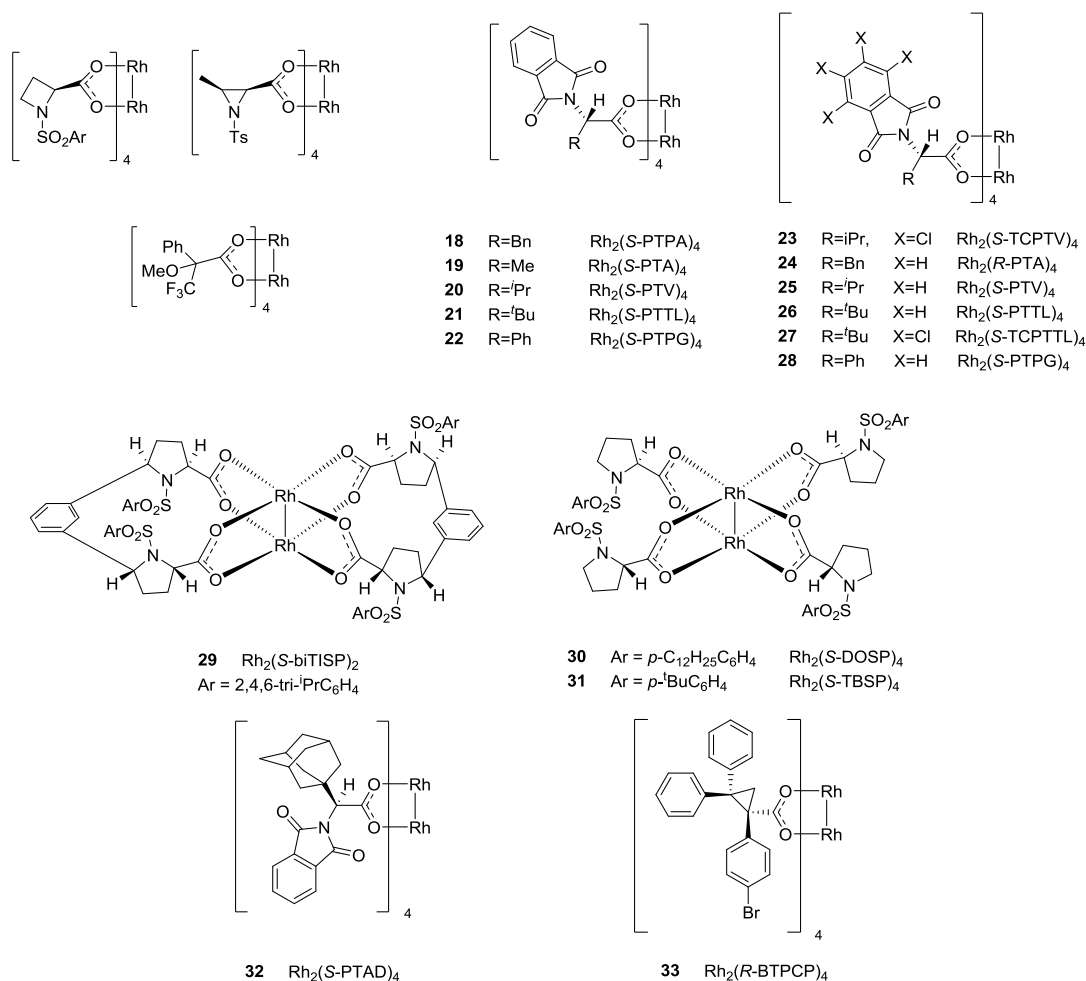


Figure 6: Selected chiral rhodium(II) carboxylates.^{23,34,35}

A major difference between achiral and chiral rhodium(II) carboxylates in catalytic performance resides in their structure. The chiral carboxylate ligands can form a chiral cavity that controls the orientation of the carbene, so that the two active sites of the rhodium complex will no longer be equal. This differentiation provides a much greater selectivity in comparison to steric hindrance.

Worth mentioning is the work published by Davies' group where they showed the development of a series of tetraprotonated rhodium(II) catalysts **29-33**.³⁷ The $\text{Rh}_2(\text{S-DOSP})_4$ (**30**) appeared to be a versatile chiral catalyst for asymmetric cyclopropanation, C-H functionalization and cycloadditions.³⁷

The high selectivity in numerous reactions was explained with a specific coordination of the diazo molecule to the active site of the rhodium(II) complex, where the formation of carbenoid occurred. The $\text{Rh}_2(\text{S-DOSP})_4$ (**30**) possesses a D_2 conformation and the rhodium-carbenoid has only one angle of approach for the substrate.³² Unlike the $\text{Rh}_2(\text{S-DOSP})_4$ (**30**), the Hashimoto's

phthalimidocarboxylates **18-28** have C_4 “all-up” conformation, supported by DFT calculations and X-ray crystallography (Figure 7).^{38,39}

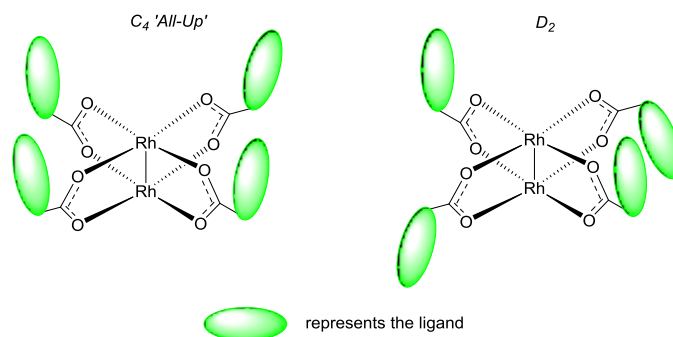
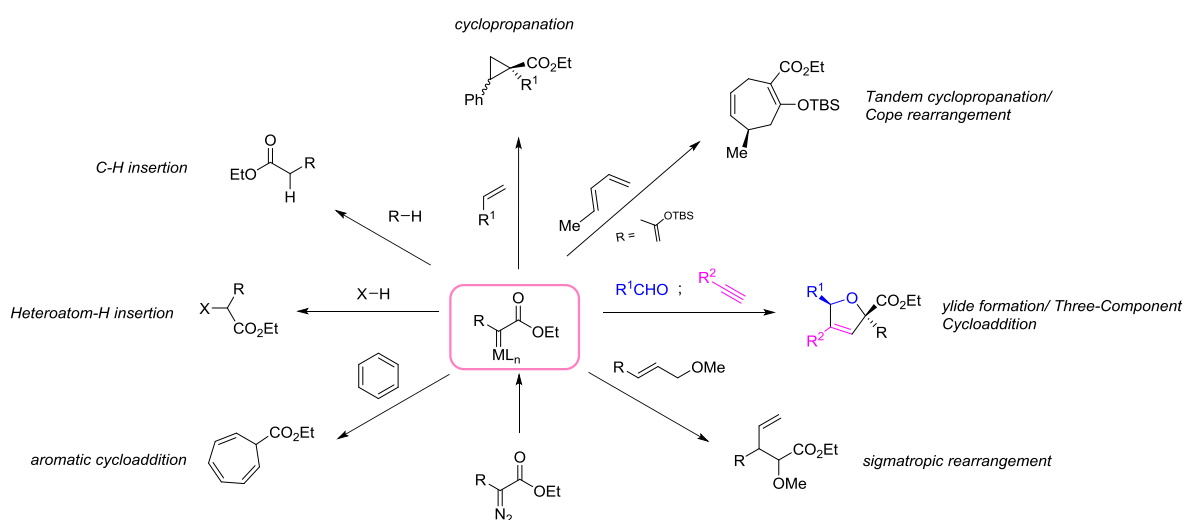


Figure 7: Different possible conformations of rhodium(II) carboxylates.^{38,39}

1.2 Rhodium(II) carbenoids and their reactivity

Diazo compounds have emerged as a versatile class of reagents in organic synthesis and for the preparation of a wide range of building blocks (Scheme 4). Furthermore, the building blocks generated from diazo compounds are a powerful tool in the synthesis of natural products and pharmaceuticals.⁴⁰⁻⁴²



Scheme 4: Diverse synthetic applications of diazo compounds in synthesis.⁴⁰⁻⁴²

The reactivity of the rhodium(II)-carbene complexes can be modulated by the carboxylate substituents (Figure 8). Increasing the electron-withdrawing ability of the ligand increases the

electrophilic nature of the metal-carbene complex, leads to the higher reactivity and, thus, to decreased selectivity.

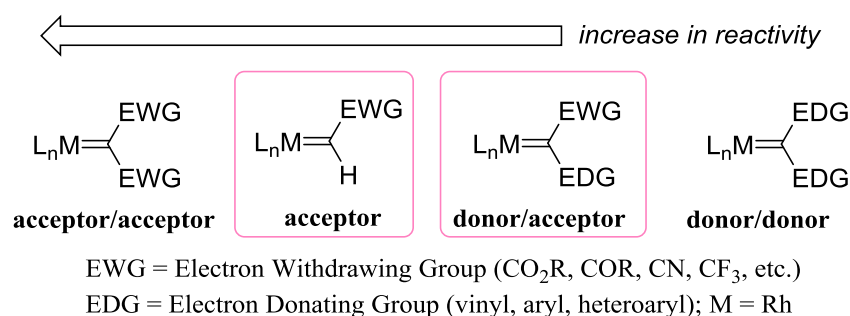
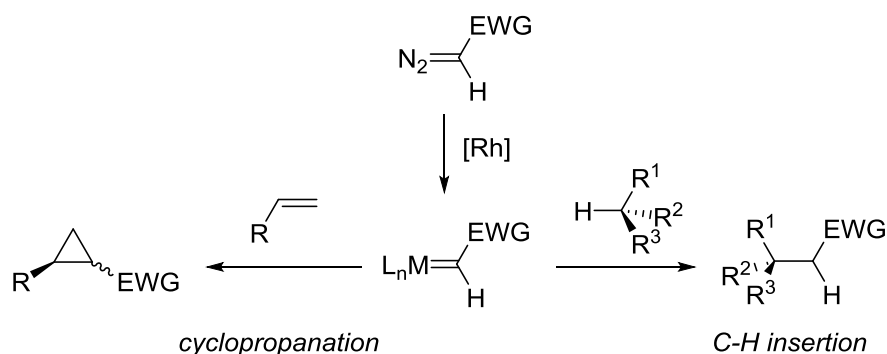


Figure 8: Scope and reactivity of the rhodium(II) carbenoids.

The acceptor/acceptor and acceptor-carbenes are moderate reactive species because the acceptor groups do not stabilize the highly electrophilic carbene center. Therefore, with respect to reactivity and selectivity, acceptor and donor/acceptor carbenoids are found to be virtuous precursors in the carbene-transfer chemistry and were chosen for this project.

Rhodium carbenoids are capable of a variety of regio- and stereoselective reactions (Scheme 4). The most well-studied carbene-transfer reaction is the cyclopropanation and C-H insertion reaction (Scheme 5). The cyclopropane ring, formed in the cyclopropanation reaction, appears in many natural substances as well as in biologically active molecules, highlighting its importance.⁴³

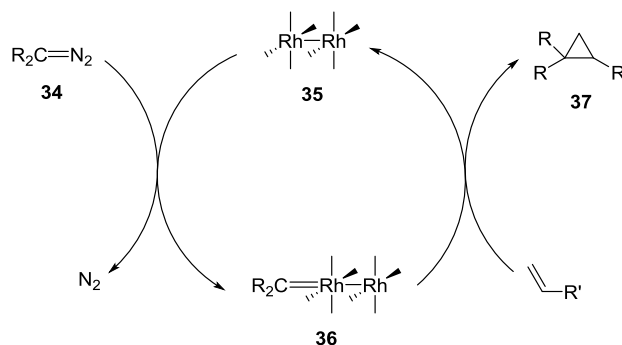


Scheme 5: Two most well-studied carbene-transfer reactions.^{44,45}

The other common reaction, C-H insertion, has become a major area of research due to its versatility in synthesis of natural products.^{44,45} Furthermore, the two reactions were chosen by us to test the catalytic performance of the new polymer catalysts.

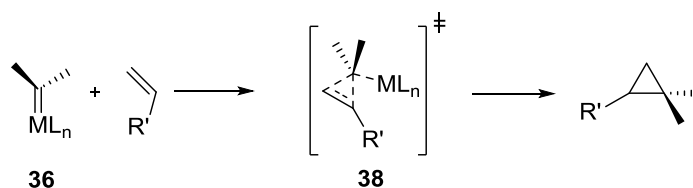
The rhodium(II) carboxylates catalyze the decomposition of the diazo compounds with liberation of N₂ (Scheme 6). The diazo compound **34** reacts with electrophilic rhodium(II) carboxylate **35**,

furnishing the rhodium(II) carbenoid **36**. Further transfer of the carbene to the alkene results in formation of cyclopropanated product **37**.



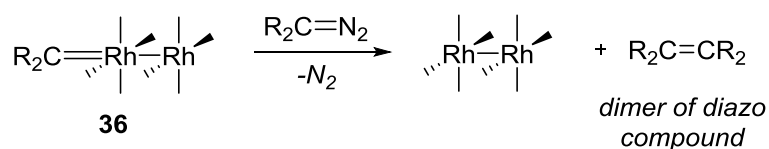
Scheme 6: Catalytic cycle for the cyclopropanation reaction catalysed by rhodium(II) carboxylate **35**. Ligands are omitted for clarity.

A proposed mechanism of cyclopropanation includes an addition of the rhodium(II) carbenoid **36** to the olefin in a concerted manner through the three-membered ring **38** in transition state (Scheme 7).³⁶



Scheme 7: Proposed mechanism of coordination of rhodium(II) carbenoid to the olefin.³⁶

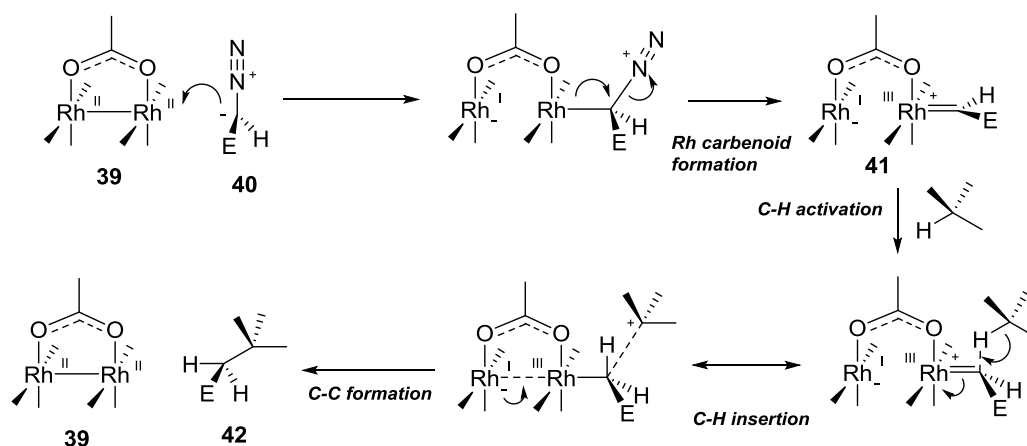
The reaction of rhodium(II) carbenoid **36** with a diazo compound results in the formation of dimers of diazo compound. Usually, the dimerization is a side reaction and desired to be suppressed (Scheme 8).



Scheme 8: Side reaction leading to formation of dimers of diazo compound. Ligands are omitted for clarity.

The C-H insertion has been studied and a plausible mechanism was proposed by Doyle *et al.*⁴⁶ The proposed mechanism was widely accepted, but additional analysis of the mechanism was performed in the group of Nakamura using DFT calculations.^{46,47} The reaction between

rhodium(II) carboxylate **39** and diazo compound **40** resulted in formation of rhodium-carbene complex **41**. Further coordination to the C-H bond, followed by C-C bond formation, generated the rhodium(II) complex **39** and the product **42** (Scheme 9).



Scheme 9: C-H activation mechanism in rhodium(II)-catalyzed reaction. Ligands are omitted for clarity.^{46,47}

In the presence of a double bond, C-H insertion reaction might compete with cyclopropanation. When $\text{Rh}_2(\text{OAc})_4$ (**5**) is used as a catalyst, the reaction results in a mixture of cyclopropanated and C-H inserted products (Table 1).⁴⁸

Table 1: Chemoselectivity in rhodium(II)-catalyzed carbene-transfer reaction.⁴⁸

Entry	Cat.	Cycloprop.	C-H insertion	Yield %
1	5 $\text{Rh}_2(\text{OAc})_4$	44	56	97
2	6 $\text{Rh}_2(\text{pbf})_4$	0	100	56
3	$\text{Rh}_2(\text{cap})_4$	100	0	76

Table 1 shows the different outcome of the reaction when different catalysts were used. Again, due to variation of the ligands around the Rh-Rh bridge, it is possible to favour the formation of the cyclopropanated or the C-H inserted product. For instance, electron rich trisubstituted alkenes can either undergo cyclopropanation or C-H insertion reaction depending on which catalyst was used (Figure 9).⁴⁹

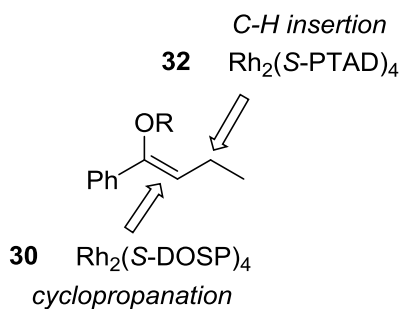
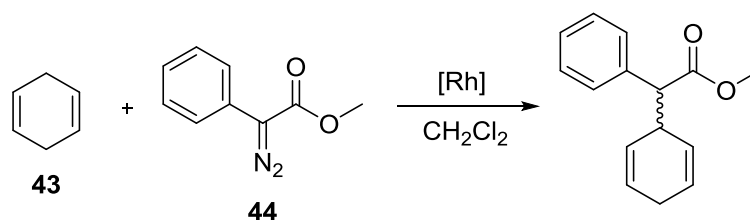


Figure 9: Role of catalyst in two competing reaction pathways.

1,4-Cyclohexadiene (**43**) is a widely used substrate for C-H insertion with methyl phenyldiazoacetate (**44**) (Scheme 10). Unlike cyclopropanation reactions, the reaction between **43** and **44** has not been extensively studied for achiral rhodium(II) carboxylates. Therefore, $\text{Rh}_2(\text{OAc})_4$ (**5**) as well as the new polymer catalysts would be used to study the reaction shown in Scheme 10.



Scheme 10: C-H insertion reaction catalyzed by rhodium(II) carboxylate.

1.3 Heterogenization of rhodium(II) carboxylates

As it was shown in Chapter 1.2, rhodium(II) carboxylates have been widely used in organic synthesis and emerged as a powerful tool in the synthesis of numerous building blocks. They are air stable, easy to handle and soluble in most polar organic solvents.

Since rhodium(II) carboxylates are being widely used, the high cost of the metal allied with the difficulty of recovery and recycling are the major factors that limit their use in both industry and academia.⁵⁰ Generally, reutilization of metal complexes can be achieved by several methods based on homogeneous and heterogeneous strategies.⁵¹⁻⁵⁴ Although each of them has advantages and disadvantages, this project is focused on the heterogeneous strategy.

Once heterogenized, the rhodium(II) carboxylate can readily be recovered by simple filtration. In addition to the easy separation, heterogeneous catalysis minimizes waste derived from catalyst

separation and disposal. Furthermore, solid catalysis allows the design of continuous flow processes, which are attractive at the industrial scale.

The first attempt to heterogenize rhodium(II) carboxylates was taken back in 1991.⁵⁵ Once immobilized, the rhodium catalyst preserved its catalytic activity. The main challenge for developing a universal immobilization method is to ensure compatibility with the different electronic and steric features of each catalyst system.

1.3.1 Covalent bonded rhodium(II) carboxylates

Generally, two classes of supports/carriers are derived – inorganic and organic. The different strategies for heterogenization of rhodium(II) carboxylates utilizing organic carriers are depicted in Figure 10.

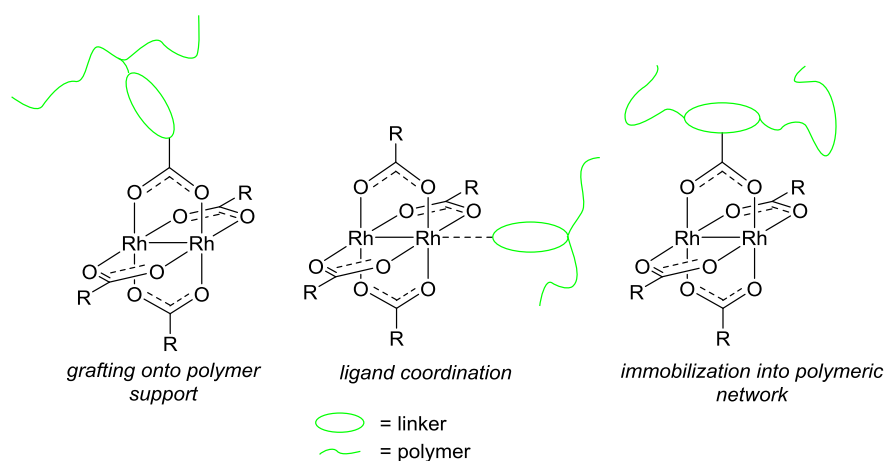
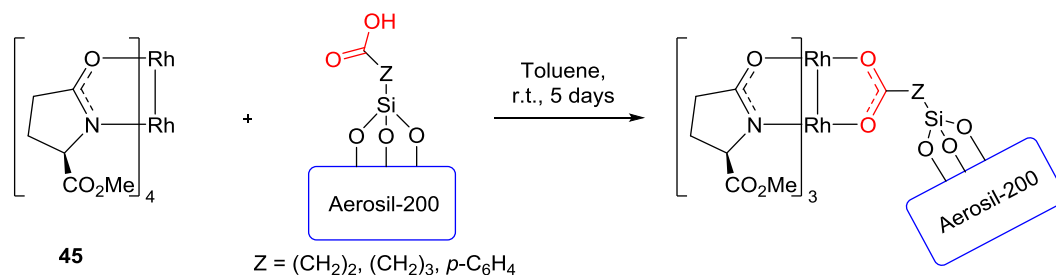


Figure 10: Strategies for immobilization of dirhodium(II) carboxylates.

The majority of rhodium(II) catalysts existing today have limited functionalization or have no functional groups that would be able to graft onto the polymeric support. As consequence, pre-functionalization or modification of existing rhodium(II) catalysts have to be accomplished in order to perform grafting. In some cases, functionalization of the solid support is also required. Ideally, the obtained heterogenized catalyst should be thermodynamically stable, recyclable and experience no leaching or degradation.

Inorganic carriers provide a significantly robust system. The access of the substrate to the catalytic site is defined by structure of the carrier and, as it was shown earlier, it might be a serious issue for the reaction selectivity.⁵⁶ As an example, Doyle's $\text{Rh}_2(5S\text{-MEPY})_4$ (**45**) was successfully immobilized on Aerosil-200 (hydrophilic fumed silica) (Scheme 11).⁵⁷



Scheme 11: Selected example of immobilization of rhodium(II) complex onto the inorganic carrier.⁵⁷

With the immobilization, the authors aimed to increase chiral induction in intermolecular reactions by bringing the catalyst and a substrate to new proximity.⁵⁷ The prepared complex was tested in Si-H insertion and provided the desired product in good yields. However, chiral induction was somewhat low and recyclability demonstrated a degradation of the catalyst already after one cycle.⁵⁸

Another example of enhancing reusability and recyclability is the use of supported catalysts in flow reactor conditions.⁵⁹ For this purpose, a highly effective immobilization of $\text{Rh}_2(\text{S-DOSP})_4$ (**30**) onto polymeric hollow fibers was reported (Figure 11).^{60,61}

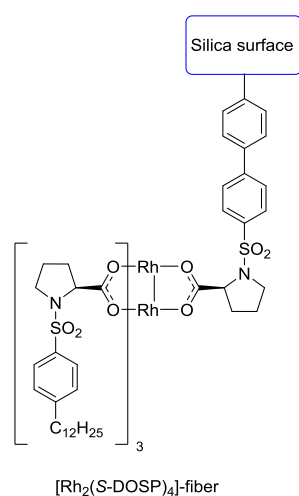


Figure 11: The immobilized $\text{Rh}_2(\text{S-DOSP})_4$ (**30**) on the silica-based support.^{60,61}

The most common resins and polymers of organic carriers are depicted in Figure 12.⁶² All catalysts were grafted on utilizing the ligand exchange method, where certain ligand modification of resin should be performed prior to immobilization. The ligand exchange method includes a reflux of the catalyst and modified polymeric resin in toluene or chlorobenzene.

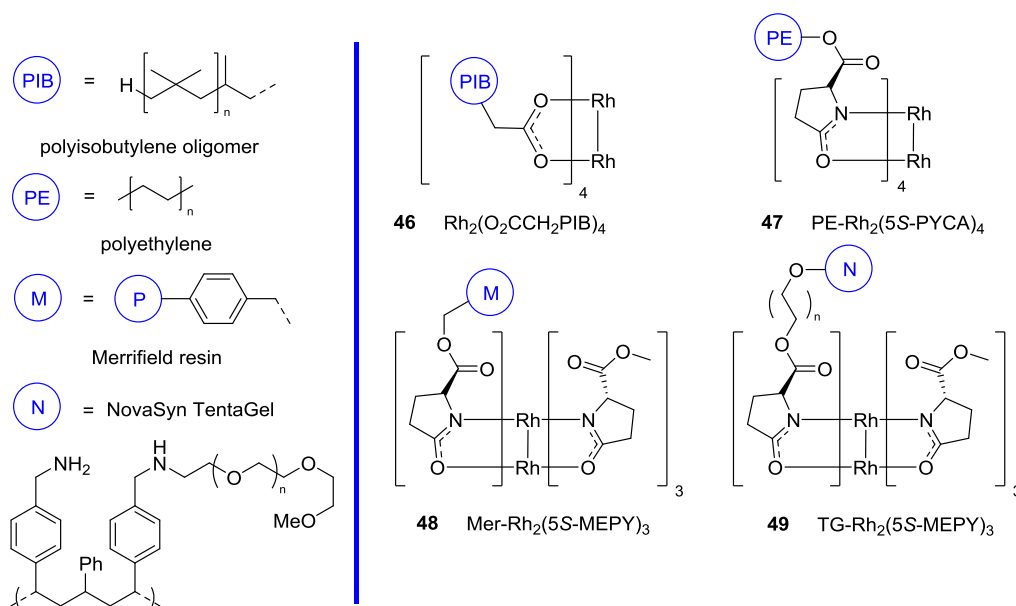
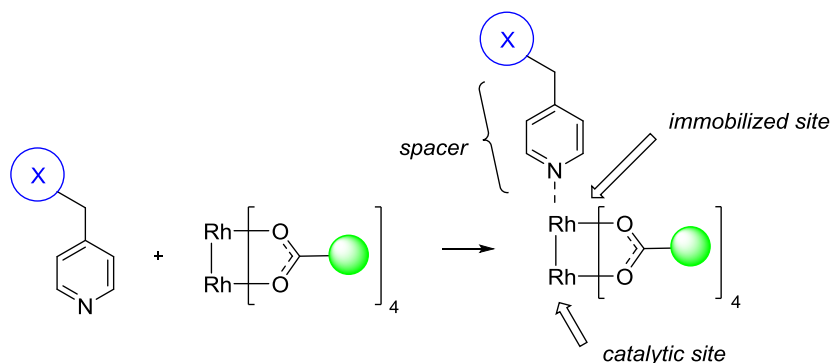


Figure 12: Selected resins and immobilized rhodium(II) catalysts 46-49.⁶²

The point of attachment and strength of the metal-ligand dissociation affects the turnover number, rates, reuse and leaching of the catalyst. These factors, with many others, should be considered in the design of new catalysts.

1.3.2 Axially coordinated rhodium(II) carboxylates



Scheme 12: General scheme for immobilization using axial coordination.⁶²

Davies and co-workers have communicated an approach for the immobilization of the chiral rhodium(II) carboxylates using the strategy depicted in Scheme 12.⁶³ In order to demonstrate the influence of the spacer between the active catalytic site and polymer support, spacers with different lengths were carried onto the polymer supports **50-52** (Figure 13).⁶⁴

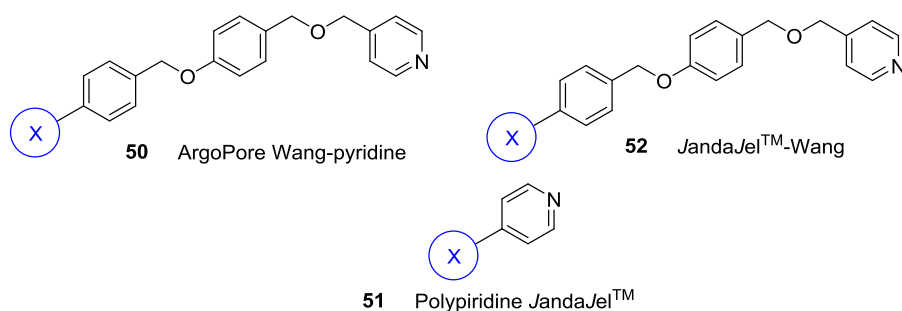


Figure 13: Polymer supports with different distances between the anchoring and the support.⁶³

Table 2: Catalytic performance of the immobilized chiral catalysts.⁶³

Entry	Cat.	Immobilization onto the support, %	ee, %
1	50 -Rh ₂ (<i>S</i> -TBSP) ₄	86	86
2	51 -Rh ₂ (<i>S</i> -TBSP) ₄	<1	-
3	52 -Rh ₂ (<i>S</i> -TBSP) ₄	97	85
4	50 -Rh ₂ (<i>S</i> -MEA _Z) ₄	61	68 (69) ^[a]
5	50 -Rh ₂ (<i>S</i> -PTTL) ₄	77	10 (13) ^[a]

[a] Enantioselectivity using homogeneous catalyst.

As it is depicted in Table 2, the length of the spacer has huge consequences on the effect of the immobilization as well as on the catalytic performance. As it was expected – the shorter the spacer, the slower the immobilization of the catalyst onto the support occurs (entry 1 and 2).

Presumably, when the active site of rhodium is close to the support, its chiral environment becomes distorted and much more sterically hindered, which leads to inefficient immobilization and catalytic performance.⁶³ It can also be concluded that enantiomeric purity of the product does not correlate with the ease of immobilization (entry 5). In addition, within the chiral coordination, the immobilized catalyst preserves its catalytic abilities, comparing to the non-immobilized monomer (entry 4).⁶⁵

To determine the efficiency of the immobilized catalysts, they were tested in standard asymmetric cyclopropanation reaction using 0.5 mol% catalyst (Table 3). In all the entries in Table 3, catalysts were recycled up to four times, yields and enantioselectivity decreased after each round.⁶⁶

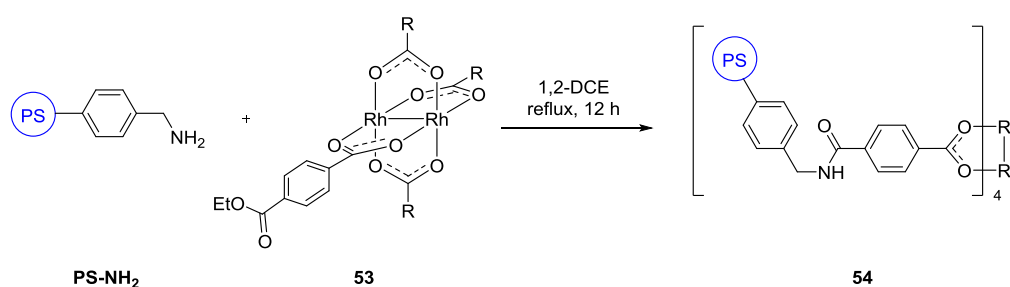
Table 3: Recyclability of the immobilized rhodium(II) carboxylates.⁶⁵

		Rh(II) heterogenized catalyst							
		toluene, r.t.							
		50 -Rh ₂ (<i>S</i> -TBSP) ₄				52 -Rh ₂ (<i>S</i> -TBSP) ₄			
Cycle ^[a]		1	2	3	4	1	2	3	4
Yield, %		92	91	89	89	92	91	90	90
ee, %		82	78	73	70	85	83	81	81

[a] The polymer catalyst was filtered after each cycle.

All the approaches above have one feature in common – they provide an “anchor-like” immobilization where only one ligand is connected to the carrier. That makes two active sites of rhodium different for catalysis, distorts the chiral surrounding, and affects the enantiocontrol. In addition, one linkage to the support affects yield and reproducibility.⁶⁷

An approach to achieve a stronger binding between the catalyst and the support was envisaged and performed by grafting rhodium(II) tetracarboxylate **53** with ester groups onto commercially available functionalized polystyrene (**PS-NH₂**) (Scheme 13).⁶⁸

**Scheme 13:** Covalent-grafted rhodium(II) carboxylate onto the resin.⁶⁷

The polymer catalyst **54** is of a special interest, because of four attaching sites that provide more robustness to the system. Therefore, the catalyst should experience less degradation under reuse. However, in the test reactions the yield was maintained at 86-81% and dropped down after three cycles.

1.4 Polymerization as bottom-up approach

The objective of this project is to immobilize derivatives of the commercially available $\text{Rh}_2(\text{OAc})_4$ (**5**), resulting in a robust, solid and reusable polymer catalysts that preserve or overcome the catalytic activity of $\text{Rh}_2(\text{OAc})_4$ (**5**). There are two ways for heterogenizing rhodium(II) carboxylates (Figure 14). All the approaches, presented in previous chapters, belong to the post-modification strategy and have one feature in common - commercially available polymer supports. Moreover, in some cases, the commercial supports should be pre-modified in order to perform grafting. The available polymer supports limit their use when the desired properties of the immobilized catalytic system should be specific, such as degree of cross-linking, porosity and swelling properties.

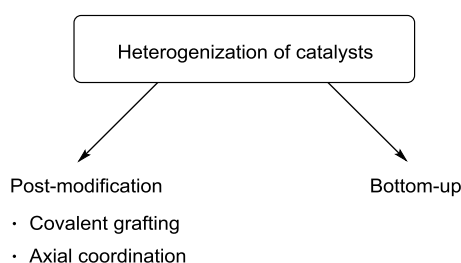
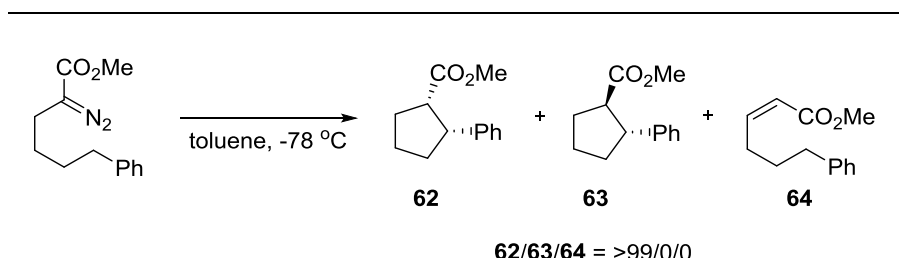


Figure 14: Two different strategies for heterogenization of rhodium(II) carboxylates.

The approach, which was chosen by us, is called bottom-up. The main idea is to copolymerize a catalyst together with monomers and cross-linkers. This enables the assembly of the final polymer catalyst with desired characteristics, like swelling, porosity and degree of cross-binding. In order to participate in polymerization, the catalyst must possess a polymerizable functional group in its molecule.

In 2010, Takeda *et al.*, reported a successful synthesis of polymer-copolymerized rhodium(II) catalysts **55-57**, by suspension polymerization of mixed rhodium(II) tetracarboxylates **58-60**, styrene and **61** (Scheme 14).^{69,70} The monomers **58-60** represent modified $\text{Rh}_2(\text{S-PTTL})_4$ (**21**), which is shown to be an efficient catalyst for intramolecular C-H insertion.⁷¹ The final copolymers **55-57** represent robust, highly selective and durable chiral heterogeneous catalysts.

Table 4: Catalytic performance of polymer rhodium(II) carboxylates by bottom-up strategy.⁷¹

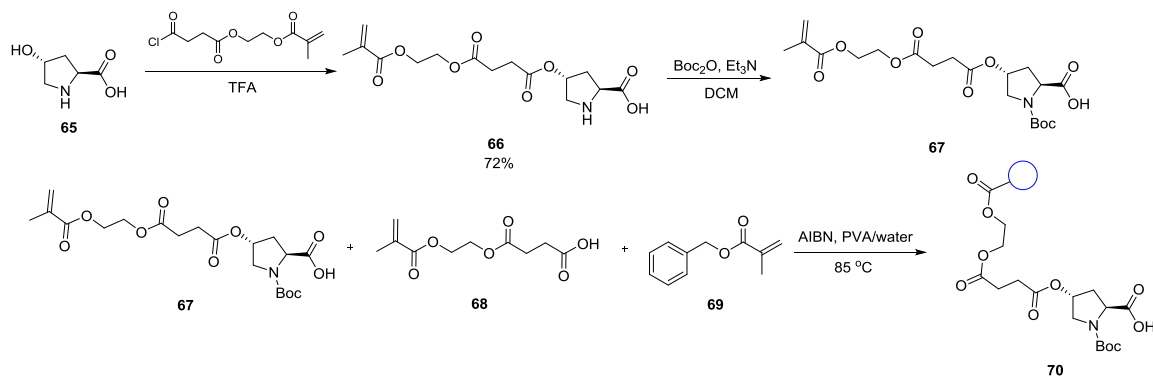
62/63/64 = >99/0/0

Entry	Cat.	Cycle no. ^[a]	Yield (62), %	ee, %
1	58	-	85	95
2	55	1	85	94
3	55	5	84	95
4	55	10	83	95
5	55	20	81	94

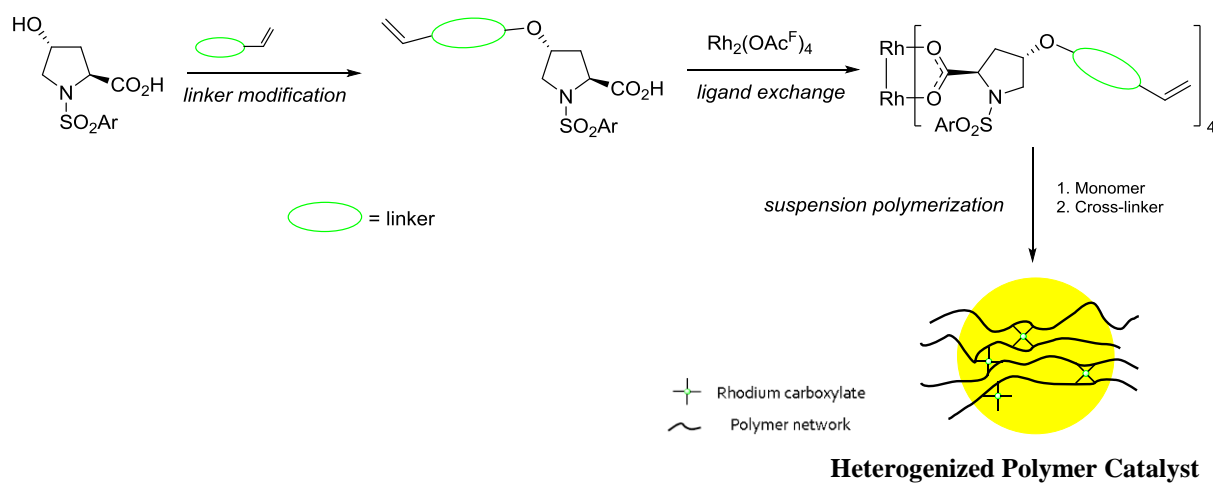
[a] The polymer catalyst was filtered after each cycle.

The bottom-up strategy for immobilization of rhodium(II) complexes is a relatively unexplored method, since very few reports are published.⁷³ Thus, we planned to synthesize analogues of $\text{Rh}_2(\text{OAc})_4$ (**5**) which contain polymerizable groups and co-polymerize them further in a bottom-up fashion. If the polymerization and catalytic testing was successful, the next step would be the synthesis of a chiral analogue of $\text{Rh}_2(\text{OAc})_4$ (**5**) and its immobilization.

The group of Tore Bonge-Hansen has an extensive experience on synthesis and immobilization of *trans*-4-hydroxy-L-proline (**65**) derivatives for both bottom-up and post-modification strategies (Scheme 15).⁷⁴ The protection of amino group in **66** resulted in **67** which was polymerized with mono-2-(methacryloyloxy) ethyl succinate (**68**), as a cross-linker, and **69**, giving heterogeneous catalytic polymer beads **70** with an excellent control of catalyst loading and a porosity of polymer network.^{74,75}

**Scheme 15:** Selected method for synthesis of bottom-up immobilized chiral organocatalyst **70**.⁷³

Being inspired by work on bottom-up immobilization of *trans*-4-hydroxy-L-proline (**65**), we envisaged a similar bottom-up method for chiral rhodium(II) carboxylates (Scheme 16).



Scheme 16: General strategy of bottom-up synthesis of immobilized chiral rhodium(II) carboxylate.

The described copolymerization strategy for polymeric immobilization of functionalized proline offers an advantageous scalability and versatility when compared to the post-modification strategy because of the tolerance and simplicity of the suspension polymerization.⁷⁶

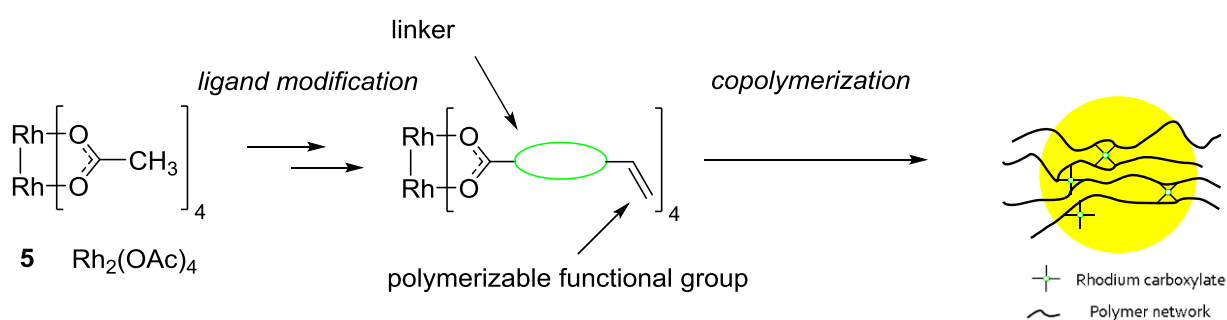
2 Results and discussion – rhodium project

In this section, the synthesis of new rhodium(II) carboxylates with polymerizable ends will be presented. Furthermore, immobilization of the rhodium(II) carboxylates using the bottom-up strategy and a detailed discussion of results will be performed.

In the end, characterization and catalytic performance of the polymer catalysts will be investigated and further discussed.

2.1 Development of novel achiral rhodium(II) carboxylates

The bottom-up approach relies upon modification of $\text{Rh}_2(\text{OAc})_4$ (**5**) with carboxylate ligands that possess a group that is capable of copolymerization. Further, the new carboxylates would be subjected to copolymerization with formation of heterogeneous, hydrophobic polymers (Scheme 17). Thus, in the new polymer-supported rhodium heterogeneous catalysts, the rhodium active component would be randomly distributed within a rigid catalytic framework that can assure more durability and recyclability of the heterogenized polymer catalysts.



Scheme 17: Bottom-up strategy for synthesis and heterogenization of analogues of $\text{Rh}_2(\text{OAc})_4$ (**5**).

At the stage of introducing new ligands, the project is divided on two parts - with achiral and chiral linkers. For achiral carboxylic acids, 4-vinylbenzoic acid (**71**) and mono-2-(methacryloyloxy) ethyl succinate (**68**) were chosen (Figure 15).

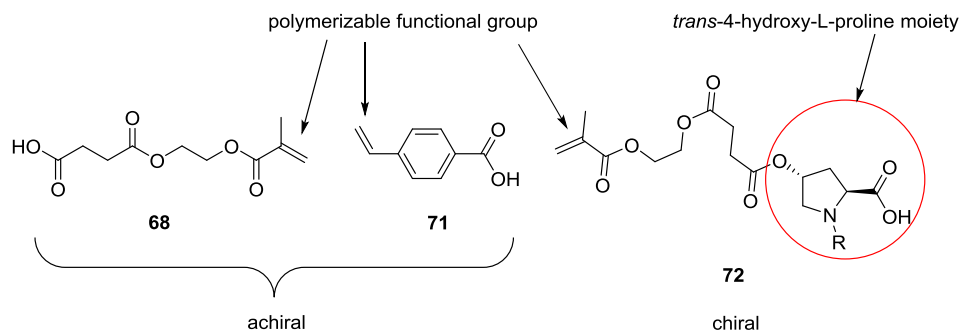


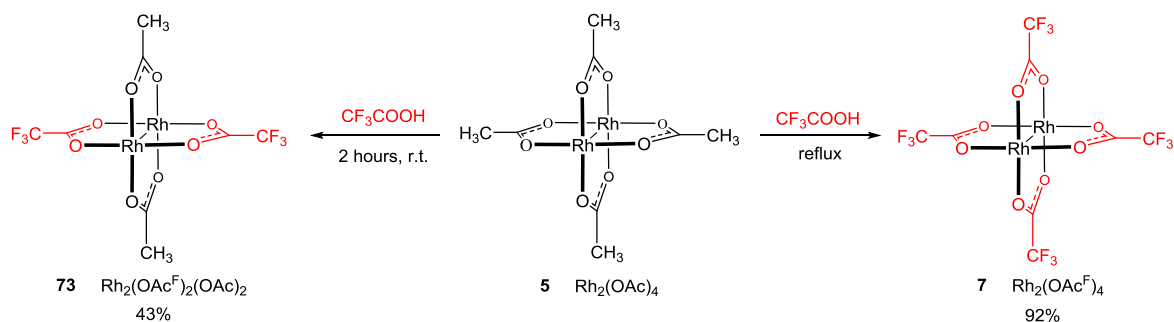
Figure 15: Ligands for synthesis of analogues of $\text{Rh}_2(\text{OAc})_4$ (**5**).

The choice of chiral carboxylic acid relied upon previous experience in Bonge-Hansen's group with functionalized *trans*-4-hydroxy-L-proline. Modifying *trans*-4-hydroxy-L-proline with a linker containing a polymerizable unit, we aimed to develop a chiral polymerizable carboxylic acid **72**.

2.1.1 Synthesis of $\text{Rh}_2(\text{OAc}^{\text{F}})_4$

In order to perform the envisaged modification of initial $\text{Rh}_2(\text{OAc})_4$ (**5**), its acetate ligands should be exchanged with more labile trifluoroacetate ligands (OAc^{F}). The trifluoroacetate groups are more susceptible to dissociate than acetate groups and, therefore, rhodium trifluorotetraacetate, $\text{Rh}_2(\text{OAc}^{\text{F}})_4$ (**7**) was chosen as a rhodium precursor. The synthesis of **7** was carried according to standard procedures found in the literature.⁷⁷

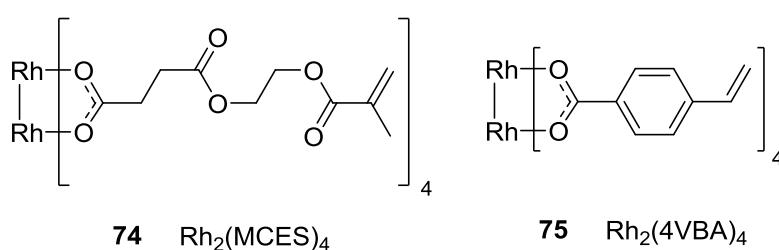
According to the literature procedure, the reaction was carried out in neat trifluoroacetic acid (TFA). The reaction was followed by TLC analysis. Under the reaction conditions mono-, di-, tri- and tetrasubstituted products were observed. Varying the temperature regime, the reaction could be pushed towards formation of a specific substituted product: under refluxing conditions – tetrasubstituted, at room temperature – disubstituted (Scheme 18).⁷⁷ After two days of reflux, all starting material was converted to the product and only tetrasubstituted complex **7** was detected.



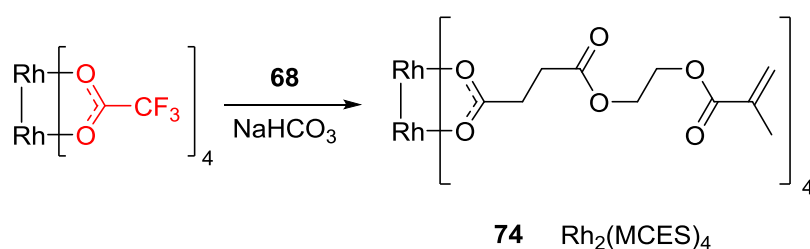
Scheme 18: Synthesis of $\text{Rh}_2(\text{OAc}^{\text{F}})_4$ (**7**) and $\text{Rh}_2(\text{OAc}^{\text{F}})_2(\text{OAc})_2$ (**73**).

The reaction profile was in agreement with previous kinetic investigations.⁷⁸ According to the kinetic studies, rate constant for formation of the disubstituted complex **73** is the greatest and nearly twice as big as for monosubstituted complex and four times bigger than for tetrasubstituted complex **7**. The kinetic data demonstrates that the disubstituted complex **73** could be formed relatively fast at room temperature, whereas the formation of the tetrasubstituted complex **7** requires harder reaction conditions, such as reflux.

2.1.2 Synthesis of tetrasubstituted rhodium(II) carboxylates: Rh₂(MCES)₄ (**74**) and Rh₂(4VBA)₄ (**75**)



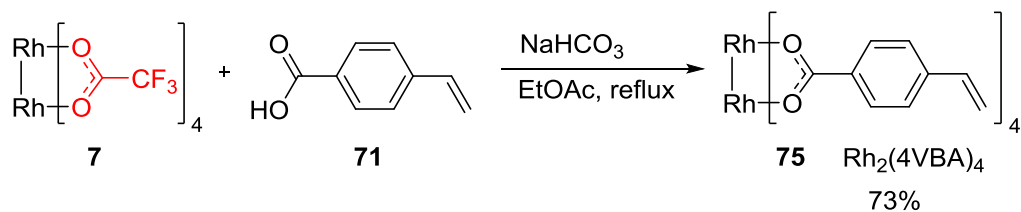
Compound **68** was the first acid investigated in the ligand exchange reaction with Rh₂(OAc^F)₄ (**7**). The acrylic acid **68** has a long spacing group between the carboxylate and the polymerizable end that gives the system its flexibility. Acrylates are usually sensitive to high temperatures and reaction conditions, so the main challenge here was to perform ligand exchange, while keeping the acrylic functional group intact. In order to push the reaction to completion, the presence of a base was found to be essential (Scheme 19).



Scheme 19: Envisaged synthesis of Rh₂(MCES)₄ (**74**).

At first, the reaction was carried at room temperature, with NaHCO₃ and acetonitrile as solvent (high tendency to coordinate to the rhodium(II) complexes). Following the reaction by the TLC analysis, a complicated mixture of compounds was observed.

In order to test the influence of the temperature, the focus was switched to the temperature stable 4-vinylbenzoic acid (**71**). This acid tolerates temperatures above 150°C without being



Scheme 21: Optimized conditions for synthesis of $\text{Rh}_2(4\text{VBA})_4$ (**75**).

In order to investigate the paddle-wheel structure of $\text{Rh}_2(4\text{VBA})_4$ (**75**), the crystals were grown and studied by single X-ray diffraction. The crystallographic structure is depicted in Figure 17 and shown to possess a paddle-wheel, $\text{Rh}_2(\text{OAc})_4$ -like structure. The crystallographic structure determination was performed by Sigurd Øien-Ødegaard.

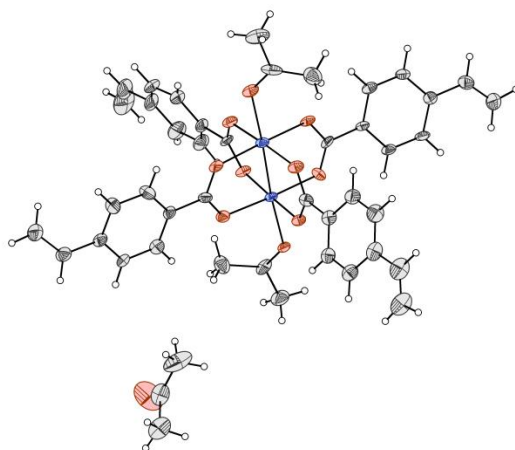
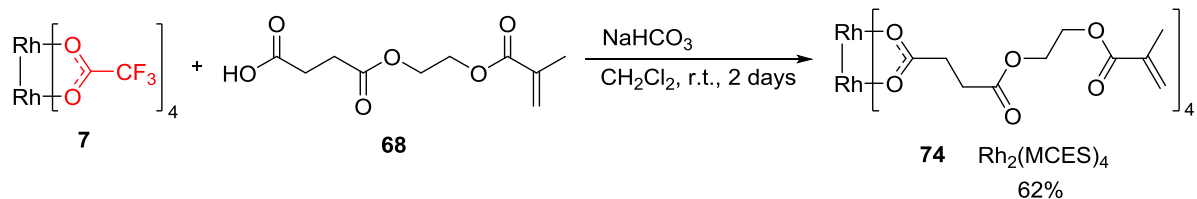


Figure 17: The ORTEP drawing of $\text{Rh}_2(4\text{VBA})_4$ (**75**) with acetone molecules coordinated in axial positions. Ellipsoids are of 50% probability.

The coordination of solvent molecules to the axial positions is observed in the crystal. This observation correlates with the ^1H NMR data that shows various molecules being present in the spectrum as axially coordinated molecules. As it was mentioned in the introduction part, removal of such coordinated molecules requires exposure to high vacuum and high temperatures for a long period of time.

Being inspired by the successful synthesis of rhodium(II) carboxylate with 4-vinylbenzoic acid (**71**), the focus was switched back to mono-2-(methacryloyloxy) ethyl succinate (**68**). Reflux at high temperature was not appropriate for the ligand exchange with mono-2-(methacryloyloxy) ethyl succinate (**68**), because of the risk of self-polymerization. Therefore, the reaction was carried out at room temperature for the increased time of 48 hours (Scheme 22).



Scheme 22: Synthesis of $\text{Rh}_2(\text{MCES})_4$ (**75**).

Interestingly, all attempts to grow a crystal of $\text{Rh}_2(\text{MCES})_4$ (**74**), which is suitable for X-ray analysis, were unsuccessful. Instead of crystals the complex **74** forms soft thin films of amorphous nature (Figure 18).

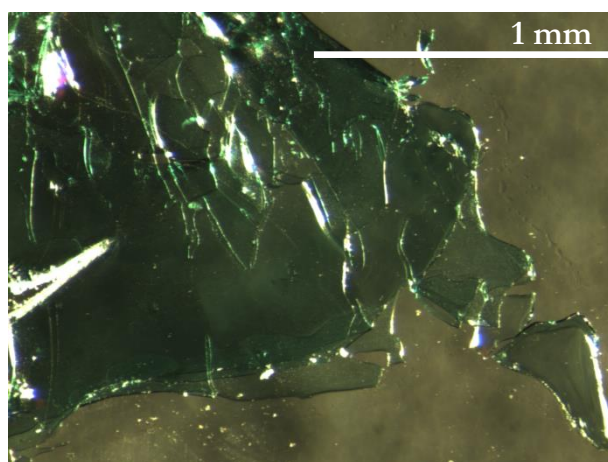
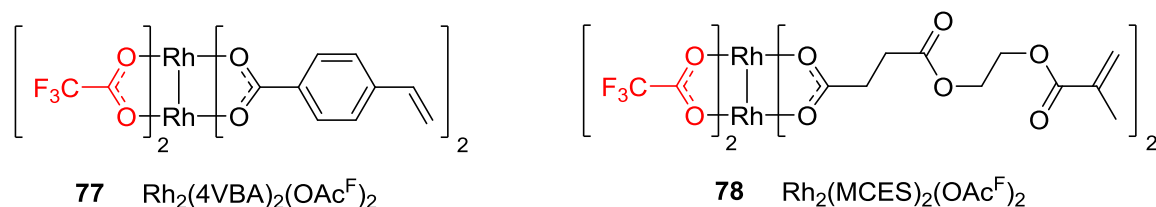


Figure 18: Attempts to grow a single crystal of $\text{Rh}_2(\text{MCES})_4$ (**74**) resulted in thin films. Microscopic picture of which is shown.

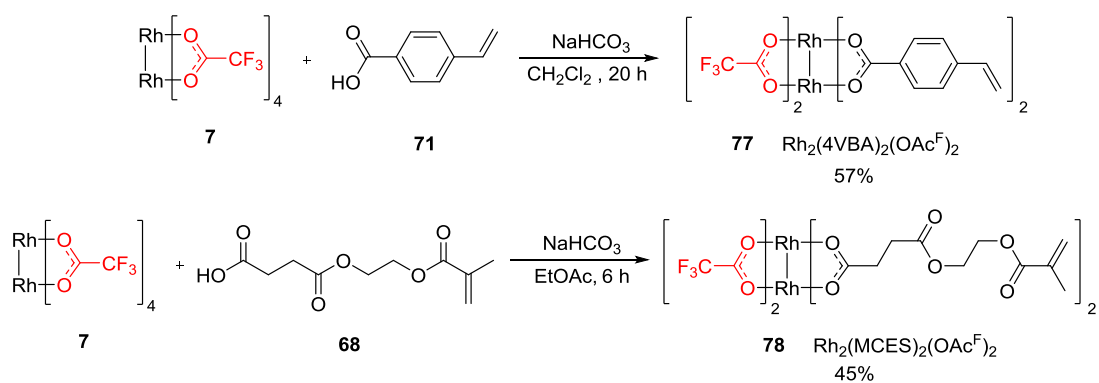
The ^{19}F NMR spectrum showed the absence of OAc^{F} -groups and the mass spectrum revealed a molecular ion top for $\text{Rh}_2(\text{MCES})_4$.

2.1.3 Synthesis of disubstituted rhodium(II) carboxylates:

$\text{Rh}_2(\text{MCES})_2(\text{OAc}^{\text{F}})_2$ (**78**) and $\text{Rh}_2(4\text{VBA})_2(\text{OAc}^{\text{F}})_2$ (**77**)



As mentioned before – room temperature favors formation of disubstituted and high temperature favors formation of tetrasubstituted complex.⁷⁸ Based on this information, the synthesis of disubstituted **77** and **78** was performed as depicted in Scheme 23.



Scheme 23: Synthesis of $\text{Rh}_2(4\text{VBA})_2(\text{OAc}^{\text{F}})_2$ (**77**) and $\text{Rh}_2(\text{MCES})_2(\text{OAc}^{\text{F}})_2$ (**78**).

Carrying out the reaction of $\text{Rh}_2(\text{OAc}^{\text{F}})_4$ with acids **71** and **68**, in the presence of base at room temperature, enabled the selective substitution of two OAc^{F} groups with two carboxylates.

The complexes **77** and **78** were characterized by spectroscopic methods as well as single crystal X-ray crystallography (Figure 19). The crystallographic structure determination was performed by Sigurd Øien-Ødegaard.

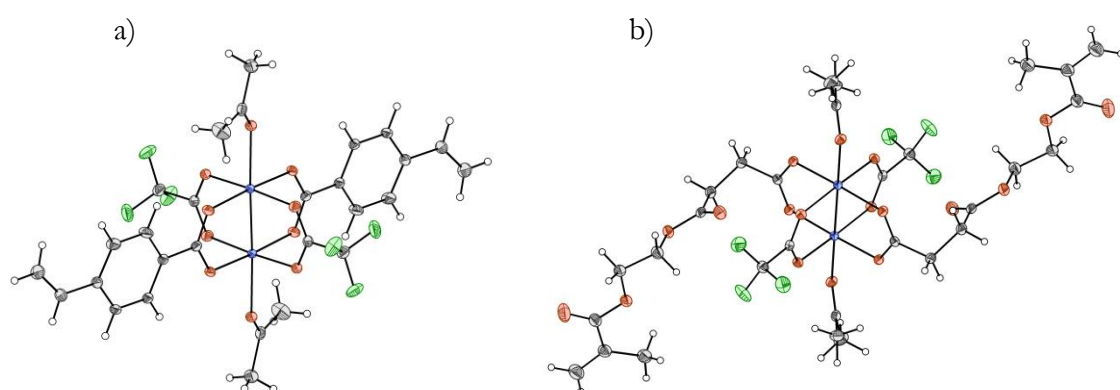


Figure 19: ORTEP-drawing of $\text{Rh}_2(4\text{VBA})_2(\text{OAc}^{\text{F}})_2$ (**77**) (a) and $\text{Rh}_2(\text{MCES})_2(\text{OAc}^{\text{F}})_2$ (**78**) (b) with ellipsoids of 50% probability. Acetone molecules are coordinated in axial positions.

It was shown that ligands are *trans* to each other and the paddle-wheel structure remains intact in both **77** and **78**.

2.2 Heterogenization by polymerization. Bottom-up in action

2.2.1 Polymerization

The homogeneous rhodium complexes **74**, **75**, **77** and **78** have one functionality in common – polymerizable groups. This groups can be involved in a polymerization process which leads to the formation of a heterogeneous network with incorporated rhodium complexes. The working hypothesis would be a synthesis of the polymer network that would hold the rhodium catalyst sites in a fixed, rigid position. Therefore, the polymers would possess the catalytic activity, be more robust and most important, would be reusable.

Due to previous experience with suspension polymerization in our group, this method was also chosen for this project. The suspension polymerization requires a two-phase system – organic and aqueous phase. The first is a hydrophobic organic solvent and the latter is water. In addition to solvents, initiator and stabilizer are also required (Table 5).

Table 5: Components and their functions, involved in suspension polymerization.

Component	Function
Mowiol™ 40-80*	Surfactant, aqueous phase
Ethyl Acetate	Organic phase
AIBN	Initiator
Styrene (79) / <i>tert</i> -butyl acrylate (80)	Monomer
Divinylbenzene (81) / Erythritol 82	Cross-linker
Rhodium(II) carboxylate	Catalyst/Cross-linker (CL)
KI	Inhibitor
Rotation speed	Bead size controller
Temperature	Activation of initiator
Degree of cross-linking	$\frac{(\text{CL} + \text{cat.})}{(\text{monomer} + \text{CL} + \text{cat.})} \cdot 100\%$

* partially hydrolyzed poly(vinyl alcohol) dissolved in water

The formed suspension is stabilized by Mowiol™ and the organic phase is distributed in the form of droplets. The size of the droplets was controlled by rotation speed. The initiation and polymerization occurred in the droplets of the organic phase. To hinder the polymerization in the organic phase, potassium iodide was added.

Exposure to high temperature initiates the polymerization inside the suspended beads. During the polymerization, ethyl acetate evaporates, the monomers copolymerize and miniscule droplets become hydrophobic. Their size is naturally controlled by rotation speed of the stirrer and the organic phase/water ratio. The ratio was found to be the most critical in the polymerization process.

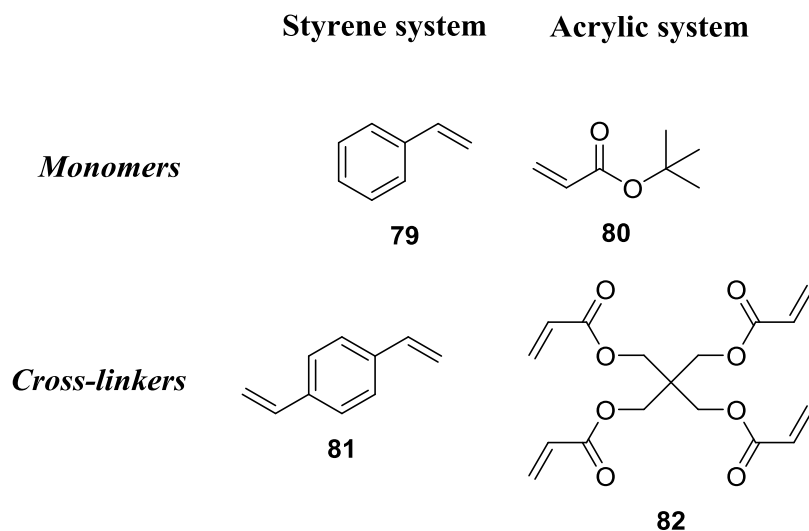


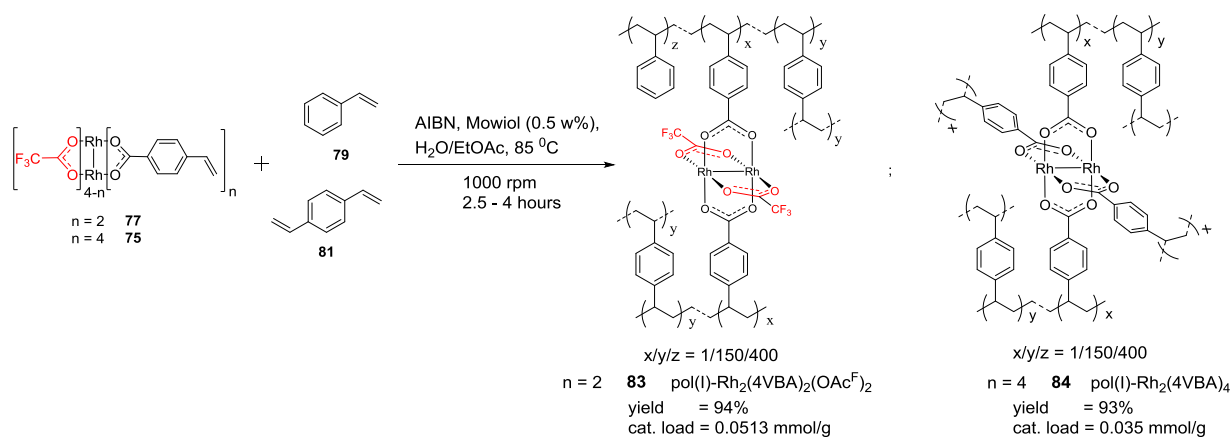
Figure 20: Two polymeric systems used in heterogenization.

The porosity of the future polymer would be controlled by the presence of cross-linkers as well as monomers that construct polymeric chains. Two systems of polymers were synthesized – styrene and acrylic system (Figure 20).

2.2.2 Synthesis of polymer catalysts – Generation I

Our objective was not only to synthesize heterogeneous polymers, but to do it in an elegant manner, so that the polymers would be easy to handle and would consist of miniscule beads. Many experiments were carried out before proper conditions were found. Among many issues, the solubility of the rhodium(II) carboxylate was the major one.

The first successful suspension polymerization resulted in colorful polymer beads for the rhodium(II) carboxylates **75** and **77**. The similar polymerization conditions, but with different monomers and cross-linkers, were applied for the vinylic (Scheme 24) and acrylic system (Scheme 25).



Scheme 24: Suspension polymerization of vinylic system – Generation I.

The di- and tetrasubstituted rhodium(II) complexes **77** and **75**, co-polymerize with styrene (**79**) and divinylbenzen (**81**). The amount of used cross-linker is closely related to the porosity of the formed polymers **83** and **84**.

The catalyst loading was based on the assumption that all the rhodium(II) carboxylate was incorporated into the polymer network. This was confirmed by a negative test of the washing residue. The calculations are provided in the experimental part (Table 16).

The degree of cross-linking was calculated as a mmol% of cross-linker in the mixture of cross-linker and monomer (see experimental part, Table 16).

In the acrylic system, pentaerythritol tetraacrylate (**82**) was used as a cross-linker and *tert*-butyl acrylate (**80**), as monomer (Scheme 25).

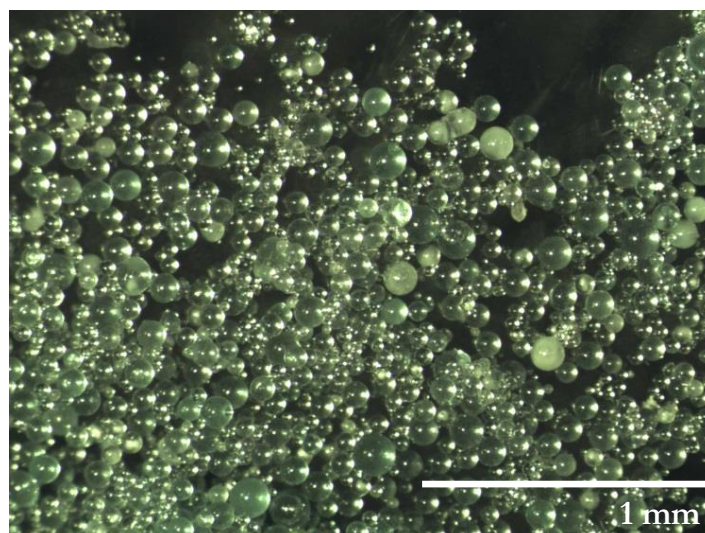


Figure 21: Selected microscopic picture of polymer catalyst – Generation I.

The microscopic pictures of the four polymeric catalysts (Generation I) are given in the appendix (Figures 104-107). In order to gain detailed information on the porosity of the synthesized polymer catalysts, SEM and TEM analysis were performed (detailed pictures are given in the appendix, Figures 111-118).

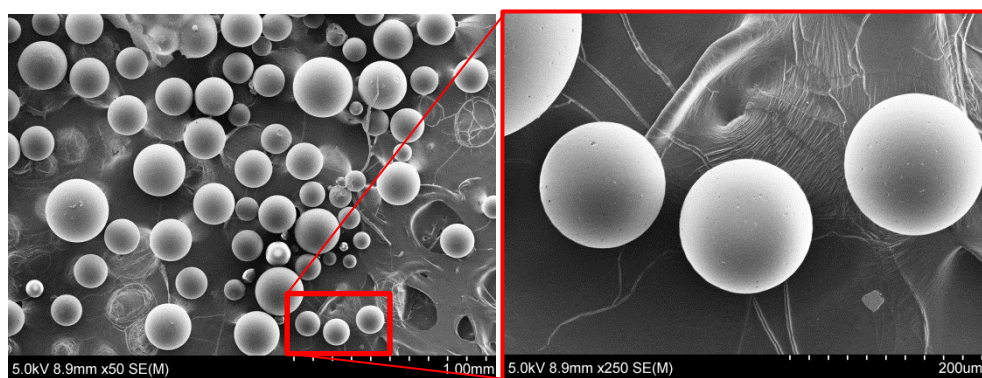


Figure 22: Selected SEM-pictures of polymer catalyst – Generation I.

Figure 22 shows the morphology of selected polymer catalyst beads with a perfect spherical shape and an average diameter of 100 μm . The size of the beads depends on the agitating rate – it decreases with increasing agitating rate. To our surprise, the surface of the analyzed polymer beads was revealed to be rock-solid with no observable porosity (Figure 22). The measurements of specific surface area of catalytic beads by BET adsorption method resulted in the absence of porosity (Figure 23). The surface area measurements were done by Dr. Evgeniy Redekop.

Adsorption/desorption isotherm

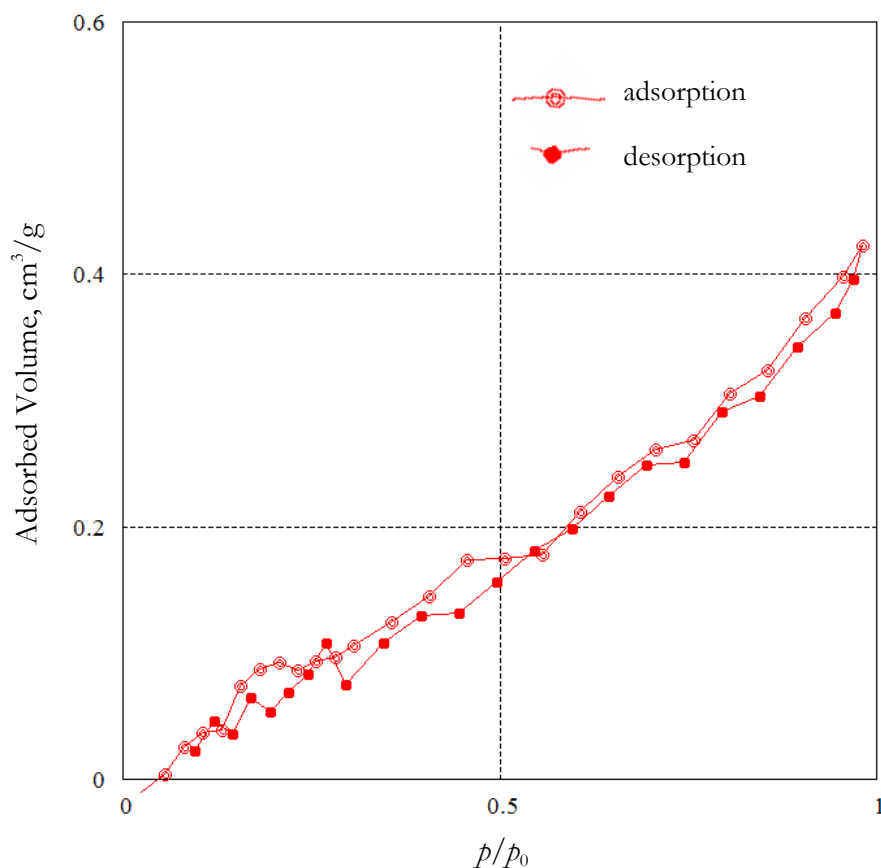


Figure 23: Isotherm of adsorption/desorption for the selected polymer catalyst of vinylic system. Measurements were performed using BET adsorption method.

The beads **83-86** appeared to be solid, glass-like with no porosity. The absence of the porosity indicates that if catalysis occurred, it would be on the rhodium component that lies on the surface of the beads. The unavailability of the rhodium-catalytic sites within the beads limits the catalytic efficiency of the polymers.

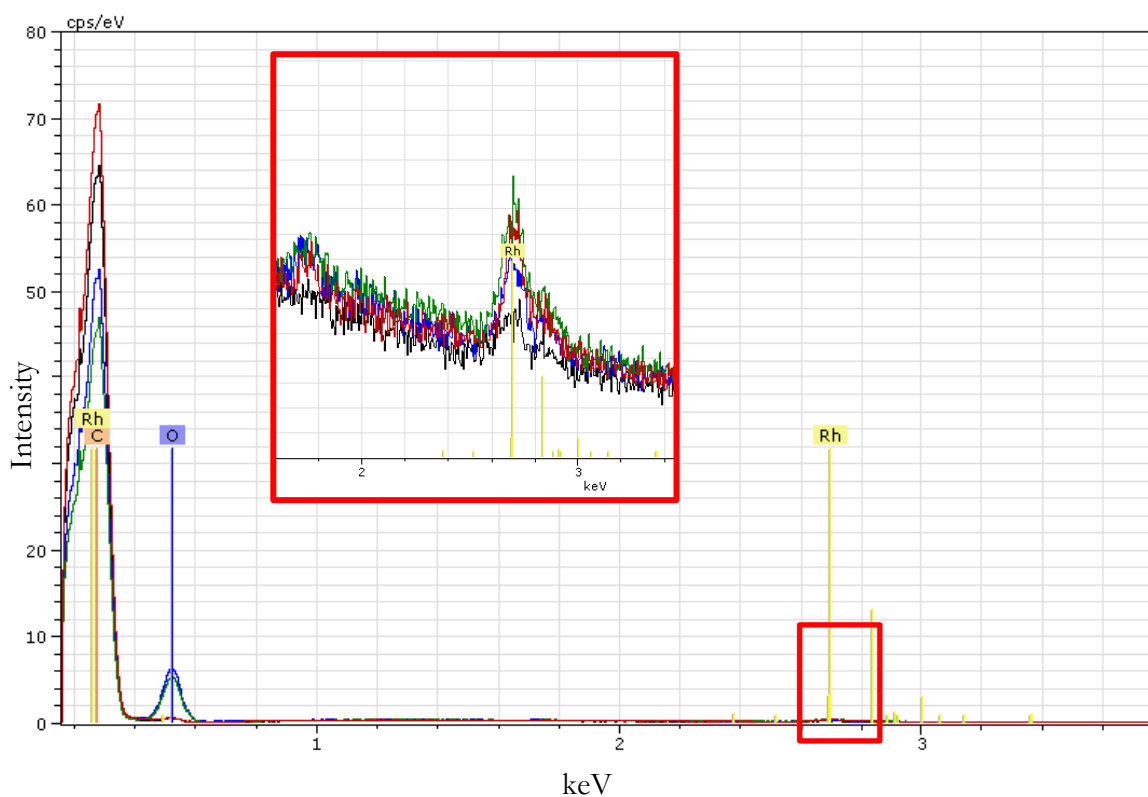
The rhodium content was measured using energy-dispersive X-ray spectroscopy (EDX). The qualitative elemental maps of elements for catalytic polymers **83-86** are shown in Figure 24. The data for the rhodium content are presented in Table 6.

Table 6: Measured Rh content in atomic%.

Rh content (in %)							
	#1 ^[a]	#2	#3	#4	#5 ^[b]	Average ^[c]	St. dev.
pol(I)-Rh ₂ (4VBA) ₄ (84)	0.12	0.08	0.08	0.10	0.09	0.094	0.017
pol(I)-Rh ₂ (MCES) ₄ (85)	0.11	0.19	0.08	0.13	0.16	0.134	0.043
pol(I)-Rh ₂ (MCES) ₂ (OAc ^F) ₂ (86)	0.09	0.12	0.08	0.08	0.09	0.092	0.016
pol(I)-Rh ₂ (4VBA) ₂ (OAc ^F) ₂ (83)	0.07	0.06	0.06	0.10	0.06	0.070	0.017

[a] First measurement. [b] Fifth measurement. [c] Rhodium content in atomic %.

pol(I)-Rh₂(4VBA)₄ - red ; pol(I)-Rh₂(MCES)₄ - green
 pol(I)-Rh₂(MCES)₂(OAc^F)₂ - blue ; pol(I)-Rh₂(4VBA)₂(OAc^F)₂ - black

**Figure 24:** Distribution of the elements calculated by EDX for the polymer catalysts – Generation I.

The measurements of Rh-content were performed five times and the average value was given in atomic percent (column “Average”) (Table 6). The atomic percent shows number of rhodium atoms out of 100 atoms of the sample. Without calibration, the measurements have significant deviation (column “St.dev.”) and cannot be quantified.

The data from Figure 24 shows relative rhodium content to carbon and oxygen atoms. The rhodium content is significantly lower than for oxygen or carbon but it depicts the successful

incorporation of the rhodium monomer into the polymer network. The SEM-EDX/TEM analysis was performed by principal engineer Michaela Salajkova.

In order to investigate the interaction between the solvent molecules and polymer network, swelling experiments were conducted.⁷⁹ The beads were soaked with dichloromethane and the difference in volume for the dry and soaked beads would represent a degree of swelling. Interestingly, no swelling was observed for any of the four catalytic polymers **83-86**. This observation, together with surface area measurements and SEM data, confirms the absence of porosity or inner cavities and could be due to the high degree of cross-linking between the polymer chains.

To elucidate a local environment around the rhodium atoms, XAS measurements were performed and, unfortunately, the results were inconclusive. The local environment of rhodium(II) could not be resolved due to low rhodium(II) content in the measured polymer samples. The new measurements required a higher rhodium(II) content and were not performed due to lack of time.

2.2.4 Synthesis of polymer catalysts – Generation II

To increase the porosity and penetration of the solvent into the polymer network, an attempt to decrease the degree of cross-linking was made. This resulted in a mixed vinyl-acrylic polymerization system where pentaerythritol tetraacrylate (**82**) was chosen as a cross-linker. The erythritol **82** was already utilized in the synthesis of acrylic polymers in Generation I and the choice of **82** as cross-linker was reasoned by the structural similarities – rhodium(II) carboxylates and cross-linker **82** have four polymerizable ends (Figure 25).

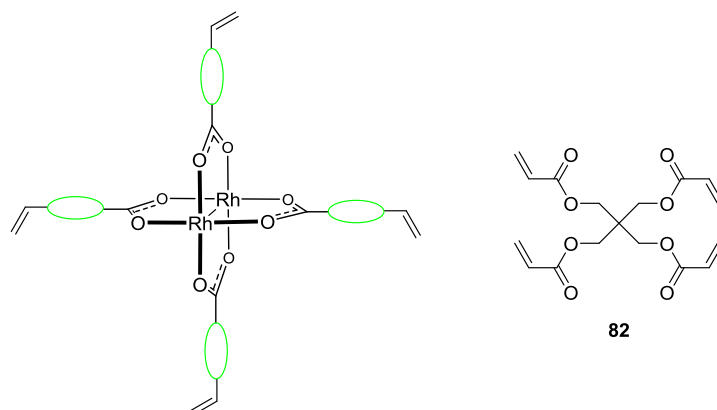
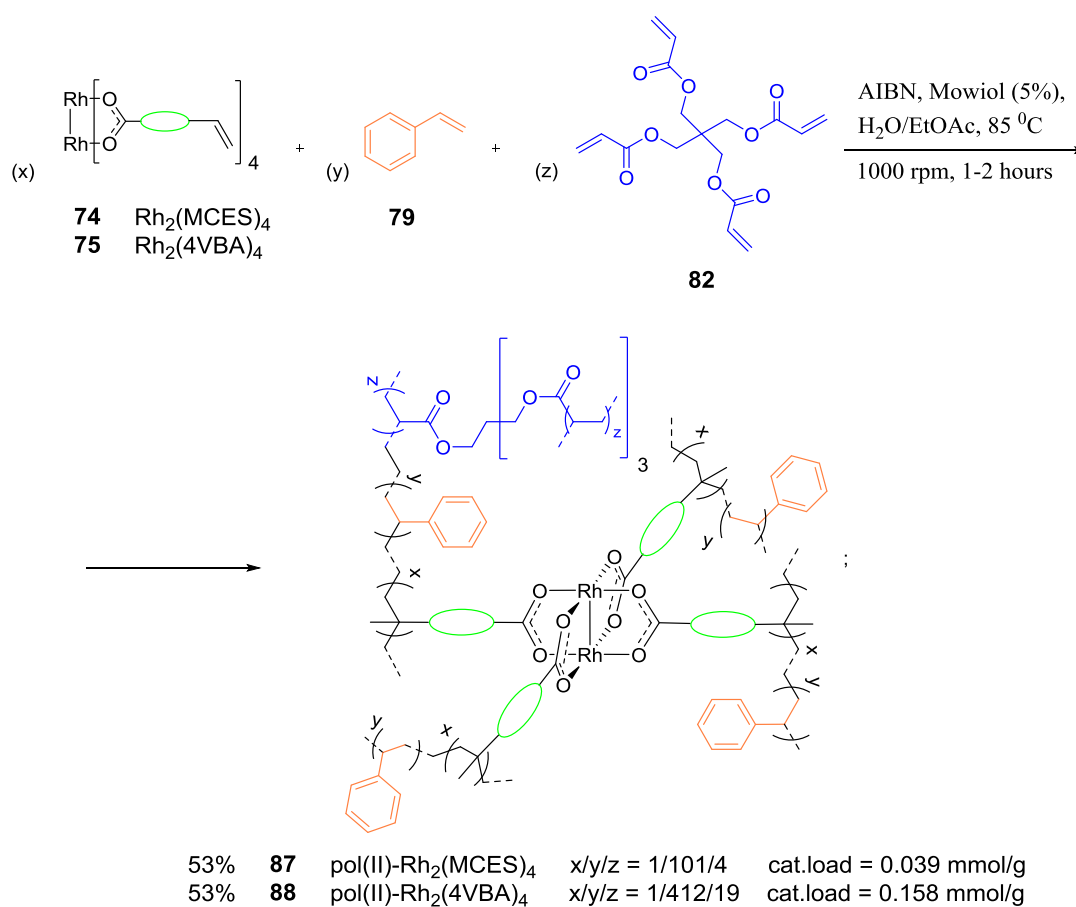


Figure 25: Similarities in structure for rhodium(II) carboxylate and cross-linker **82**.

In the new system, the polymerization method remains the same and both the rhodium(II) carboxylate together with **82** would control the degree of cross-linking. As in the previous polymer catalysts (Generation I), Mowiol™ was chosen to be an aqueous phase and a surfactant. The other parameters remained unchanged. Numerous attempts were made before optimal conditions and a suitable degree of cross-linking was found (Scheme 26). Thus, the degree of cross-linking was decreased from 26% (in the vinylic system) and 15% (in the acrylic system) to 5%.



Scheme 26: Suspension polymerization that leads to the formation of polymer catalysts – Generation II.

2.2.5 Characterization of polymer catalysts – Generation II

The polymer catalysts were characterized by microscopy analysis, SEM-EDX, TEM analysis and surface area measurements.

The polymer catalysts are colored spherical beads that are hard in dry form (a) and soft when swollen (b) (Figure 26). In order to quantify the degree of swelling, the following test was performed. A thin glass capillary tube was charged with polymer beads in dry state and filled with

dichloromethane until the beads stopped to grow. The difference in height between the swollen and dry state defines degree of swelling.

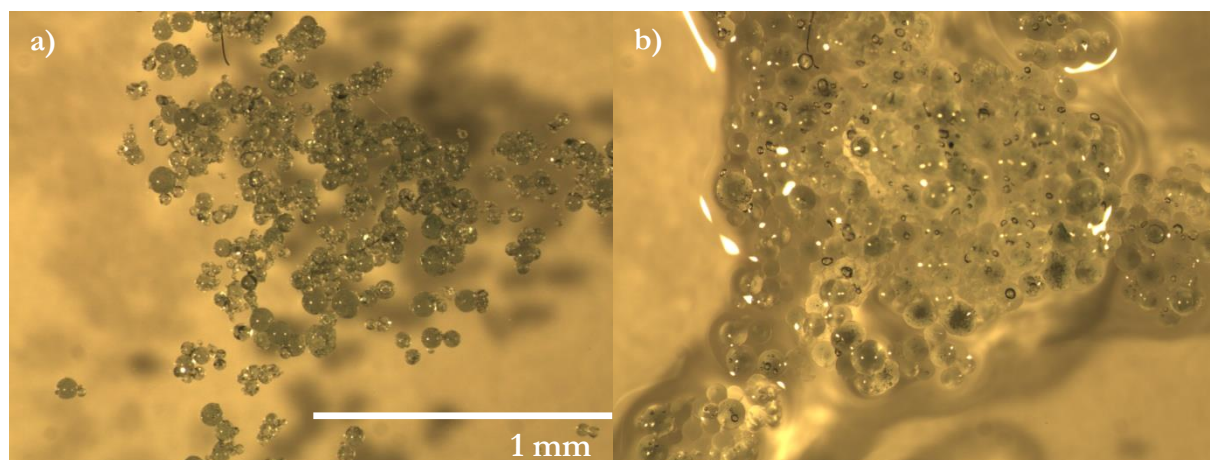


Figure 26: Microscopic picture of the selected polymer catalyst in dry (a) and swollen in CH₂Cl₂ (b) state.

The swelling of the beads indicates that more immobilized rhodium carboxylates became available for the solvent molecules and the substrate. With a lower degree of cross-linking, the polymer becomes more friable. The degree of swelling for pol(II)-Rh₂(MCES)₄ (**87**) and pol(II)-Rh₂(4VBA)₄ (**88**) was measured to be 120 and 100% respectively.

To investigate the surface and morphology, scanning electron microscopy (SEM) and transmission electron microscopy (TEM) were performed (Figure 27 and 28). More SEM and TEM pictures can be found in appendix (Figures 119-122).

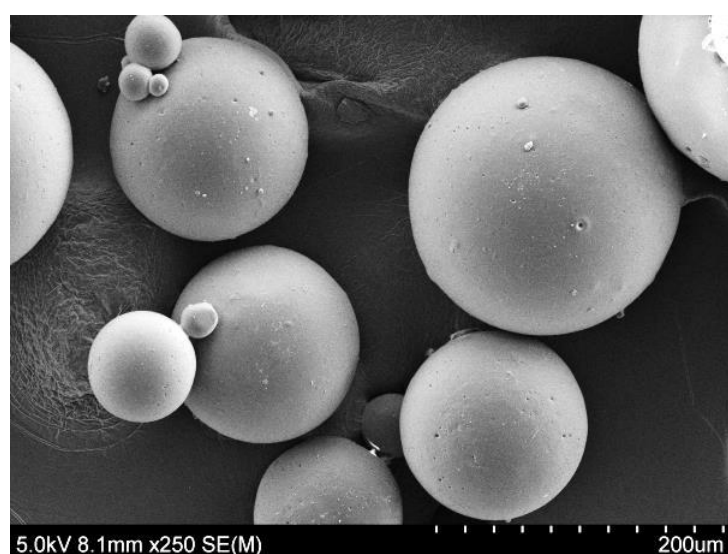


Figure 27: SEM picture of selected polymer catalyst.

Although results from swelling tests suggested a presence of porosity, the SEM picture shows a rock-solid, flat surface with no cracks or deformation observed (Figure 27). The analysis of the cross-section of a selected polymeric bead in non-swollen and swollen states was performed using TEM (Figure 28). The TEM pictures demonstrate a uniform nature of the polymer bead with no visible porosity in both swollen and non-swollen state.

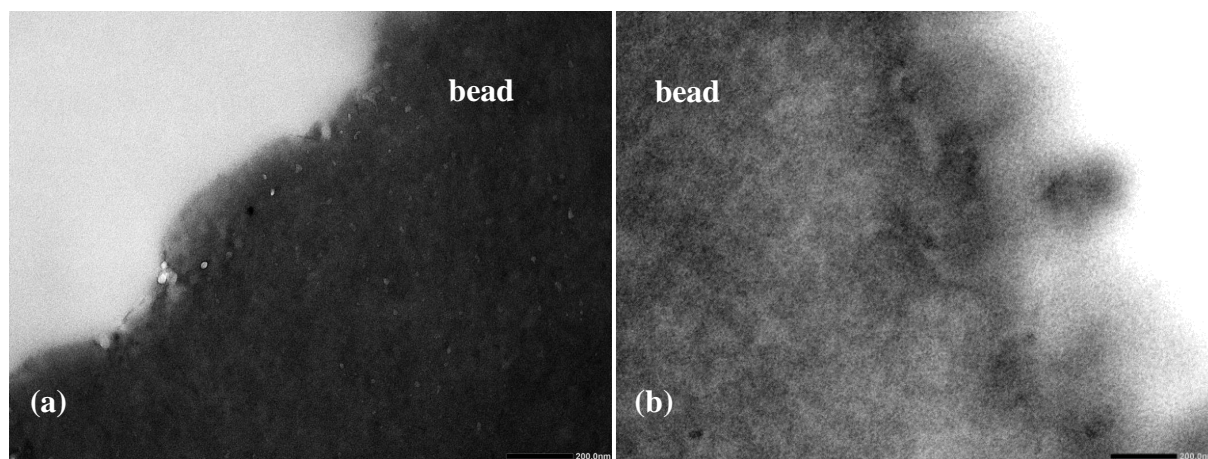


Figure 28: TEM pictures of selected polymer catalyst in non-swollen (a) and swollen (b) state.

In order to estimate the porosity, specific surface area measurements were performed. The measurements were performed using BET adsorption method and revealed no porosity for both $\text{pol(II)-Rh}_2(\text{MCES})_4$ (**87**) and $\text{pol(II)-Rh}_2(4\text{VBA})_4$ (**88**).

The rhodium content was measured using energy-dispersive X-ray spectroscopy (EDX). The qualitative elemental maps of elements for catalytic polymers **88-89** are shown in Figure 29. The data for rhodium content is presented in Table 7.

In the polymer catalysts of the Generation II, higher catalyst loading was observed in comparison to the Generation I. The presented data in Table 7 were not calibrated and the real Rh-content was not possible to calculate. However, it is possible to estimate the relative Rh-content, which was calculated to be approximately 3.4 times greater for $\text{pol(II)-Rh}_2(4\text{VBA})_4$ (**88**) than for $\text{pol(II)-Rh}_2(\text{MCES})_4$ (**87**) (column “Average”). The EDX measured relative Rh-content correlates well with theoretic ratio for Rh-loading in the polymer catalysts (experimental section, Table 18).

Table 7: Measured Rh content in atomic%.

Rh content (in %)							
	#1 ^[a]	#2	#3	#4	#5 ^[b]	Average ^[c]	St. dev.
pol(II)-Rh ₂ (4VBA) ₄ (88)	0.33	0.68	0.64	1.10	0.78	0.706	0.277
pol(II)-Rh ₂ (MCES) ₄ (87)	0.13	0.23	0.27	0.22	0.20	0.210	0.051

[a] First measurement. [b] Fifth measurement. [c] Rhodium content in atomic %.

pol(I)-Rh₂(4VBA)₄ - blue ; pol(I)-Rh₂(MCES)₄ - red

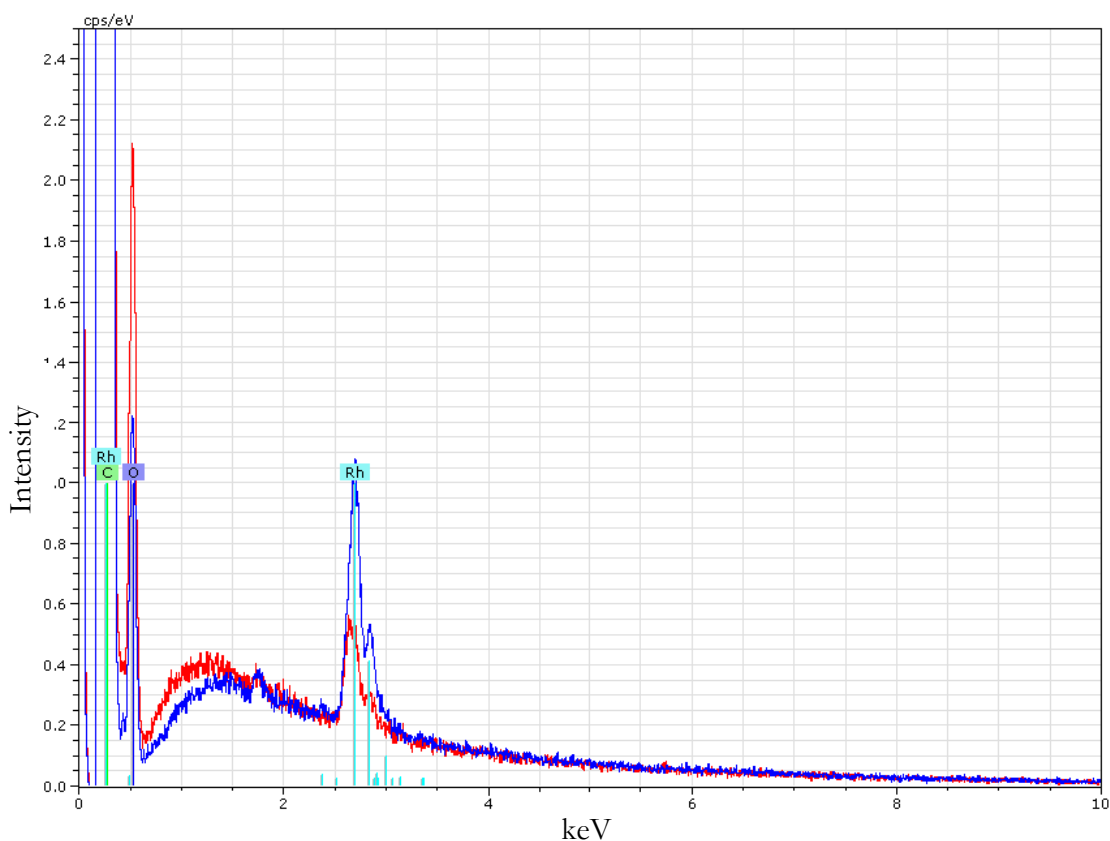
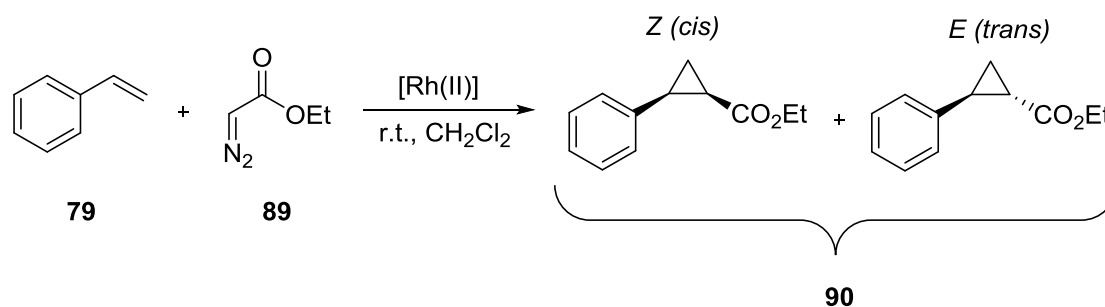


Figure 29: Distribution of the elements calculated by EDX for the polymer catalysts – Generation II.

The SEM-EDX/TEM analysis was performed by principal engineer Michaela Salajkova.

2.3 Catalytic performance of novel heterogenized rhodium(II) catalysts

Cyclopropanation of alkenes with diazo compounds has been used as a benchmark reaction to evaluate new heterogeneous catalysts for carbenoid reactions.⁸⁰ Therefore, the studies to investigate the heterogenized catalysts using the standard intermolecular cyclopropanation of styrene (**79**) with ethyl diazoacetate (EDA) (**89**) were initiated (Scheme 27).



Scheme 27: Test reaction for evaluation of Rh(II)-polymer catalysts.

In the benchmark reaction 5 equiv. of styrene (**79**) reacted with 1 equiv. EDA (**89**) in the presence of 1 mol% rhodium(II) carboxylate as a catalyst. The reaction was carried out in dry CH₂Cl₂, with a dropwise addition of EDA in CH₂Cl₂ over 30 minutes and stirring at room temperature for 2 hours.

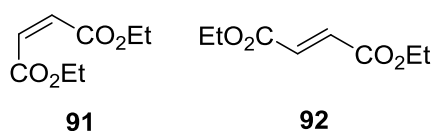


Figure 30: Products of dimerization of EDA.

The cyclopropanation reaction implies formation of two diastereomers **90** – Z (*cis*) and E (*trans*) (Scheme 27). The *cis* and *trans* products were isolated and characterized once. Further, the yields were measured using mesitylene as an internal standard. In the cyclopropanation reaction, the rhodium(II) carbenoid can transfer the carbene group onto the diazo compound which results in formation of two by products - diethyl maleate (**91**) and diethyl fumarate (**92**). The formation of **91** and **92** is considered undesirable and the dimerization reaction is preferred to be suppressed.

The results of performance of polymer catalysts in cyclopropanation reaction are given in Table 8.

Table 8: Catalytic performance of polymer catalysts – Generation I.

Entry ^[a]	Cat.	Cat. [mol %]	EDA dimer, [%]	Product, <i>cis/trans</i> ^[b]	Yield [%] ^[c]
1	5 Rh ₂ (OAc) ₄	1	trace*	39/61	82
2	7 Rh ₂ (OAc ^F) ₄	1	6	45/55	40
3	85 pol(I)-Rh ₂ (MCES) ₄	1	trace	41/59	63
4	84 pol(I)-Rh ₂ (4VBA) ₄	1	trace	51/49	81
5 ^[d]	86 pol(I)-Rh ₂ (MCES) ₂ (OAc ^F) ₂	1	7	48/52	46
6 ^[f]	83 pol(I)-Rh ₂ (4VBA) ₂ (OAc ^F) ₂	1	trace	50/50	39
7 ^[e]	83 pol(I)-Rh ₂ (4VBA) ₂ (OAc ^F) ₂	1	trace	42/58	24

[a] Reaction was performed by a dropwise addition of EDA over 30 min. Polymer catalysts were swollen in CH₂Cl₂ and styrene before reaction with EDA was added. After addition, the reaction mixture was agitated for 2 hours. [b] Diastereomeric excess was measured by NMR. [c] Yield was measured by NMR spectroscopy with mesitylene as an internal standard. [d] 84 % conversion of EDA in 2 hours. [e] 82 % conversion of EDA in 2 hours. [f] Full conversion of EDA in 24 hours. * the yield of EDA dimer <3 % was considered as a trace.

Entry 1 and 2 in Table 8 show a significant influence of the OAc vs OAc^F group, which resulted in almost half the yield. Presumably, the drop in yield is due to high lability of the trifluoroacetate groups which also can be observed by comparing the polymer disubstituted catalysts (entry 5 and 3). The trend of yield <50% is observed for all the fluorinated, immobilized analogues of Rh₂(OAc)₄ (entry 5, 6, 7). Interestingly, the polymer catalyst pol(I)-Rh₂(4VBA)₄ (**84**) possessed the highest catalytic activity with the yield of 81%, which is comparable with non-immobilized Rh₂(OAc)₄ (entry 4).

To summarize Table 8, the tetrasubstituted polymer catalysts **84** and **85** performed better than disubstituted and fluorinated polymer catalysts **86** and **83** (entry 3 and 4 vs 5 and 6). As it was discussed in Section 2.2.3, the tested polymer catalysts have no porosity and although they are not able to swell, the yields in some cases were comparable to Rh₂(OAc)₄. That indicates that the catalysis occurs on the surface of the beads and that the internal rhodium(II) component is not available for catalysis.

The tetrasubstituted pol(I)-Rh₂(MCES)₄ (**85**) and pol(I)-Rh₂(4VBA)₄ (**84**) show the best catalytic activity and, therefore, the corresponding rhodium(II) carboxylates Rh₂(MCES)₄ (**74**) and Rh₂(4VBA)₄ (**75**) were chosen for synthesis of polymer catalysts with less degree of cross binding – Generation II polymer catalysts. The new polymer catalysts pol(II)-Rh₂(MCES)₄ (**87**) and pol(II)-Rh₂(4VBA)₄ (**88**) were tested in the cyclopropanation reaction (Table 9).

Table 9: Catalytic performance of polymer catalysts – Generation II.

Entry ^[a]	Cat.	Cat. [mol %]	EDA dimer, %	Product, <i>cis/trans</i> ^[b]	Yield [%] ^[c]
1	5 Rh ₂ (OAc) ₄	1	trace	39/61	82
3	87 pol(II)-Rh ₂ (MCES) ₄	1	trace	42/58	81
4	88 pol(II)-Rh ₂ (4VBA) ₄	1	trace	47/53	91

[a] Reaction was performed by a dropwise addition of EDA over 30 min. Polymer catalysts were swollen in CH₂Cl₂ and styrene before reaction with EDA was added. After addition, the reaction mixture was agitated for 2 hours. [b] Diastereomeric excess was measured by NMR. [c] Yield was measured by NMR spectroscopy with mesitylene as an internal standard.

The less cross-linked polymer catalysts pol(II)-Rh₂(MCES)₄ (**87**) and pol(II)-Rh₂(4VBA)₄ (**88**) possess higher catalytic activity with improved yields in comparison to their previous analogues pol(I)-Rh₂(MCES)₄ (**85**) and pol(I)-Rh₂(4VBA)₄ (**84**) (Table 8). The improved yields are presumably due to increased amount of Rh-active sites exposed to the catalysis. Therefore, the catalysis occurs not only on the surface, but also within the beads.

Interestingly, the polymer catalysts **87** and **88** possess the same and even higher catalytic activity than the original Rh₂(OAc)₄ (**5**). Thus, the novel polymer catalysts pol(II)-Rh₂(MCES)₄ (**87**) and pol(II)-Rh₂(4VBA)₄ (**88**) can be used as alternative to the existing Rh₂(OAc)₄ (**5**). That satisfies the original idea of the project and opens new prospectives for the immobilized post-modified rhodium(II) carboxylates.

To investigate how efficient polymer catalysts could convert diazo compound, the cyclopropanation reaction was performed with a 0.01 mol% polymer catalysts together with the non-polymerized rhodium(II) carboxylates **74** and **75** (Table 10). It was observed a significantly different behaviour in the catalytic activity for the non-polymerized and polymerized rhodium(II) carboxylates.

Table 10: Catalytic performance of polymer catalysts – Generation II.

Entry ^[a]	Cat.	Cat. [mol %]	EDA dimer, %	Product, <i>cis/trans</i> ^[b]	Yield [%] ^[c]
1	5 Rh ₂ (OAc) ₄	0.01	trace	42/58	60
2	75 Rh ₂ (4VBA) ₄	0.01	trace	46/54	30
3	74 Rh ₂ (MCES) ₄	0.01	BDL	42/58	81
4	88 pol(II)-Rh ₂ (4VBA) ₄	0.01	BDL	42/58	15
5	87 pol(II)-Rh ₂ (MCES) ₄	0.01	BDL	44/58	9

[a] Reaction was performed by a dropwise addition of EDA over 1.5 hours. Polymer catalysts were swollen in CH₂Cl₂ and styrene before reaction with EDA was added. After addition, the reaction mixture was agitated for 24 hours. [b] Diastereomeric excess was measured by NMR. [c] Yield was measured by NMR spectroscopy with mesitylene as an internal standard.

In either case, the polymerized catalysts performed significantly worse than their monomers. The most severe drop in yield was observed for the pair $\text{Rh}_2(\text{MCES})_4$ / $\text{pol(II)-Rh}_2(\text{MCES})_4$ (entry 3 vs 5 in Table 10). Presumably, the immobilization has a certain effect on the rhodium local environment.

To our surprise, the non-polymerized $\text{Rh}_2(\text{MCES})_4$ (**75**) possesses a significantly higher carbene-transfer activity in comparison to the original $\text{Rh}_2(\text{OAc})_4$ (**5**) (entry 3 vs 1 in Table 10). Apparently, the polymerization has an impact onto the catalytic activity of the rhodium(II) complex.

The general procedure for the described cyclopropanation reaction (Scheme 27) was performed *via* a dropwise addition of EDA (**89**). The dropwise addition minimizes the formation of dimers of the diazo compound. The non-dropwise addition of the EDA was investigated utilizing polymer catalysts (Table 11).

Table 11: One-pot addition of the diazo compound **89**.

Entry ^[a]	Cat.	Cat. [mol %] ^[b]	EDA dimer, %	Product, <i>cis/trans</i> ^[c]	Yield [%] ^[d]
1	5 $\text{Rh}_2(\text{OAc})_4$	0.1	7	36/64	72
2	84 $\text{pol(I)-Rh}_2(4\text{VBA})_4$	0.1	trace	46/54	46
3 ^[e]	84 $\text{pol(I)-Rh}_2(4\text{VBA})_4$	1	trace	44/56	25
4	87 $\text{pol(II)-Rh}_2(\text{MCES})_4$	1	trace	45/55	74

[a] Reaction was performed by adding EDA in non-dropwise manner. Reaction time – 24 hours. [b] Polymer catalysts were swollen in CH_2Cl_2 and styrene before reaction with EDA was performed. [c] Diastereomeric excess was measured by NMR. [d] Yield was measured by NMR spectroscopy with mesitylene as an internal standart. [e] Reaction time - 2 hours. 85% EDA conversion was observed.

The polymer catalysts from Generation I, gave cyclopropanated products in yield less than 50% (entry 2 and 3). The low yields are probably due to the inability of inner rhodium active sites to participate in the catalysis. The Generation II catalyst increases the yield almost two times and is comparable to the original $\text{Rh}_2(\text{OAc})_4$ (entry 4 vs 1). Interestingly, only traces of EDA-dimers (**91** and **92**) for all immobilized catalysts were observed under non-dropwise conditions.

To investigate the reusability and the robustness of the polymer catalysts, repetitive experiments were conducted (Table 12).

Table 12: Investigation of reusability of the $\text{pol(II)-Rh}_2(4\text{VBA})_4$ (**88**).

Cycle ^[a]	1	2	3	4	5	6	7
Yield ^[b] , %	91	96	92	88	85	62	78
<i>trans/cis</i> ^[b] , %	55/45	55/45	55/45	55/45	55/45	55/45	55/45

[a] The cyclopropanation reaction with 1 mol% catalyst. The catalyst was recovered by filtration. [b] Diastereomeric excess and yield were measured by ¹H NMR.

The catalyst was tested in the cyclopropanation reaction and was recovered by filtration after each cycle. After seven cycles, the yield dropped to 78%, indicating either leaching or degradation of the catalyst. However, the *trans/cis* ratio remained constant during all 7 cycles. The investigation of recyclability of $\text{pol(II)-Rh}_2(4\text{VBA})_4$ (**88**) was performed by master student Bård Sundslø.

The polymer catalyst $\text{pol(II)-Rh}_2(\text{MCES})_4$ (**87**) was also investigated for reusability (Table 13).

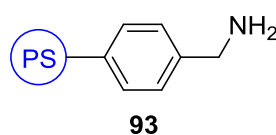
Table 13: Investigation of reusability of the $\text{pol(II)-Rh}_2(\text{MCES})_4$ (**87**).

Cycle ^[a]	1	2	3	4	5	6	7
Yield ^[b] , %	81	81	82	82	57	43	44
<i>trans/cis</i> ^[b] , %	58/42	58/42	58/42	58/42	58/42	58/42	58/42

[a] The cyclopropanation reaction with 1 mol% catalyst. The catalyst was recovered by filtration. [b] Diastereomeric excess and yield were measured by ¹H NMR.

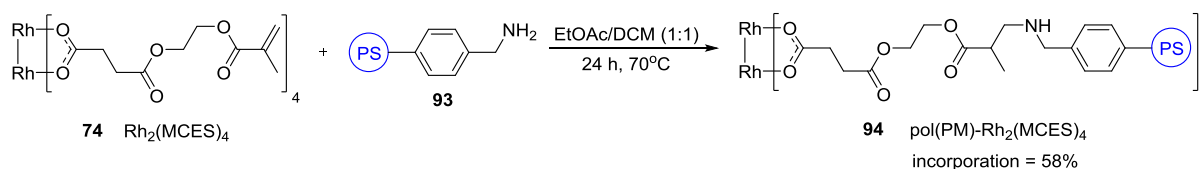
The yield remained over 80% during the first four cycles and then began to decrease. As in case with $\text{pol(II)-Rh}_2(4\text{VBA})_4$ (**88**), the *trans/cis* ratio remained constant during all 7 cycles.

2.3.1 Heterogenization by post-modification strategy



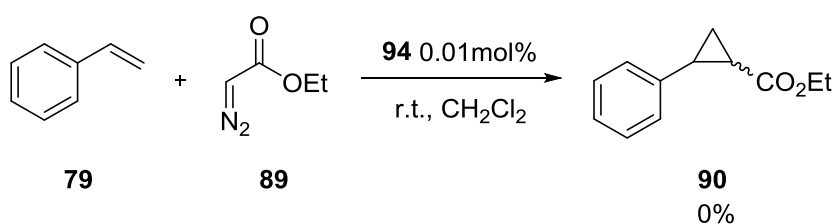
As it was discussed in Chapter 1.4, the catalytic activity of immobilized analogues of $\text{Rh}_2(\text{OAc})_4$ synthesized using bottom-up approach expected to be significantly higher than with a post-modification approach. In order to compare the two approaches, the synthesis of post-modified rhodium(II) carboxylate was performed.

The post-modification strategy implies grafting the rhodium(II) carboxylates onto the polymer support. The grafting occurs between the active polymerizable groups of $\text{Rh}_2(\text{MCES})_4$ (**74**) and (Aminomethyl)polystyrene (**93**) (Scheme 28).



Scheme 28: The post-modification strategy for immobilization of $\text{Rh}_2(\text{MCES})_4$ (74).

In order to enable the comparison with polymer catalysts using bottom-up strategy, the post-modified catalyst **94** was subjected to cyclopropanation reaction (Scheme 29).



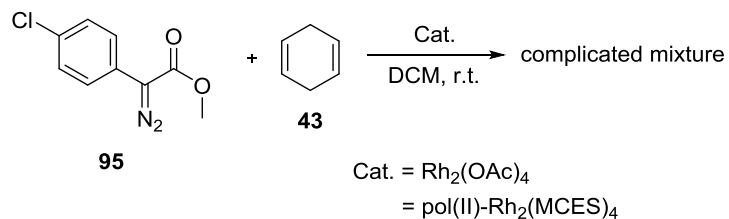
Scheme 29: The cyclopropanation reaction utilizing polymer catalyst immobilized by post-modification strategy.

The post-modified polymer catalyst possesses significantly lower catalytic activity than polymer catalysts synthesized in the bottom-up strategy. In the cyclopropanation reaction, 22% conversion of EDA was achieved with no observed cyclopropanated product (Scheme 29). The main difference in bottom-up and post-modification strategies is that in the latter the rhodium catalyst adjusts its structure to the structure of attached polymer. Whereas in bottom-up approach the polymer structure adjusts to the structure of the rhodium catalyst.

Thus, the efficiency of bottom-up strategy over the post-modification in synthesis of polymer rhodium(II) carboxylates was demonstrated.

2.3.2 Polymer catalysts performance in C-H insertion reaction

To investigate the catalytic activity of the polymer catalysts further, C-H insertion reactions were carried out (Scheme 30). The $\text{Rh}_2(\text{OAc})_4$ -catalyzed and $\text{pol}(\text{II})\text{-Rh}_2(\text{MCES})_4$ -catalyzed reaction between 1,4-cyclohexadiene (**43**) and methyl 2-(4-chlorophenyl)-2-diazoacetate (**95**) resulted in a complicated mixture of products (the crude ^1H NMR spectrum can be found in the appendix, Figure 128).



Scheme 30: Rh-catalyzed C-H insertion reaction.

No desired product **96** was observed and GC-MS analysis revealed the formation of **97** as well as numerous products of complicated nature.

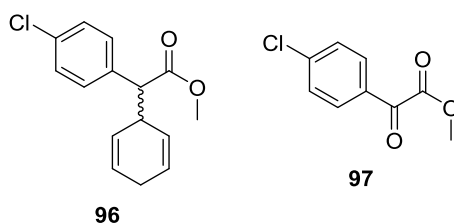


Figure 31: Desired product **96** and observed minor product **97**.

Investigations of the chemoselectivity of $\text{Rh}_2(\text{OAc})_4$ (**5**) and $\text{pol(II)-Rh}_2(\text{MCES})_4$ (**87**) in C-H insertion reactions were not explored further and left for future projects.

3 Synthesis of novel chiral rhodium(II) carboxylates

The Bonge-Hansen's group has worked extensively with immobilized prolinates, where *trans*-4-hydroxy-L-proline (**65**) works as a source of chirality. In order to synthesize new, chiral rhodium(II) carboxylate, the substrate should possess a carboxylic group as well as a polymerizable end. These two groups were envisaged to be attached to *trans*-4-hydroxy-L-proline, in which the nitrogen atom is protected with a phenylsulphonyl group (Figure 32).

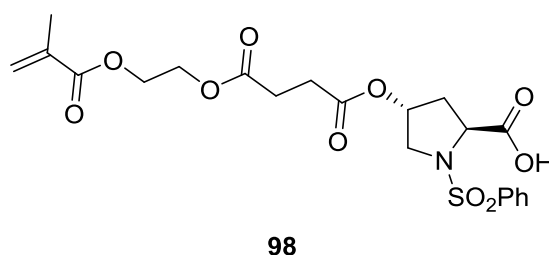


Figure 32: Envisaged chiral ligand **98** for synthesis of chiral polymer catalysts.

A former master student of our group, Massoud Kaboli, successfully synthesized a chiral rhodium complex **99**. (Massoud Kaboli, master thesis, 2008)

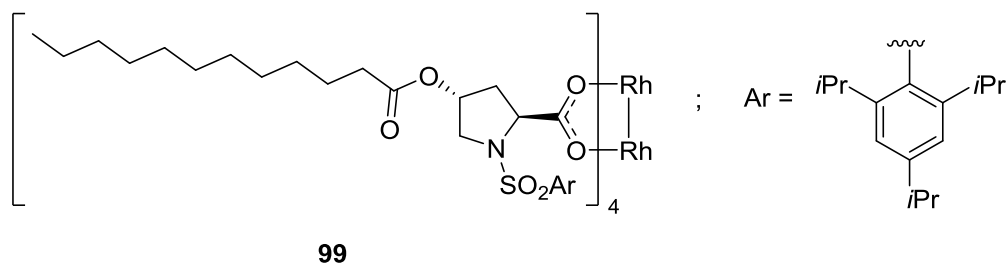
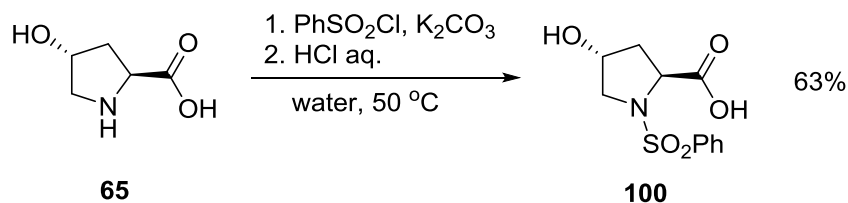


Figure 33: Chiral rhodium(II) complex **99** synthesized by Massoud Kaboli.

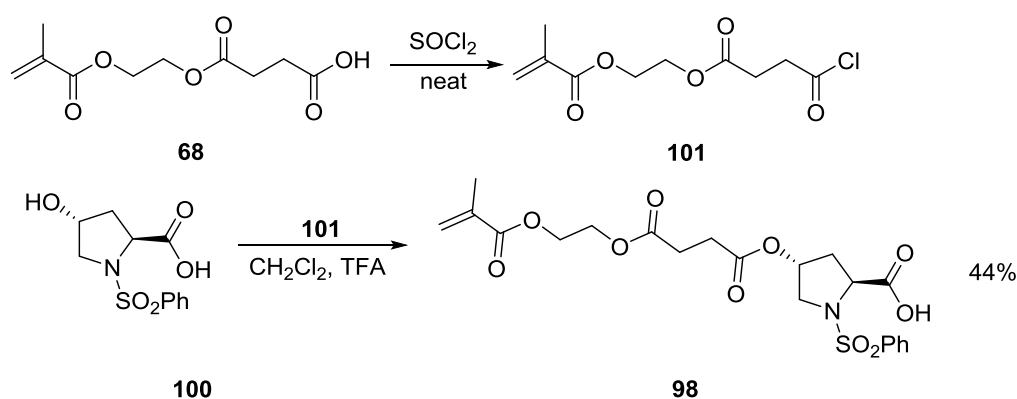
The synthesis of the desired chiral ligand **98** was performed in a similar manner as Massoud's complex **99**. The only difference was the fatty acid chain, which was substituted with already known mono-2-(methacryloyloxy) ethyl succinate (**68**).

Compound **100** was synthesized from *trans*-4-hydroxy-L-proline (**65**), with protection of amino group in the first step (Scheme 31).



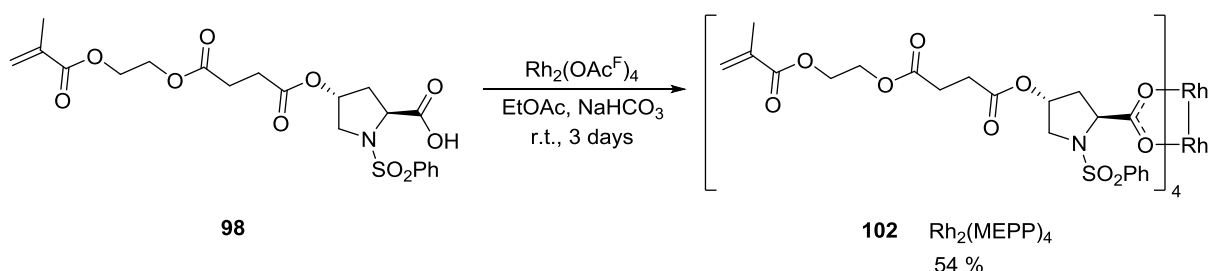
Scheme 31: Protection of the amino group in reaction of **65** with phenylsulphonyl chloride.

The obtained **100** was subjected to acylation with mono-2-(methacryloyloxy) ethyl succinate (**68**), which was converted to acyl chloride **101** in a step prior to acylation (Scheme 32). The acylation was performed in the mixture of CH₂Cl₂ and TFA at room temperature overnight.



Scheme 32: Synthesis of chiral ligand **98**.

The chiral ligand **98** was subjected to ligand exchange with Rh₂(OAc^F)₄ as rhodium precursor. The ligand exchange was performed in a manner, similar with synthesis of achiral ligands, i.e. in EtOAc and with sodium bicarbonate as a base (Scheme 33).



Scheme 33: Synthesis of chiral rhodium complex Rh₂(MEPP)₄ (**102**) – Generation I.

The obtained chiral Rh₂(MEPP)₄ (**102**) was subjected to detailed studies. The ¹H NMR spectrum shows an additional signal for a proton that sits on the 4th position in the proline moiety (Figure 34).

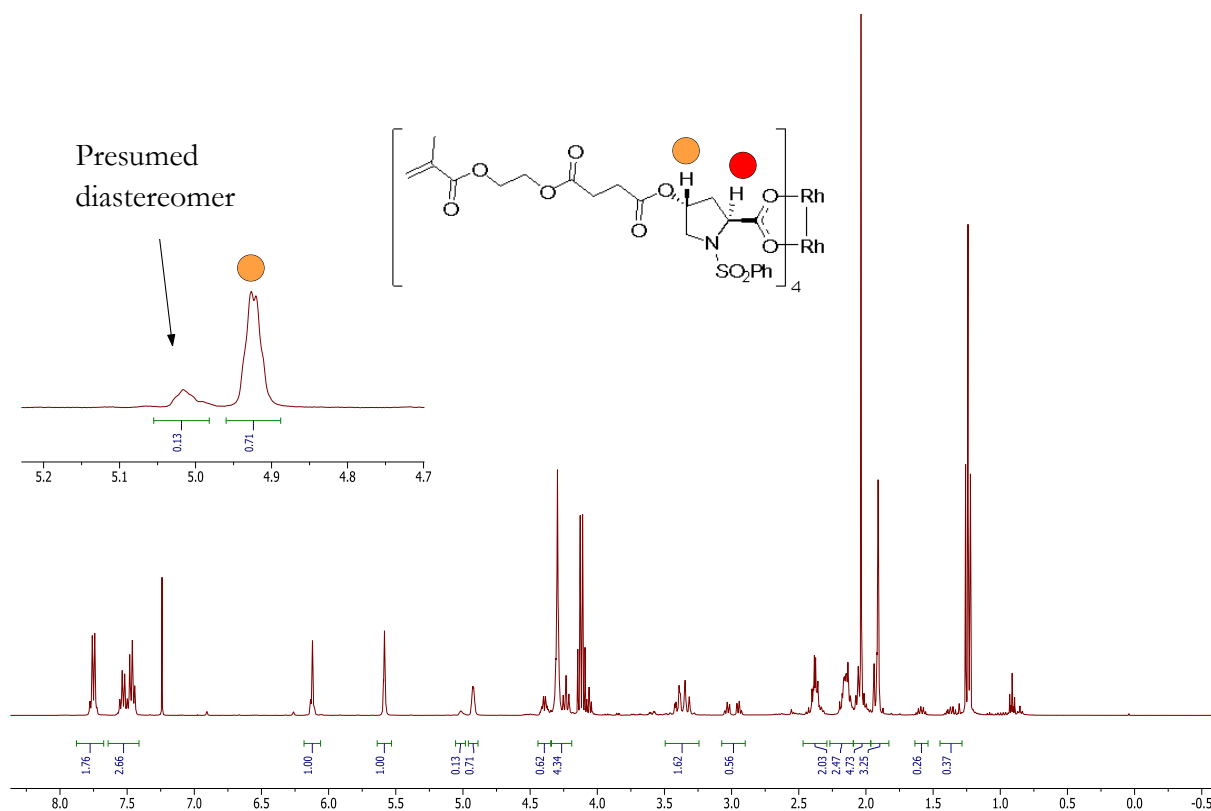


Figure 34: ^1H NMR spectrum of $\text{Rh}_2(\text{MEPP})_4$ (**102**). Epimerization occurs at the proton, marked with a red circle.

The ^1H NMR spectrum given in Figure 34, suggests that the isolated compound **102** consists of two stereoisomers. The assumption was investigated with HPLC analysis, where two peaks were observed. The area under the curves correlates with relative abundance of each isomer (see appendix for more information, Figure 110).

One possible reason for a formation of the diastereomer is the acidity of the proton in the proline moiety (circled in red in Figure 34). The base in the reaction mixture could induce the epimerization.

Several attempts were made to suppress the epimerization: exclusion of the base and use of different temperature regimes. None of the attempts were successful and the mixture of diastereomers was observed in all the reactions.

Comparing compound **99**, that was made by Massoud Kabouli, with our compound **102**, it can be proposed that the spacer group between the polymerizable end and functionalized proline could have an effect that favors epimerization. Based on this observation, another modification of chiral functionalized proline **103** was proposed (Figure 35).

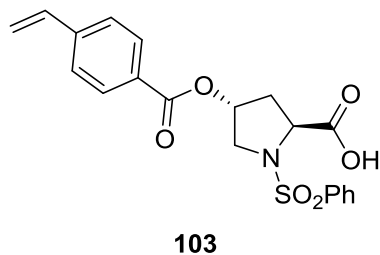
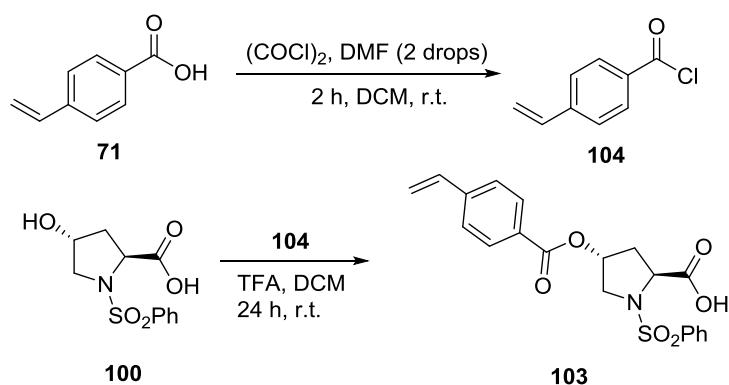


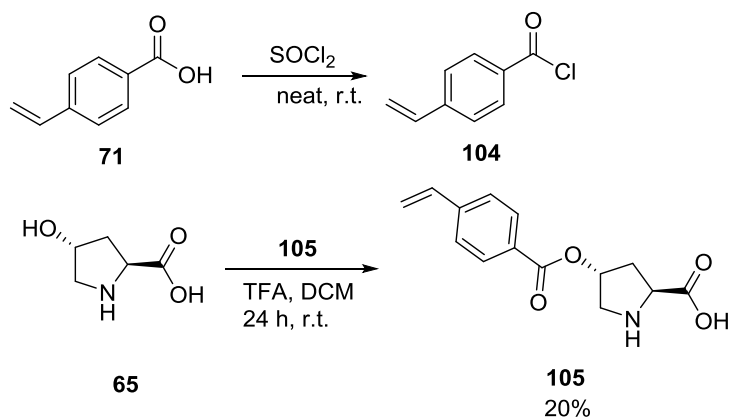
Figure 35: Chiral ligand for rhodium(II) carboxylate formation - Generation II.

The (2*S*,4*R*)-4-hydroxy-1-(phenylsulphonyl)pyrrolidine-2-carboxylic acid (**100**) was subjected to acylation with the acyl chloride **104**, generated from the 4-vinylbenzoic acid (**71**) and thionyl chloride (Scheme 34).



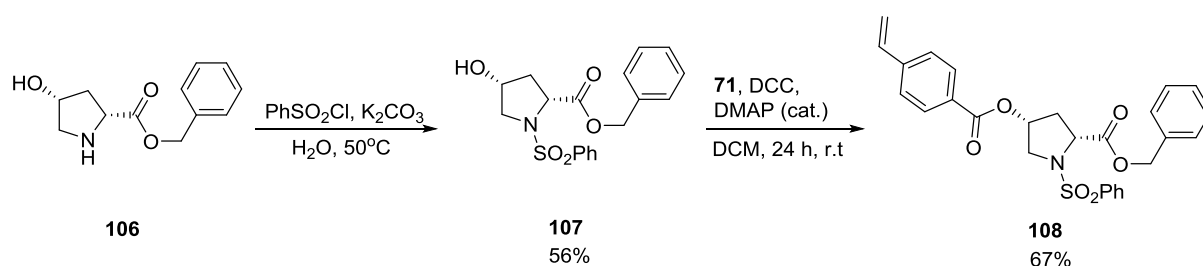
Scheme 34: Envisaged reaction sequence leading to formation of the **103**.

The generation of the reported acyl chloride **104** of 4-vinylbenzoic acid (**71**) did not work,⁸¹ thus the following acylation of **100** was not attempted. Hence, we focused on direct acylation of *trans*-4-hydroxy-L-proline (**65**) with acyl chloride **104** (Scheme 35).



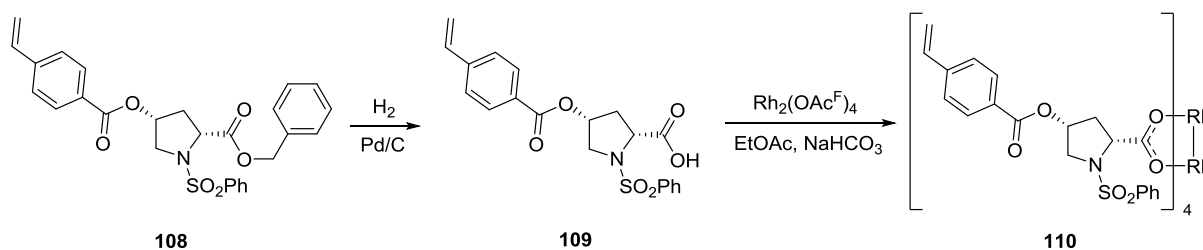
Scheme 35: Attempt to synthesize a chiral rhodium(II) carboxylate **105**.

The target compound **105** was synthesized in poor yield (20%) and required additional purification of the obtained material. These disadvantages made us switch focus to the last attempt of synthesis of the chiral ligand (Scheme 36). The starting benzyl (2*R*,4*R*)-4-hydroxypyrrolidine-2-carboxylate (**106**) was converted to sulfonyl amide **107**. Treatment of **107** with 4-vinylbenzoic acid (**71**) and *N,N'*-dicyclohexylcarbodiimide (DCC) in the presence of 4-dimethylaminopyridine (DMAP) resulted in formation of (2*R*,4*R*)-1-(phenylsulfonyl)-4-((4-vinylbenzoyl)oxy)pyrrolidine-2-carboxylate (**108**) in 67% yield.



Scheme 36: Synthesis of a chiral rhodium(II) carboxylate **108**.

The synthesized **108** was expected to be reduced to (2*R*,4*R*)-1-(phenylsulfonyl)-4-((4-vinylbenzoyl)oxy)pyrrolidine-2-carboxylic acid (**109**). Following ligand exchange with $\text{Rh}_2(\text{OAc}^{\text{F}})_4$ in the EtOAc would result in the chiral rhodium(II) carboxylate **110** (Scheme 37).



Scheme 37: Planned reaction sequence that was not performed due to the lack of time.

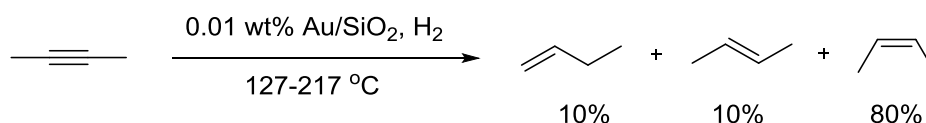
Unfortunately, the planned synthesis in Scheme 51 was not accomplished due to the lack of time.

4 Introduction to the gold project

4.1 General introduction and historical aspects

For many years, gold has been considered as a noble, unreactive metal.⁸² However, during the past 40 years, gold became a subject of growing interest due to its catalytic versatility in various organic transformations – from hydrogenation of olefines to construction of heterocyclic complexes.⁸³⁻⁸⁶

The first catalytic reaction that opened perspectives for gold catalysis was a hydrogenation under heterogeneous conditions catalyzed by metallic gold deposited on silica (Scheme 38).^{87,88} Later, Ito *et al.* reported the first example of a gold-catalyzed aldol reaction, which was shown to be the first example of asymmetric gold catalysis.⁸⁹ Although a gold-catalyzed homogeneous hydrogenation was first mentioned in 1974, it took almost two decades until the interest for the homogeneous gold catalysis arose again.



Scheme 38: Gold-catalyzed selective reduction of alkynes.⁸⁸

In the beginning of the 21st century the groups of Hashmi, Yang and He extended the homogeneous catalysis for gold introducing the comprehensive studies on both inter- and intramolecular nucleophilic additions with oxygen-based nucleophiles and demonstrated a high potential of aryl C-H activation.⁹⁰⁻⁹²

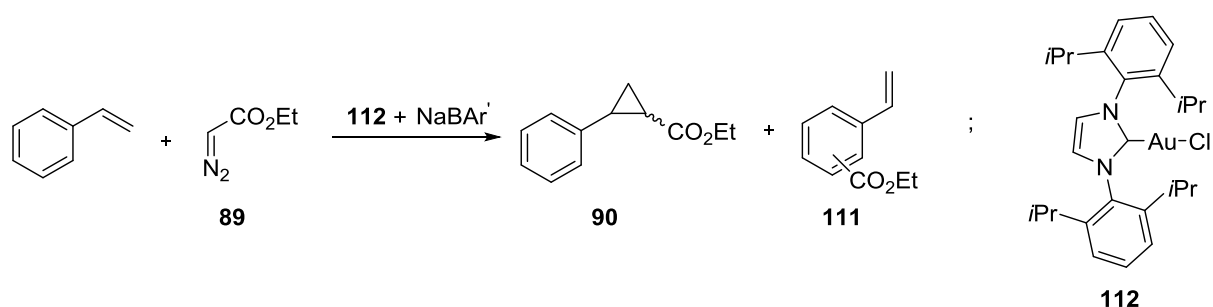
In addition to the potential applications in organic synthesis, gold found a promising future in nanomedicine and biomedicine.⁹³ Its rich properties on a nanoscale allowed it to be used in biodiagnostics,⁹⁴ cancer nanotechnology,⁹⁵ drug delivery⁹⁶ and photothermal therapy.⁹⁷

4.2 Gold(I) catalysis in carbene-transfer reactions

The first gold-catalyzed carbene-transfer reaction was reported back in 2005 by Nolan *et al.*⁹⁸ Since then, interest in carbenoid chemistry utilizing gold as a catalyst has grown significantly. Continuous development of gold catalysts triggered the discovery of novel transformations in which gold performed better than other metals.

By 2010 it was already known that gold(I) can not only catalyze the decomposition of diazocompounds but also transfer the carbene groups onto numerous substrates with high regioselectivity.⁹⁹ In 2015 Guanyang *et al.* reported an exceptionally remarkable gold(I)-catalyzed cross-coupling of diazo compounds.¹⁰⁰

Fructos *et al.* reported the gold(I)-catalyzed carbene transfer to aromatic hydrocarbons, olefins, alcohols and amines.¹⁰¹ For the cyclopropanation reaction catalyzed by **112**, a complicated mixture of isomers **111** as well as the cyclopropanated product **90** was observed (Scheme 39).



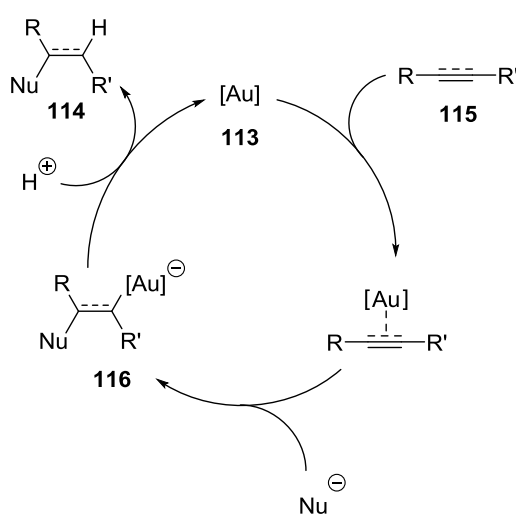
Scheme 39: Gold(I)-catalyzed carbene transfer in cyclopropanation reaction.¹⁰¹

As it was illustrated in Scheme 39, the gold(I) catalysis of **112** in the carbene-transfer reactions is not as selective as rhodium catalysis (see Chapter 1 for rhodium catalyzed carbene-transfer reactions). Thus, the selectivity in the carbene-transfer reaction catalyzed by other gold(III) complexes was decided to be investigated in this project.

4.3 Nucleophilic addition to π -systems

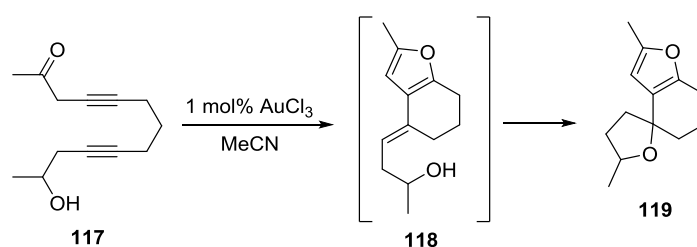
4.3.1 Coordination to alkenes and alkynes

Being a carbophilic Lewis acid, gold(I) and (III) species are able to activate C-C multiple bonds towards nucleophilic attack.¹⁰² Interaction of the gold species **113** with the π -bond of **115** increases the electrophilic character of the alkyne/alkene, thus enabling the attack of nucleophiles in an intra- or intermolecular manner with a formation of intermediate **116** (Scheme 40).¹⁰³ Further protodemetalation regenerates the gold complex **113** and the product **114**. Additions of nucleophiles to coordinated unsaturated species at gold complexes are key steps in gold catalysis.



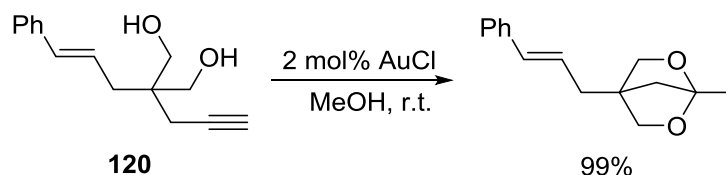
Scheme 40: Proposed gold-catalyzed activation of C-C multiple bonds.¹⁰²

Tandem reactions of coordination and nucleophilic addition were presented by Hashmi and co-workers as a new, promising strategy for C-C bond formation and construction of complex structures (Scheme 41).⁹⁰ Scheme 41 demonstrates a sequence of intramolecular gold(III)-coordination/nucleophilic attack in compound **117**. A nucleophile can successfully be a C-C triple bond as well as an oxygen atom in the carbonyl and the hydroxy group. The formed intermediate **118** reacts further forming the polycyclic compound **119**. This complicated example shows the versatility of the rather simple mechanism in Scheme 40.



Scheme 41: Sequence of coordination and nucleophilic attack leading to polycyclic compound.⁹⁰

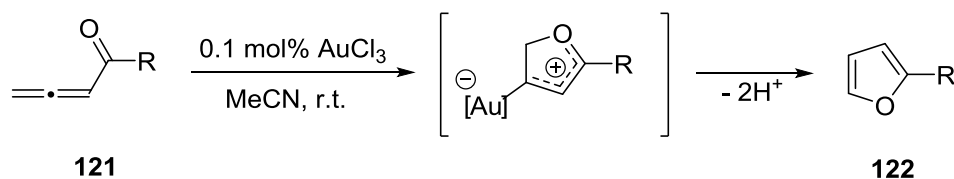
The selectivity of gold coordination was shown by Genet *et al.* (Scheme 42) where the selective coordination of the gold(I) chloride to the alkyne rather than to the alkene center in compound **120** was illustrated.¹⁰⁴



Scheme 42: Chemoselectivity in gold(I)-catalyzed C-C triple bond activation.¹⁰⁴

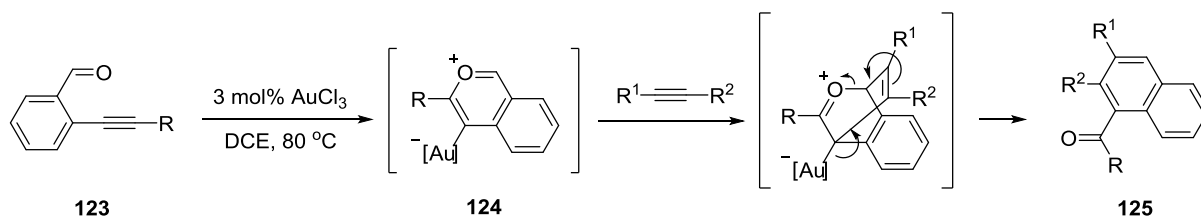
4.3.2 Coordination to other π -systems

If the presented nucleophile is conjugated, cycloisomerization after coordination might occur. This was demonstrated in a gold(III)-catalyzed intramolecular reaction in the allene **121** (Scheme 43).⁹⁰ The allene **121** coordinates to the gold(III) complex and the carbonyl oxygen atom attacks as an intramolecular nucleophile, leading directly to the functionalized furan **122**.



Scheme 43: Gold(III)-catalyzed synthesis of substituted furans.⁹⁰

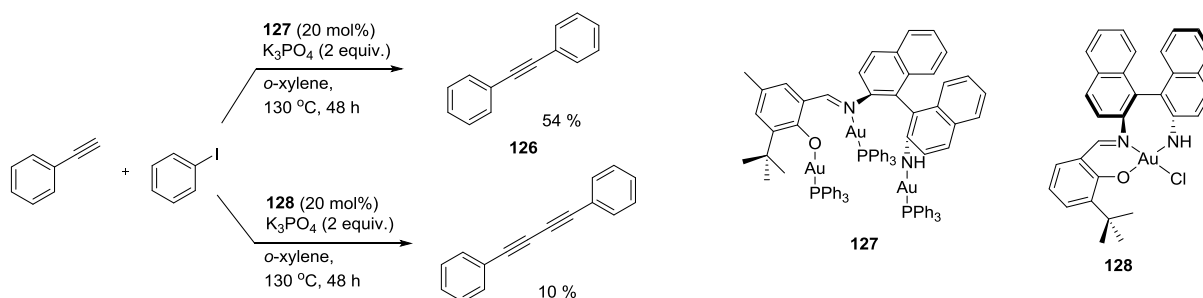
In another example, a gold(III)-catalyzed intramolecular reaction in **123** led to the formation of the highly reactive intermediate **124**. The intermediate **124** reacts in cycloaddition manner with alkyne molecule, furnishing the product **125** (Scheme 44).¹⁰⁵



Scheme 44: Bimolecular gold(III)-catalyzed cycloaddition.¹⁰⁵

The tandem of π -bond coordination and further nucleophilic attack found applications in many other transformations like ring enlargements,¹⁰⁶ enyne cyclization¹⁰⁷ and CO-activation.¹⁰⁸

An interesting feature of gold(I) and gold(III) catalysis is the ability to replace copper and palladium catalysts in the Sonogashira coupling.¹⁰⁹ Corma *et al.* demonstrated the differences between gold(I) and gold(III) species under copper(I) and palladium(0) free conditions (Scheme 45).¹⁰⁹ Gold(III) complexes seemed to catalyze the desired homocoupling reaction whereas gold(I) seemed to be responsible for the formation of alkylation product **126**.



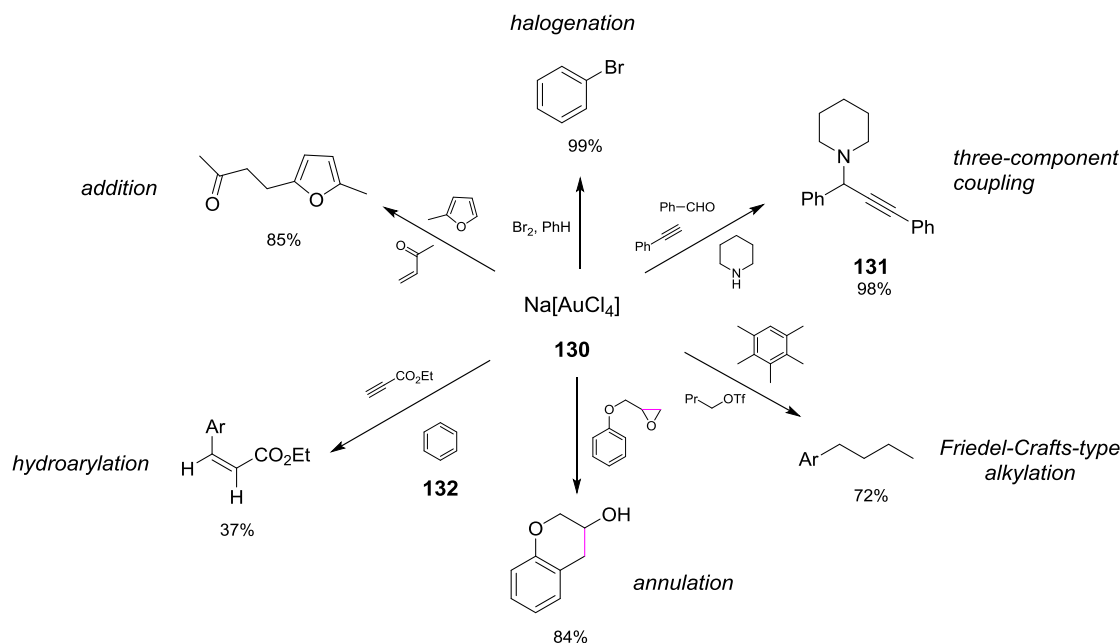
Scheme 45: The gold-catalyzed Sonogashira coupling.¹⁰⁹

However, further studies of the Sonogashira reactions by Corma and co-workers led to investigations of gold metal nanoparticles supported on nanocrystalline ceria (Au/CeO_2). During the studies of the catalyst, the presence of gold in three oxidation states +1, +3 and 0 were revealed, suggesting a possible tandem catalysis for Au(I) and Au(III).

4.4 Gold(III)-catalyzed C-H activation reactions and gold(III) cyclometalated complexes

The most used gold(III) complexes are inorganic salts such as $Na[AuCl_4]$ and $AuBr_3$. However, catalytic activity of organometallic gold(III) species requires further investigations and, fortunately, more and more publications on their synthesis are being reported.¹¹⁰

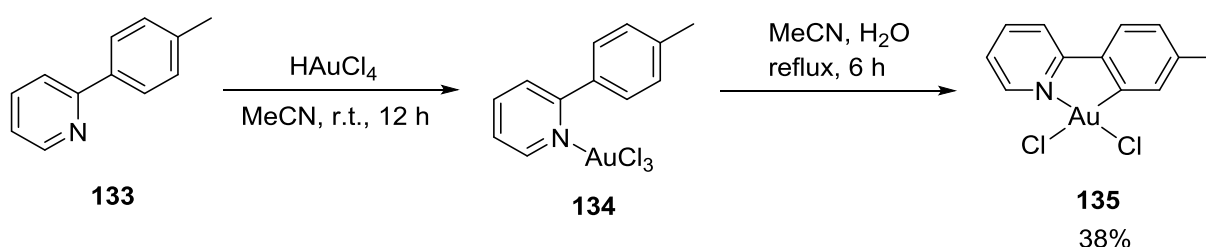
Gold(III) mediated C-H aryl functionalizations have been intensively studied since the first report by Kharasch *et al.* in 1931, with mostly gold(III) inorganic salts used as catalysts.¹¹¹ A short overview of reactions catalyzed by sodium chloroaurate (**130**) is represented in Scheme 46.^{90,92,112-114} Unlike the three-component coupling leading to the formation of **131** and hydroarylation of **132** (described in Chapter 5), the intramolecular annulation, Friedel-Crafts alkylation, halogenation and addition reactions will not be extensively described in this project.



Scheme 46: The utilization of inorganic gold(III) complex as a catalyst in organic transformations.^{90,92,112-114}

By introducing new ligands and counterions in AuCl_3 , it is possible to make complex organometallic gold(III) compounds. Here, cyclometalated gold(III) complexes are of special interest, because of the extensive studies that have been accomplished in the group where this project took place – the group of Professor Mats Tilset.

The cyclometalated gold complexes are known already for 40 years. They are organometallic compounds that contain a dative bond between the heteroatom and metal as well as a metal-carbon σ -bond.¹¹⁵ The first synthesis of the cyclometalated gold(III) complexes involved mercury(II) compounds and led to poor yields.¹¹⁶ Later, Henderson *et al.* used **133** in order to perform direct cyclometalation with $\text{H}[\text{AuCl}_4]$ with 38% yield (Scheme 47).¹¹⁷



Scheme 47: Synthesis of gold(III) cyclometalated complex **135**.¹¹⁷

Substitution of halogen atoms in gold(III) complexes with new ligands (or ancillary ligands) alters the local environment around the gold(III) atom.¹¹⁸ In these systems the remaining ligand (a counterion) may be able to detach, leaving an open, vacant coordination site. The dissociation

trans to the carbon leads to the thermodynamically stable “naked” gold ion. However, further formal insertion would lead to thermodynamically unstable product. In practice, the formal insertion was observed *trans* to the nitrogen, giving thermodynamically stable insertion products (Figure 36).¹¹⁹

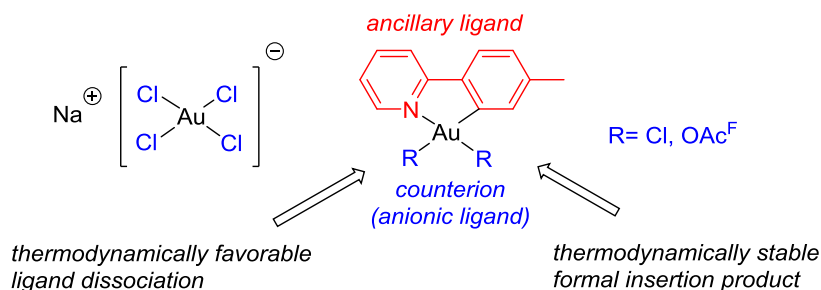


Figure 36: The role of ligands and counterions in complex gold molecules.

The electronic structure of the ligand influences the acidic character of the gold(III) ion in the catalytic cycle and affects the stability of the intermediates.¹²⁰ At the same time, the counterion affects the kinetic and thermodynamic profile of the catalytic reaction, modulating the regio- and stereoselectivity.¹²¹

Having a chloride as leaving group limits the coordination of a substrate to the gold center, because of the poor ability of the chloride to dissociate. However, introduction of a silver ion in the system facilitates the cleavage of the chloride in form of AgCl and thus creating a vacant catalytic site, leaving the gold atom “naked” (Figure 37). This method was widely used in many of the reactions described so far.^{90,92,112-114} Thus exchanging the halogen atom with a more labile group enhances the potential reactivity of the gold complex.

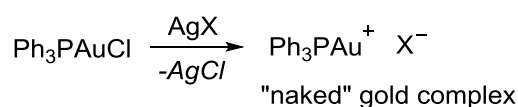
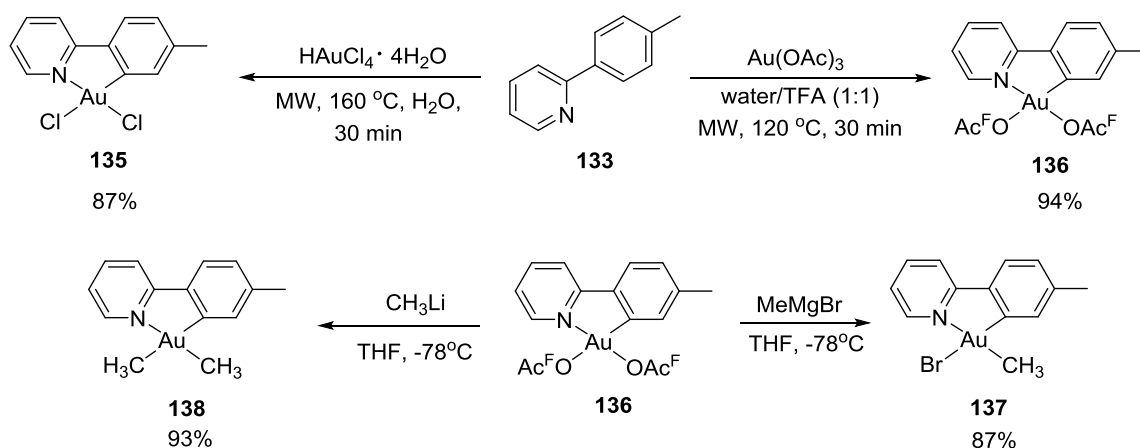


Figure 37: Formation of gold(I) complex with a vacant coordination site.

Tilset and co-workers, implemented microwave heating in the cyclometalation reaction and reported a substantial increase in yield for **135**, reduction of reaction time, simplified work-up as well as suppression of undesired side reactions (Scheme 48):¹²²



Scheme 48: Synthesis of cyclometalated gold(III) complexes in Tilstet's group.^{122,123}

A microwave assisted reaction between 2-(*p*-tolyl)pyridine (*tpy*) (**133**) and Au(OAc)₃ in a mixture of TFA and water resulted in the formation of Au(*tpy*)(OAc^F)₂ (**136**) in high yields. The complex Au(*tpy*)(OAc^F)₂ (**136**) reacted with methyl magnesium bromide in THF furnishing Au(*tpy*)BrMe (**137**) in 87% yield.¹²³

Synthesis and catalytic testing of the cyclometalated gold(III) complexes presented the starting point of the work presented in this project. Compounds **135-138** have the 2-(*p*-tolyl)pyridine (*tpy*) ligand in common and two coordinated anionic ligands *cis* and *trans* to nitrogen. Au(*tpy*)(OAc^F)₂ (**136**) was reported by a former doctoral student in our group, Dr. Eirin Langseth, and is a compound of special interest because of its labile trifluoroacetate groups that readily dissociate to give a vacant coordination site.¹²³

The influence of the leaving groups on the catalytic activity of the complexes **135-138** is the main focus of this project (Figure 38).

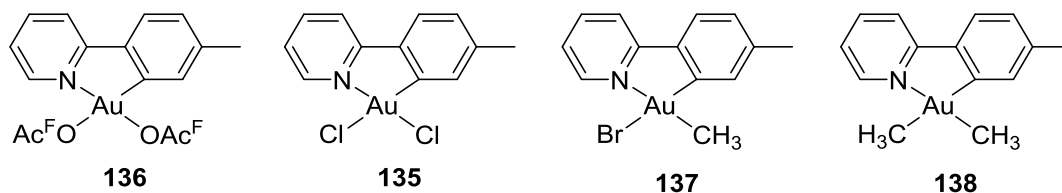
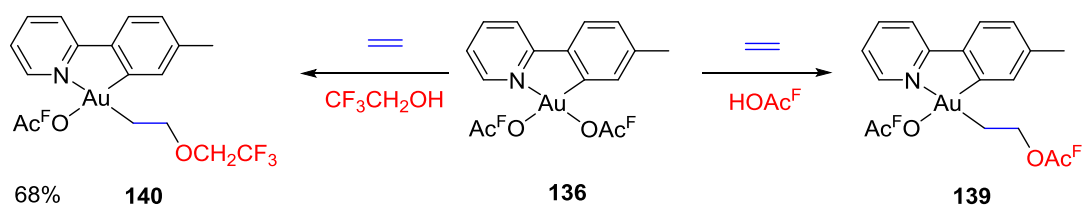


Figure 38: Gold(III) cyclometalated complexes, synthesized in Tilstet's group.^{122,123}

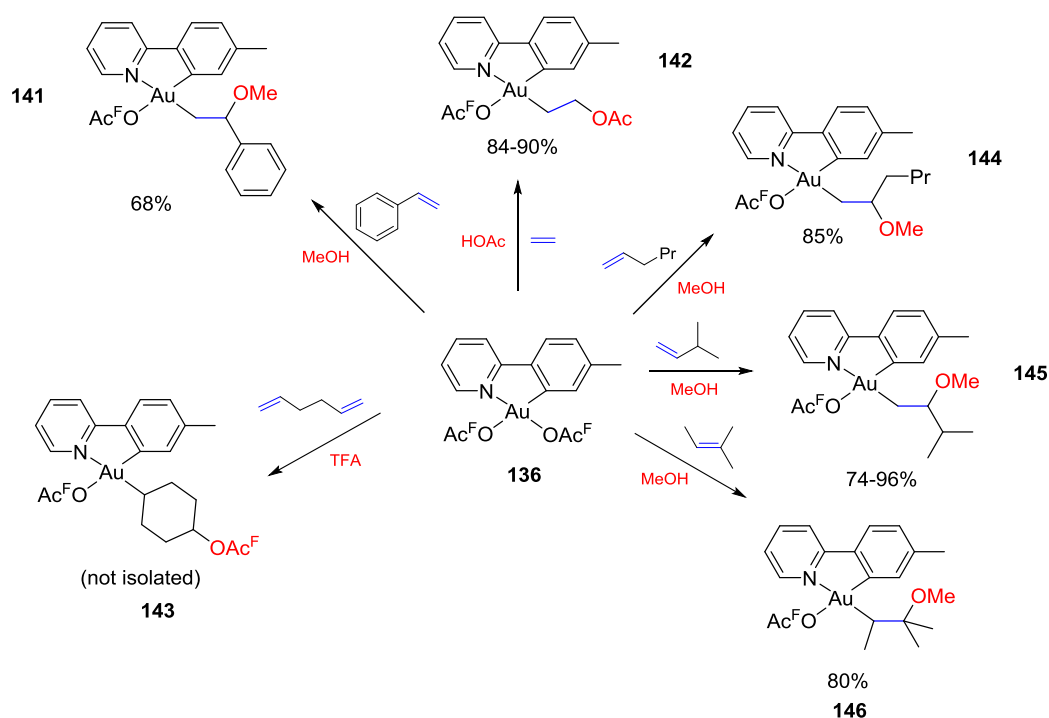
The reactivity of Au(*tpy*)(OAc^F)₂ (**136**), towards a wide variety of alkenes has previously been studied in the group of Tilstet.¹²⁴ Formal insertion of ethylene molecule into the Au-O bond of **136** has been thoroughly investigated by Dr. Eirin Langseth (Scheme 49).¹²⁴



Scheme 49: Ethylene formal insertion to the Au(tpy)(OAc^F)₂ (**136**).¹²⁴

The insertion of ethylene occurs in the position *trans* to the nitrogen atom in the tpy-ligand of **136**. Interestingly, the presence of an external nucleophile alters the reaction outcome. Thus, the reaction between **136** and ethylene in trifluoroethanol (TFE) gave the alkyl gold(III) complex **140** in good yields.

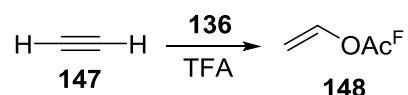
In general, the alkene insertion to the gold(III) complex (**136**) is governed by associative substitution of the OAc^F in a position *trans* to nitrogen with the alkene followed by a nucleophilic addition to furnish the new gold(III) alkyl complex (Scheme 50). The mechanism was probed by DFT calculations.¹²⁵



Scheme 50: Reactivity of **136** towards a wide variety of alkenes.

PhD student, Marte Sofie Holmsen, investigated the reactivity of Au(tpy)(OAc^F)₂ (**136**) towards different alkenes with methanol as a nucleophile (Scheme 50). Addition of the nucleophile at the

internal position of the double bond in terminal alkenes lead to the Markovnikov products **144**, **145** and **146** in good yields. (Holmsen, M. S., unpublished results, 2015) However, in the case of ethyne **147**, the nucleophilic addition in TFA led to catalytic formation of **148** with 14-33 TON (Scheme 51).



Scheme 51: Gold(III)-catalyzed acetylene functionalization.

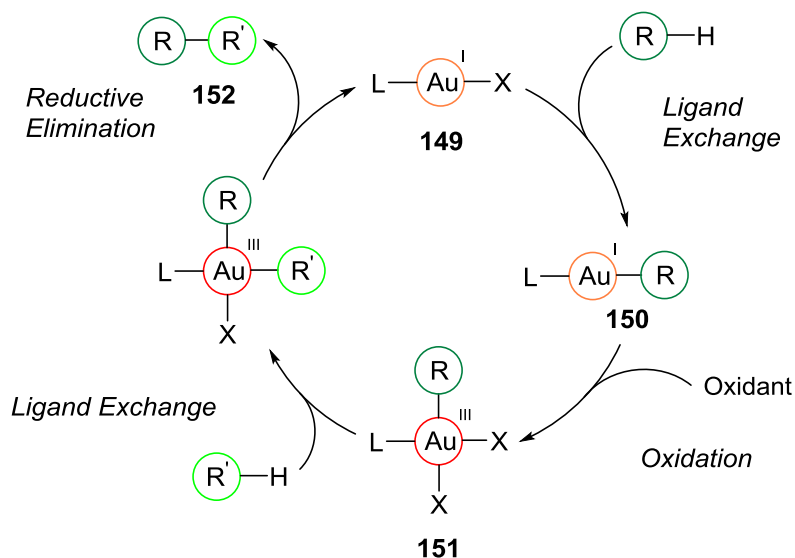
This is the first evidence of catalysis with the cyclometalated gold(III) complex **136** in our group. (Holmsen, M. S., unpublished results, 2015)

Former master (now PhD) student Franziska Stefanie Ihlefeldt contributed a lot with further investigations of formal insertion reactions of dienes and electron-poor alkenes. The formation of **143** and **141** (for styrene in Scheme 50) in reaction of $\text{Au}(\text{tpy})(\text{OAc}^{\text{F}})_2$ with hexadiene and styrene correspondently, was reported. (Ihlefeldt, F. S., unpublished results, 2015)

4.5 Tandem Au(I) and Au(III) system

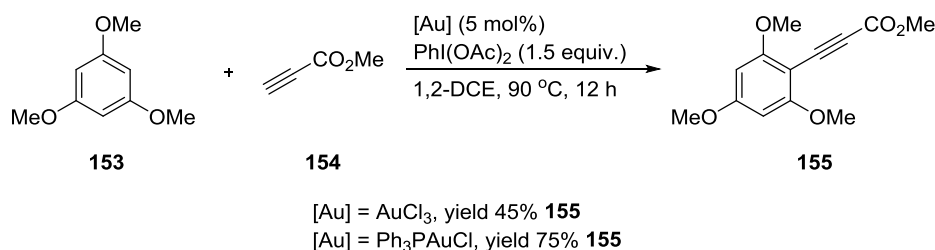
Most of the reactions described in Sections 4.3 and 4.4 were successfully catalyzed by both inorganic and organometallic gold(I) and gold(III) species in decent yields. In either oxidation state, gold complexes react as carbophilic π -acid, being resistant in redox activity due to high redox potential of the $\text{Au}^{\text{I}}/\text{Au}^{\text{III}}$ ($E_0 = +1.41 \text{ V}$)¹²⁶. However, utilization of gold(I) and (III) species in tandem, significantly extended the scope of coupling reactions by performing C-H functionalization and C-C oxidative coupling under homogeneous conditions. This was achieved by introducing an external oxidative agent that could keep the catalytic circle of $\text{Au}^+/\text{Au}^{3+}$ alive (Scheme 52).¹²⁷

In the presence of an internal oxidant, the gold(I) complex **149** could be oxidized to gold(III). Complex **150**, formed in a ligand exchange reaction, was oxidized to **151** with an external oxidative agent. Followed by a reductive elimination, **152** is liberated and gold(I) complex **149** is regenerated (Scheme 52).¹²⁸



Scheme 52: The C-C coupling, catalyzed by gold(I)/(III) tandem.¹²⁸

The gold-catalyzed ethynylation in Scheme 53 was studied in the group of Cristina Nevado where the catalytic activity for both gold(I) and (III) was demonstrated.¹²⁹ The 1,3,5-trimethoxybenzene (**153**) was coupled with **154** in 1,2-dichloroethane in a reaction catalyzed by gold(I) or gold(III) complexes. The $\text{PhI}(\text{OAc})_2$ was utilized as the external oxidative agent. This work encouraged us to study gold(III) cyclometalated complexes **135-138** as catalysts for such aryl functionalization.



Scheme 53: Ethynylation of arenes catalysed by gold(I) or gold(III) complexes.¹²⁹

4.5.1 Multicomponent reactions

Over the past few decades multicomponent coupling reactions (MCRs) have become a powerful tool in organic synthesis. Catalyzed by numerous transition metals, the MCRs have attracted significant interest due to atom economy and ease of performance.^{130,131}

Marvelous work showing the significant synthetic potential of MCRs was reported by Chernyak and Gevornyak, where they applied MCRs towards drug synthesis and developed mild reaction

conditions utilizing copper catalysis for a one-pot synthesis of AlpidemTM and ZolpidemTM – anxiolytic drugs (Figure 39).¹³²

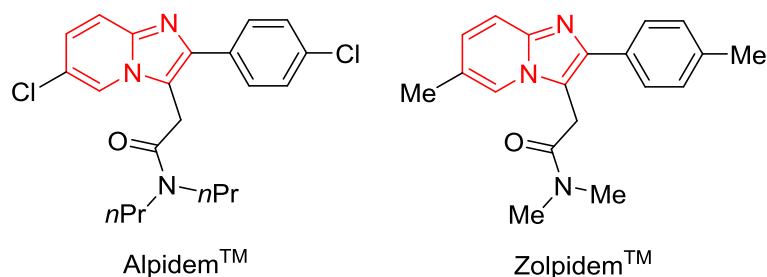
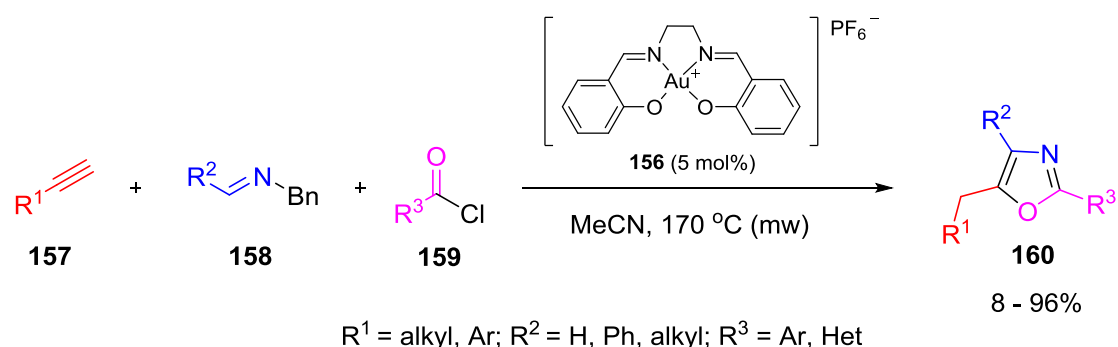


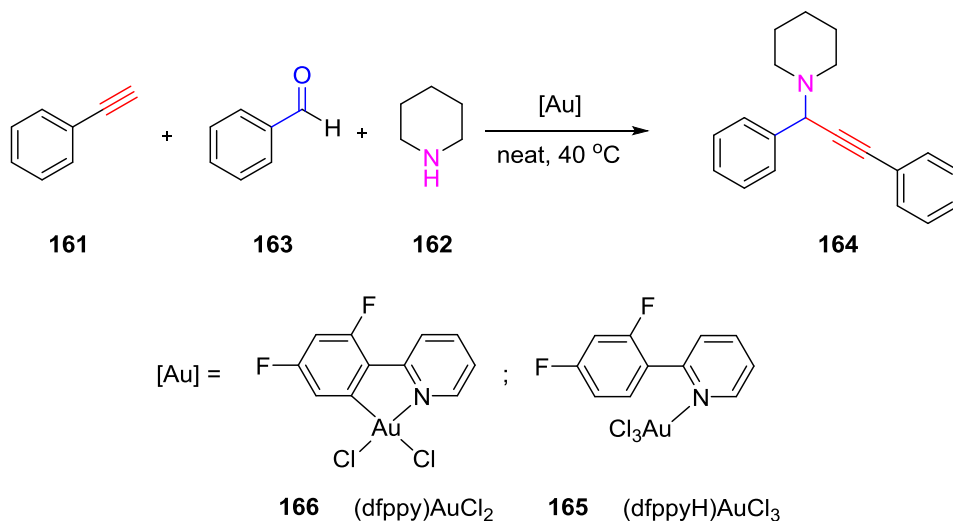
Figure 39: Selected examples of drugs, synthesized in MCRs.¹³²

Despite its effectivity and high yields, the method utilizing copper catalyst in water is limited to imines generated from arylamines and aromatic aldehydes. Further development of MCRs for synthesis of propargylamines led to the discovery of the exceptional catalytic activity of gold species. Recent work by Strand *et al.* has demonstrated the catalytic activity of the gold(III) salen complex **156** in the reaction of terminal alkynes **157** with *N*-benzylimines **158** and acid chlorides **159** in water, providing substituted oxazoles **160** in high yields (Scheme 54).¹³³



Scheme 54: Three-component synthesis of oxazoles catalysed by gold(III)-salen complex.¹³³

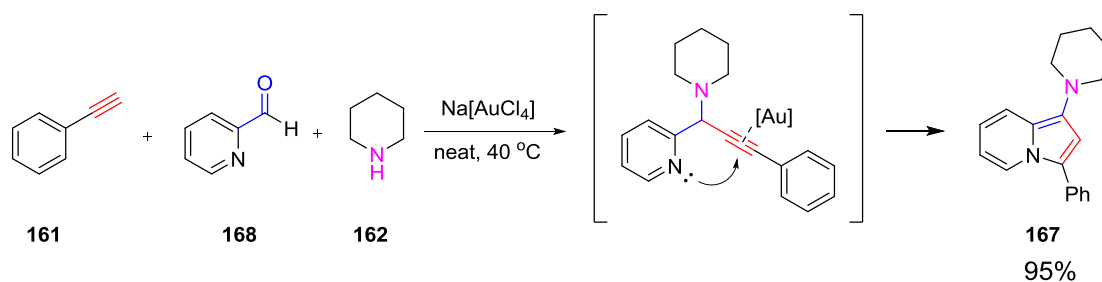
Strand *et al.* investigated the catalytic activity of cyclometalated *vs* non-cyclometalated gold(III) complexes in the synthesis of trisubstituted oxazoles and the parent A³ three-component coupling reaction (Scheme 55). The gold(III)-catalyzed reaction between phenylacetylene (**161**), piperidine (**162**) and benzaldehyde (**163**) under solvent-free conditions resulted in the functionalized propargylamine **164**. Both the non- and cyclometalated complexes **165** and **166** were shown to be efficient catalysts for such multicomponent reactions: yields were over 80%, low temperature and solvent-free conditions (Scheme 55).¹³⁴



Entry	Catalyst	Yield [%]
1	(dfppyH)AuCl ₃	100
2	(dfppy)AuCl ₂	71

Scheme 55: Gold(III)-catalyzed MCR in synthesis of propargylamine **164**.¹³⁴

Interestingly, the triple bond in the formed propargylamine **164** could be activated by coordination with the remaining gold(III) catalyst and undergo a nucleophilic attack in an inter- or intramolecular fashion. This attractive approach was demonstrated in the group of Liu, where the gold(III)-catalyzed formation of substituted aminoindolizine **167** from pyridine-2-aldehyde (**168**), phenylacetylene (**161**) and piperidine (**162**) was reported (Scheme 56).¹³⁵



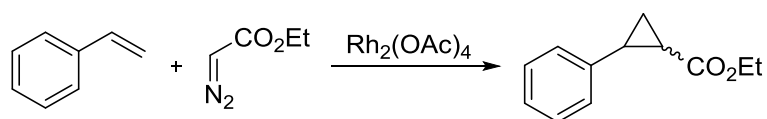
Scheme 56: Gold(III)-catalyzed three-component synthesis of aminoindolizine **167**.¹³⁵

In this project the catalytic activity of the cyclometalated **135-138** complexes (Figure 38) in the MCRs will be investigated. Also in this case it was anticipated that complexes with labile ligands (good leaving groups) would perform better in the catalysis.

5 Results and discussion – gold project

5.1 Cyclopropanation reaction

As it was described in the introduction to rhodium chemistry (Chapter 1), rhodium(II) carboxylates are the most efficient catalysts for carbene-transfer reactions. In order to investigate the catalytic activity in carbene-transfer reactions, the cyclometalated gold(III) complex **136** was employed as a catalyst for the cyclopropanation reaction between styrene and ethyldiazoacetate (EDA) (Scheme 57). This reaction is considered to be a standard reaction for carbenoid chemistry, where Rh(II) species are usually being used (Scheme 57).



Scheme 57: Cyclopropanation reaction utilizing Rh-complex as a catalyst.⁴³

Recalling Section 4.2, Fructos *et al.* reported the catalytic behavior of gold(I) complex **112** in the transfer of a carbene to aromatic hydrocarbons, olefins, alcohols and amines.¹⁰¹ In the case of the cyclopropanation reaction, a mixture of isomers was observed (Figure 40).

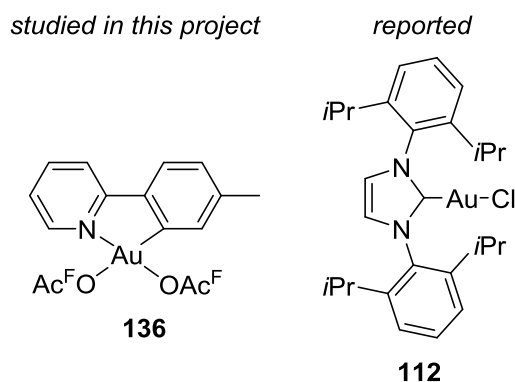
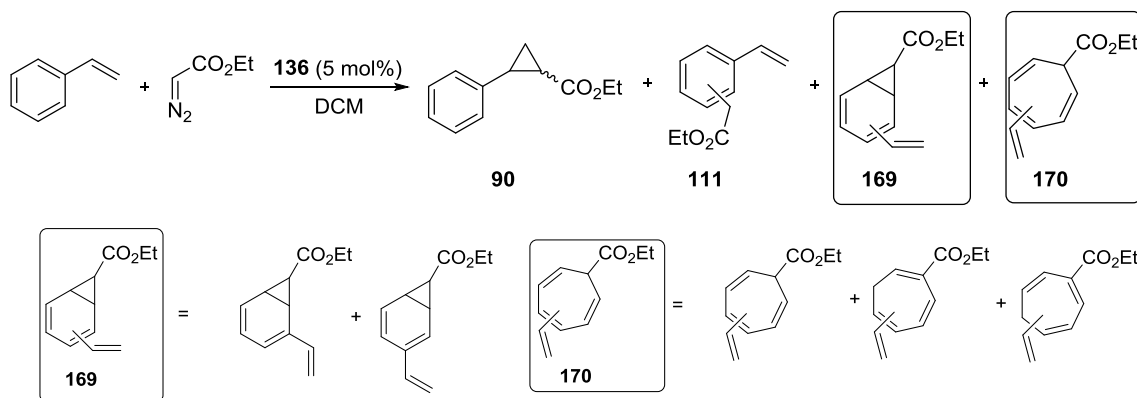


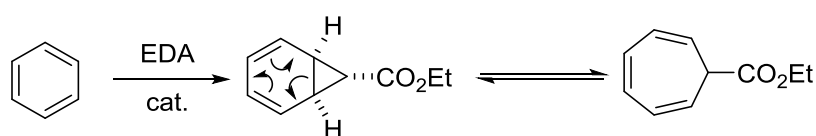
Figure 40: Gold complexes for cyclopropanation reaction.

The use of 5 mol% (with respect to EDA) **136** as a catalyst at 70°C led to the formation of a mixture of isomers and different products (Scheme 58). The analysis of the resulting mixture by GC-MS and comparing the NMR data with literature data revealed a formation of 5-10 different isomers with the same molecular mass and the same fragmentation pattern in the mass spectrum.



Scheme 58: Cyclopropanation reaction, catalyzed by **136**.

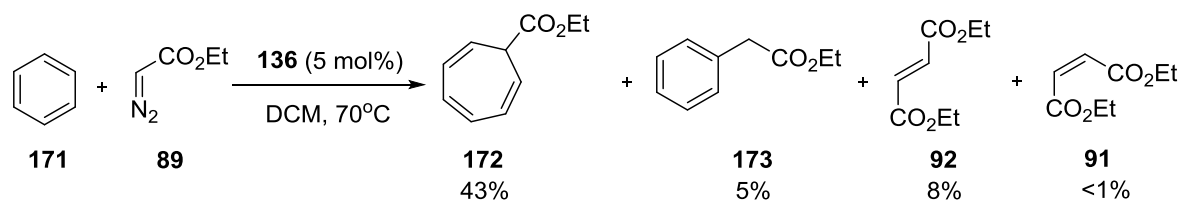
The GC-MS analysis revealed formation of cyclopropanated styrene **90** (*cis/trans* - 40/60) as well as C-H insertion products **111**. Interestingly, both norcaradienes **169** and cycloheptatrienes **170** were observed as major products of the reaction. Their formation can be explained by (2+1)-annulation and following 6π -electrocyclization in Buchner fashion (Scheme 59).¹³⁶



Scheme 59: Ring opening in Buchner reaction.¹³⁶

136-catalyzed transfer of the carbene onto styrene occurred in a non-selective manner and resulted in a complicated mixture of products. To suppress one of the two competing reactions (cyclopropanation and C-H insertion) a less reactive substrate **171** with no functional groups was chosen.

The 5 mol% of gold complex **136** induced the functionalization of benzene (**171**) with EDA (**89**) to give a mixture of cycloheptatriene **172**, formed in Buchner reaction, and ethyl fumarate **92**, the diazo cross-coupled product (Scheme 60). The NMR analysis confirmed a consumption of diazoacetate (**89**) within 30 minutes.



Scheme 60: Gold(III)-catalyzed carbene-transfer onto benzene.

A small amount of the C-H insertion product **173** was observed. Interestingly, with rhodium(II) tetraacetate ($\text{Rh}_2(\text{OAc})_4$ (**5**)) as catalyst, the yield of **172** is 40% with no formation of dimers of EDA or C-H insertion product **173**.¹³⁶

When the reaction was carried out using 2.5 mol% of $\text{Au}(\text{tpy})(\text{OAc}^{\text{F}})_2$ (**136**), the diazo cross-coupled products **92** and **91** were observed as the major products and cyclopentatriene **172** as the minor product.

To gain a deeper insight in the reaction mechanism, the reaction between benzene and ethyl diazoacetate (**89**) was carried out in an NMR tube. The biggest issue here was the low solubility of $\text{Au}(\text{tpy})(\text{OAc}^{\text{F}})_2$ (**136**) in deuterated benzene. Therefore, we could not obtain a good resolution of the spectrum (Figure 41).

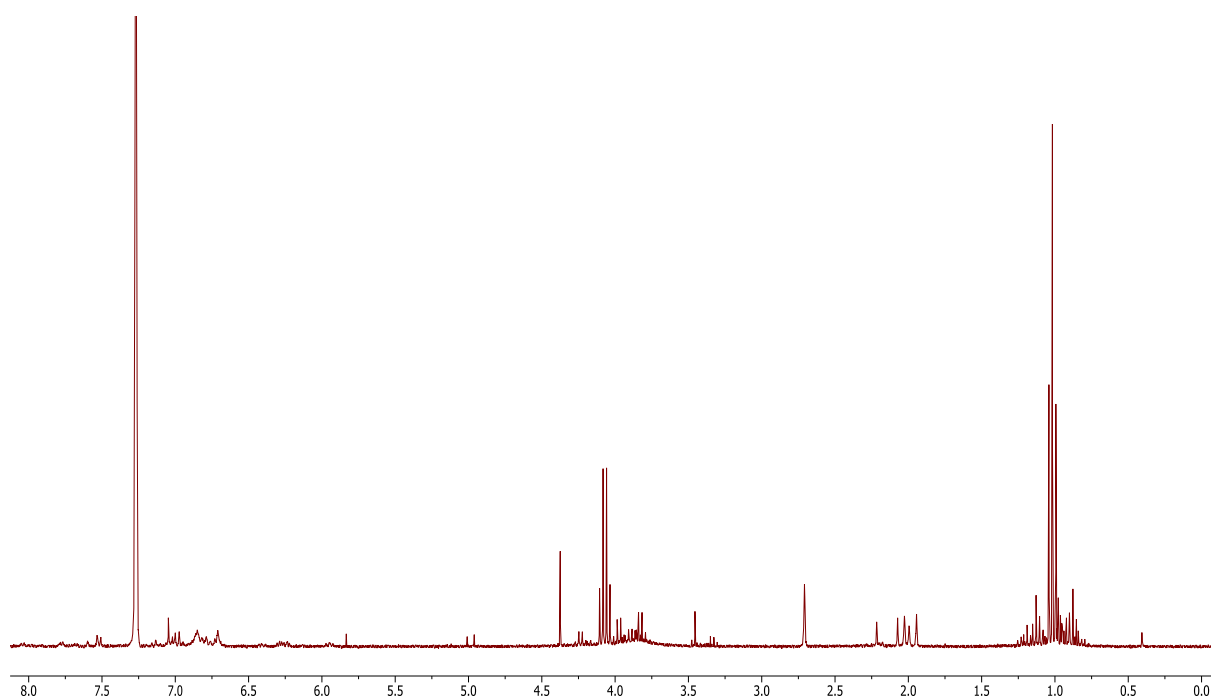


Figure 41: The ¹H NMR spectrum of the reaction between benzene and EDA catalysed by **136**.

The reaction mixture shows complicated content within minutes, due to cross-reactions of formed carbene with tpy ligand of **136**. All attempts to grow crystals suitable for X-ray analysis failed.

A short summary: $\text{Au}(\text{tpy})(\text{OAc}^{\text{F}})_2$ (**136**), transfers the carbene group onto benzene and styrene with poor selectivity. The resulted mixture of products consists of the carbene insertion products into a C-H bond and products from the cyclopropanation reaction.

5.2 Multicomponent reactions

As it was described in Section 4.5.1, the multicomponent reactions (MCRs) were studied with gold(I) and gold(III) species as catalysts. In this project complexes $\text{Au}(\text{tpy})(\text{OAc}^{\text{F}})_2$ (**136**), $\text{Au}(\text{tpy})(\text{Cl})_2$ (**135**), $\text{Au}(\text{tpy})\text{BrMe}$ (**137**) and $\text{Au}(\text{tpy})(\text{Me})_2$ (**138**) were examined in the MCRs. The four complexes have different groups with different abilities to dissociate from the central gold(III) ion (Figure 42).

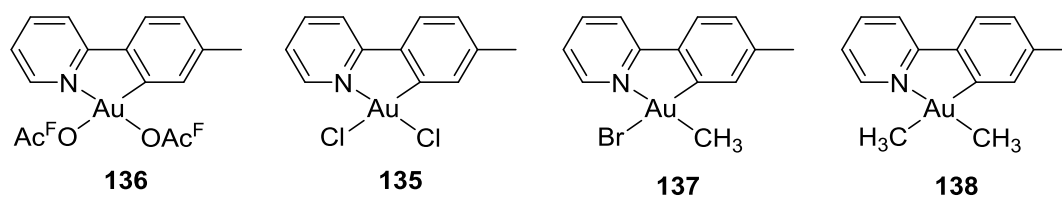


Figure 42: The investigated gold(III) complexes in MCRs.

It was believed that $\text{Au}(\text{tpy})(\text{OAc}^{\text{F}})_2$ (**136**) would be the most reactive complex because of the good leaving OAc^{F} groups.

Benzaldehyde (**163**), piperidine (**162**) and phenylacetylene (**161**) were chosen as substrates. The reactions were carried out under solvent-free conditions and different temperature regimes. The results are given in Table 14.

Table 14: Gold(III)-catalyzed formation of propargylamine **164**.

Entry	Cat.	Cat. [mol %]	Temp, °C	Yield ^[a] , %
1	136	1	40	65
2	136	2	40	81
3	136	0.5	40	42
4	136	0.5	80	97
5	136	0.25	80	68
6	135	1	40	90
7	135	1	80	89
8	135	0.5	80	96
9	135	0.25	80	81
10	137	1	40	trace
11	137	1	80	81
12	137	0.5	80	26
13	138	1	80	80
14	138	0.5	80	34
15	135	0.5	40	18
16	none	none	80	0

[a] Yields were measured by ¹H NMR spectroscopy with mesitylene as an internal standard.

Most of the complexes **135-137** catalyze the reaction in Table 14 with yields higher than 60%. The catalytic ability of the investigated gold(III) complexes was shown by carrying out the reaction in the absence of gold species where no product was observed (entry 16).

The yields increase dramatically with higher temperatures (entry 3 and 4). The temperature regime noticeably affects the catalytic performance for all catalysts, except Au(tpy)(Cl)₂ (**135**) (entry 6 and 7). At 40°C no reaction occurs with Au(tpy)BrMe (**137**), whereas Au(tpy)(Cl)₂ (**135**) catalyzes the reaction with 90% yield (entry 10 and 6).

Increase of the catalyst loading for Au(tpy)(OAc)^F₂ (**136**), resulted in increased yield at all temperatures. The same tendency was observed for Au(tpy)BrMe (**137**) (entries 10, 11 and 12) and Au(tpy)(Me)₂ (**138**) (entry 13 and 14). However, no dramatic effect on catalyst loading for Au(tpy)(Cl)₂ (**135**) was observed, reporting yields >80% for all cases (entries 6-9).

Complex $\text{Au}(\text{tpy})(\text{Me})_2$ (**138**) is of special interest because of its two methyl groups that are considered to be poor leaving groups. Although they are poor leaving groups, the catalysis occurs in a high yield at 80°C (entry 13). It becomes obvious that under elevated temperatures the gold(III) complexes possess approximately the same catalytic activity. Whereas at much lower temperatures, the catalytic activity decreases with a given tendency: $\text{Au}(\text{tpy})\text{Cl}_2 > \text{Au}(\text{tpy})(\text{OAc}^{\text{F}})_2 > \text{Au}(\text{tpy})\text{BrMe}$.

In principle, the C-C triple bond in product **164** could be further coordinated to the gold(III) complex and subjected to nucleophilic attack. In Section 4.5.1 was shown that substitution of the benzaldehyde (**163**) with pyridine-2-carbaldehyde (**168**) results in intramolecular attack onto the activated C-C triple bond.

Table 15: Gold(III)-catalyzed formation of aminoindolizine **167**.

Entry	Cat.	Cat. [mol %]	Temp, °C	Time, h	Yield ^[a] , %
1	NaAuCl_4	1	40	1.5	95
2	136	1	60	2	60
3	136	1	80	2	85
4	135	1	60	3	30
5	135	1	80	2	85
6	135	0.5	80	2	80
7	137	0.5	80	2	trace
8	137	1	80	24	9
9	138	1	80	24	trace

[a] Yields were measured by ^1H NMR spectroscopy with mesitylene as an internal standard.

In order to catalyze the formation of aminoindolizine **167**, catalysts should be able to coordinate to the C-C triple bond twice during the one catalytic cycle.

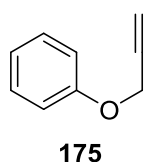
At 80°C, the differences in catalytic activity become significant: 85, 85, 9 and 0% yield for $\text{Au}(\text{tpy})(\text{OAc}^{\text{F}})_2$ (**136**), $\text{Au}(\text{tpy})(\text{Cl})_2$ (**135**), $\text{Au}(\text{tpy})\text{BrMe}$ (**137**) and $\text{Au}(\text{tpy})(\text{Me})_2$ (**138**), respectively. Thus, the nature of the leaving group plays an important role in the system with double coordination in one catalytic cycle. The deprived yields for the complexes $\text{Au}(\text{tpy})\text{BrMe}$ (**137**) and $\text{Au}(\text{tpy})(\text{Me})_2$ (**138**) correlate well with the poor ability of the methyl groups to dissociate.

At lower temperatures, $\text{Au}(\text{tpy})(\text{OAc}^{\text{F}})_2$ (**136**) catalyzes the reaction with higher yields than $\text{Au}(\text{tpy})(\text{Cl})_2$ (**135**) (entry 2 and 4). This correlates well with the ability of the groups to dissociate.

5.3 Alkyne insertion

As it was depicted in Chapter 4.4, the cyclometalated gold(III) complexes readily react with numerous alkenes. When it comes to alkynes, only the simplest representative was investigated – acetylene. Thus, the objective was to investigate the reaction of cyclometalated gold(III) complexes with different alkynes – phenylacetylene (**174**) and phenyl propargyl ether (**175**).

5.3.1 Phenyl propargyl ether (**175**)



The reaction of phenyl propargyl ether (**175**) with $\text{Au}(\text{tpy})(\text{OAc}^{\text{F}})_2$ (**136**) in CD_2Cl_2 was first performed in an NMR tube and followed by ^1H NMR. The general procedure involved taking a reference spectrum of the gold complex **136** in CD_2Cl_2 , introducing the alkyne in a second step and monitoring the reaction development by ^1H NMR within certain time periods (usually 1 hour). The procedure was also applied for monitoring the reaction by ^{19}F NMR. The reference spectrum for phenyl propargyl ether (**175**) is depicted in Figure 43.

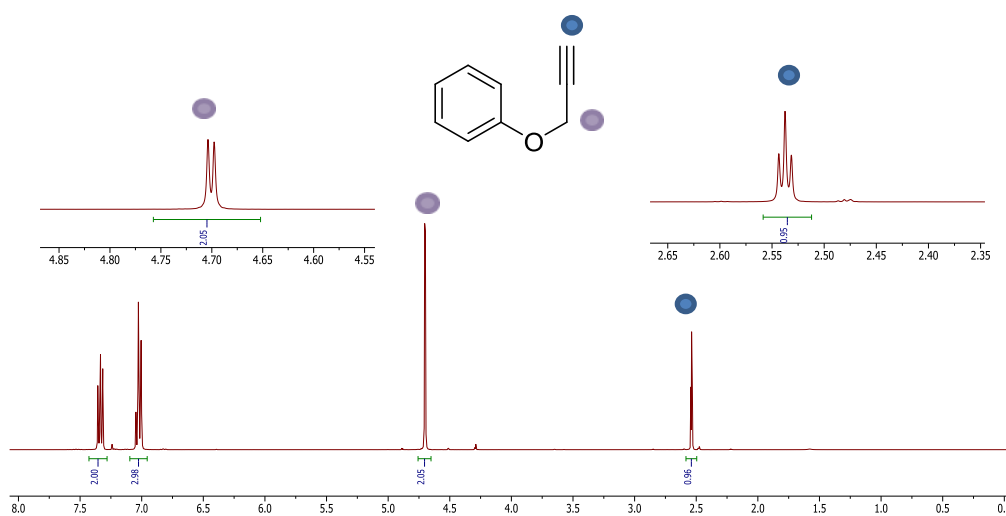


Figure 43: ^1H NMR (CDCl_3 , 400 MHz) of the phenyl propargyl ether (**175**).

Phenyl propargyl ether has two signals for the non-aromatic region: a doublet for the methylene group at 4.70 ppm and a triplet for the acetylenic proton at 2.54 ppm (Figure 43). After dissolving $\text{Au}(\text{tpy})(\text{OAc}^{\text{F}})_2$ (**136**) and phenyl propargyl ether (**175**) in the NMR tube, a spectrum was recorded (Figure 44).

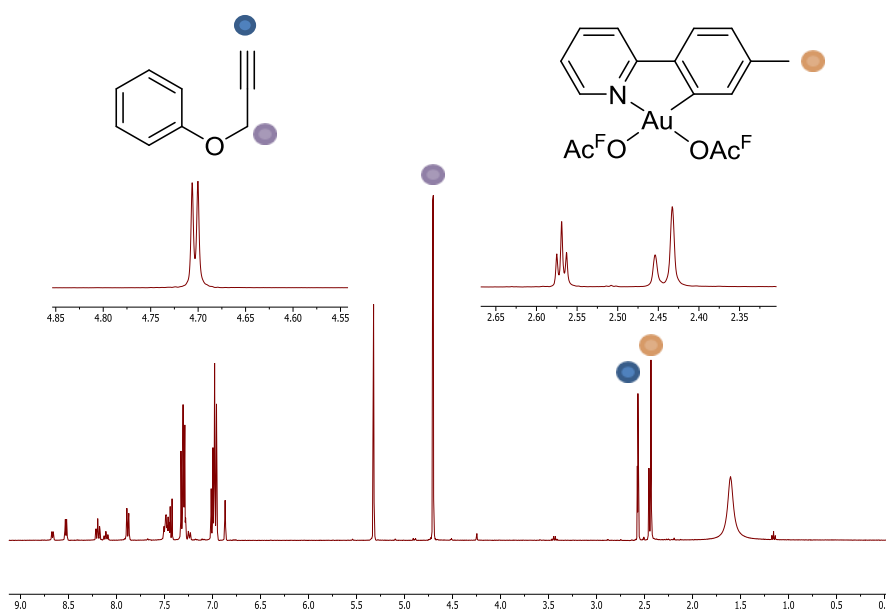


Figure 44: ^1H NMR (CD_2Cl_2 , 400 MHz) of the reaction between $\text{Au}(\text{tpy})(\text{OAc}^{\text{F}})_2$ (**136**) and phenyl propargyl ether (**175**) right after mixing.

Shifted signals for methyl and aromatic groups, in comparison to the starting gold(III) complex, indicate an immediate formation of a new species with a methyl group signal at 2.45 ppm. The aromatic signals for the unknown species have a similar coupling pattern to the starting $\text{Au}(\text{tpy})(\text{OAc}^{\text{F}})_2$ (**136**) complex. That postulates that the tpy ligand remained intact and coordination occurred to Au(III)-ion in the $\text{Au}(\text{tpy})(\text{OAc}^{\text{F}})_2$ complex (Figure 45).

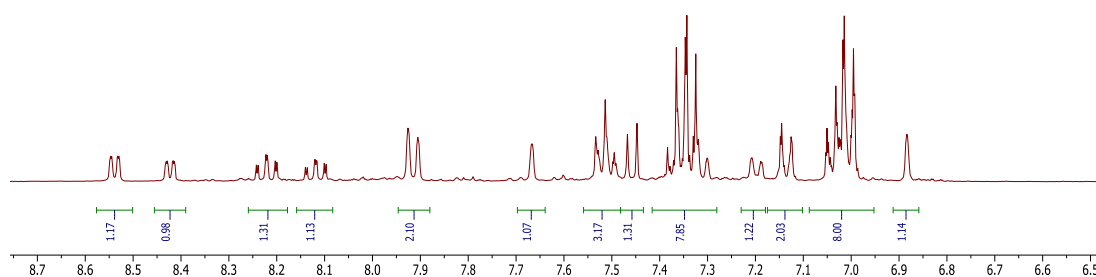


Figure 45: Close-up view of the aromatic region of the reaction mixture of $\text{Au}(\text{tpy})(\text{OAc}^{\text{F}})_2$ and phenyl propargyl ether.

The concentration of the unknown complex decreases over time, which indicates its further transformations during the experiment (Figure 46).

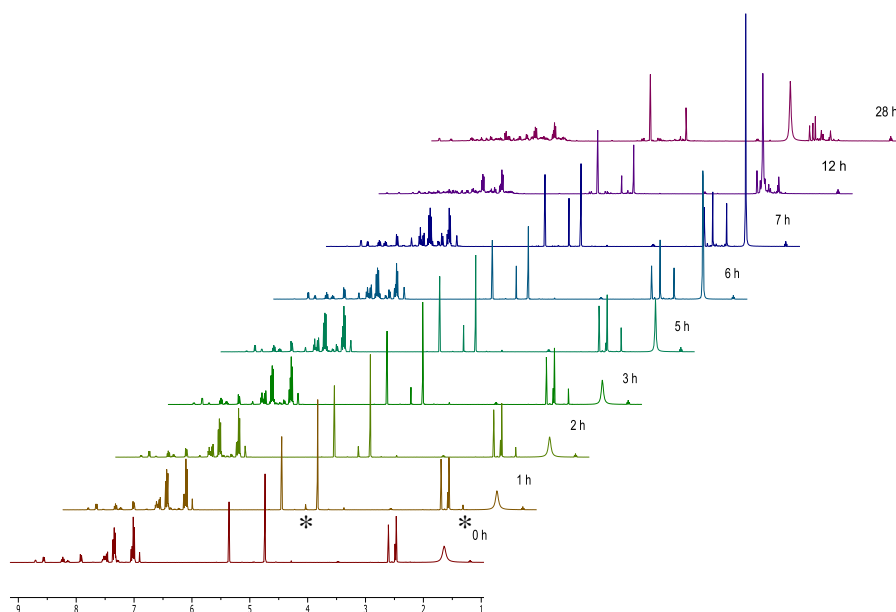


Figure 46: Development of the reaction of $\text{Au}(\text{tpy})(\text{OAc}^{\text{F}})_2$ (**136**) and phenyl propargyl ether in CD_2Cl_2 followed by ^1H NMR (400 MHz). Peaks marked with “*” are at 4.91 ppm and 2.19 ppm.

This assumption is consistent with the ^{19}F NMR spectra, where an immediate formation of a complex that undergoes further transformations was observed (Figure 47).

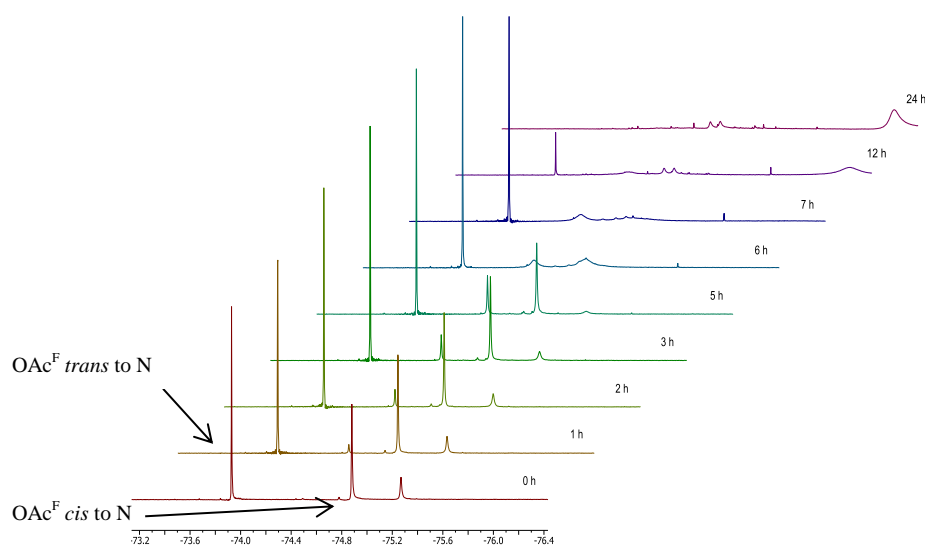


Figure 47: Development of the reaction between $\text{Au}(\text{tpy})(\text{OAc}^{\text{F}})_2$ (**136**) and phenyl propargyl ether in CD_2Cl_2 followed by ^{19}F NMR (376 MHz).

On the basis of previous experience with alkene and alkyne insertions, the main indicator of formal insertion to the gold(III) complex is a downfield shift of the singlet at 6.90 ppm. During the first 7 hours, no formal insertion occurred, which indicated the absence of intermediate depicted in Figure 48. After 7 hours the shift occurs, indicating a possible formation of insertion products. However, the mixture becomes complicated and leaves, therefore, no possibility to interpret the intermediates that are involved.

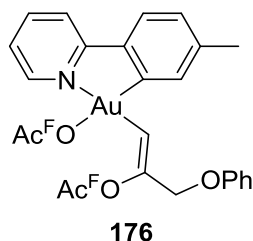
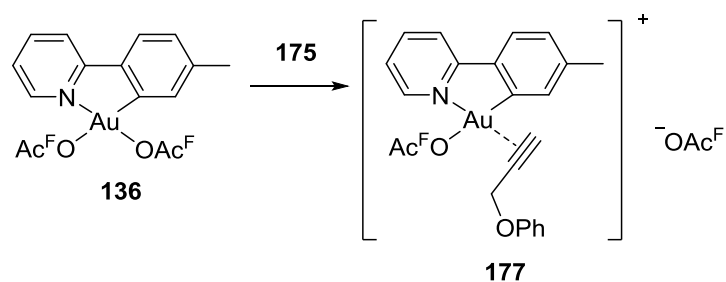


Figure 48: Expected insertion product **176**.

As shown in Figure 46, the reaction did not proceed in a clean and defined manner. After 12 hours, signals in the aromatic and aliphatic region became indistinguishable, which indicated the complicated pathway of the reaction leading to the mixture of products.

During the first 7 hours, the peak at 4.91 ppm (*) and the peak at 2.19 ppm (*) were observed (Figure 46). These two peaks are considered to be related, because their ratio remains 2:3 during the 7 hours. With respect to the region where these two peaks appeared, they were assumed to be $-\text{CH}_2-$ and $-\text{CH}_3$ groups, respectively.

The described above scenario is possible when the phenyl propargyl ether would coordinate to the gold atom, so that the methylene hydrogens of the ether and the methyl group of the tpy ligand would experience different environment (Scheme 61). Integration of the peaks led to a 60/40 ratio of $\text{Au}(\text{tpy})(\text{OAc}^{\text{F}})_2$ and the new formed complex **177** (Figure 45).



Scheme 61: Possible reaction pathway for the reaction of $\text{Au}(\text{tpy})(\text{OAc}^{\text{F}})_2$ with phenyl propargyl ether.

In order to elucidate the structure of the formed compounds, MS studies were conducted. Two MS-ionization techniques were used in this project – electrospray (ESI) and electron impact (EI). The first technique can be used to analyze non-volatile compounds, such as organometallic complexes or salts. The second one is useful for analysis of organic compounds.

ESI mass spectra depicted an instant formation of species with m/z 533 and 454. The concentration of the latter decreased over time, while the concentration of the peak with m/z 533 increased and reached its maximum after 7 hours. Corresponding molecular ions were found to be $[\text{Au}(\text{tpy})_2]^+$ (**181**) and its fragment (m/z 454), indicating primary formation of the complex $[\text{Au}(\text{tpy})_2]^+$ at the beginning of the reaction (Figure 49).

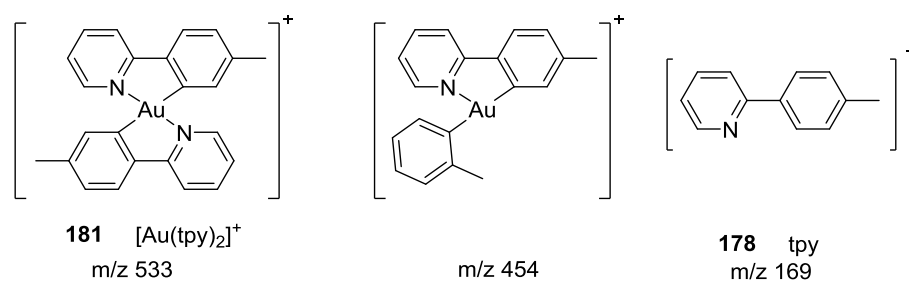
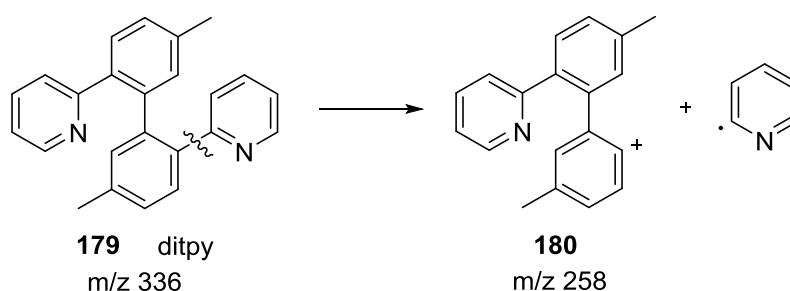


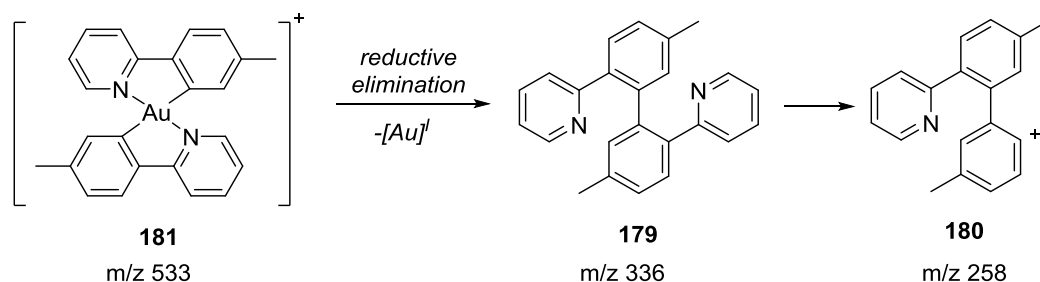
Figure 49: Proposed structures for the observed intermediates.

EI mass spectra demonstrated the rise of peak with m/z 169 and 258 with their maximum after 7 hours. The first is considered to be a free tpy ligand **178** and the second is a fragment of a dimerized tpy **180**. The EI-MS provides useful information about volatile organic molecules that do not contain the Au-atom.



Scheme 62: Proposed structures for intermediates.

Molecules **179** and **181** were found to be dominant in the reaction mixture during the first 7 hours. Interestingly, the origin of the ditpy **179** with m/z 336 can be understood combining ESI and EI MS data. Compound **179** could be formed within reductive elimination of complex **181** (Scheme 63).



Scheme 63: Proposed mechanism of formation of observed intermediates.

Formation of $[\text{Au}(\text{tpy})_2]^+$ (**181**) was proven *via* single crystal X-ray analysis. The crystal suitable for X-ray analysis was grown in the reaction mixture, using the vapor-diffusion method. However, formation of such species was discovered before by a former exchange student in our group, Yannick Wencke. The mechanism of how these species convert into each other still remains unsolved. Interestingly, the MS studies revealed the same destruction pathway for $\text{Au}(\text{tpy})(\text{OAc}^{\text{F}})_2$, regardless of what substrate it reacted with.

5.3.2 Phenyl acetylene (**174**)

The reaction of $\text{Au}(\text{tpy})(\text{OAc}^{\text{F}})_2$ (**136**) with phenyl acetylene (**174**) was performed in order to investigate the plausible gold-alkyne complex and gain an insight into the mechanism of coupling reactions. The reaction was studied by ^1H (300 MHz) and ^{19}F NMR (282 MHz) in two different solvent systems: CD_2Cl_2 and $\text{CD}_2\text{Cl}_2/\text{TFA}$. The NMR spectra were recorded until the gold “mirror” in the NMR tube was formed or the composition of the reaction mixture became too complicated. The reference spectrum of the starting material before and after the mixing is depicted in Figure 50 and 51.

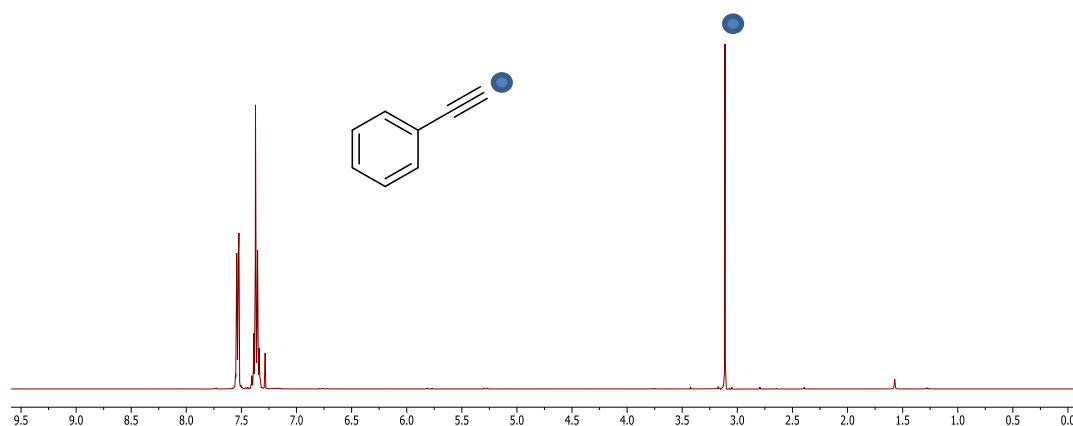


Figure 50: ^1H NMR (300 MHz, Chloroform-*d*) spectrum of phenyl acetylene (**174**).

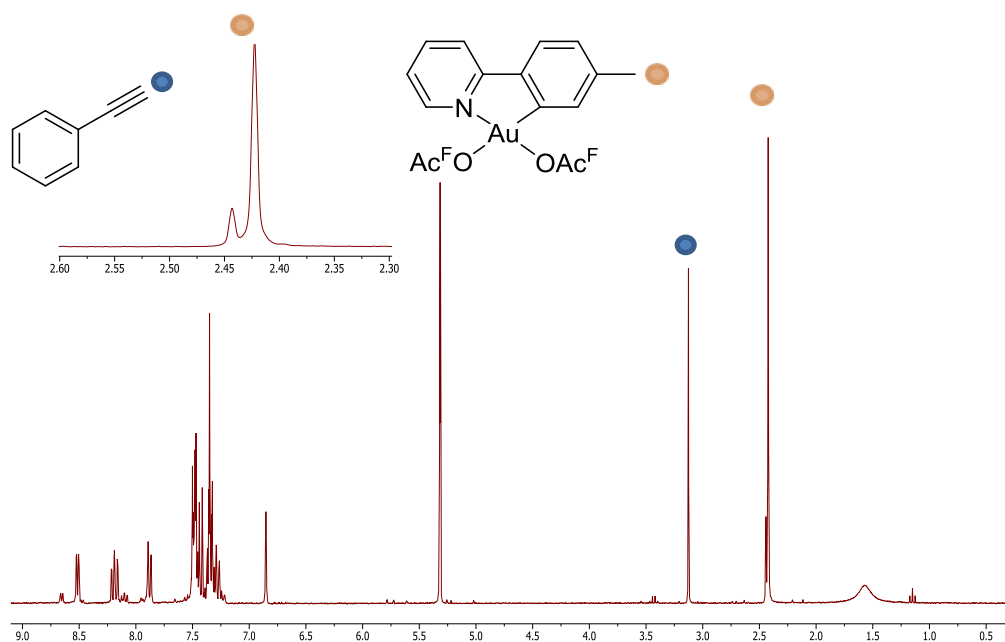


Figure 51: ^1H NMR (300 MHz, $\text{Dichloromethane-}d_2$) spectrum recorded right after mixing the reagents.

When phenyl acetylene was introduced to the gold complex **136**, the signal of the methyl group in the starting gold complex **136** at 2.42 ppm, shifts downfield to 2.44 ppm. In addition, a shift of the aromatic signals occurs. Growth of new signals could be explained by an immediate formation of a gold-alkyne complex. This assumption is consistent with the ^{19}F NMR spectrum, recorded right after mixing the reagents, where the third peak presumably belongs to the free TFA (Figure 52).

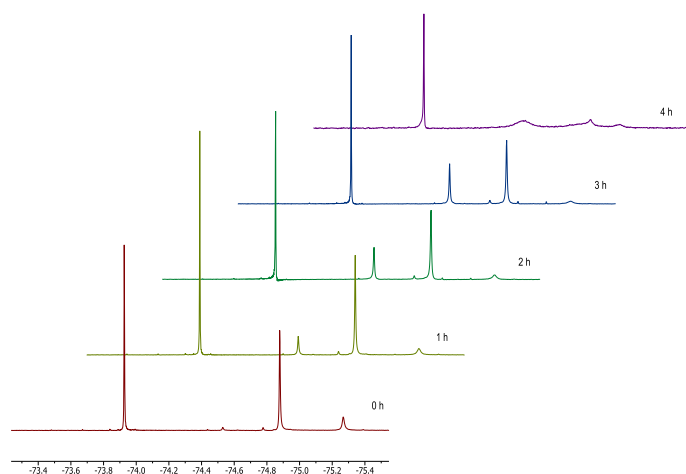


Figure 52: ^{19}F NMR (282 MHz, $\text{Dichloromethane-}d_2$) study of reaction development.

No shift of the peak at 6.85 ppm and lack of signals in the “olefinic” region indicate the absence of plausible insertion complex **182** or **183** (Figure 53).

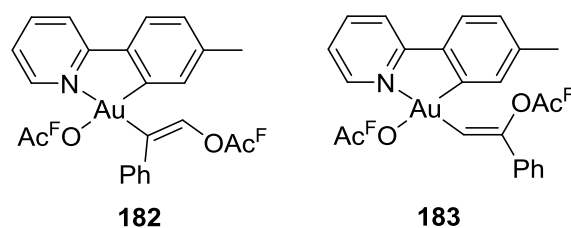


Figure 53: Proposed structures of intermediates **182** and **183**.

During the whole 12 hours, the acetylenic proton at 3.13 ppm remains unshifted (Figure 54).

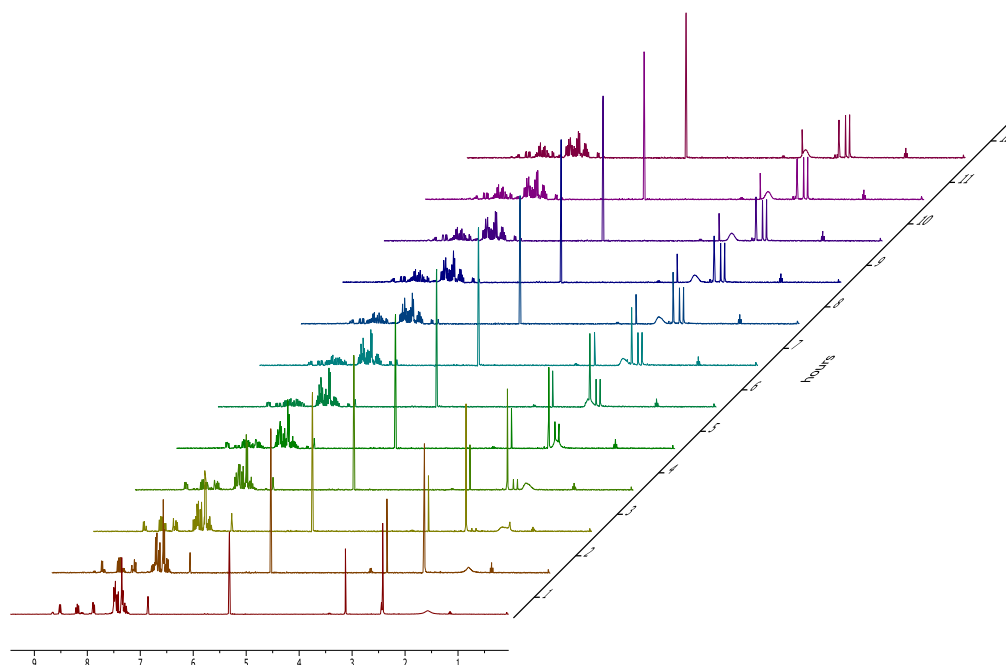


Figure 54: Development of the reaction between Au(tpy)(OAc^F)₂ (**136**) and phenyl acetylene in CD₂Cl₂ followed by ¹H NMR (300 MHz).

According to the formation of a new methyl signal at 2.44 ppm and the unaltered acetylenic signal, it was assumed that the first complex that could probably be formed would be **184** (Figure 55).

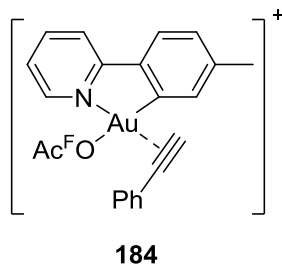


Figure 55: Proposed structure of intermediate.

According to ^{19}F NMR data, this complex exists only for the first 1-2 hours and further undergoes numerous transformations: oxidative coupling, reductive elimination, etc. (Figure 52).

Being inspired by the work conducted in the group of Tilsted, the reaction was carried out in the presence of TFA. As it can be seen from Figure 56, the reaction proceeded much faster and no further changes occurred after 2 hours.

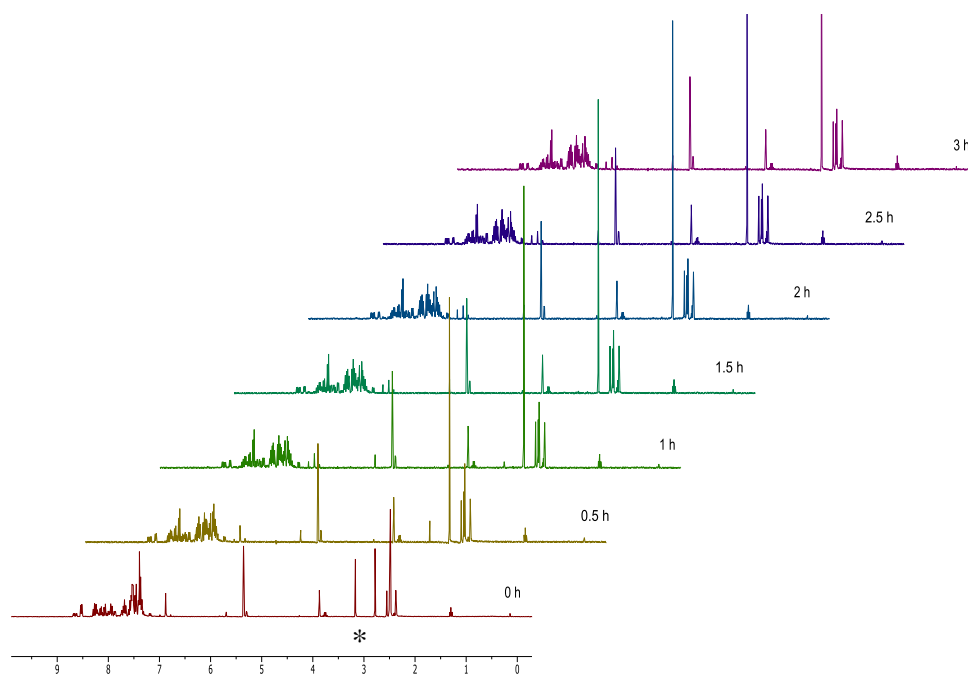
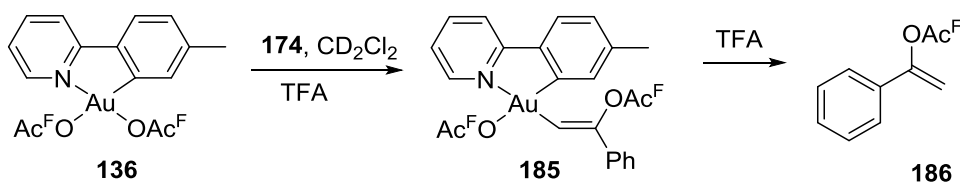


Figure 56: Development of the reaction between $\text{Au}(\text{tpy})(\text{OAc}^{\text{F}})_2$ (**136**) and phenyl acetylene in CD_2Cl_2 and TFA followed by ^1H NMR (300 MHz). Peak marked with “*” is at 3.13 ppm.

The NMR data revealed a lot of information. First, the signal of the acetylenic proton at 3.13 ppm (*) decreases and disappears within 2 hours, which indicates the full conversion of the phenyl acetylene (Figure 56). Secondly, two doublets appeared in the olefinic region, which designated formation of an insertion product **185** (Scheme 64).



Scheme 64: Possible reaction pathway between phenyl acetylene (**174**) and **136**.

All attempts to isolate the intermediate **185** were unsuccessful due to decomposition.

MS-analysis, as in the case of phenyl propargyl ether **175** (see Section 5.3.1), reveals formation of ions with m/z 533, 454 and 169 (Figure 57).

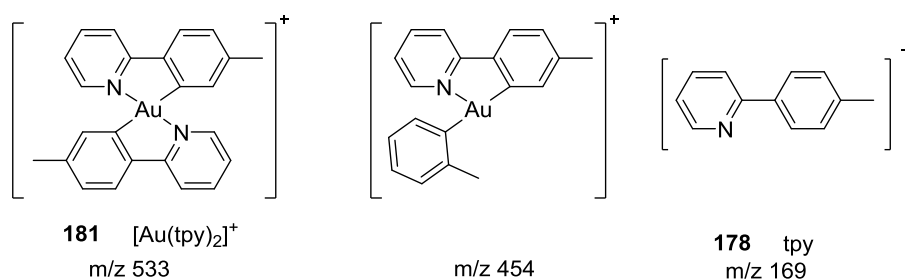
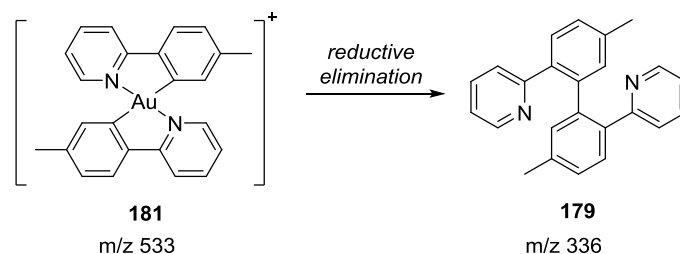


Figure 57: Proposed structures for observed ions in the MS-spectrum.

5.3.3 Conclusions regarding the alkyne insertion

Although no products were isolated and characterized, the NMR experiments together with MS-analysis show similar destruction patterns for $\text{Au}(\text{tpy})(\text{OAc}^{\text{F}})_2$, regardless the substrate it reacted with. The degradation of $\text{Au}(\text{tpy})(\text{OAc}^{\text{F}})_2$ in both cases resulted in formation of the $[\text{Au}(\text{tpy})_2]^+$ (**181**) complex, which undergoes a reductive elimination with formation of ditpy-molecule **179** (Scheme 65).

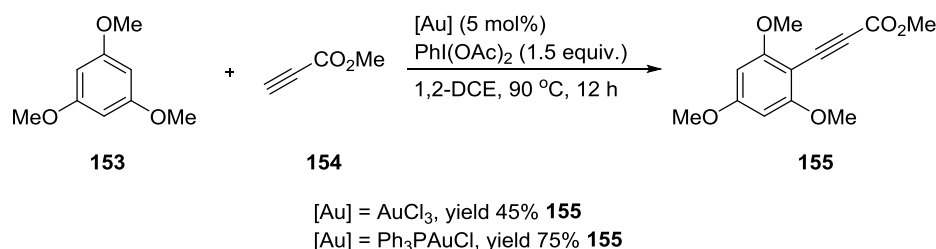


Scheme 65: Proposed structures for products of degradation of $\text{Au}(\text{tpy})(\text{OAc}^{\text{F}})_2$.

The origin of $[\text{Au}(\text{tpy})_2]^+$ (**181**) complex remains unsolved.

5.4 Gold-catalyzed ethynylation of arenes

As it was discussed in Chapter 4.5, a gold-catalyzed ethynylation of 1,3,5-trimethoxybenzene (**153**) with ethyl propiolate (**154**) resulted in the C-C coupled product **155** in high yield (Scheme 66).



Scheme 66: Ethynylation of arenes catalysed by gold(I) or gold(III) complexes.

The reaction was performed utilizing two gold(III) cyclometalated complexes - Au(tpy)(OAc)^F₂ (**136**) and Au(tpy)Cl₂ (**135**) (Figure 58).

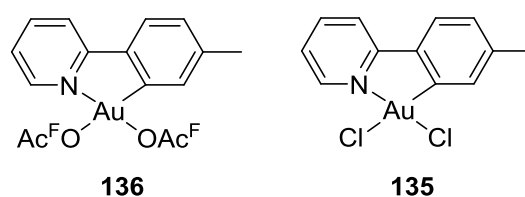
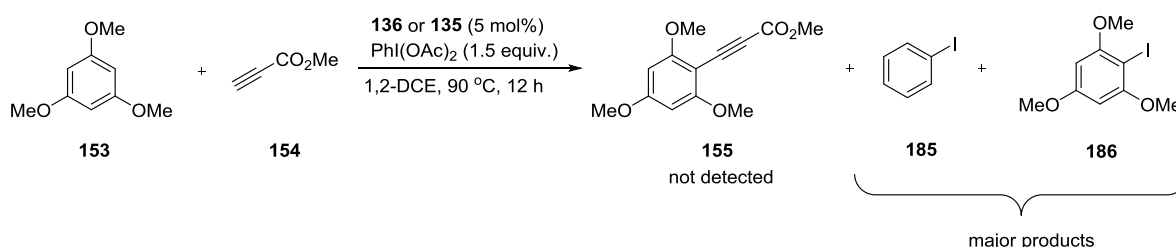


Figure 58: Investigated gold(III) cyclometalated complexes.

The reaction, catalyzed by **136** and **135**, was analyzed by ¹H NMR and GC-MS. Under the conditions described in the literature none of the complexes provided the desired product **155**. Instead, iodobenzene (**185**) and 2-iodo-1,3,5-trimethoxybenzene (**186**) were observed (Scheme 67).



Scheme 67: Ethynylation catalyzed by gold(III) cyclometalated complexes **136** and **135**.

In addition to the observed products, a lot of starting material **153** was recovered. When the reaction was performed in the absence of PhI(OAc)₂, starting material 1,3,5-trimethoxybenzene

(**155**) and ethyl propiolate (**154**) were recovered. In the absence of gold(III) complexes **136** and **135**, iodobenzene (**185**) and 2-iodo-1,3,5-trimethoxybenzene (**186**) were observed as minor products.

The observed results suggest the disability of the cyclometalated gold(III) complexes **136** and **135** to be involved in tandem gold(I)/gold(III) reaction.

6 Conclusions and Future Prospects

The preparation and characterization of four novel Rh(II)-monomers ($\text{Rh}_2(4\text{VBA})_4$ (**75**), $\text{Rh}_2(\text{MCES})_4$ (**74**), $\text{Rh}_2(4\text{VBA})_2(\text{OAc}^{\text{F}})_2$ (**77**) and $\text{Rh}_2(\text{MCES})_2(\text{OAc}^{\text{F}})_2$ (**78**)), were successfully performed. The novel Rh(II)-monomers were successfully immobilized in a bottom-up fashion, giving six hydrophilic, solid polymer catalysts – $\text{pol}(\text{I})\text{-Rh}_2(4\text{VBA})_4$ (**84**), $\text{pol}(\text{I})\text{-Rh}_2(\text{MCES})_4$ (**85**), $\text{pol}(\text{I})\text{-Rh}_2(4\text{VBA})_2(\text{OAc}^{\text{F}})_2$ (**83**), $\text{pol}(\text{I})\text{-Rh}_2(\text{MCES})_2(\text{OAc}^{\text{F}})_2$ (**86**), $\text{pol}(\text{II})\text{-Rh}_2(4\text{VBA})_4$ (**88**) and $\text{pol}(\text{II})\text{-Rh}_2(\text{MCES})_4$ (**87**).

The two prepared polymer catalysts ($\text{pol}(\text{II})\text{-Rh}_2(4\text{VBA})_4$ (**88**) and $\text{pol}(\text{II})\text{-Rh}_2(\text{MCES})_4$ (**87**)) possessed the best catalytic activity among the other prepared polymer catalysts, which is comparable to the commercially available $\text{Rh}_2(\text{OAc})_4$.

The dependence of polymer structure on the catalytic activity of the immobilized rhodium(II) carboxylates was investigated. The high degree of cross-linking retarded the catalytic activity of the prepared immobilized rhodium(II) carboxylates.

The advantages of the bottom-up strategy over the post-modification one were revealed. The bottom-up strategy enables the assembly of the polymer catalysts with a desired polymer network, which is crucial for the availability of the rhodium(II) catalyst in the catalysis. Post-modified $\text{pol}(\text{PM})\text{-Rh}_2(\text{MCES})_4$ (**94**) was synthesized and compared with the one prepared with the bottom-up strategy. It was shown that the post-modified polymer catalyst possesses lower catalytic activity in comparison to the bottom-up polymer catalyst.

The synthesis of $\text{Rh}_2(\text{MEPP})_4$ (**102**) surprisingly resulted in the epimerization of the chiral rhodium(II) carboxylate. The attempt to synthesize other chiral rhodium(II) carboxylates was not accomplished due to lack of time.

One way of continuing this project is to complete the synthesis and immobilization of chiral rhodium(II) carboxylates. The detailed studies on the polymer catalysts as well as investigation of their catalytic activity have to be performed. It would be also interesting to extend the scope of the synthesized achiral polymer catalysts.

Regarding the polymer for immobilization, a main goal is the synthesis of the polymer that can swell in most of the organic solvents. The assembly of a flow reactor utilizing a heterogenized rhodium(II) carboxylates is a far future goal.

Cyclometalated gold(III) complexes were found to catalyze numerous organic reactions. The nature of the leaving group affected the catalytic activity of the cyclometalated gold(III) complexes. The cyclometalated gold(III) complexes bearing alkyl groups as ligands possess lower catalytic activity in comparison to Au(tpy)(OAc^F)₂ (**136**) and Au(tpy)Cl₂ (**135**). The differences in the catalytic activity of Au(tpy)(OAc^F)₂ (**136**) and Au(tpy)Cl₂ (**135**) were inconclusive due to few experiments.

Presumably, both the organic ligand (tpy) and anionic ligands influence the catalytic activity at the gold(III) atom. In order to tune the activity, new cyclometalated gold(III) complexes should be synthesized and investigated in future.

The formal insertion reactions of alkynes to Au(tpy)(OAc^F)₂ proceeded *via* a complex pathway and no intermediates were isolated. Under the reaction conditions, decomposition products of the gold(III) complexes were observed. The pathway for the decomposition was assumed to be independent of the alkyne substrate used in the reaction. Further investigations of the decomposition of the cyclometalated gold(III) complexes is interesting to perform.

7 Experimental Section

General

Solvents used as reaction media were used as delivered from Sigma-Aldrich unless stated otherwise. CH_2Cl_2 was dried using the MB SPS-800 Solvent Purification System from MBraun. Distilled water was used. $\text{Au}(\text{OAc})_3$ was purchased from Alfa Aesar and ABCR. Argon gas was used to perform reactions under inert atmosphere. NMR-solvents were used as delivered from Sigma Aldrich, Cambridge Isotope Laboratories and Eurisotop. Thin layer chromatography was performed on 60 F_{254} silica coated aluminum plates from Merck. Flash chromatography was performed on silica gel from Merck (Silicagel 60, 40-0.60 μm , 460 m^2/g , pH 6.5-7.5) either manually or with an Isco Inc. CombiFlash Companion with PeakTrack software (v.1.4.10). Distilled hexane was used. Eluents used were on of technical grade.

^1H , ^{13}C and ^{19}F NMR experiments were recorded in CD_2Cl_2 , CD_3CN , Acetone- d_6 , Methanol- d_4 , TFA- d or DMSO- d_6 using either a Bruker Avance DPX200, DPX300, AVII400 or AVIII400 instrument with residual solvent peaks as references (CHD_2CN ($\delta\text{H} = 1.94$ ppm), CHDCl_2 ($\delta\text{H} = 5.32$ ppm), TFA- d ($\delta\text{C} = 116.6$ ppm, 164.2 ppm), DMSO- d_6 ($\delta\text{C} = 39.5$ ppm) or CD_2Cl_2 ($\delta\text{C} = 54.0$ ppm)). Chemical shifts (δ) are given in parts per million (ppm) and coupling constants (J) are given in Hertz (Hz). Multiplicities are abbreviated as: s - singlet; d - doublet; t - triplet; dd - doublet of doublets; dt - doublet of triplets; td - triplet of doublets; ddt - doublet of doublets of triplets; m - multiplet; br. - broad.

Mass spectra were obtained on Bruker MAXIS II ETD (ESI) and Scion 436-GC TQ (EI) spectrometer by Osamu Sekiguchi. SEM was performed with secondary electron detector using FE-SEM (Hitachi S-4800) operated at 5 kV. EDX spectra collected at 15 kV (500000 counts; Bruker Xflash Detector 4030). Images were collected using TEM (JEOL JEM 1400Plus) operated at 120 kV. Thin sections were prepared using Ultramicrotome (Leica Ultracut UCT) equipped with a diamond knife (Diatome). X-ray data was collected using Bruker D8 Venture, CMOS detector diffractometer. Microscopic pictures were taken on OLYMPUS ACH 1X microscope. Surface area measurements were performed using BELSORP-MINI II instrument. FTIR spectra were recorded on Perkin Elmer Spectrum One instrument.

The temperatures of decomposition for rhodium(II) carboxylates were measured to be over 300°C.

7.1 Experimental section for the rhodium project

7.1.1 Synthesis of $\text{Rh}_2(\text{OAc}^{\text{F}})_4$ (rhodium(II) trifluoroacetate),¹⁴ 7

A dry round bottom flask was charged with $\text{Rh}_2(\text{OAc})_4$ (100 mg, 0.226 mmol) and trifluoroacetic acid (TFA) (4 ml). The reaction flask was equipped with a water cooler and the mixture was stirred, under reflux for 2 days. The reaction mixture was cooled down and TFA was removed in vacuum to give a dark blue residue of the product in a quantitative yield.

Spectroscopic data was in agreement with reported literature data.¹⁴

^1H NMR (400 MHz, Methanol- d_4): δ Only signals of solvents are present - ethyl acetate and methanol- d_4 .

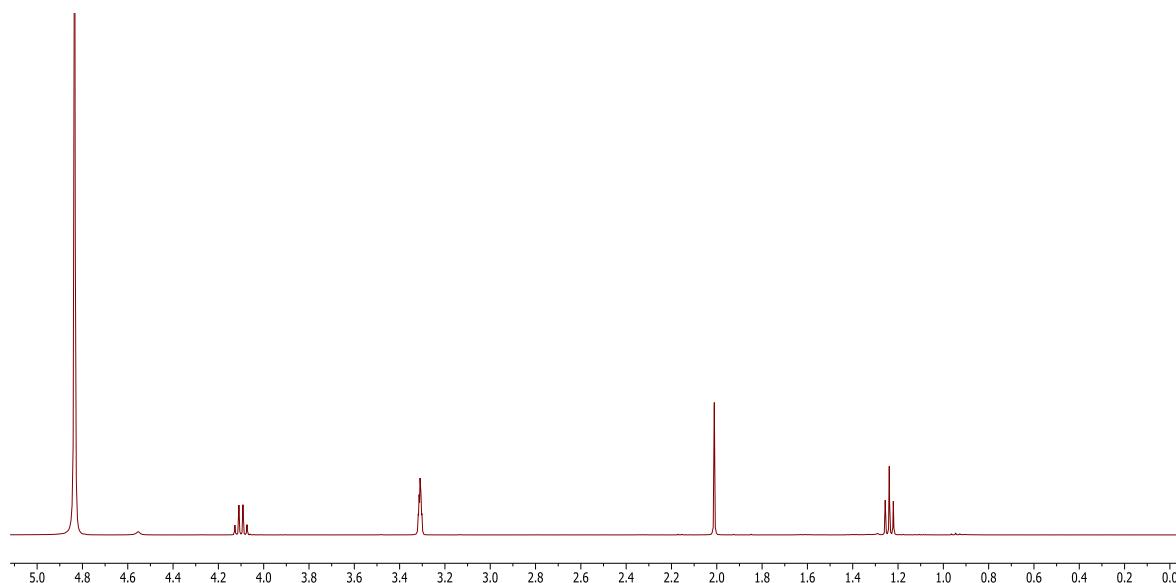


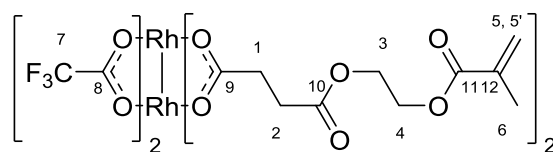
Figure 59: ^1H NMR (400 MHz, Methanol- d_4) spectrum of $\text{Rh}_2(\text{OAc}^{\text{F}})_4$. Only solvent signals present.

^{19}F NMR (188 MHz, Methanol- d_4): δ -76.05

MS (ESI, MeOH) m/z : 680.9 [$M+\text{Na}^+$]

HRMS (MeOH): calculated for $\text{Rh}_2\text{C}_8\text{O}_8\text{F}_{12}\text{Na}^+$ [$M+\text{Na}^+$] 680.8627, found 680.8630 (Δ 0.0003 ppm).

7.1.2 Synthesis of $\text{Rh}_2(\text{MCES})_2(\text{OAc}^{\text{F}})_2$, **78**



78

To a 10 ml round bottom flask was added $\text{Rh}_2(\text{OAc}^{\text{F}})_4$ (30 mg, 0.05 mmol, 1.0 equiv.), mono-2-(Methacryloyloxy) ethyl succinate (**68**) (63 mg, 0.27 mmol, 6.0 equiv.), NaHCO_3 (24 mg, 0.29 mmol), ethyl acetate (3 ml) and the reaction mixture was stirred at ambient temperature for 6 hours. The dark green-blue solution was washed with saturated NaHCO_3 solution and the organic phase was concentrated under reduced pressure. The product mixture was purified by column chromatography (EtOAc:hexane/1:2) and gave 18 mg of a green solid product $\text{Rh}_2(\text{MCES})_2(\text{OAc}^{\text{F}})_2$ in 45 % yield.

The purified product was crystallized from acetone/hexane and gave crystals suitable for single crystal X-ray diffraction.

$^1\text{H NMR}$ (400 MHz, Chloroform-*d*) δ 6.57 (s, H-5, 1H), 5.96 (s, H-5', 1H), 4.46 – 4.38 (m, H-4, 2H), 4.38 – 4.30 (m, H-3, 2H), 2.57 (dd, H-2, $J = 7.8, 5.0$ Hz, 2H), 2.46 (dd, H-1, $J = 7.9, 5.3$ Hz, 2H), 2.04 (t, H-6, $J = 1.2$ Hz, 3H).

$^{13}\text{C NMR}$ (100 MHz, Chloroform-*d*) δ 193.51 (C-9), 172.32 (C-10), 168.28 (C-11), 136.22 (C-12), 125.18 (C-5), 62.99 (C-3), 62.05 (C-4), 51.91 (C-2), 29.68 (C-1), 18.58 (C-6). Signals of $-\text{CF}_3$ group were not observed.

$^{19}\text{F NMR}$ (188 MHz, Methanol-*d*₄): δ -76.5

FTIR: 1735 cm^{-1} (-COOR), 1592, 1431 cm^{-1} (COO).

MS (ESI, MeOH) m/z : 912.8 [$M+\text{Na}^+$]

HRMS (MeOH): calculated for $\text{Rh}_2\text{C}_{24}\text{O}_{16}\text{H}_{26}\text{F}_6\text{Na}^+$ [$M+\text{Na}^+$] 912.9127, found 912.9145 (Δ 0.0018 ppm).

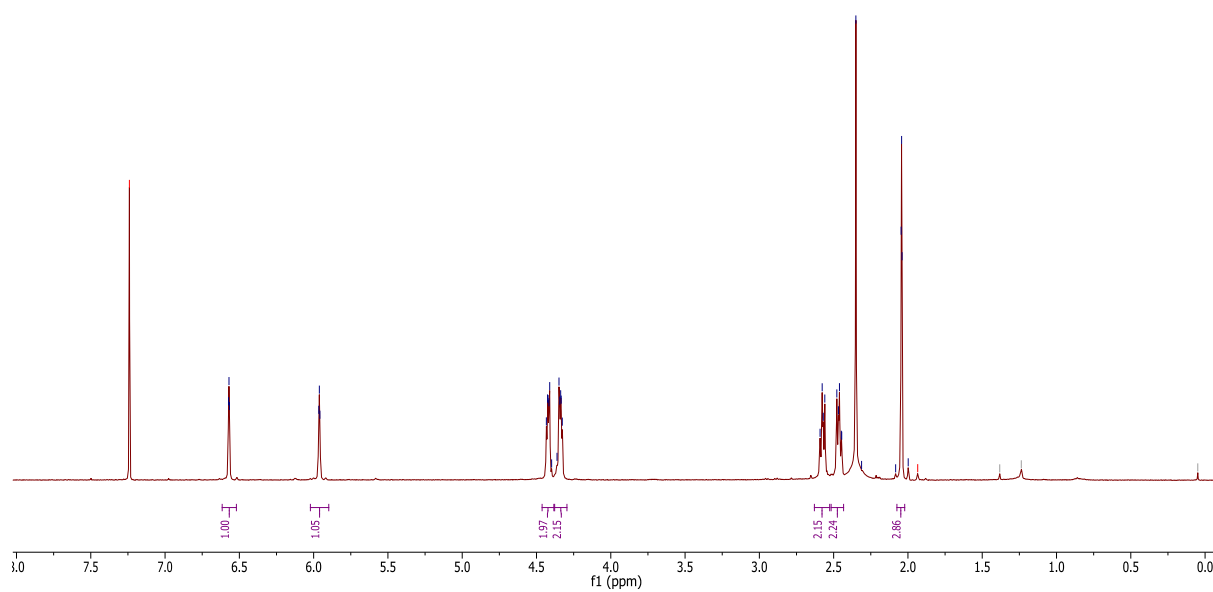


Figure 60: ^1H NMR (400 MHz, Chloroform-*d*) spectrum of $\text{Rh}_2(\text{MCES})_2(\text{OAc}^{\text{F}})_2$ (**78**). Singlet at 2.27 ppm is due to coordinated water.

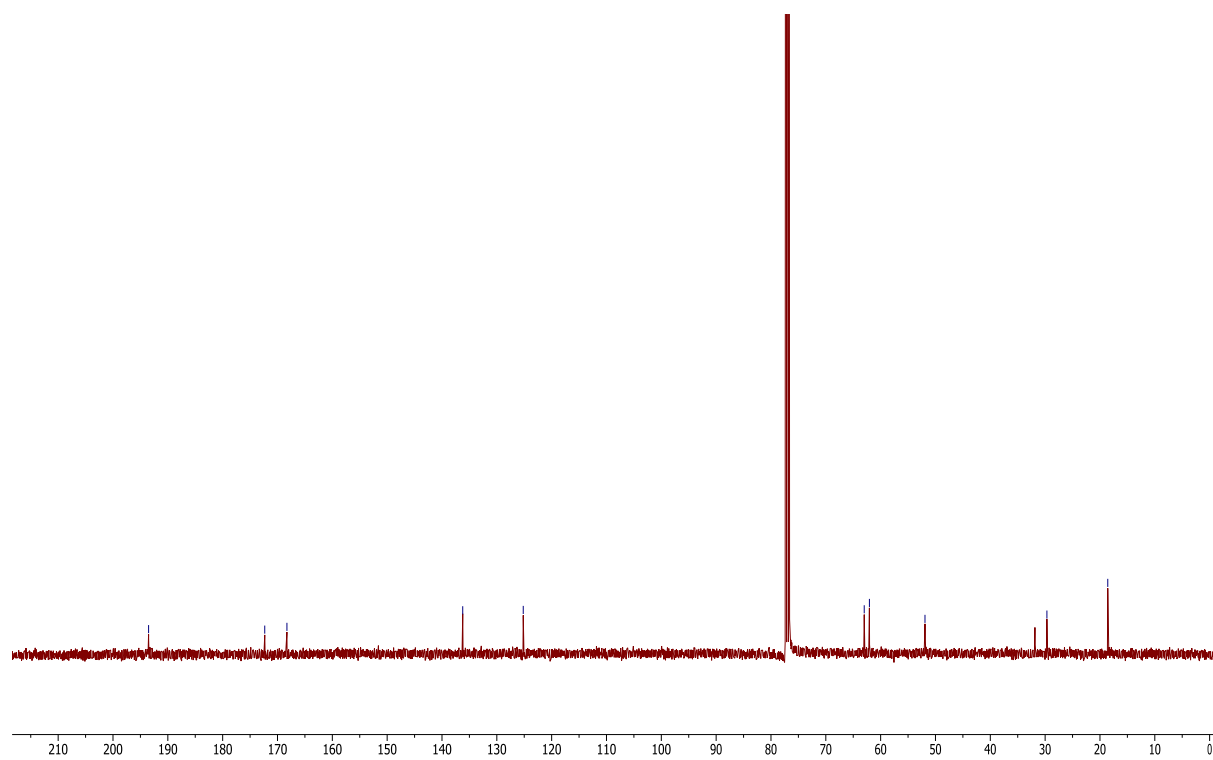
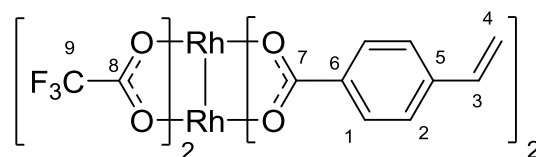


Figure 61: ^{13}C NMR (100 MHz, Chloroform-*d*) spectrum of $\text{Rh}_2(\text{MCES})_2(\text{OAc}^{\text{F}})_2$ (**78**).

7.1.3 Synthesis of $\text{Rh}_2(4\text{VBA})_2(\text{OAc}^{\text{F}})_2$, **77**



77

A dry, round bottom flask was charged with $\text{Rh}_2(\text{OAc}^{\text{F}})_4$ (30 mg, 0.046 mmol, 1 equiv.), 4-vinylbenzoic acid (**71**) (61 mg, 0.41 mmol, 9.0 equiv.), NaHCO_3 (24 mg, 0.29 mmol, 6.4 equiv.) and dichloromethane (5 ml). The mixture was stirred at ambient temperature for 20 hours. The dark green-blue solution was washed with saturated NaHCO_3 solution and the organic phase was concentrated in vacuum. The product mixture was purified by column chromatography (EtOAc:hexane/1:1) and gave 19 mg of a green solid product $\text{Rh}_2(4\text{VBA})_2(\text{OAc}^{\text{F}})_2$ in 57 % yield. The purified product was crystallized from acetone/hexane and gave crystals suitable for X-ray diffraction.

$^1\text{H NMR}$ (400 MHz, Chloroform-*d*) δ 7.88 (d, H-1, $J = 8.4$ Hz, 2H), 7.27 (d, H-2, $J = 8.4$ Hz, 2H), 6.64 (dd, H-3, $J = 17.6, 10.9$ Hz, 1H), 5.74 (d, H-4, $J = 17.6$ Hz, 1H), 5.26 (d, H-4', $J = 10.9$ Hz, 1H).

$^{13}\text{C NMR}$ (100 MHz, Methanol-*d*₄) δ 187.08 (C-7), 142.89 (C-5), 137.36 (C-6), 131.76 (C-2), 130.11 (C-1), 126.73 (C-3), 116.54 (C-4). Signals of $-\text{CF}_3$ group were not observed.

$^{19}\text{F NMR}$ (376 MHz, Methanol-*d*₄): -76.08

FTIR: 1700-2000 cm^{-1} (vinyl group), 1685, 1652 cm^{-1} (COO).

MS (ESI, MeOH) m/z : 748.9 [$M+\text{Na}^+$]

HRMS (MeOH): calculated for $\text{Rh}_2\text{C}_{22}\text{O}_8\text{H}_{14}\text{F}_6\text{Na}^+$ [$M+\text{Na}^+$] 748.8601, found 748.8594 (Δ 0.007 ppm).

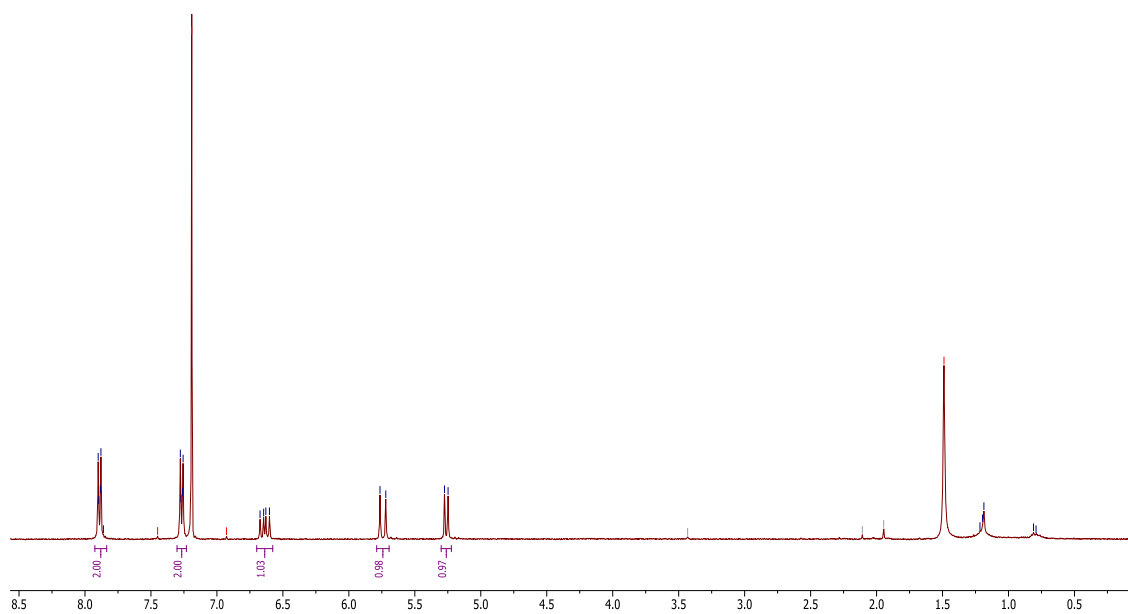


Figure 62: ^1H NMR (400 MHz, Chloroform- d) spectrum of $\text{Rh}_2(4\text{VBA})_2(\text{OAc}^{\text{F}})_2$ (**77**). Singlet at 1.5 ppm is due to water.

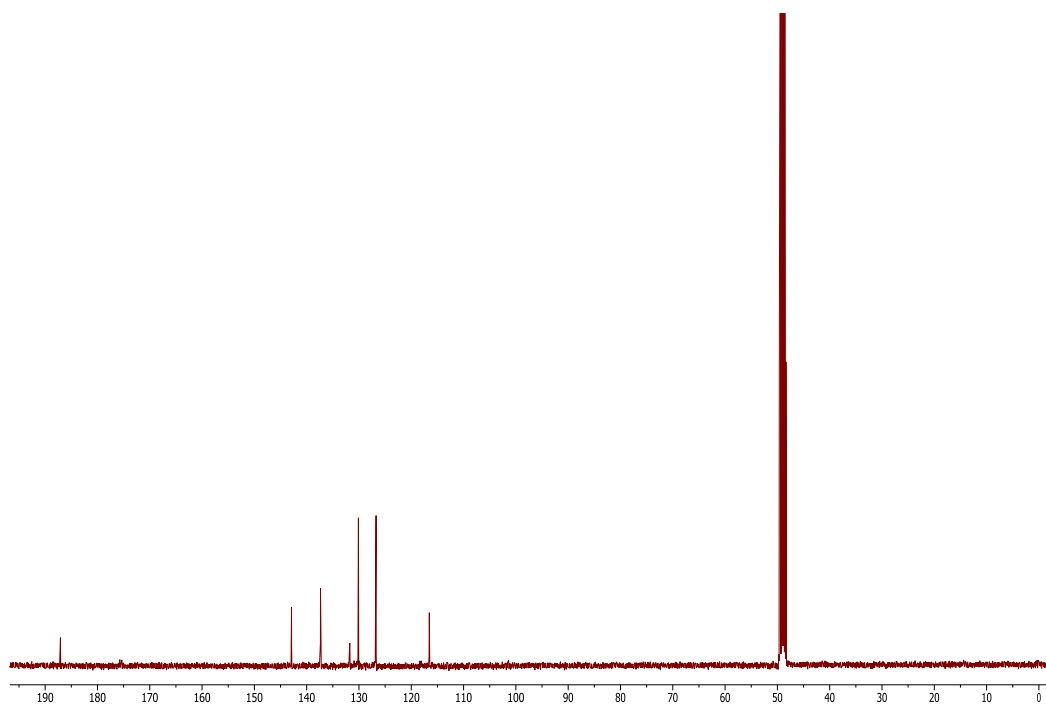
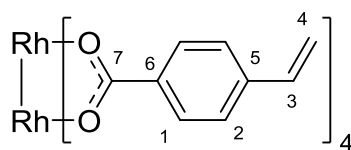


Figure 63: ^{13}C NMR (100 MHz, Methanol- d_4) spectrum of $\text{Rh}_2(4\text{VBA})_2(\text{OAc}^{\text{F}})_2$ (**77**).

7.1.4 Synthesis of $\text{Rh}_2(4\text{VBA})_4$ (Rhodium(II) tetra-4-vinylbenzoate), **75**



75

To a 10 ml round bottom flask was added $\text{Rh}_2(\text{OAc}^{\text{F}})_4$ (20 mg, 0.03 mmol, 1.0 equiv.), 4-vinylbenzoic acid (**71**) (31 mg, 0.21 mmol, 7.0 equiv.), NaHCO_3 (19 mg, 0.18 mmol, 6.0 equiv.), ethyl acetate (3 ml) and refluxed for 3 hours in an oil bath. The dark green-blue solution was washed with saturated NaHCO_3 solution and the organic phase was concentrated in vacuum. The product mixture was purified by column chromatography (EtOAc:hexane/1:2) and gave 20 mg of a green solid product $\text{Rh}_2(4\text{VBA})_4$ in 73% yield.

The purified product was crystallized from acetone/hexane and gave crystals suitable for X-ray diffraction.

^1H NMR (400 MHz, Acetonitrile- d_3) δ 7.77 (d, H-1, $J = 8.2$ Hz, 2H), 7.34 (d, H-2, $J = 8.2$ Hz, 2H), 6.68 (dd, H-3, $J = 17.6, 10.9$ Hz, 1H), 5.79 (dd, H-4, $J = 17.5, 1.1$ Hz, 1H), 5.26 (dd, H-4', $J = 10.9, 1.1$ Hz, 1H).

^{13}C NMR (100 MHz, Acetonitrile- d_3) δ 185.87 (C-7), 141.89 (C-5), 136.81 (C-6), 131.59 (C-2), 129.51 (C-1), 126.61 (C-3), 118.26 (C-4).

^{19}F NMR (188 MHz, Acetonitrile- d_3) No signals detected.

MS (ESI, MeOH) m/z : 817.0 [$M+\text{Na}^+$]

HRMS (MeOH): calculated for $\text{Rh}_2\text{C}_{36}\text{O}_8\text{H}_{28}\text{Na}^+$ [$M+\text{Na}^+$], 816.9792 found 816.9776 (Δ 0.0016 ppm).

FTIR: 1594, 1550 cm^{-1} (COO), 1550 cm^{-1} (C-C stretch aromatics), 1893-1969 cm^{-1} (vinyl group).

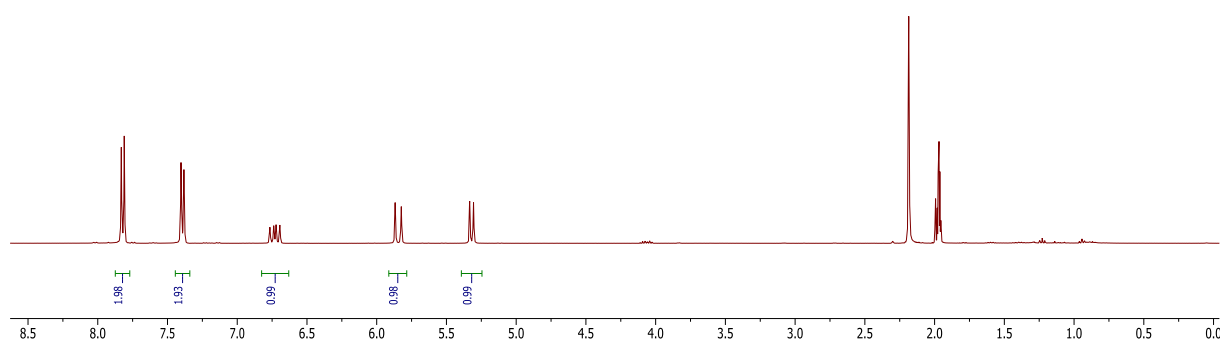


Figure 64: ^1H NMR (400 MHz, Acetonitrile- d_3) spectrum of $\text{Rh}_2(4\text{VBA})_4$ (**75**). Signal at 2.18 ppm is due to coordinated acetone.

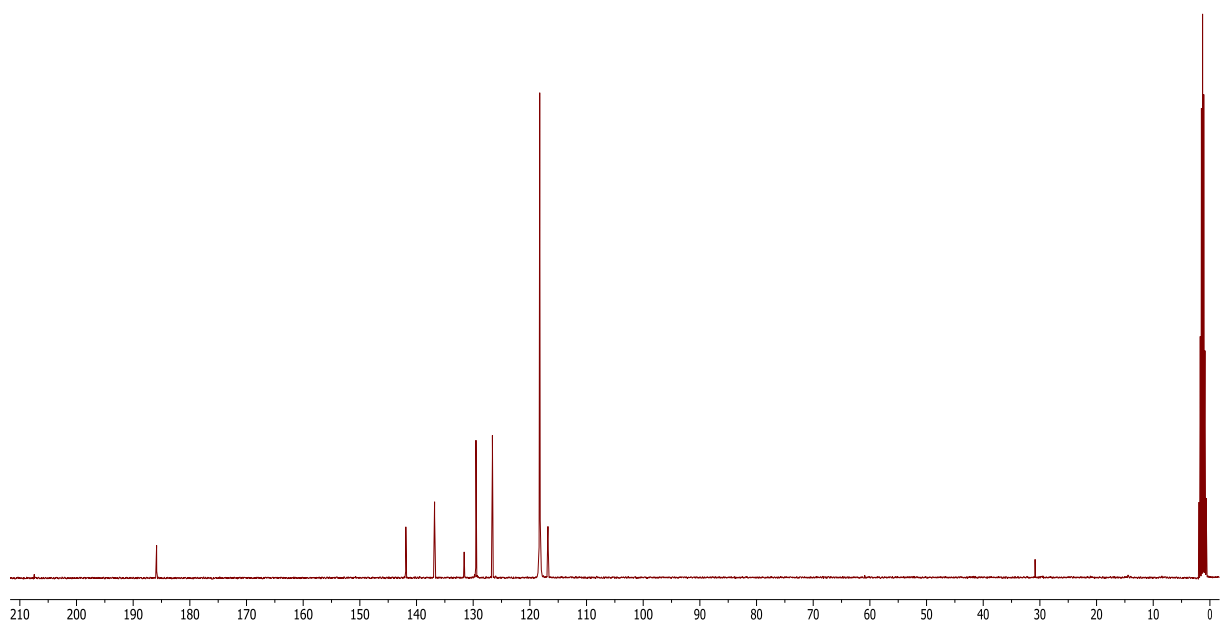
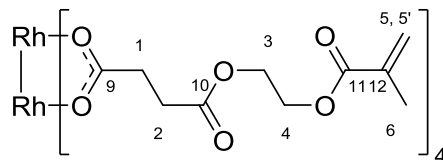


Figure 65: ^{13}C NMR (100 MHz, Acetonitrile- d_3) spectrum of $\text{Rh}_2(4\text{VBA})_4$ (**75**). Signals at 30.84 ppm and 207 ppm are due to coordinated acetone.

7.1.5 Synthesis of Rh₂(MCES)₄ (Rhodium(II) tetra-4-(2-(methacryloyloxy)ethoxy)-4-oxobutanoate), 74



74

To a 10 ml round bottom flask was added Rh₂(OAc)₄ (20 mg, 0.03 mmol, 1.0 equiv.), mono-2-(Methacryloyloxy) ethyl succinate (**68**) (63 mg, 0.27 mmol, 9 equiv.), NaHCO₃ (24 mg, 0.29 mmol, 9 equiv.), CH₂Cl₂ (3 ml) and stirred at ambient temperature for 3 days. The dark green-blue solution was washed with saturated NaHCO₃ solution and the organic phase was concentrated in vacuum. The product mixture was purified by column chromatography (EtOAc:hexane/2:1) and gave 21 mg of a green solid product Rh₂(MCES)₄ in 62 % yield.

¹H NMR (400 MHz, Methanol-*d*₄) δ 6.17 (s, H-5, 1H), 5.72 (s, H-5', 1H), 4.39 – 4.34 (m, H-4, 2H), 4.31 (m, H-3, 2H), 2.54 (m, H-2, 2H), 2.44 (m, H-1, 2H), 1.98 (s, H-6, 3H).

¹³C NMR (100 MHz, Methanol-*d*₄) δ 192.35 (C-9), 173.98 (C-10), 168.52 (C-11), 137.46 (C-12), 126.46 (C-5), 63.83 (C-3), 63.32 (C-4), 32.36 (C-2), 30.60 (C-1), 18.49 (C-6).

¹⁹F NMR (188 MHz, Acetonitrile-*d*₃) No signals detected.

MS (ESI, MeOH) *m/z*: 1145.1 [*M*+Na⁺]

HRMS (MeOH): calculated for Rh₂C₄₀O₂₄H₅₂Na⁺ [*M*+Na⁺] 1145.6272, found 1145.0878 (Δ 0.54 ppm).

FTIR: 1734 cm⁻¹ (COOR ester), 1591 cm⁻¹ (COO⁻).

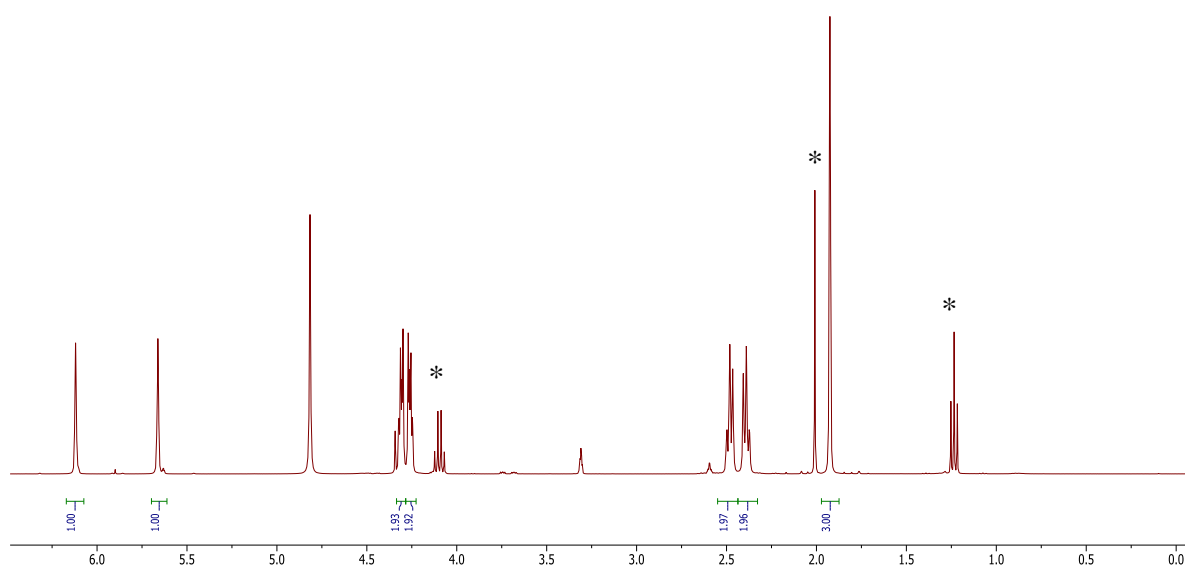


Figure 66: ^1H NMR (400 MHz, Methanol- d_4) spectrum of $\text{Rh}_2(\text{MCES})_4$ (**74**). Coordinated ethyl acetate signals are marked with *.

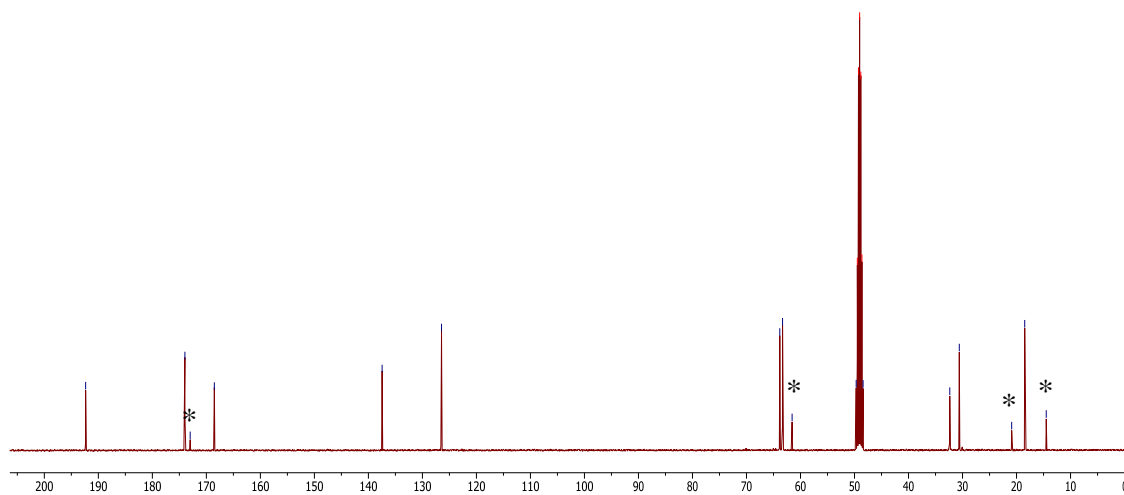
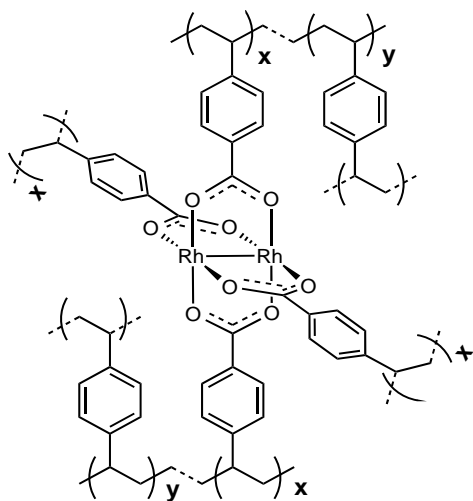


Figure 67: ^{13}C NMR (100 MHz, Methanol- d_4) spectrum of $\text{Rh}_2(\text{MCES})_4$ (**74**). Coordinated ethyl acetate signals are marked with *.

7.1.6 Synthesis of $\text{pol(I)-Rh}_2(4\text{VBA})_4$, 84



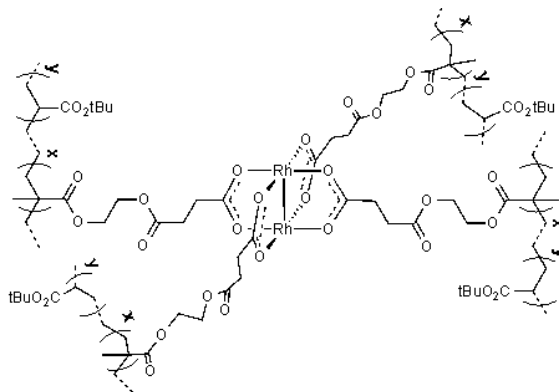
A 25 ml round-bottom flask was charged with styrene (0.6 g, 5.77 mmol) and 1,4-divinylbenzene (0.26 g, 1.972 mmol). In a separate flask $\text{Rh}_2(4\text{VBA})_4$ (**75**), (22 mg, 0.028 mmol) was dissolved in ethyl acetate (0.4 ml). Three drops of acetone were used to increase solubility of the rhodium complex. The mixture was added carefully to the solution of monomers prepared above. To the resulting mixture, 0.5% aqueous polyvinyl alcohol (Mowiol 40-88, 3.5 ml) together with potassium iodide (2 mg) (inhibits polymerization in the aqueous phase) were added. 2,2'-azobisisobutyronitrile (AIBN) (0.008 g, 0.049 mmol) was dissolved in 0.25 ml ethyl acetate and carefully added to the resulting mixture under vigorous stirring. The suspension was polymerized at 85 °C for 4 hours at a constant rate of 1000 rpm.

The suspension was cooled to room temperature and poured into a beaker together with a water/methanol mixture (15/15 ml). The beads were allowed to settle by gravity and the supernatant was decanted off. The polymer beads were filtered, washed with water and dichloromethane and dried at room temperature to give 0.8 g of glassy, light-green polymer beads in 93% yield. The filtrate was extracted with dichloromethane and the organic layer was dried in vacuum. NMR of the residue showed absence of signals for the rhodium ligands which indicates the 100 % incorporation of the rhodium monomer **75**.

Swelling's test: the polymer beads were suspended in CH_2Cl_2 and no visible swelling was observed.

Microscopic and SEM/TEM pictures as well as IR spectrum can be found in the appendix (Figures 92, 104, 111 and 112).

7.1.8 Synthesis of $\text{pol}(\text{I})\text{-Rh}_2(\text{MCES})_4$, **85**



A 25 ml round-bottom flask was charged with $\text{Rh}_2(\text{MCES})_4$ (**74**) (28 mg, 0.025 mmol), *tert*-butyl acrylate (0.6 g, 4.68 mmol), pentaerythritol tetraacrylate (**82**) (0.28 g, 0.80 mmol) and ethyl acetate (0.8 ml). Three drops of acetone were used to increase solubility of the rhodium complex.

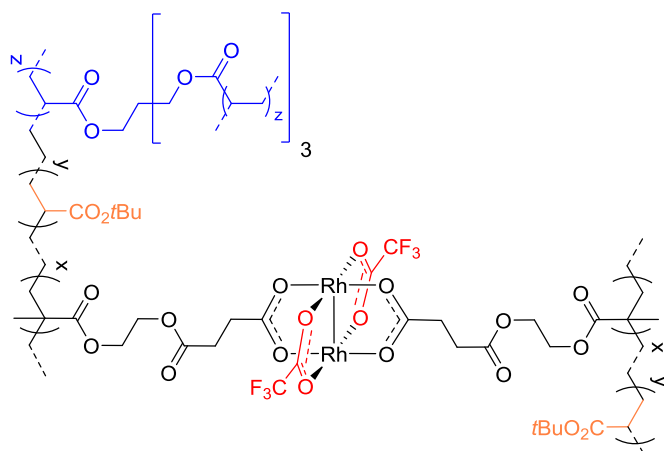
To the resulting mixture, 0.5% aqueous polyvinyl alcohol (Mowiol 40-88, 3.5 ml) together with potassium iodide (2 mg) (inhibits polymerization in the aqueous phase) were added. 2,2'-azobisisobutyronitrile (AIBN) (0.008 g, 0.049 mmol) was dissolved in 0.25 ml ethyl acetate and carefully added to the resulting mixture under vigorous stirring. The suspension was polymerized at 85 °C for 1 hour at a constant rate of 1000 rpm.

The suspension was cooled to room temperature and poured into a beaker together with a water/methanol (15/15 ml). The beads were allowed to settle by gravity and the supernatant was decanted off. The polymer beads were filtered, washed with water and dichloromethane and dried at room temperature to give 0.78 g of glassy, blue-green polymer beads in 89% yield. The filtrate was extracted with dichloromethane and the organic layer was dried in vacuum. NMR of the residue showed absence of signals for the rhodium ligands which indicates the 100 % incorporation of the rhodium monomer **74**.

Swelling's test: the polymer beads were suspended in CH_2Cl_2 and no visible swelling was observed.

Microscopic and SEM/TEM pictures as well as IR spectrum can be found in the appendix (Figures 93, 105, 113 and 114).

7.1.9 Synthesis of $\text{pol}(\text{I})\text{-Rh}_2(\text{MCES})_2(\text{OAc}^{\text{F}})_2$, **86**



A 25 ml round-bottom flask was charged with $\text{Rh}_2(\text{MCES})_2(\text{OAc}^{\text{F}})_2$ (**78**) (25 mg, 0.028 mmol), *tert*-butyl acrylate (0.6 g, 4.68 mmol), pentaerythritol tetraacrylate (**82**) (0.27 g, 0.77 mmol) and ethyl acetate (0.8 ml). Three drops of acetone were used to increase solubility of the rhodium complex. To the resulting mixture, 0.5% aqueous

polyvinyl alcohol (Mowiol 40-88, 3.5 ml) together with potassium iodide (2 mg) (inhibits polymerization in the aqueous phase) were added. 2,2'-azobisisobutyronitrile (AIBN) (0.008 g, 0.049 mmol) was dissolved in 0.25 ml ethyl acetate and carefully added to the resulting mixture under vigorous stirring. The suspension was polymerized at 85 °C for 1 hour at a constant rate of 1000 rpm.

The suspension was cooled to room temperature and poured into a beaker together with a water/methanol (15/15 ml). The beads were allowed to settle by gravity and the supernatant was decanted off. The polymer beads were filtered, washed with water and dichloromethane and dried at room temperature to give 0.8 g of glassy, blue-green polymer beads in a 92% yield. The filtrate was extracted with dichloromethane and the organic layer was dried in vacuum. NMR of the residue showed absence of signals for the rhodium ligands which indicates the 100 % incorporation of the rhodium monomer **78**.

Swelling's test: the polymer beads were suspended in CH_2Cl_2 and no visible swelling was observed.

Microscopic and SEM/TEM pictures as well as IR spectrum can be found in the appendix (Figures 94, 106, 115 and 116).

Table 16: Components for suspension polymerization of styrene system – Generation I.

Component	pol(I)-Rh ₂ (4VBA) ₄	pol(I)-Rh ₂ (4VBA) ₂ (OAc ^F) ₂
Mowiol 40-80 (0.5 w%)	3.5 ml	3.5 ml
Ethyl Acetate	0.65 ml	0.75 ml
AIBN	0.008 g	0.008 g
Styrene (79)	0.6 g (5.77 mmol)	0.6 g (5.77 mmol)
Divinylbenzene (81) + rhodium(II) carboxylate	2 mmol (26 mmol% of styrene+cross-linker+cat.)	2 mmol (26 mmol% of styrene+cross-linker+cat.)
KI	2 mg	2 mg
Rotation speed	1000 rpm	1000 rpm
Temperature	85°C	85°C
Degree of cross-linking	26 %	26 %

$$\text{Catalyst loading (pol(I)-Rh}_2\text{(4VBA)}_4) = \frac{n(\text{rhodium(II)carboxylate})}{m(\text{synthetized polymer})} = \frac{0.028 \text{ mmol}}{0.8 \text{ g}} = 0.035 \text{ mmol/g}$$

$$\text{Catalyst loading (pol(I)-Rh}_2\text{(4VBA)}_2\text{(OAc}^F\text{)}_2) = \frac{n(\text{rhodium(II)carboxylate})}{m(\text{synthetized polymer})} = \frac{0.041 \text{ mmol}}{0.8 \text{ g}} = 0.0513 \text{ mmol/g}$$

$$\begin{aligned} \text{Degree of cross-linking (pol(I)-Rh}_2\text{(4VBA)}_4) &= \frac{n(\text{cross-linker})+n(\text{rhodium(II) carboxylate})}{n(\text{cross-linker})+n(\text{rhodium(II) carboxylate})+n(\text{styrene})} = \\ &= \frac{n(\text{divinylbenzene})+n(\text{Rh}_2\text{(4VBA)}_4)}{n(\text{divinylbenzene})+n(\text{Rh}_2\text{(4VBA)}_4)+n(\text{styrene})} = \frac{1.972 \text{ mmol} + 0.028 \text{ mmol}}{1.972 \text{ mmol} + 0.028 \text{ mmol} + 5.77 \text{ mmol}} = 0.26 ; 26\% \end{aligned}$$

$$\begin{aligned} \text{Degree of cross-linking (pol(I)-Rh}_2\text{(4VBA)}_2\text{(OAc}^F\text{)}_2) &= \frac{n(\text{cross-linker})+n(\text{rhodium(II) carboxylate})}{n(\text{cross-linker})+n(\text{rhodium(II) carboxylate})+n(\text{styrene})} = \\ &= \frac{n(\text{divinylbenzene})+n(\text{Rh}_2\text{(4VBA)}_2\text{(OAc}^F\text{)}_2)}{n(\text{divinylbenzene})+n(\text{Rh}_2\text{(4VBA)}_2\text{(OAc}^F\text{)}_2)+n(\text{styrene})} = \frac{1.95 \text{ mmol} + 0.041 \text{ mmol}}{1.95 \text{ mmol} + 0.041 \text{ mmol} + 5.77 \text{ mmol}} = \\ &0.26 ; 26\% \end{aligned}$$

Table 17: Components for suspension polymerization of acrylic system – Generation I.

Component	pol(I)-Rh ₂ (MCES) ₄	pol(I)-Rh ₂ (MCES) ₂ (OAc ^F) ₂
Mowiol 40-80 (0.5 w%)	3.5 ml	3.5 ml
Ethyl Acetate	1.05 ml	1.05 ml
AIBN	0.008 g	0.008 g
<i>tert</i> -butyl acrylate (80)	0.6 g (4.68 mmol)	0.6 g (4.68 mmol)
pentaerythritol tetraacrylate (82) + rhodium(II) carboxylate	0.825 mmol (15 mmol% of styrene+cross-linker+cat.)	0.798 mmol (15 mmol% of styrene+cross-linker+cat.)
KI	2 mg	2 mg
Rotation speed	1000 rpm	1000 rpm
Temperature	85°C	85°C
Degree of cross-linking	15 %	15 %

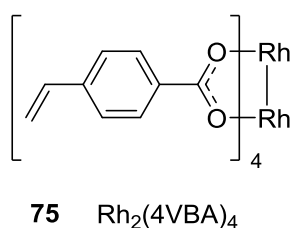
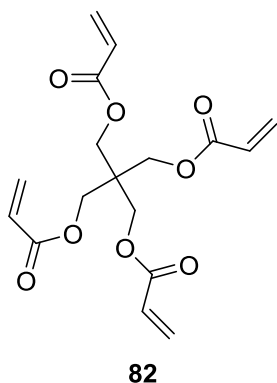
$$\text{Catalyst loading (pol(I)-Rh}_2\text{(MCES)}_4) = \frac{n(\text{rhodium(II)carboxylate})}{m(\text{synthetized polymer})} = \frac{0.025 \text{ mmol}}{0.78 \text{ g}} = 0.032 \text{ mmol/g}$$

$$\text{Catalyst loading (pol(I)-Rh}_2\text{(MCES)}_2\text{(OAc}^F\text{)}_2) = \frac{n(\text{rhodium(II)carboxylate})}{m(\text{synthetized polymer})} = \frac{0.028 \text{ mmol}}{0.8 \text{ g}} = 0.035 \text{ mmol/g}$$

$$\begin{aligned} \text{Degree of cross-linking (pol(I)-Rh}_2\text{(MCES)}_4) &= \\ \frac{n(\text{cross-linker})+n(\text{rhodium(II) carboxylate})}{n(\text{cross-linker})+n(\text{rhodium(II) carboxylate})+n(\text{acrylate})} &= \frac{n(\mathbf{82})+n(\text{Rh}_2(\text{MCES})_4)}{n(\mathbf{82})+n(\text{Rh}_2(\text{MCES})_4)+n(\text{acrylate})} = \\ \frac{0.8 \text{ mmol} + 0.025 \text{ mmol}}{0.8 \text{ mmol} + 0.025 \text{ mmol} + 4.68 \text{ mmol}} &= 0.15 ; 15\% \end{aligned}$$

$$\begin{aligned} \text{Degree of cross-linking (pol(I)-Rh}_2\text{(4VBA)}_2\text{(OAc}^F\text{)}_2) &= \\ \frac{n(\text{cross-linker})+n(\text{rhodium(II) carboxylate})}{n(\text{cross-linker})+n(\text{rhodium(II) carboxylate})+n(\text{acrylate})} &= \frac{n(\mathbf{82})+n(\text{Rh}_2(\text{MCES})_2(\text{OAc}^F)_2)}{n(\mathbf{82})+n(\text{Rh}_2(\text{MCES})_2(\text{OAc}^F)_2)+n(\text{acrylate})} = \\ \frac{0.77 \text{ mmol} + 0.028 \text{ mmol}}{0.77 \text{ mmol} + 0.028 \text{ mmol} + 4.68 \text{ mmol}} &= 0.15 ; 15\% \end{aligned}$$

7.1.10 Synthesis of $\text{pol(II)-Rh}_2(4\text{VBA})_4$, **88**



A 25 ml round-bottom flask was charged with styrene (0.6 g, 5.77 mmol) and pentaerythritol tetraacrylate (**82**) (81 mg, 0.23 mmol). A separate flask was charged with $\text{Rh}_2(4\text{VBA})_4$ (**75**), (45 mg, 0.057 mmol) and ethyl acetate (1 ml). Five drops of acetone were added to increase the solubility of the rhodium complex. The resulting mixture was carefully added to the solution of monomers prepared above.

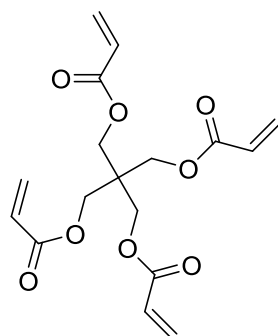
The resulting solution was combined with 0.5% aqueous polyvinyl alcohol (Mowiol 40-88, 3.5 ml) and 1 mg potassium iodide (inhibits polymerization in the aqueous phase). 2,2'-azobisisobutyronitrile (AIBN) (0.008 g, 0.049 mmol) was dissolved in ethyl acetate (0.5 ml) and carefully added to the combined mixture under vigorous stirring. The suspension was polymerized at 85 °C for 1.5 hours at a constant rate of 1000 rpm.

The suspension was cooled to room temperature and poured into a beaker together with a water/methanol (15/15 ml). The beads were allowed to settle by gravity and the supernatant was decanted off. The polymer beads were filtered, washed with water and dichloromethane and dried at room temperature to give 0.36 g of blue-green polymer beads in a 50 % yield.

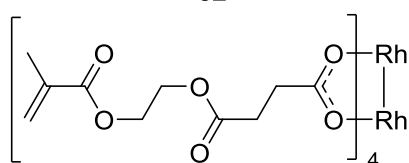
Swelling's test: the polymer beads were suspended in CH_2Cl_2 and significant swelling was observed. The degree of swelling was measured to be 100%.

Microscopic and SEM/TEM pictures as well as IR spectrum can be found in the appendix (Figures 97, 109, 121 and 122).

7.1.11 Synthesis of $\text{pol(II)-Rh}_2(\text{MCES})_4$, **87**



82



74 $\text{Rh}_2(\text{MCES})_4$

A 25 ml round-bottom flask was charged with styrene (0.6 g, 5.77 mmol) and pentaerythritol tetraacrylate (**82**) (95 mg, 0.27 mmol). A separate flask was charged with $\text{Rh}_2(\text{MCES})_4$ (**74**), (16 mg, 0.014 mmol) and ethyl acetate (1 ml). Five drops of acetone were added to increase the solubility of the rhodium complex. The mixture was carefully added to the solution of monomers prepared above.

The resulting solution was combined with 0.5% aqueous polyvinyl alcohol (Mowiol 40-88, 3.5 ml) and 1 mg potassium iodide (inhibits polymerization in the aqueous phase). 2,2'-azobisisobutyronitrile (AIBN) (0.008 g, 0.049 mmol) was dissolved in ethyl acetate (0.5 ml) and carefully added to the combined mixture under vigorous stirring. The suspension

was polymerized at 85 °C for 1.5 hours at a constant rate of 1000 rpm.

The suspension was cooled to room temperature and poured into a beaker together with water/methanol (15/15 ml). The beads were allowed to settle by gravity and the supernatant was decanted off. The polymer beads were filtered, washed with water and dichloromethane and dried at room temperature to give 0.36 g of blue polymer beads in a 51 % yield.

Swelling's test: the polymer beads were suspended in CH_2Cl_2 and significant swelling was observed. The degree of swelling was measured to be 120%.

Microscopic and SEM/TEM pictures as well as IR spectrum can be found in the appendix (Figures 96, 108, 119 and 120).

Table 18: Components for suspension polymerization of mixed system – Generation II

Component	pol(II)-Rh ₂ (MCES) ₄	pol(II)-Rh ₂ (4VBA) ₄
Mowiol 40-80 (0.5 w%)	3.5 ml	3.5 ml
Ethyl Acetate	1.5 ml	1.5 ml
AIBN	0.008 g	0.008 g
Styrene (79)	5.77 mmol	5.77 mmol
Pentaerythritol tetraacrylate (82) + rhodium(II) carboxylate	0.284 mmol	0.287 mmol
KI	2 mg	2 mg
Rotation speed	1000 rpm	1000 rpm
Temperature	85°C	85°C
Degree of cross-linking	5%	5 %

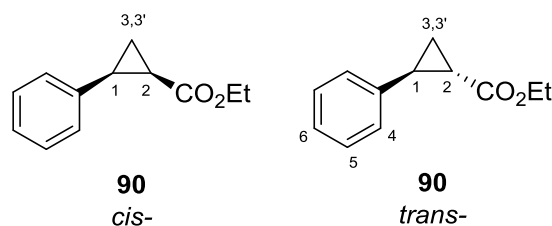
$$\text{Catalyst loading (pol(II)-Rh}_2\text{(MCES)}_4) = \frac{n(\text{rhodium(II)carboxylate})}{m(\text{synthetized polymer})} = \frac{0.014 \text{ mmol}}{0.36 \text{ g}} = 0.039 \text{ mmol/g}$$

$$\text{Catalyst loading (pol(II)-Rh}_2\text{(4VBA)}_4) = \frac{n(\text{rhodium(II)carboxylate})}{m(\text{synthetized polymer})} = \frac{0.057 \text{ mmol}}{0.36 \text{ g}} = 0.158 \text{ mmol/g}$$

$$\begin{aligned} \text{Degree of cross-linking (pol(I)-Rh}_2\text{(MCES)}_4) &= \\ \frac{n(\text{cross-linker})+n(\text{rhodium(II) carboxylate})}{n(\text{cross-linker})+n(\text{rhodium(II) carboxylate})+n(\text{styrene})} &= \frac{n(82)+n(\text{Rh}_2(\text{MCES})_4)}{n(82)+n(\text{Rh}_2(\text{MCES})_4)+n(\text{styrene})} = \\ \frac{0.27 \text{ mmol} + 0.014 \text{ mmol}}{0.27 \text{ mmol} + 0.014 \text{ mmol} + 5.77 \text{ mmol}} &= 0.05 ; 5\% \end{aligned}$$

$$\begin{aligned} \text{Degree of cross-linking (pol(I)-Rh}_2\text{(4VBA)}_4) &= \\ \frac{n(\text{cross-linker})+n(\text{rhodium(II) carboxylate})}{n(\text{cross-linker})+n(\text{rhodium(II) carboxylate})+n(\text{styrene})} &= \frac{n(82)+n(\text{Rh}_2(4\text{VBA})_4)}{n(\text{XX})+n(\text{Rh}_2(4\text{VBA})_4)+n(\text{styrene})} = \\ \frac{0.23 \text{ mmol} + 0.057 \text{ mmol}}{0.23 \text{ mmol} + 0.057 \text{ mmol} + 5.77 \text{ mmol}} &= 0.05 ; 5\% \end{aligned}$$

7.1.12 General procedure for intermolecular cyclopropanation of styrene with EDA, catalyzed by rhodium(II) tetraacetate (5)



A 50 ml round-bottomed flask equipped with a stir bar was charged with $\text{Rh}_2(\text{OAc})_4$ (**5**) (4 mg, 0.009 mmol, 1 mol% of EDA) and styrene (0.456 g, 4.38 mmol, 5 equiv.) in CH_2Cl_2 (6 ml). A mixture of ethyl diazoacetate (0.10 g, 0.88 mmol, 1 equiv.) in CH_2Cl_2 (12 ml) was added dropwise under vigorous stirring for 35 min. After stirring for additional 1 hour, the volatiles were removed in vacuum. The crude product was purified by silica column chromatography (EtOAc:hexane/1:10) to obtain the final product as a mixture of diastereomers. Both are known compounds and the NMR data agreed with the data in the literature.¹³⁷

Further, no isolation of products was performed. Yields were measured by NMR using an internal standard.

***trans*-2-Phenylcyclopropane-1-carboxylic acid ethyl ester:** ^1H NMR (300 MHz, Chloroform-*d*) δ 7.35 – 7.26 (m, H-4, 2H), 7.26 – 7.21 (m, H-6, 1H), 7.16 – 7.09 (m, H-5, 2H), 4.20 (q, $-\text{CH}_2\text{CH}_3$, $J = 7.1$ Hz, 2H), 2.61 – 2.48 (m, H-2, 1H), 1.98 – 1.89 (m, H-1, 1H), 1.68 – 1.57 (m, H-3, 1H), 1.39 – 1.25 (m, H-3', $-\text{CH}_2\text{CH}_3$, 4H).

***cis*-2-Phenylcyclopropane-1-carboxylic acid ethyl ester:** ^1H NMR (300 MHz, Chloroform-*d*) δ 7.38 – 7.15 (m, Ph-, 5H), 3.89 (q, $-\text{CH}_2\text{CH}_3$, $J = 7.1$ Hz, 2H), 2.68 – 2.54 (m, H-2, 1H), 2.17 – 2.03 (m, H-1, 1H), 1.79 – 1.68 (m, H-3, 1H), 1.41 – 1.25 (m, H-3', 1H), 0.99 (t, $-\text{CH}_2\text{CH}_3$, $J = 7.1$ Hz, 3H).

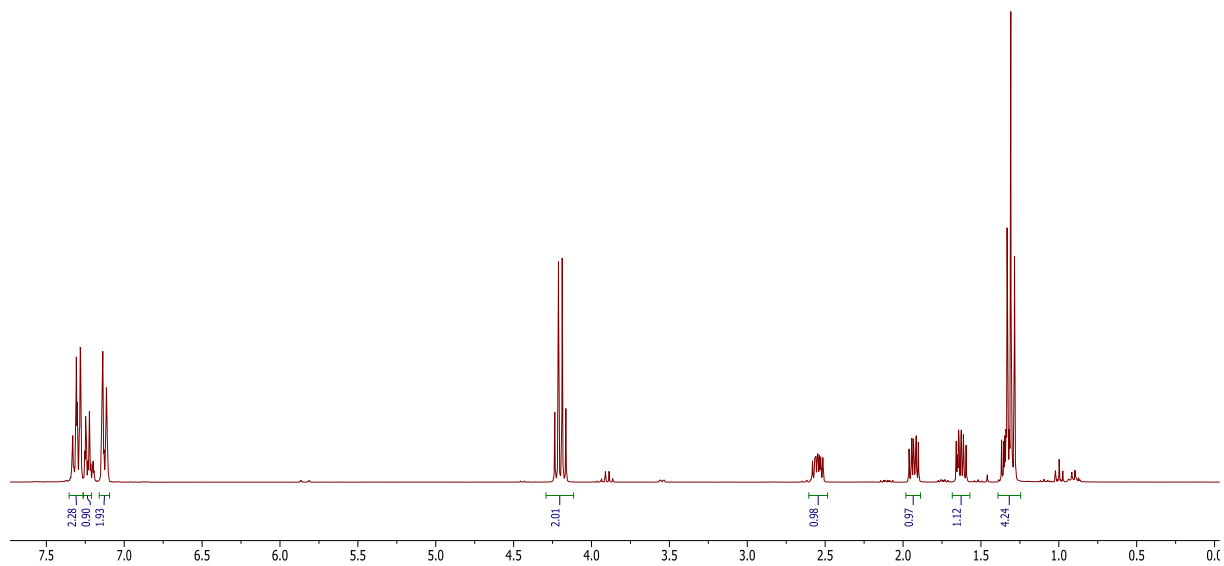


Figure 68: ^1H NMR (300 MHz, Chloroform-*d*) spectrum of *trans*-2-Phenylcyclopropane-1-carboxylic acid ethyl ester (**90**).

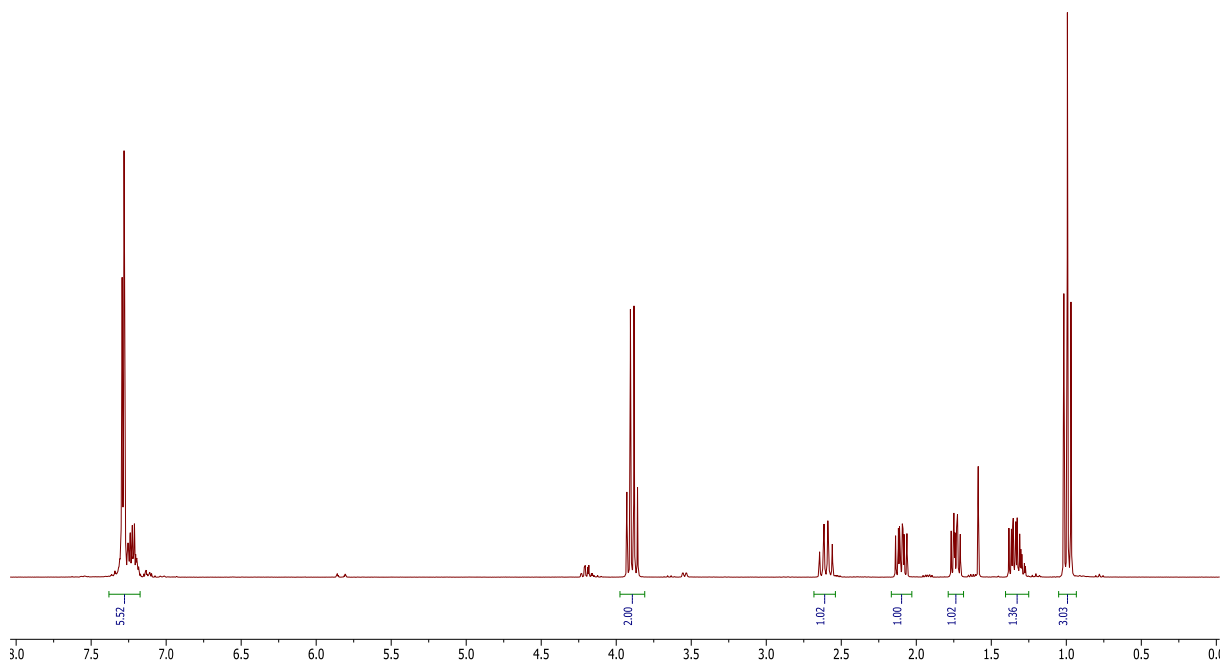


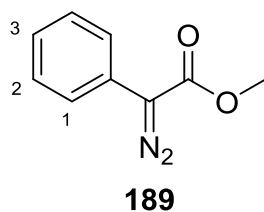
Figure 69: ^1H NMR (300 MHz, Chloroform-*d*) spectrum of *cis*-2-Phenylcyclopropane-1-carboxylic acid ethyl ester (**90**).

7.1.13 General procedure for intermolecular cyclopropanation of styrene with EDA, catalyzed by heterogenized Rh-containing polymers.

A 50 ml round-bottomed flask equipped with a stirring bar was charged with Rh-containing polymer beads (1 mol% with respect to ethyl diazoacetate) in CH_2Cl_2 (3 ml) and left stirring for 30 min for pre-swelling. A solution of ethyl diazoacetate (0.10 g, 0.88 mmol, 1 equiv.) in CH_2Cl_2 (12 ml) was added dropwise under vigorous stirring for 35 min. After stirring for additional 1 hour, the polymeric catalyst was recovered by filtration and mesitylene (122 μl , 0.88 mmol, 1.0 equiv.) was added to the reaction filtrate. A small fraction of reaction mixture was then concentrated under reduced pressure. The yield and the *trans/cis* ratio were determined from the NMR analysis.

The selected NMR spectrum of the analyzed reaction crude is given in the appendix as an example (Figure 127).

7.1.14 Synthesis of Methyl 2-diazo-2-phenylacetate, ¹³⁸ 189



To the methyl 2-(4-chlorophenyl)acetate (1 g, 6.7 mmol, 1 equiv.) in CH₃CN (5 ml) was added p-ABSA (1.26 g, 7.3 mmol, 1.1 equiv.) and the mixture was stirred at room temperature. The flask was cooled to 0°C under argon and DBU (1.8 ml, 12 mmol, 1.8 equiv.) was added in one portion. The flask was warmed to room temperature and stirred for two hours. The reaction mixture was quenched with a saturated solution of ammonium chloride and the aqueous layer was extracted with diethyl ether (2x10 ml). The combined organic layers were dried over MgSO₄ and concentrated under reduced pressure. Purification through column with silica gel gave 1 g product, as red oil, in 86% yield. This is a known compound and the NMR data agreed with the data in the literature.¹³⁸

¹H NMR (400 MHz, Chloroform-*d*) δ 7.51 (d, H-1, *J* = 7.6 Hz, 2H), 7.45 – 7.37 (m, H-2, 2H), 7.21 (t, H-3, *J* = 7.7, 6.8 Hz, 1H), 3.89 (s, -OMe, 3H).

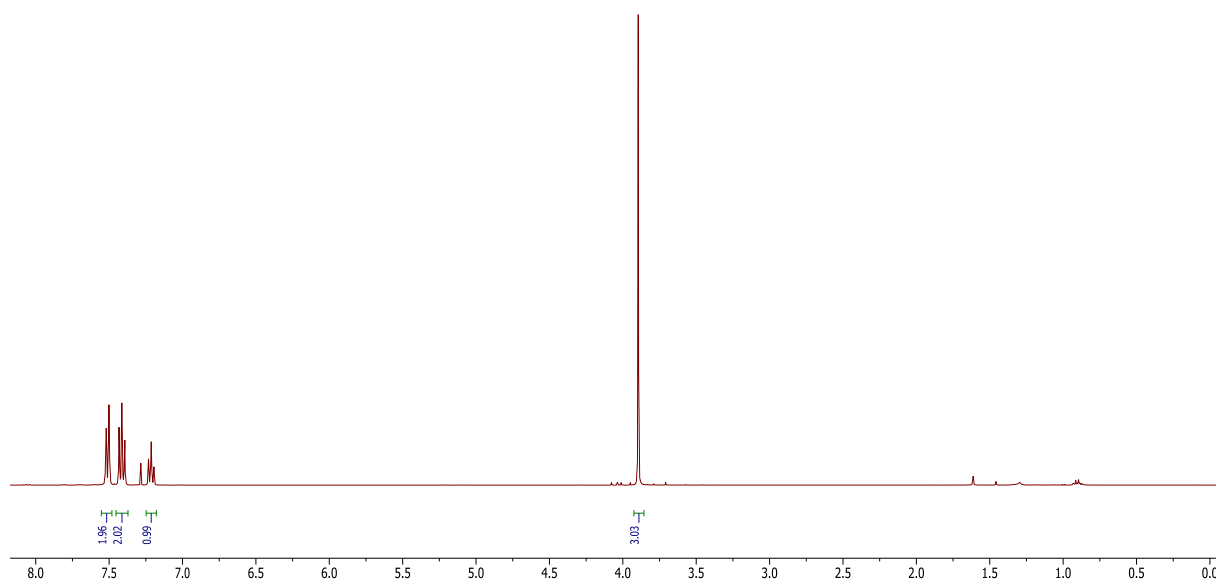
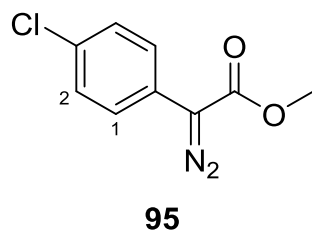


Figure 70: ¹H NMR (400 MHz, Chloroform-*d*) spectrum of methyl 2-diazo-2-phenylacetate (**189**).

7.1.15 Synthesis of Methyl 2-(4-chlorophenyl)-2-diazoacetate,⁴⁴ 95



To the methyl phenylacetate (1 g, 6.7 mmol, 1 equiv.) in CH₃CN (5 ml) was added p-ABSA (1.26 g, 7.3 mmol, 1.1 equiv.) and the mixture was stirred at room temperature. The flask was cooled to 0°C under Argon and DBU (1.8 ml, 12 mmol, 1.8 equiv.) was added in one portion. The flask was warmed to room temperature and stirred for two hours. The reaction mixture was quenched with saturated solution of ammonia chloride and aqueous layer was extracted with diethyl ether (2x10 ml). The combined organic layers were dried over MgSO₄, and concentrated under reduced pressure. Purification through column with silica gel gave 0.784 g product, as orange solid, in 56% yield. This is a known compound and the NMR data agreed with the data in the literature.⁴⁴

¹H NMR (300 MHz, Chloroform-*d*) δ 7.51 – 7.40 (m, H-1, 2H), 7.40 – 7.32 (m, H-2, 2H), 3.89 (s, -CH₃, 3H).

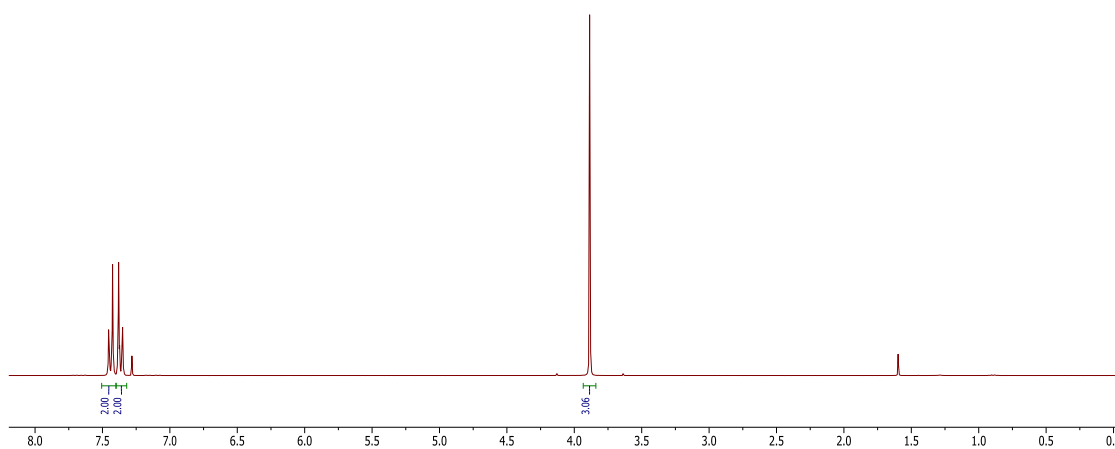
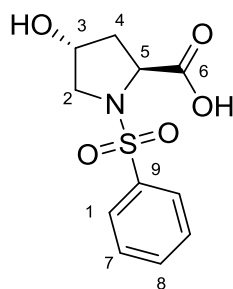


Figure 71: ¹H NMR (400 MHz, Chloroform-*d*) spectrum of methyl 2-(4-chlorophenyl)-2-diazoacetate (95).

7.1.16 Synthesis of (2*S*,4*R*)-4-hydroxy-1-(phenylsulphonyl)pyrrolidine-2-carboxylic acid, **100**



100

A 100 ml round-bottom flask was charged with *trans*-4-hydroxy-L-proline (1 g, 7.63 mmol, 1 equiv.), potassium carbonate (2.32 g, 16.8 mmol, 2.2 equiv.) in water (50 ml) and heated to 50°C. After dissolving, benzenesulfonyl chloride (1.62 g, 9.18 mmol, 1.2 equiv) was added and the reaction mixture was left stirring overnight. To the reaction mixture an aqueous solution of HCl (to pH=3) was added and extracted with EtOAc. The organic phase was dried over MgSO₄. Evaporation of EtOAc in vacuum resulted in 1.3 g viscous liquid of the product **100** in 63% yield.

¹H NMR (300 MHz, Methanol-*d*₄) δ 7.94 – 7.83 (m, H-1, 2H), 7.72 – 7.52 (m, Ph-, 3H), 4.33 (m, H-3, 1H), 4.26 (t, H-5, *J* = 7.9 Hz, 1H), 3.58 (dd, H-2, *J* = 10.9, 4.1 Hz, 1H), 3.31 (m, H-2', 2H), 2.09 (m, H-4, 2H).

¹³C NMR (100 MHz, Acetone-*d*₆) δ 207.45 (C-6), 138.65 (C-9), 133.52 (C-1), 129.67 (C-7), 128.32 (C-8), 70.02 (C-3), 57.17 (C-5), 39.95 (C-2), 30.59 (C-4).

MS (ESI, MeOH) *m/z*: 294.0 [*M*+Na⁺]

HRMS (MeOH): calculated for C₁₁O₅H₁₃NSNa⁺ [*M*+Na⁺] 294.2796, found 294.2801 (Δ 0.0005).

FTIR: O-H (-OH group) stretch (3407 cm⁻¹), O-H (-COOH group) (2600-3100 cm⁻¹), C=O stretch (1715 cm⁻¹)

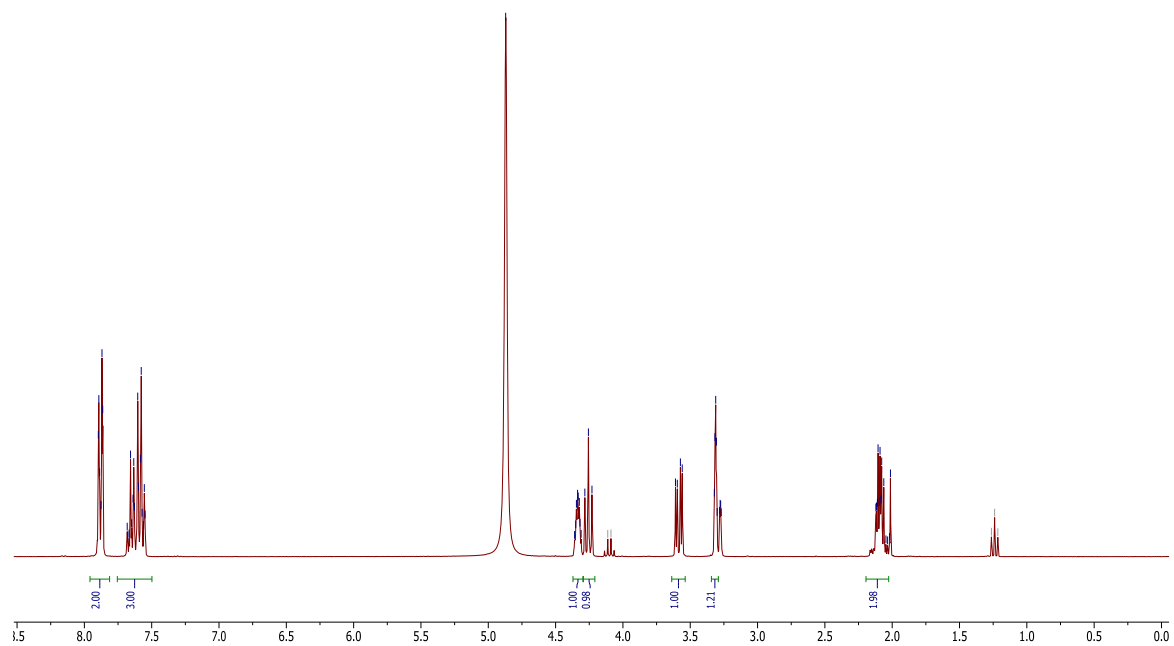


Figure 72: ^1H NMR (300 MHz, Methanol- d_4) spectrum of **100**. Extra signals are due to ethyl acetate residue.

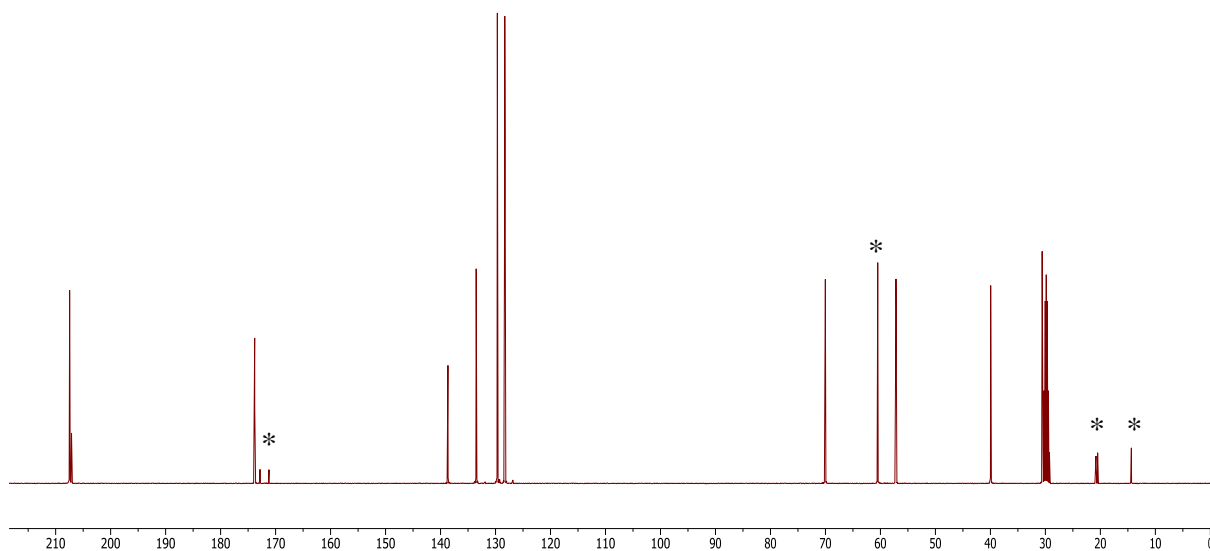
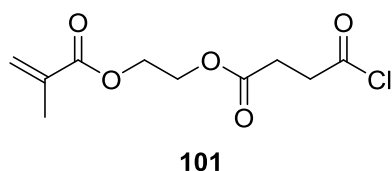
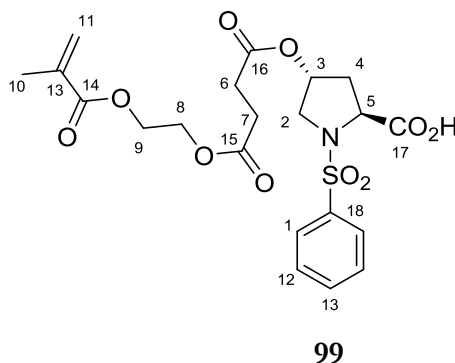


Figure 73: ^{13}C NMR (100 MHz, Acetone- d_6) spectrum of **100**. Ethyl acetate signals are marked with *.

7.1.17 Synthesis of (2*S*,4*R*)-4-((4-(2-(methacryloyloxy)ethoxy)-4-oxobutanoyl)oxy)-1-(phenylsulfonyl)pyrrolidine-2-carboxylic acid, **99**



A 10 ml round-bottom flask was charged with mono-2-(Methacryloyloxy) ethyl succinate (**68**) (1.388 g, 6.035 mmol, containing 750 ppm MEHQ) in neat SOCl₂ (2.4 ml). The mixture was stirred at the room temperature for 30 min and at

50°C for 1 hour. The excess SO₂Cl₂ was removed in vacuum and 2-methacryloyloxyethylsuccinyl chloride was obtained in a quantitative yield. This is a well-known compound¹³⁹.

A round bottom flask was charged with **100** (828 mg, 3.05 mmol), CH₂Cl₂ (3 ml) and TFA (3 ml) under vigorous stirring. The mixture was stirred for 30 min, the crude methacrylic acid chloride **101** was added, and the reaction mixture was stirred at room temperature for 24 hours. The volatile components were removed under reduced pressure to give a nearly colorless, syrupy solution. Column chromatography on silica gel with CH₂Cl₂/CH₃OH/CH₃COOH (90%/5%/5%) gave 649 mg of **99**, as colorless oil (yield 44%).

¹H NMR (300 MHz, Chloroform-*d*) δ 7.97 – 7.78 (m, H-1, 2H), 7.68 – 7.40 (m, H-12, H-13, 3H), 6.17 – 6.00 (s, H-11, 1H), 5.62 – 5.47 (s, H-11', 1H), 5.20 – 5.07 (m, H-3, 1H), 4.41 – 4.20 (m, H-8, H-9, H-5, 5H), 3.68 (dd, H-2, *J* = 12.5, 3.8 Hz, 1H), 3.51 (d, H-2', *J* = 12.5 Hz, 1H), 2.53 – 2.01 (m, H-6, H-7, H-4, 7H), 1.89 (s, H-10, 3H).

¹³C NMR (100 MHz, Chloroform-*d*) δ 175.69 (C-14), 172.28 (C-17), 168.28 (C-15), 167.62 (C-16), 137.82 (C-11), 136.30 (C-13), 133.61 (C-18), 129.62 (C-1), 128.15 (C-12), 126.64 (C-13), 73.33 (C-3), 66.77 (C-5), 62.99 (C-8), 62.77 (C-9), 61.72 (C-2), 54.50 (C-6), 39.68 (C-7), 37.07 (C-4), 28.98 (C-10).

MS (ESI, MeOH) *m/z*: 506.1 [*M*+Na⁺]

HRMS (MeOH): calculated for C₂₁O₁₀H₂₅NSNa⁺ [*M*+Na⁺] 506.4793, found 506.4803 (Δ 0.001).

FTIR: 2500-3100 cm^{-1} (Aromatic C-H stretch and O-H stretch), 1710-1730 cm^{-1} (COOR), 2975 cm^{-1} (vinyl group).

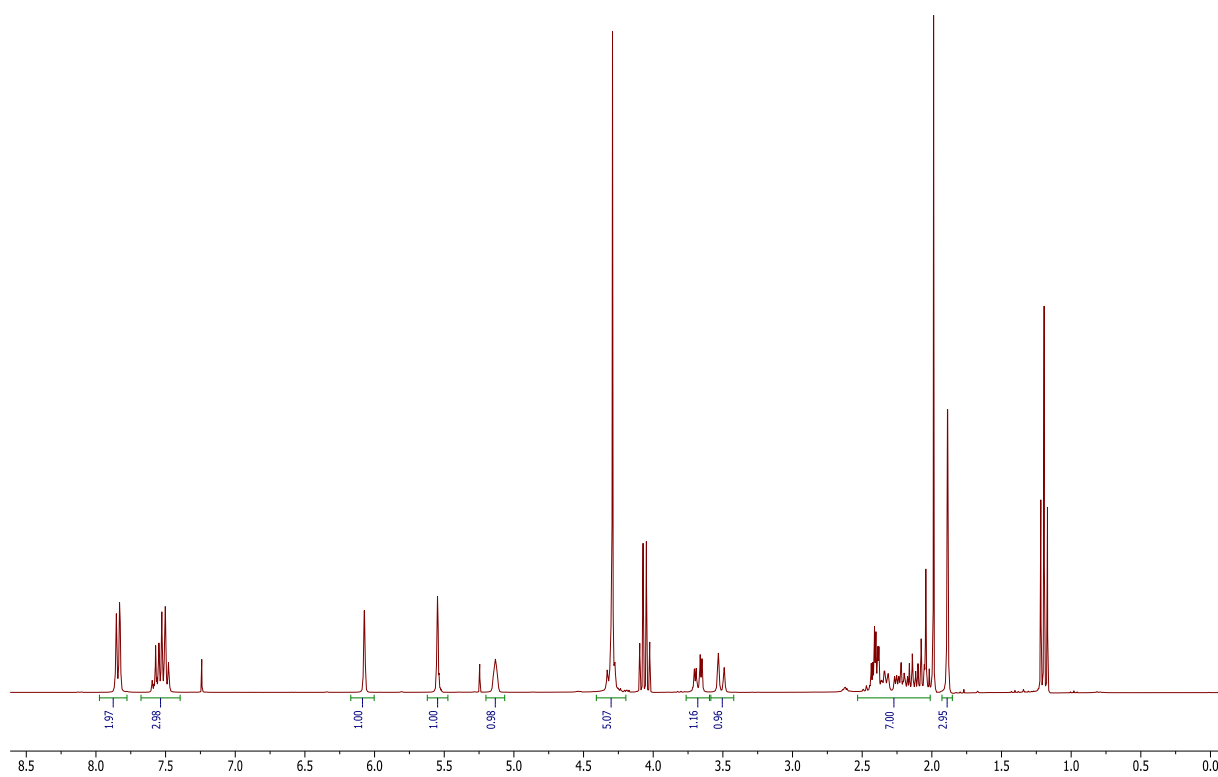


Figure 74: ^1H NMR (300 MHz, Chloroform-*d*) spectrum of **99**. Extra signals are due to ethyl acetate residue.

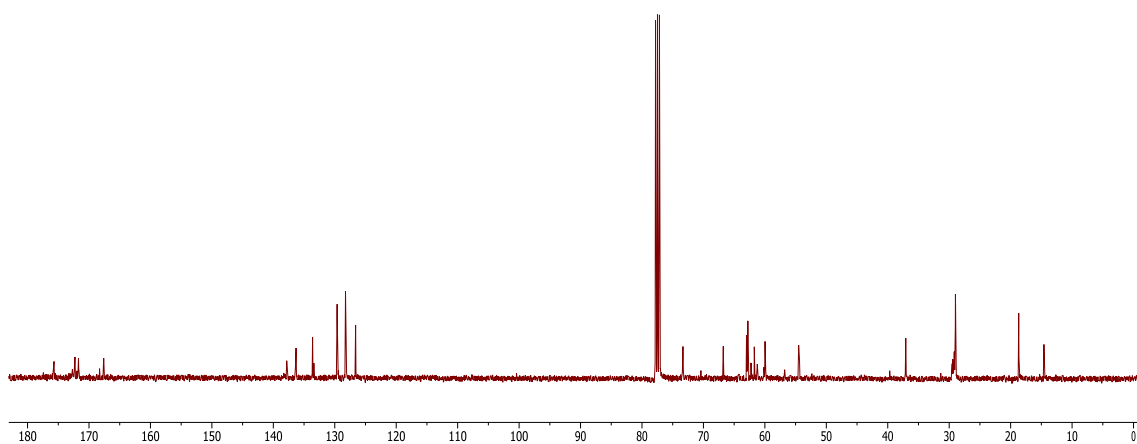
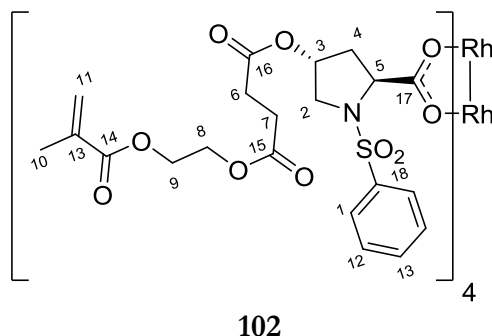


Figure 75: ^{13}C NMR (100 MHz, Chloroform-*d*) spectrum of **99**.

7.1.18 Synthesis of Rh₂(MEPP)₄, 102



A round bottom flask was charged with **99** (132 mg, 0.273 mmol, 6 equiv), Rh₂(OAc^F)₄ (30 mg, 0.046 mmol, 1 equiv.) and sodium bicarbonate (23 mg, 0.273 mmol, 6 equiv.) in EtOAc (5 ml). The reaction mixture was stirred at room temperature for 3 days. The green solution was then washed with saturated solution of sodium bicarbonate and the organic phase was dried over MgSO₄. Removing the solvent in vacuum gave a green, viscous residue which was purified by column chromatography (EtOAc:hexane/2:1), giving a 53 mg of purified, viscous product in 54% yield.

¹H NMR (400 MHz, Chloroform-*d*) δ 7.83 – 7.67 (m, H-1, 2H), 7.61 – 7.38 (m, H-12, H-13, 3H), 6.14 (s, H-11, 1H), 5.61 (s, H-11', *J* = 1.4 Hz, 1H), 4.92 (m, H-3, 1H), 4.47 – 4.34 (m, H-5, 1H), 4.35 – 4.26 (m, H-8, H-9, 4H), 4.23 (m, H-2, 1H), 3.45 – 3.28 (m, H-6, 2H), 2.42 – 2.34 (m, H-7, 2H), 2.19 – 2.10 (m, H-4, 2H), 1.92 (s, H-10, 3H).

¹³C NMR (100 MHz, Chloroform-*d*) δ 191.44 (C-17), 171.84 (C-16), 171.47 (C-15), 171.14 (C-14), 167.13 (C-13), 138.50 (C-18), 135.86 (C-1), 132.70 (C-12), 129.01 (C-13), 127.68 (C-11), 73.38 (C-3), 62.47 (C-5), 62.35 (C-8), 53.67 (C-9), 36.63 (C-7), 29.24 (C-6), 28.63 (C-2), 18.25 (C-4), 13.68 (C-10).

¹⁹F NMR (188 MHz, Methanol-*d*₄): no signals observed.

MS (ESI, MeCN) *m/z*: 2159.2 [*M*+Na⁺]

HRMS (MeOH): calculated for Rh₂C₈₄O₄₀H₉₆N₄S₄Na⁺ [*M*+Na⁺], 2158.7271 found 2158.7282 (Δ 0.0011).

FTIR: O-H stretch (3454 cm⁻¹), COO⁻ (1611 cm⁻¹), ester groups (1738 cm⁻¹), vinyl group (2950-2927 cm⁻¹).

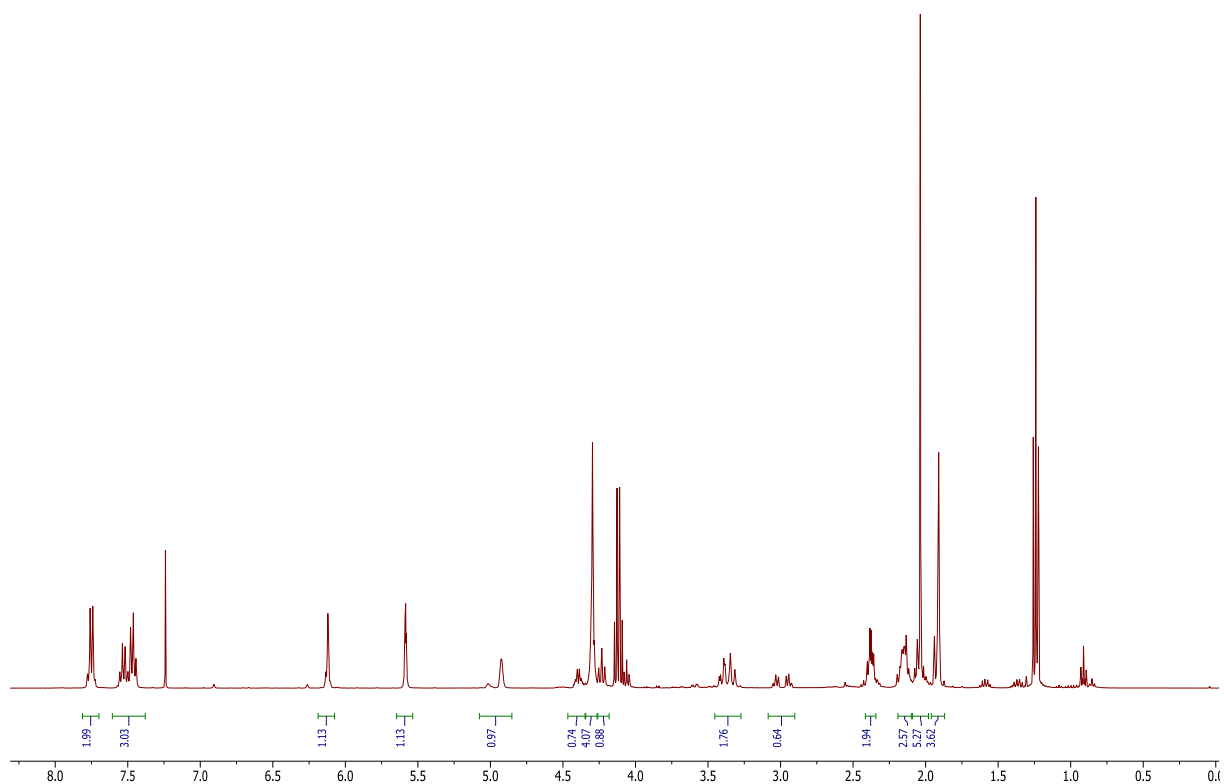


Figure 76: ^1H NMR (400 MHz, Chloroform-*d*) spectrum of **103**. Extra signals are due to coordinated ethyl acetate.

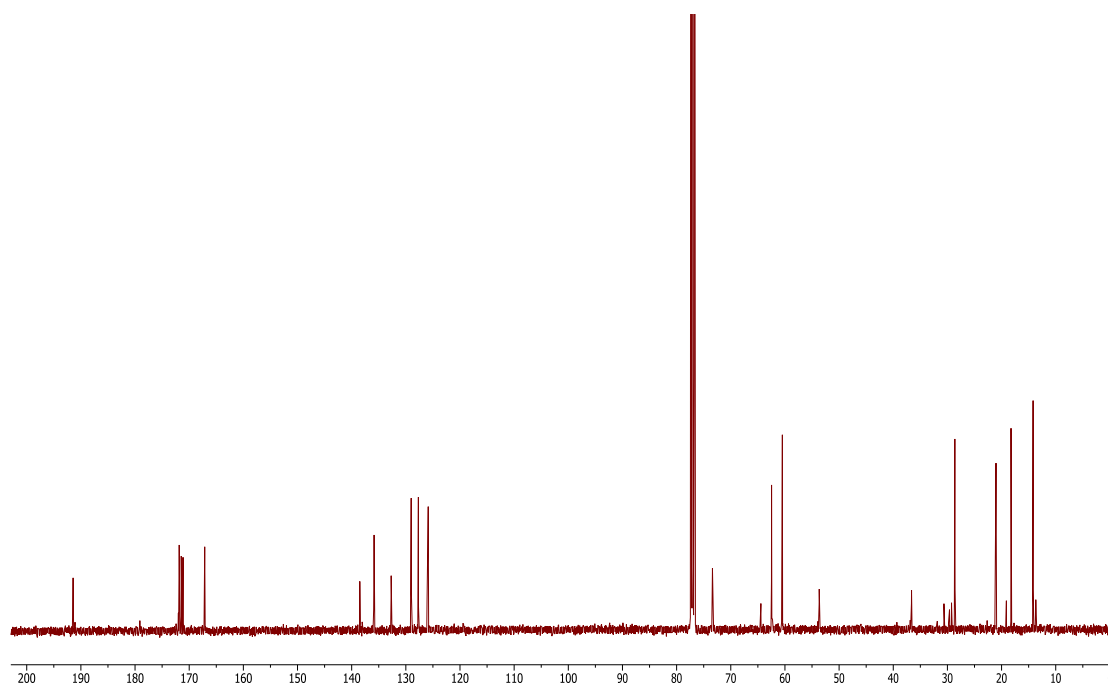
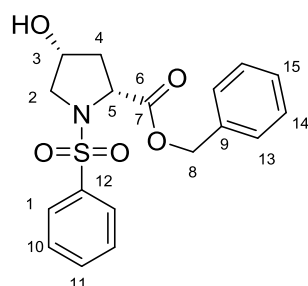


Figure 77: ^{13}C NMR (100 MHz, Chloroform-*d*) spectrum of **103**.

7.1.19 Synthesis of benzyl (2*R*,4*R*)-4-hydroxy-1-(phenylsulfonyl)pyrrolidine-2-carboxylate, 107



107

A 100 ml round-bottom flask was charged with benzyl *cis*-4-hydroxy-L-prolinate (tosilate salt) (**106**) (0.5 g, 1.27 mmol, 1 equiv.), potassium carbonate (0.39 g, 2.83 mmol, 2.2 equiv.) in water (100 ml) and heated to 50°C. After dissolving, benzenesulfonyl chloride (0.27 g, 1.53 mmol, 1.2 equiv) was added and the reaction mixture was left stirring overnight. The reaction mixture was extracted with CH₂Cl₂, organic phase was dried over MgSO₄ and the volatiles were removed in vacuum. The crude product was purified by silica column chromatography (EtOAc:hexane/1:1), as the eluent to obtain 0.51 g of the final product as a colorless oil in 56% yield.

¹H NMR (400 MHz, Chloroform-*d*) δ 7.83 (d, H-1, *J* = 8.3 Hz, 2H), 7.62 – 7.53 (m, H-11, 1H), 7.52 – 7.43 (m, H-10, 2H), 7.41 – 7.29 (m, Ph-, 5H), 5.17 (dd, H-8, *J* = 19.8, 11.9 Hz, 2H), 4.41 (dd, H-5, *J* = 9.7, 2.0 Hz, 1H), 4.36 – 4.26 (m, H-3, 1H), 3.52 (d, -OH, *J* = 9.8 Hz, 1H), 3.37 (dd, H-2, *J* = 10.3, 3.7 Hz, 2H), 2.21 – 2.11 (m, H-4, 1H), 2.11 – 2.04 (m, H-4', 1H).

¹³C NMR (100 MHz, Chloroform-*d*) δ 173.52 (C-7), 137.59 (C-12), 134.95 (C-1), 133.12 (C-9), 129.17 (C-13), 128.68 (C-10), 128.61 (C-14), 128.36 (C-11), 127.51 (C-15), 71.00 (C-3), 67.84 (C-5), 59.21 (C-6), 56.98 (C-2), 38.72 (C-4).

MS (ESI, MeOH) *m/z*: 384.2 [*M*+Na⁺]

HRMS (MeOH): calculated for C₁₈O₅H₁₉NSNa⁺ [*M*+Na⁺] 384.4024, found 384.4010 (Δ 0.0014).

FTIR: 3483 cm⁻¹ (O-H stretch), 1538 cm⁻¹ (carbonyl group), 1550 cm⁻¹ (C-C stretch aromatics).

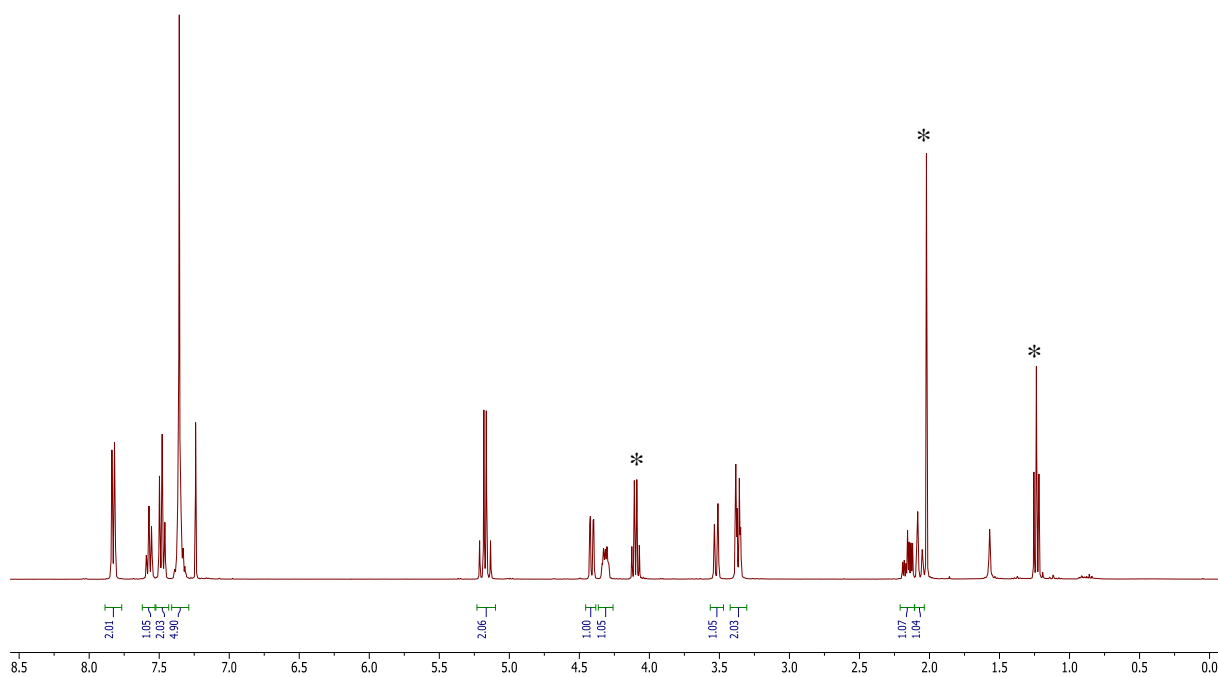


Figure 78: ^1H NMR (400 MHz, Chloroform-*d*) spectrum of **107**. Extra signals are due to ethyl acetate and marked with *.

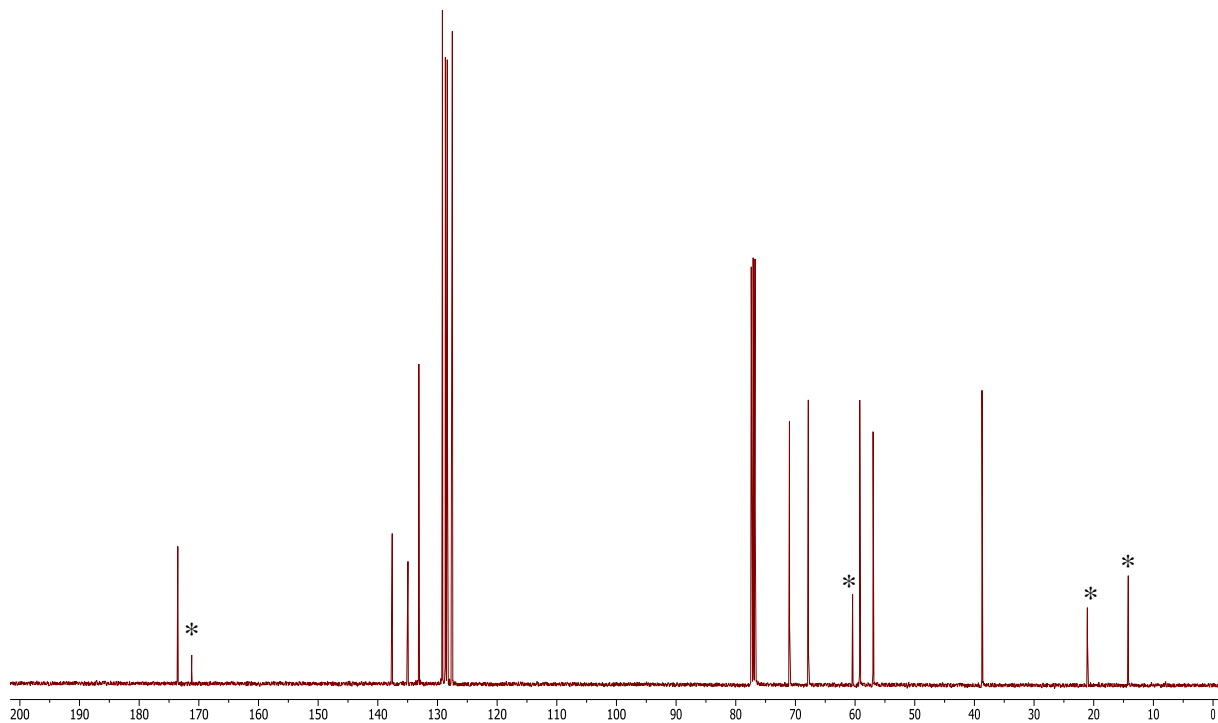
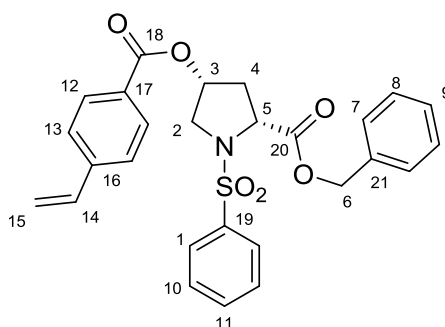


Figure 79: ^{13}C NMR (100 MHz, Chloroform-*d*) spectrum of **107**. Ethyl acetate signals are marked with *.

7.1.20 Synthesis of benzyl (2*R*,4*R*)-1-(phenylsulfonyl)-4-((4-vinylbenzoyl)oxy)pyrrolidine-2-carboxylate, **108**



108

A round-bottom flask was charged with benzyl (2*R*,4*R*)-4-hydroxy-1-(phenylsulfonyl)pyrrolidine-2-carboxylate (**107**) (180 mg, 0.498 mmol, 1 equiv.) and 4-vinylbenzoic acid (68.4 mg, 0.486 mmol, 0.93 equiv.) in CH₂Cl₂ (3 ml). To the resulting solution was added dropwise a mixture of DCC (96 mg, 0.435 mmol, 0.93 equiv.) and DMAP (0.57 g, 0.00462 mmol, 0.00925 equiv) in CH₂Cl₂ (5 ml) over period 1 hour. After stirring overnight, the reaction mixture was then filtered and the filtrate was washed with water. The organic phase was concentrated under the reduced pressure and the residue was purified in silica gel (EtOAc:hexane/1:1), giving a 164 mg of product in 67% yield.

¹H NMR (400 MHz, Chloroform-*d*) δ 7.97 – 7.88 (m, H-12, 2H), 7.85 – 7.77 (m, H-13, 2H), 7.61 – 7.53 (m, H-11, 1H), 7.52 – 7.44 (m, H-10, 2H), 7.41 – 7.32 (m, H-1, 2H), 7.28 – 7.18 (m, Ph-, 7H), 6.71 (dd, H-14, *J* = 17.6, 10.9 Hz, 1H), 5.83 (dd, H-15, *J* = 17.6, 0.8 Hz, 1H), 5.47 – 5.41 (m, H-3, 1H), 5.37 (dd, H-15', *J* = 10.9, 0.8 Hz, 1H), 5.08 (dd, H-6, *J* = 17.4, 12.6 Hz, 2H), 4.69 (dd, H-5, *J* = 9.5, 2.2 Hz, 1H), 3.74 (dd, H-2, *J* = 11.4, 5.2 Hz, 1H), 3.62 – 3.52 (m, H-2', 1H), 2.53 – 2.42 (m, H-4, 1H), 2.42 – 2.24 (m, H-4', 1H).

¹³C NMR (100 MHz, Acetone-*d*₆) δ 206.19 (C-18), 171.73 (C-20), 165.77 (C-17), 143.21 (C-16), 139.13 (C-1), 136.89 (C-19), 133.92 (C-12), 130.73 (C-14), 130.14 (C-13), 129.76 (C-21), 129.25 (C-7), 128.89 (C-8), 128.71 (C-9), 128.40 (C-11), 127.07 (C-10), 117.25 (C-15), 74.37 (C-3), 67.49 (C-5), 60.66 (C-6), 54.66 (C-2), 37.04 (C-4).

MS (ESI, MeOH) *m/z*: 514.1 [*M*+Na⁺]

HRMS (MeOH): calculated for C₂₇O₆H₂₅NSNa⁺ [*M*+Na⁺] 514.5460, found 514.1294 (Δ 0.4166).

FTIR: 1638 cm⁻¹ (ester groups), 1550 cm⁻¹ (C-C stretch aromatics).

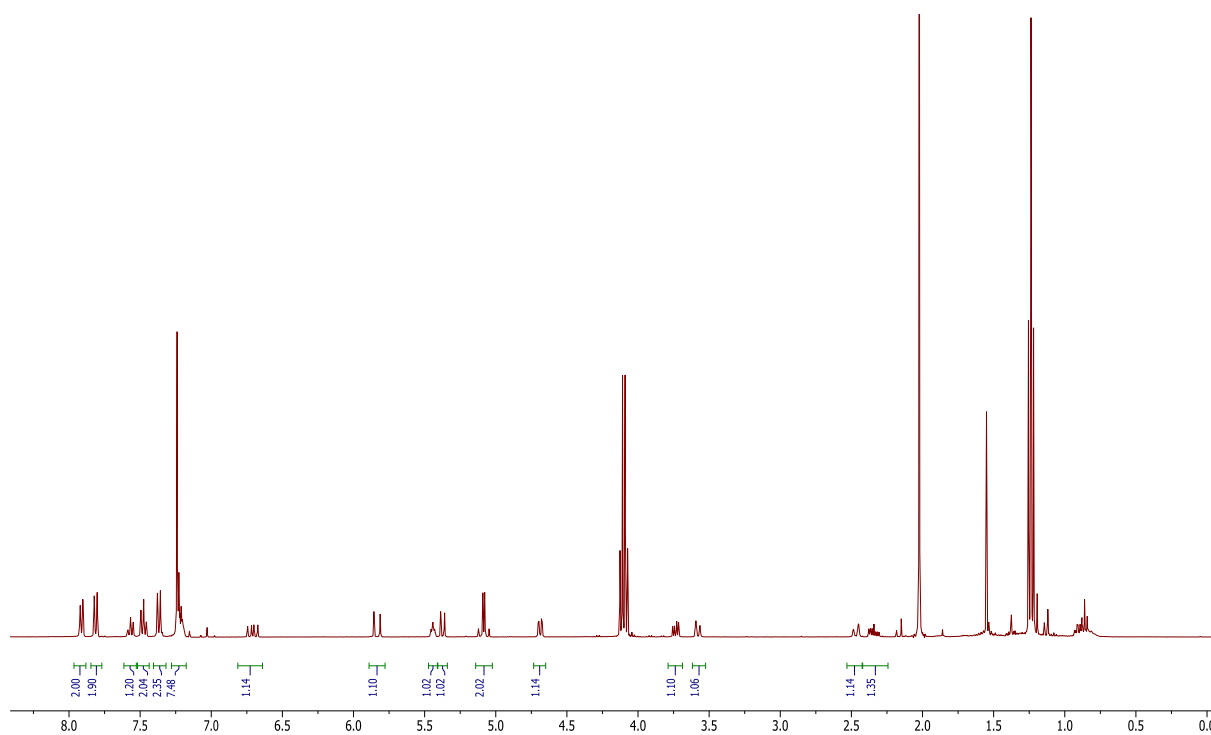


Figure 80: ^1H NMR (400 MHz, Chloroform- d) spectrum of **108**. Extra signals are due to ethyl acetate.

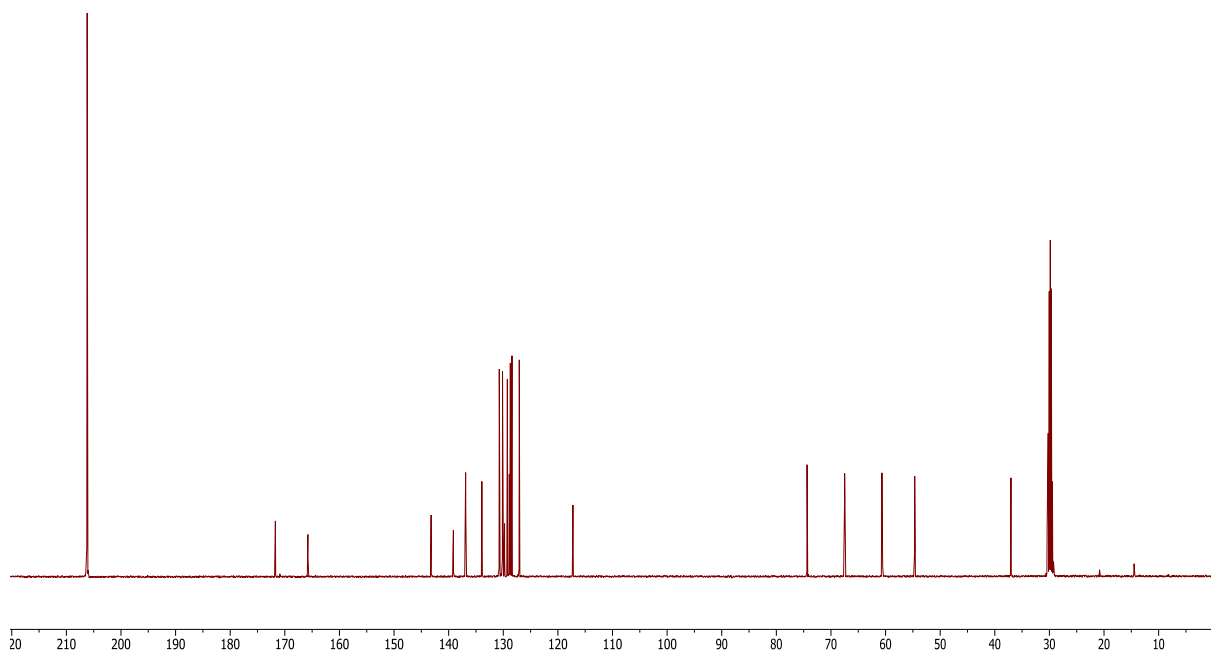
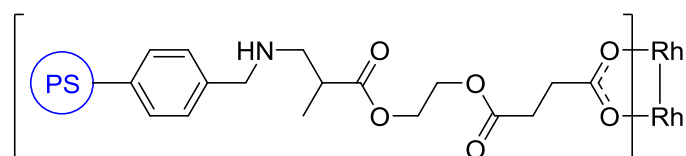


Figure 81: ^{13}C NMR (100 MHz, Acetone- d_6) spectrum of **108**.

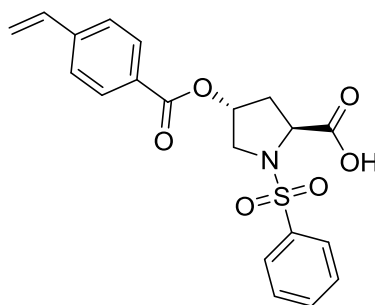
7.1.21 Heterogenization of $\text{Rh}_2(\text{MCES})_4$ by post-modification approach – Synthesis of $\text{pol}(\text{PM})\text{-Rh}_2(\text{MCES})_4$, **94**



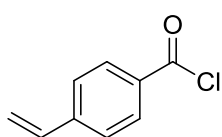
94

A round bottom flask was charged with (Aminomethyl)polystyrene (82 mg, 4 equiv.) in CH_2Cl_2 (2 ml) and left swelling for 30 min. In a separate flask $\text{Rh}_2(\text{MCES})_4$ (**74**) (23 mg, 0.0205 mmol, 1 equiv.) was dissolved in 5 ml ethyl acetate. The combined solutions were stirred at 70°C for 24 hours. Filtration resulted in 90 mg green beads of **94** with 58% incorporation of the monomer **74**.

7.1.22 Attempt at synthesis of (2R,4R)-1-(phenylsulfonyl)-4-((4-vinylbenzoyl)oxy)pyrrolidine-2-carboxylic acid, **103**



103

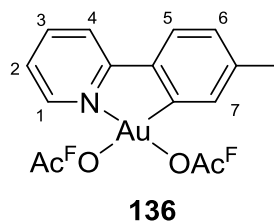


104

A round-bottom flask was charged with 4-vinylbenzoic acid (**71**) (36 mg, 0.24 mmol, 2 equiv.) in thionyl chloride (1 ml) and stirred at 50°C . After 2 hours, thionyl chloride was evaporated in vacuum and the residue (4-vinylbenzoyl chloride) was re-dissolved in CH_2Cl_2 (1 ml). The resulting mixture was transferred to a flask with a solution of (2*S*,4*R*)-4-hydroxy-1-(phenylsulphonyl)pyrrolidine-2-carboxylic acid (**100**) (40 mg, 0.122 mmol, 1 equiv.) in CH_2Cl_2 (1 ml) with zinc chloride (26 mg, 0.19 mmol, 1.5 equiv.) and stirred at room temperature. When all the starting material had reacted (TLC control), the reaction mixture was washed with water (3x25 ml), the organic phase was dried over MgSO_4 and volatiles were removed under reduced pressure. The resulting crude was subjected to column chromatography ($\text{MeOH}:\text{CH}_2\text{Cl}_2/1:20$). ^1H NMR analysis of isolated products revealed absence of target compound **103**.

7.2 Experimental section for the gold project

7.2.1 Synthesis of $\text{Au}(\text{tpy})(\text{OAc}^{\text{F}})_2$,¹²³ **136**



A microwave vessel was charged with $\text{Au}(\text{OAc})_3$ (0.384 g, 1.03 mmol, 1.00 equiv.), 2-(*p*-tolyl)pyridine (186 μl , 1.09 mmol, 1.06 equiv.) in a mixture of water and TFA (15/15 ml). The resulting mixture was heated in the microwave oven at 120 $^{\circ}\text{C}$. After 30 min of heating, the reaction mixture was cooled to ambient temperature and decanted over to an Erlenmeyer flask. The product was precipitated by adding 50 ml of water and cooling with ice bath. The product was washed on a fine frit with water (3 x 5 ml), diethyl ether (5 ml) and dried giving 0.53 g of the product in 87% yield.

Spectroscopic data was in agreement with reported literature data.¹²³

^1H NMR (300 MHz, CF_3COOD) δ 8.71 (d, H-1, $J = 6.4$ Hz, 1H), 8.40 (m, H-3, 1H), 8.10 (d, H-4, $J = 7.9$ Hz, 1H), 7.68 (m, H-2, 1H), 7.60 (d, H-5, $J = 7.4$ Hz, 1H), 7.49 (d, H-6, $J = 8.4$ Hz, 1H), 7.03 (s, H-7, 1H), 2.60 (s, $-\text{CH}_3$, 3H).

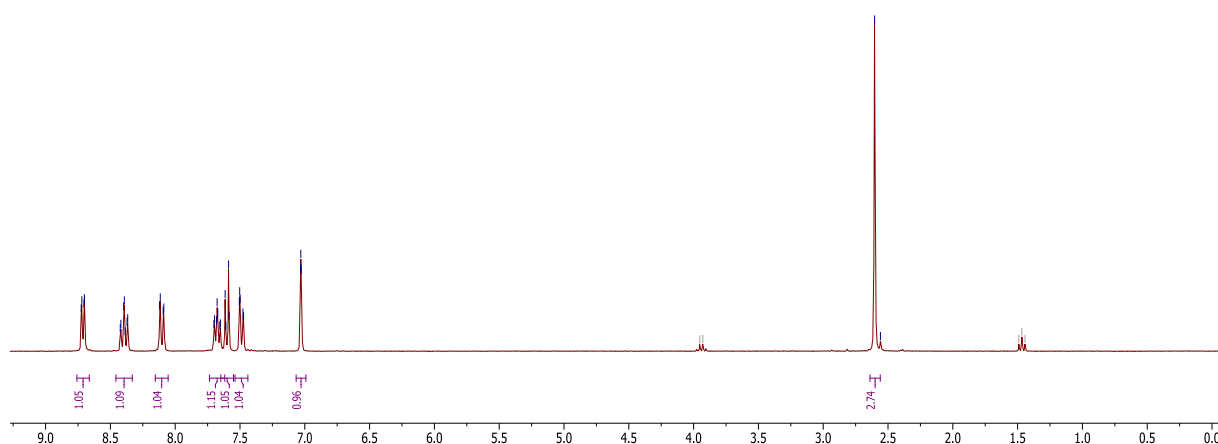
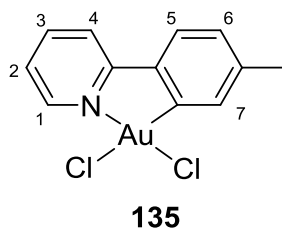


Figure 82: ^1H NMR (300 MHz, CF_3COOD) of $\text{Au}(\text{tpy})(\text{OAc}^{\text{F}})_2$ (**136**). Peaks at 1.5 and 3.95 ppm are due to diethyl ether residue.

7.2.2 Synthesis of Au(tpy)Cl₂,¹⁴⁰ **135**



A round bottom flask was charged with metallic gold (0.192 g, 0.976 mmol), hydrochloric acid (6 ml) and nitric acid (2 ml). After all gold dissolved, the volatiles were removed in vacuum, giving a yellow crystalline product of HAuCl₄·3H₂O. The flask with HAuCl₄·3H₂O was charged with water (30 ml), 2-(*p*-tolyl)pyridine (167 μl, 0.165 mmol) and the resulting mixture was heated in the microwave oven at 160 °C for 30 min. After the mixture was cooled, product was collected on a fine frit, washed with water (3 x 5 ml), acetonitrile (3 x 5 ml) and dried under the stream of air giving 0.280 g of the product in 66% yield.

Spectroscopic data was in agreement with reported literature data.¹⁴⁰

¹H NMR (300 MHz, DMSO-*d*₆) δ 9.49 (d, H-1, *J* = 6.2 Hz, 1H), 8.43 – 8.30 (m, H-3, H-4, 2H), 7.85 (d, H-5, *J* = 7.9 Hz, 1H), 7.72 (m, H-2, 1H), 7.62 (s, H-7, 1H), 7.31 (d, H-6, *J* = 7.5 Hz, 1H), 2.41 (s, CH₃, 3H).

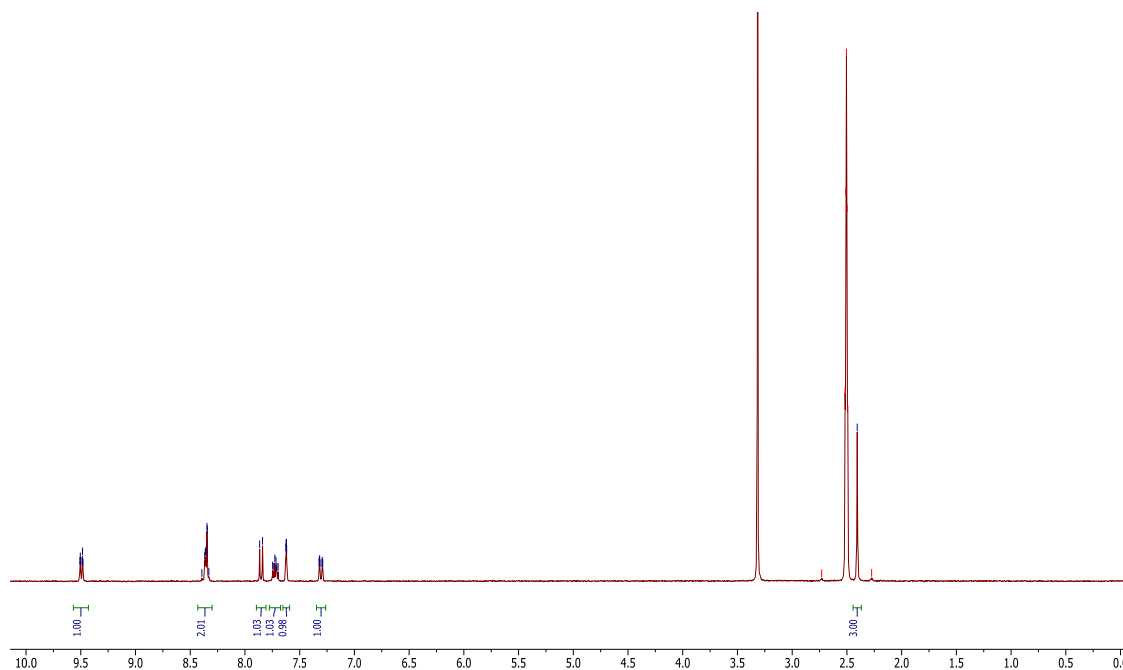
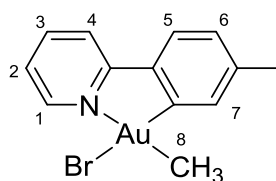


Figure 83: ¹H NMR (300 MHz, DMSO-*d*₆) of Au(tpy)Cl₂ (**135**). Peak at 3.3 is due to water signal.

7.2.3 Synthesis of Au(tpy)BrMe,¹²³ **137**



137

A round bottom flask was charged with Au(tpy)(OAc^F)₂ (**136**) (0.100 g, 0.169 mmol, 1.00 equiv.) in THF (10 ml) and the solution was cooled in a dry ice/acetone bath. CH₃MgBr (28.6 mg, 0.24 mmol, 1.40 equiv.) was added to the reaction mixture. The formed milky suspension was stirred for an hour in a dry ice/acetone bath and then for 1 hour at room temperature. After 1 hour, volatiles were removed under reduced pressure. The resulting solid was dissolved in CH₂Cl₂ (25 ml) and washed with water (3 x 25 ml). Removing the solvent from the organic phase, 64.5 mg of the product was obtained in 83 % yield.

Spectroscopic data was in agreement with reported literature data.¹²³

¹H NMR (400 MHz, Methylene Chloride-*d*₂) δ 9.53 (d, H-1, *J* = 5.9 Hz, 1H), 7.99 (dd, H-3, *J* = 9.1, 7.3 Hz, 1H), 7.92 (d, H-4, *J* = 8.1 Hz, 1H), 7.69 (d, H-5, *J* = 7.9 Hz, 1H), 7.44 (dd, H-2, *J* = 7.2, 5.6 Hz, 1H), 7.32 (s, H-7, 1H), 7.20 (d, H-6, *J* = 8.7 Hz, 1H), 2.43 (s, ArCH₃, 3H), 1.63 (s, AuCH₃, 3H).

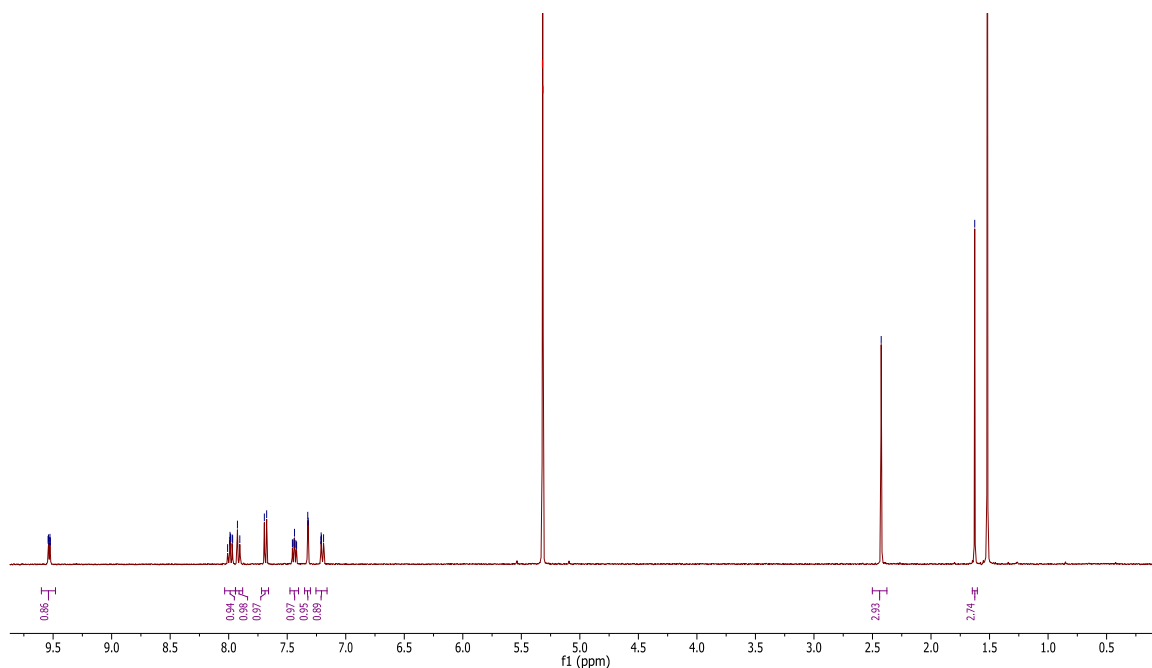
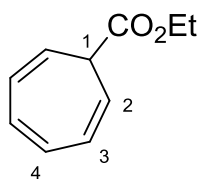


Figure 84: ¹H NMR (400 MHz, CD₂Cl₂) of Au(tpy)BrMe (**137**). Peak at 1.5 is due to the water residue.

7.2.4 Synthesis of ethyl cyclohepta-2,4,6-triene-1-carboxylate,¹³⁶ **172**



172

A round bottom flask was charged with Au(tpy)(OAc)^F₂ (**136**) (26 mg, 0.044 mmol, 5 mol %) was dissolved in benzene (2 ml) and EDA (0.10 g, 0.88 mmol, 1 equiv.) was added. The reaction mixture was stirred at 70°C. After 30 min no EDA was detected in the reaction mixture. The volatiles were removed under reduced pressure and the crude product was purified by silica column chromatography (EtOAc:Hexane/1:9) to obtain 0.62 g of the final product as colorless oil in 43% yield.

Spectroscopic data were in agreement with reported literature data.¹³⁶

¹H NMR (200 MHz, Chloroform-*d*) δ 6.70 (m, H-4, 2H), 6.42 – 6.18 (m, H-3, 2H), 5.48 (m, H-2, 2H), 4.30 (q, -CH₂CH₃, *J* = 7.1 Hz, 2H), 2.58 (m, H-1, 1H), 1.50 – 1.17 (m, -CH₃, 3H).

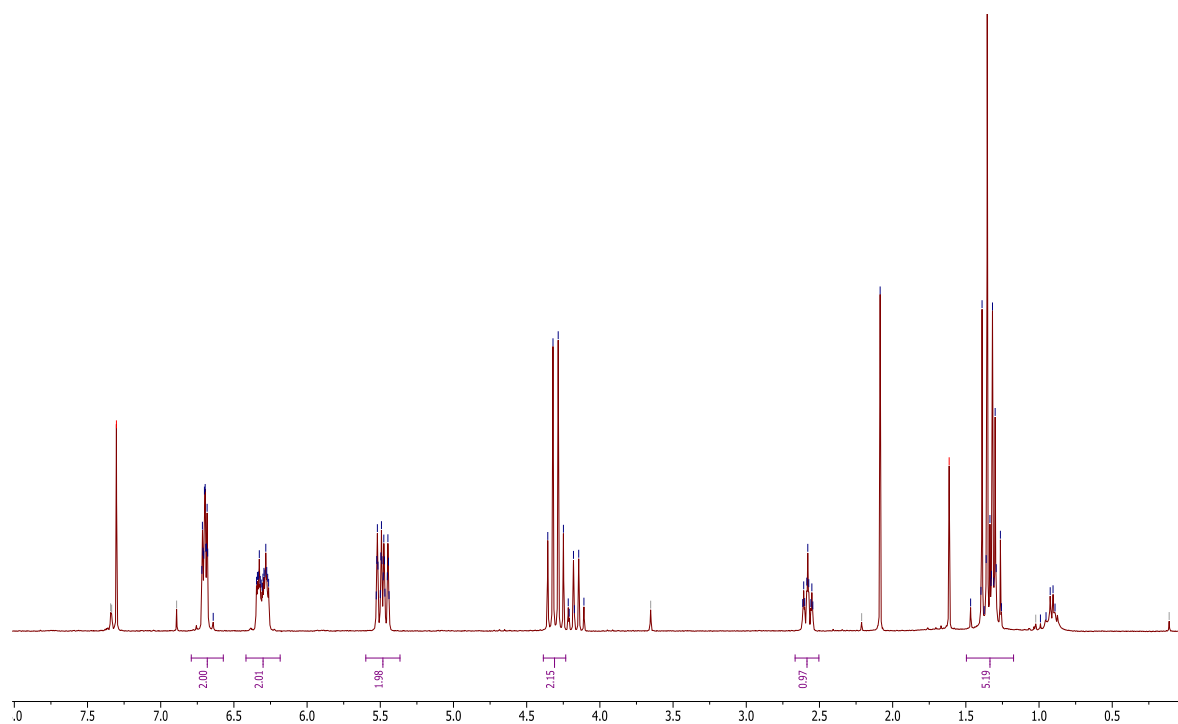
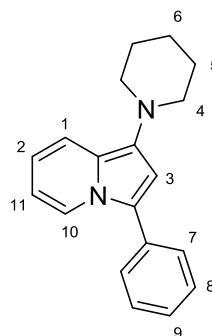


Figure 85: ¹H NMR (200 MHz, Chloroform-*d*) of cycloheptatriene **172**. Extra peaks are due to water and ethyl acetate residue.

7.2.5 Synthesis of 3-phenyl-1-(piperidin-1-yl)indolizine,^{141,142} **167**



167

A round-bottom flask was charged with 2-pyridinecarboxaldehyde (321 mg, 3 mmol, 1.0 equiv.), piperidine (281 mg, 3.3 mmol, 1.1 equiv.) and phenylacetylene (368 mg, 3.6 mmol, 1.2 equiv.). To the resulting mixture $\text{Au}(\text{tpy})(\text{OAc})_2$ (**136**) (18 mg, 0.03 mmol, 0.01 equiv.) was added and stirred at 80°C for 2 hours. The product mixture was purified by column chromatography (EtOAc:hexane/1:9) and gave 705 mg of a viscous, dark-yellow product **167** in 85 % yield. Spectroscopic data were in agreement with reported literature data.^{141,142}

¹H NMR (300 MHz, Chloroform-*d*) δ 8.17 (d, H-10, $J = 7.2$ Hz, 1H), 7.61 – 7.50 (m, H-7, 2H), 7.49 – 7.36 (m, H-8, H-11, 3H), 7.33 – 7.25 (m, H-2, 1H), 6.66 (s, H-3, 1H), 6.50 (m, H-9, 1H), 6.36 (dd, H-1, $J = 7.5$ Hz, 6.4 Hz, 1H), 3.10 – 2.87 (m, H-4, 4H), 1.66 – 1.49 (m, H-5, 3H), 1.51 – 1.70 (m, H-6, 2H).

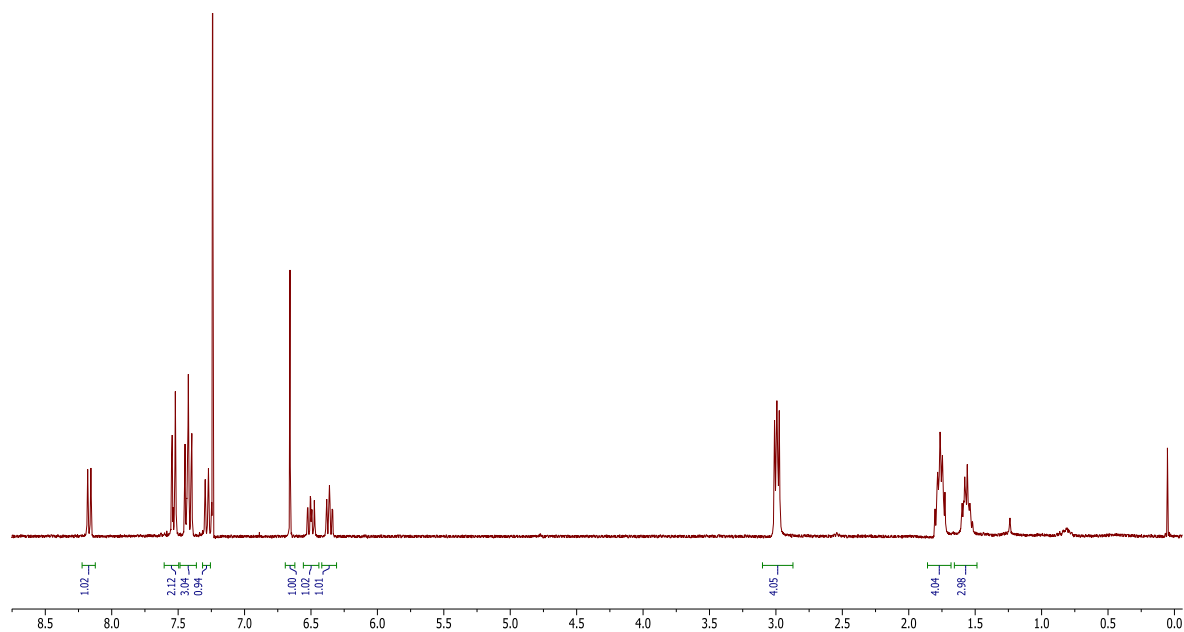
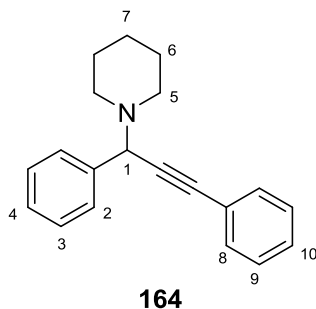


Figure 86: ¹H NMR (300 MHz, Chloroform-*d*) of 3-phenyl-1-(piperidin-1-yl)indolizine (**167**).

7.2.6 Synthesis of 1-(1,3-diphenylpro-2-yn-1-yl)piperidine, **164**



A round-bottom flask was charged with benzaldehyde (202 μl , 2 mmol, 1.0 equiv.), piperidine (218 μl , 2.2 mmol, 1.1 equiv.) and phenylacetylene (330 μl , 3 mmol, 1.5 equiv.). To the resulting mixture $\text{Au}(\text{tpy})(\text{OAc})_2$ (**136**) (18 mg, 0.03 mmol, 0.01 equiv.) was added and stirred at 80°C for 20 hours. The product mixture was purified by column chromatography (EtOAc:hexane/1:9) and gave 386 mg of a viscous product **164** in 70 % yield.

Spectroscopic data were in agreement with reported literature data.¹³⁴

^1H NMR (300 MHz, Chloroform-*d*) δ 7.73 – 7.62 (m, H-8, 2H), 7.62 – 7.48 (m, H-2, 2H), 7.44 – 7.31 (m, H-9, H-3, H-5, H-10, 6H), 4.84 (s, H-1, 1H), 2.60 (t, H-5, $J = 5.4$ Hz, 4H), 1.76 – 1.55 (m, H-6, 5H), 1.55 – 1.42 (m, H-7, 2H).

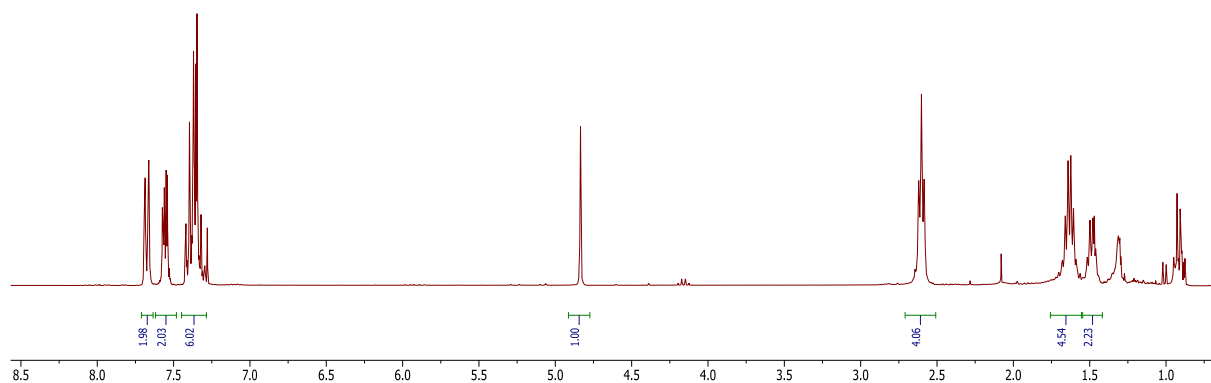


Figure 87: ^1H NMR (300 MHz, Chloroform-*d*) of 1-(1,3-diphenylpro-2-yn-1-yl)piperidine (**164**). Extra signals are due to undistilled hexane.

7.2.7 Cyclopropanation reaction utilizing Au(tpy)(OAc^F)₂ as a catalyst

A round bottom flask was charged with Au(tpy)(OAc^F)₂ (**136**) (26 mg, 0.044 mmol), styrene (0.456 g, 4.38 mmol, 5 eq) and CH₂Cl₂ (3 ml). The resulting mixture was stirred and EDA (0.10 g, 0.88 mmol, 1.0 eq) in CH₂Cl₂ (12 ml) was added dropwise for 35 min. After stirring for an additional 20 hours at reflux, a small fraction of the reaction mixture was taken in order to perform ¹H NMR analysis.

7.2.8 General procedure for A³ coupling for synthesis of propargylamine 164

A round bottom flask was charged with the respective gold complex and phenylacetylene (165 μl, 1.5 mmol). Benzaldehyde (101 μl, 1.0 mmol) and piperidine (109 μl, 1.1 mmol) were added under solvent-free conditions and the resulting mixture was heated for 24 hours. The reaction mixture was then cooled to ambient temperature and mesitylene (70 μl, 0.5 mmol) was added. Conversion of benzaldehyde and the yield of target compound were determined by ¹H NMR using mesitylene as an internal standard.

7.2.9 General procedure for A³ coupling for synthesis of indolizine 167

To a mixture of the respective gold complex, 2-pyridinecarboxaldehyde (107 mg, 1 mmol, 1 equiv.), piperidine (93.7 mg, 1.1 mmol, 1.1 equiv.) and phenylacetylene (122.6 mg, 1.2 mmol, 1.2 equiv.) were added under solvent-free conditions. The resulting mixture was stirred at 80°C for 2 hours. The yield of the reaction was determined by ¹H NMR using mesitylene as an internal standard.

7.2.10 Procedure for gold(III)-catalyzed ethynylation reaction¹²⁹

To a solution of 1,3,5-trimethoxybenzene (**153**) (77 mg, 0.46 mmol, 2 equiv.), iodobenzene diacetate (111 mg, 0.34 mmol, 1.5 equiv.), NaHCO₃ (22 mg, 0.26 mmol, 1.05 equiv.) and the ethyl propiolate (**154**) (23 mg, 0.23 mmol, 1 equiv.) in anhydrous 1,2-dichloroethane (3 ml) was added Au(tpy)(OAc^F)₂ (7 mg, 0.01 mmol, 0.05 equiv.). The reaction mixture was stirred at 90°C for 12 hours. The analysis of ¹H NMR spectrum revealed the absence of the target compound **155**.

7.2.11 NMR experiment – reaction of Au(tpy)(OAc^F)₂ with phenylacetylene (174)

An NMR-tube was charged with Au(tpy)(OAc^F)₂ (**136**) (5 mg, 0.0085 mmol), phenylacetylene (**74**) (0.9 μl, 0.0085 mmol) and dichloromethane-*d*₂. The ¹H NMR spectra were recorded at room temperature.

7.2.12 NMR experiment – reaction of Au(tpy)(OAc^F)₂ with phenyl propargyl ether (175)

An NMR-tube was charged with Au(tpy)(OAc^F)₂ (**136**) (5 mg, 0.0085 mmol), phenyl propargyl ether (**175**) (1.1 μl, 0.0085 mmol) and dichloromethane-*d*₂. The ¹H NMR spectra were recorded at room temperature.

Appendix

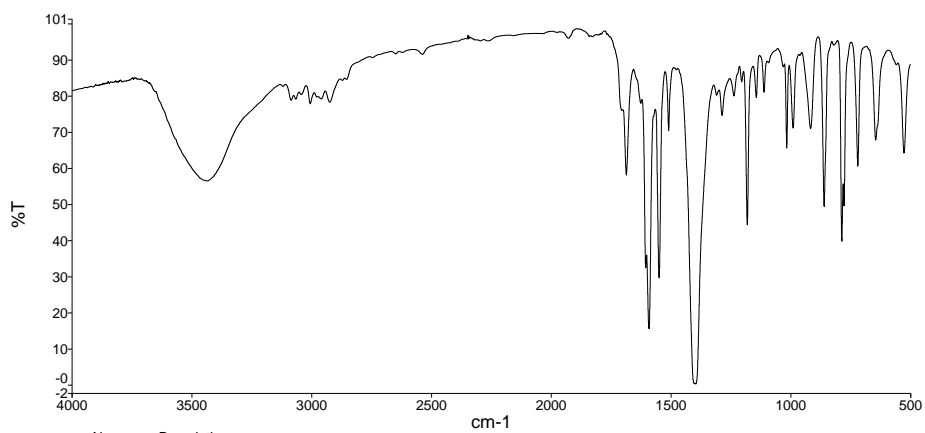


Figure 88: FTIR spectrum of $\text{Rh}_2(4\text{VBA})_4$ (75).

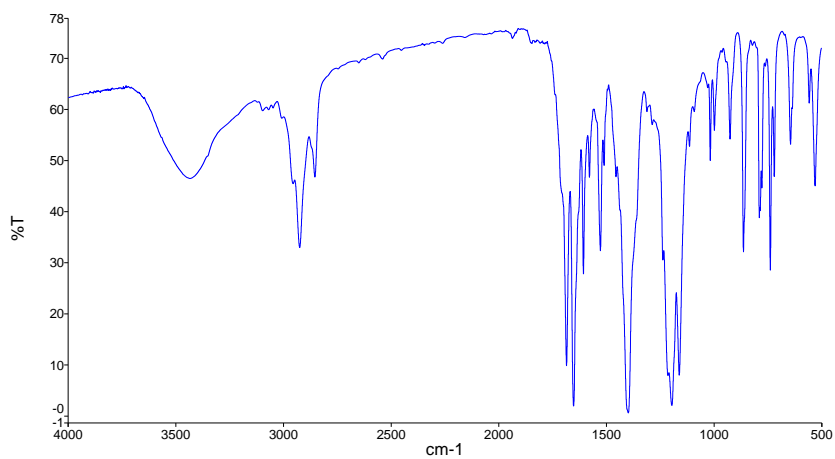


Figure 89: FTIR spectrum of $\text{Rh}_2(4\text{VBA})_2(\text{OAc}^F)_2$ (77).

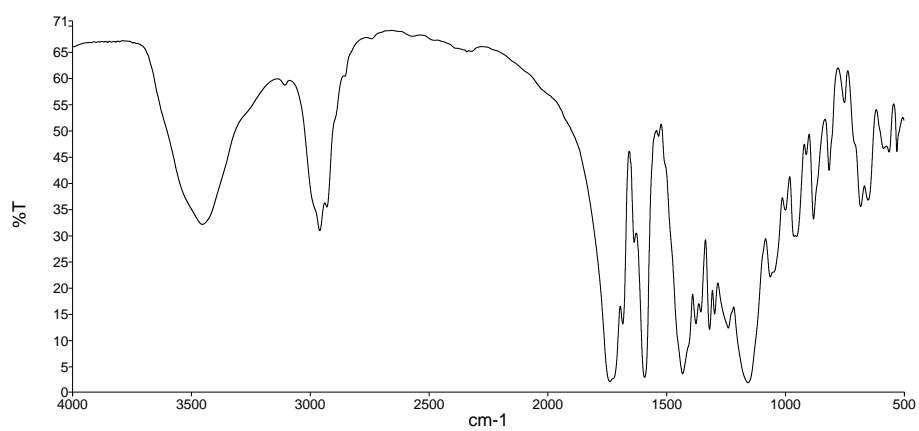


Figure 90: FTIR spectrum of $\text{Rh}_2(\text{MCES})_4$ (74).

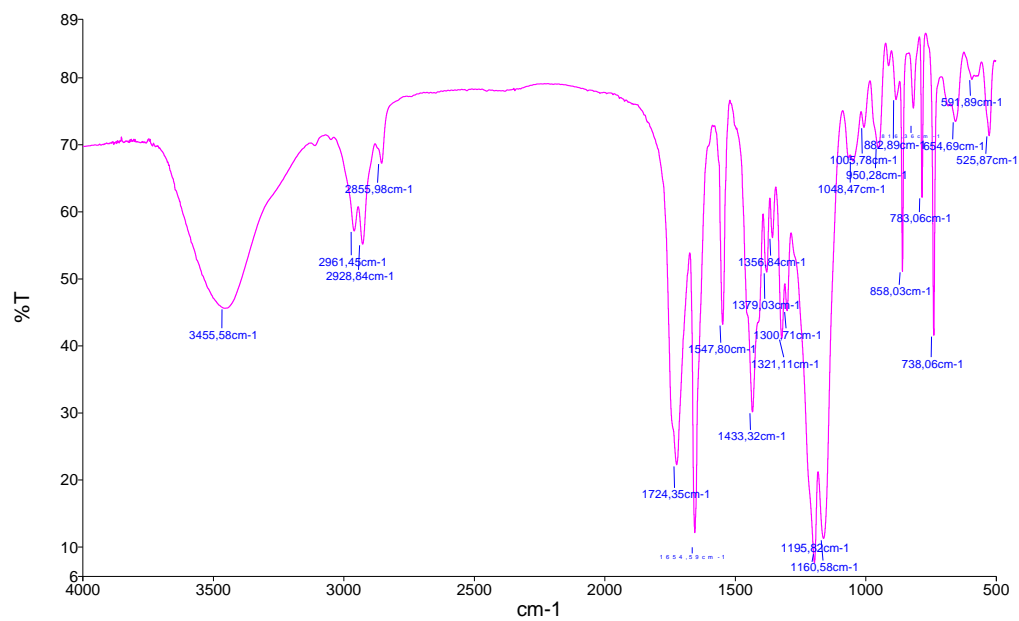


Figure 91: FTIR spectrum of $\text{Rh}_2(\text{MCES})_2(\text{OAc})_2$ (**78**).

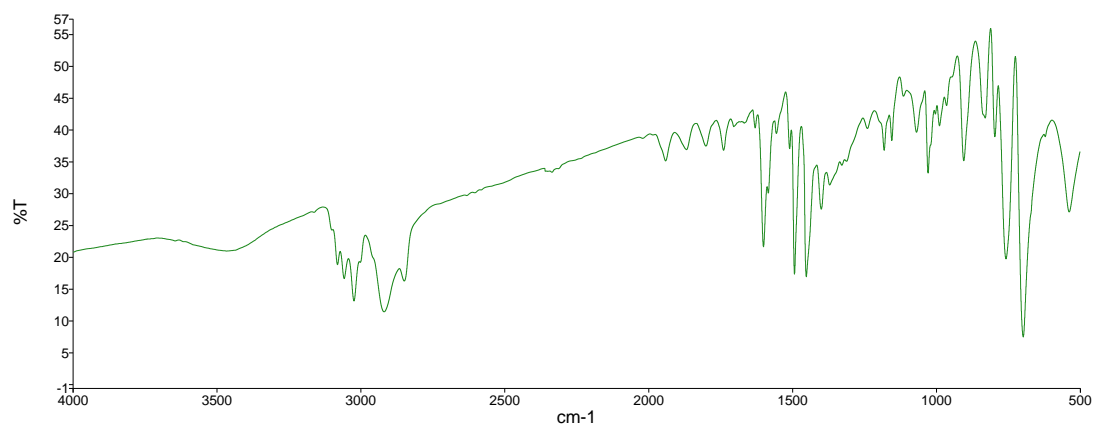


Figure 92: FTIR spectrum of $\text{pol(I)-Rh}_2(4\text{VBA})_4$ (**84**).

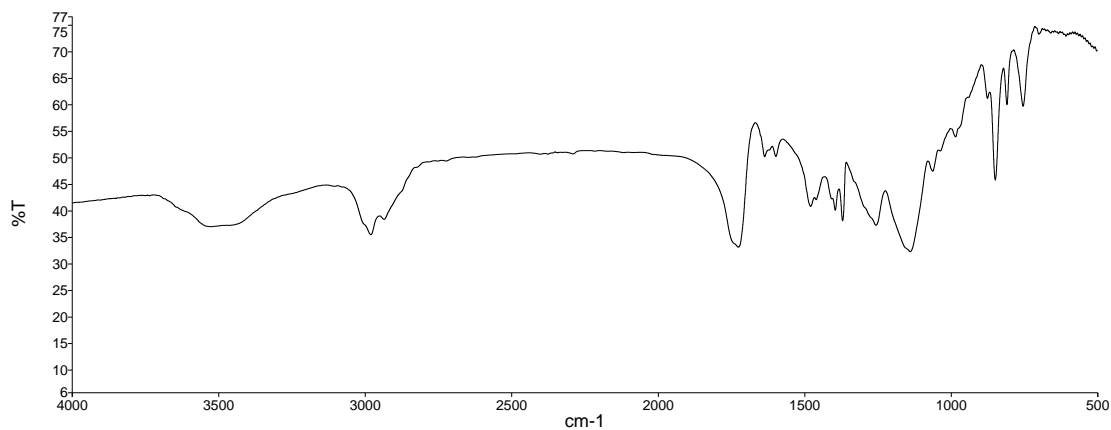


Figure 93: FTIR spectrum of $\text{pol(I)-Rh}_2(\text{MCES})_4$ (**85**).

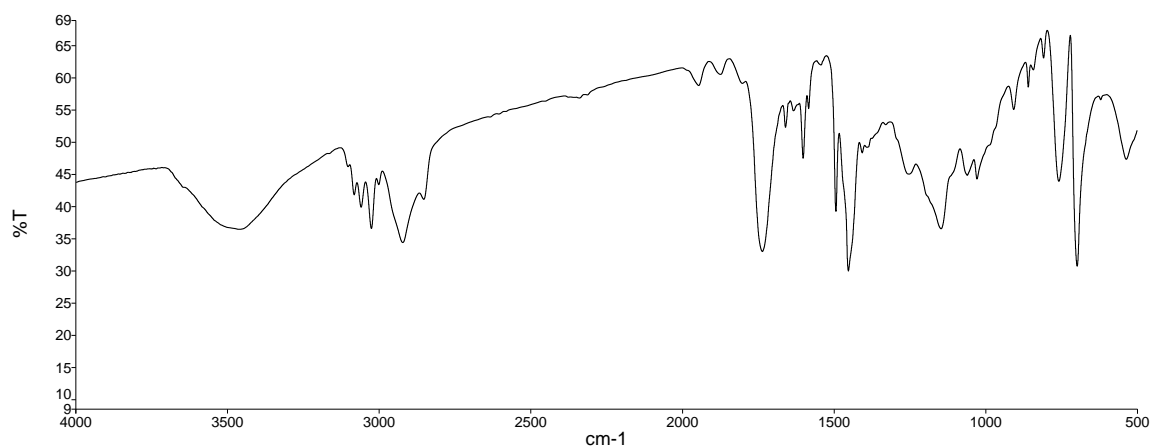


Figure 94: FTIR spectrum of $\text{pol(I)-Rh}_2(\text{MCES})_2(\text{OAc}^F)_2$ (**86**).

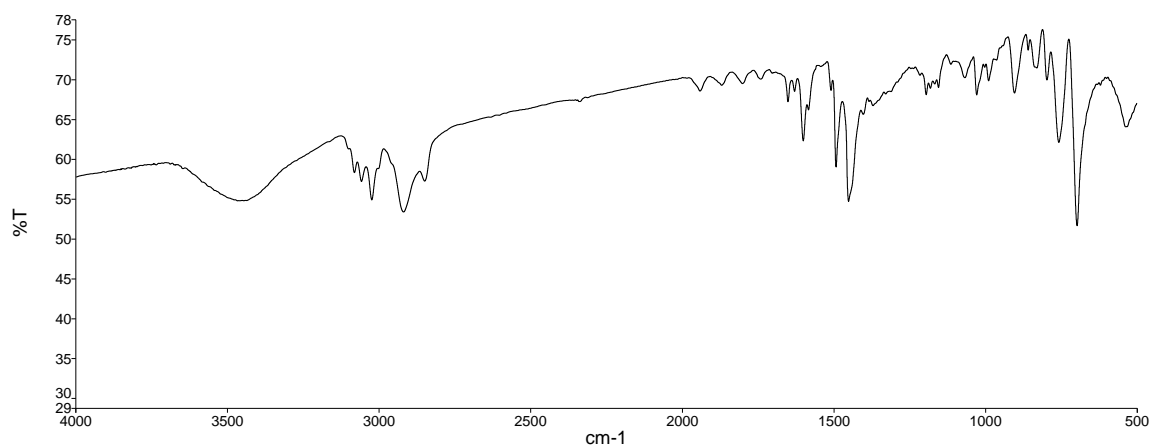


Figure 95: FTIR spectrum of $\text{pol(I)-Rh}_2(4\text{VBA})_2(\text{OAc}^F)_2$ (**83**).

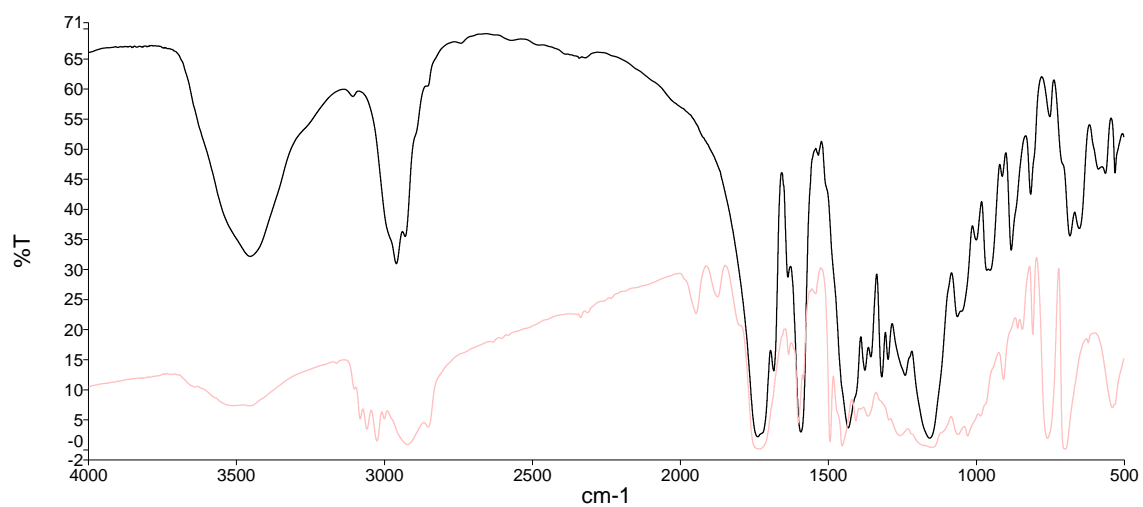


Figure 96: FTIR spectra of $\text{pol(II)-Rh}_2(\text{MCES})_4$ (**87**) (red) and $\text{Rh}_2(\text{MCES})_4$ (**74**) (black).

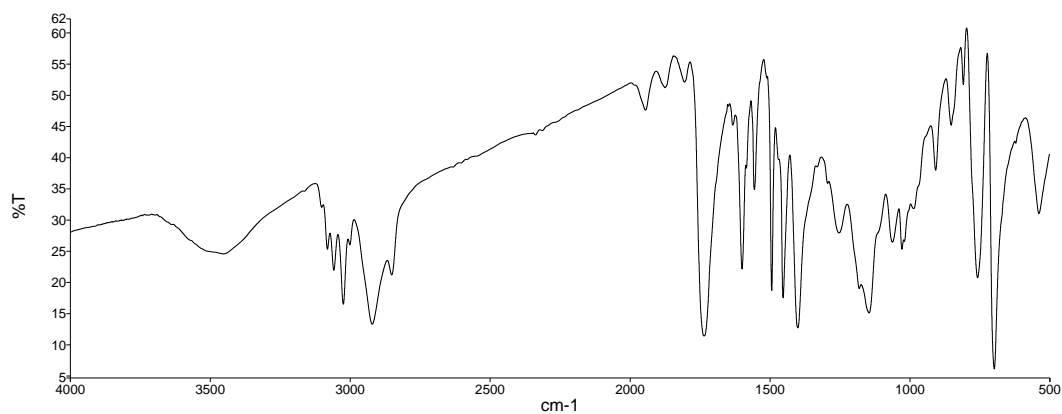


Figure 97: FTIR spectrum of $\text{pol(II)-Rh}_2(4\text{VBA})_4$ (**88**).

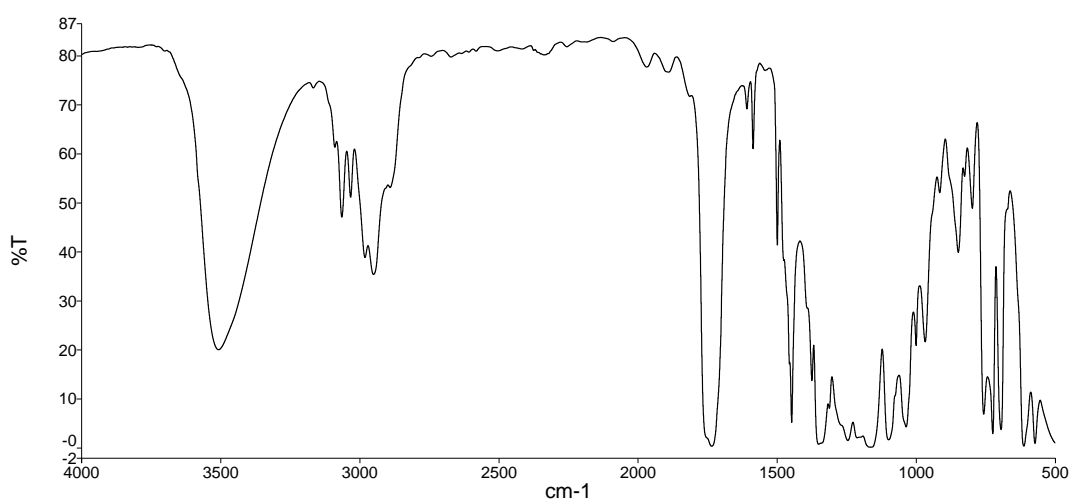


Figure 98: FTIR spectrum of $(2R,4R)$ -4-hydroxy-1-(phenylsulfonyl)pyrrolidine-2-carboxylate (**107**).

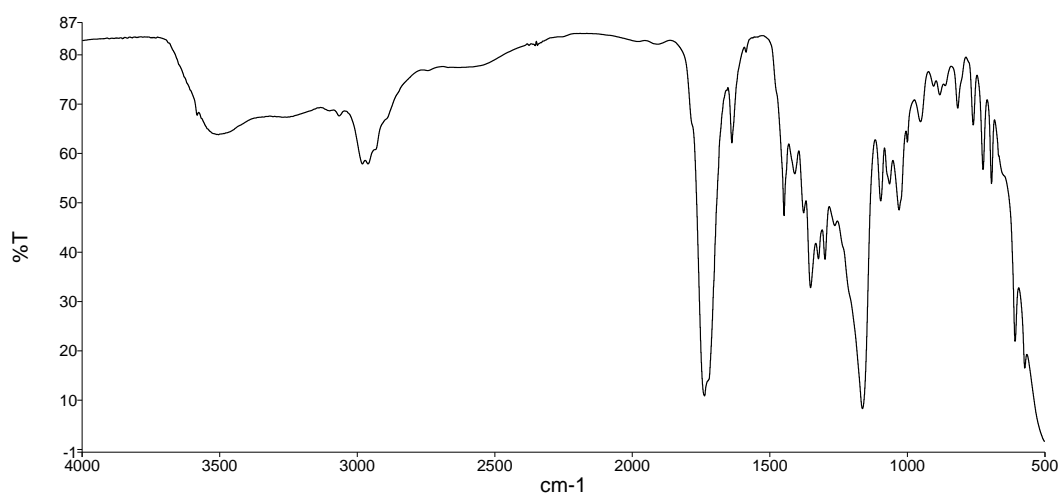


Figure 99: $(2S,4R)$ -4-((4-(2-(methacryloyloxy)ethoxy)-4-oxobutanoyl)oxy)-1-(phenylsulfonyl)pyrrolidine-2-carboxylic acid (**99**).

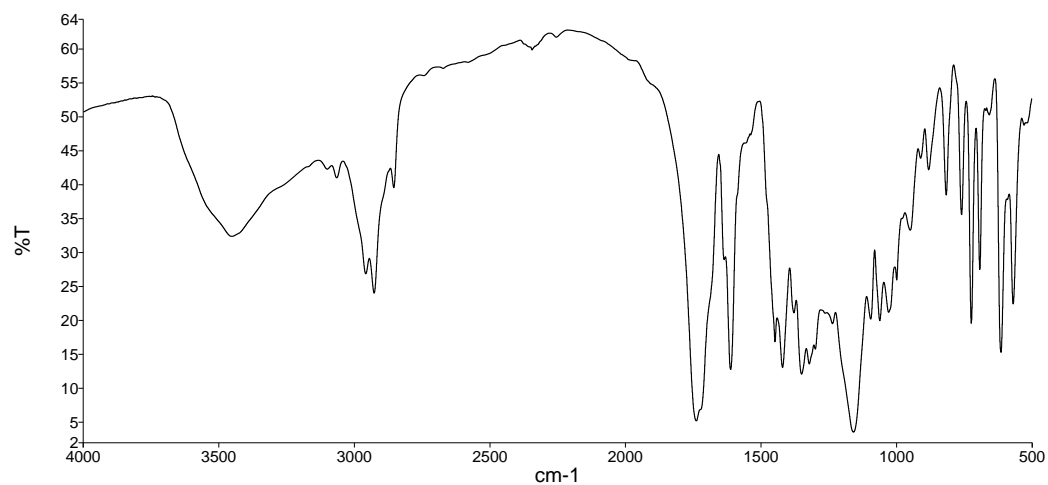


Figure 100: FTIR spectrum of $\text{Rh}_2(\text{MEPP})_4$ (**102**).

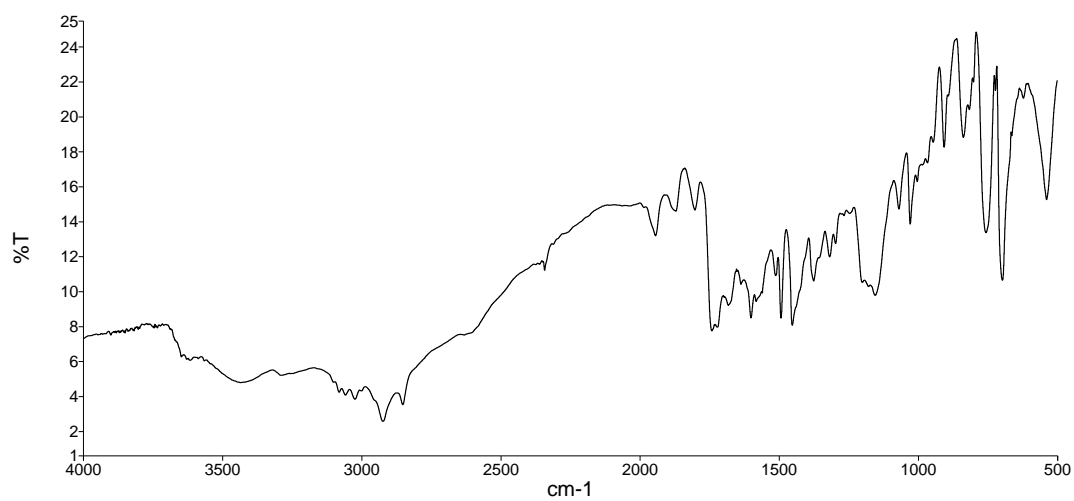


Figure 101: FTIR spectrum of $\text{pol}(\text{PM})\text{-Rh}_2(\text{MCES})_4$ (**94**).

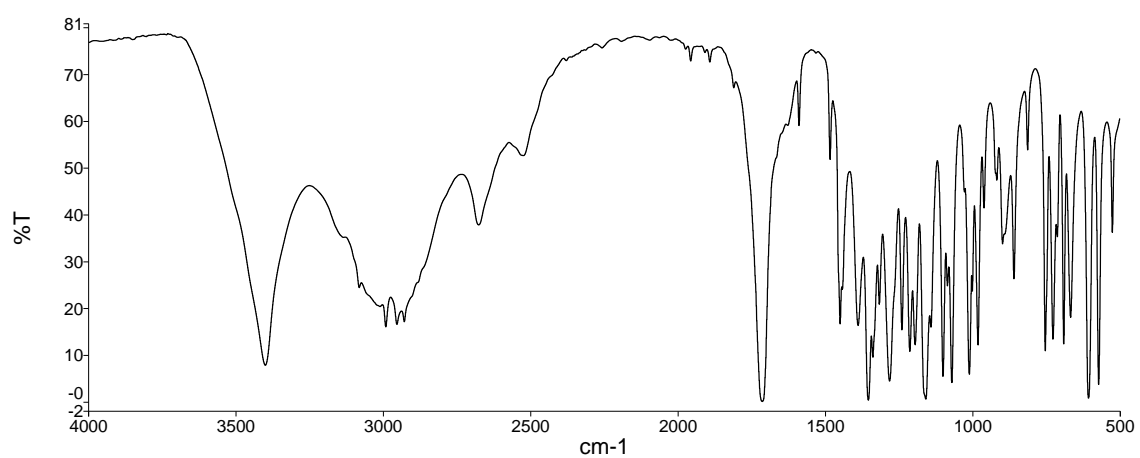


Figure 102: FTIR spectrum of $(2S,4R)\text{-4-hydroxy-1-(phenylsulphonyl)pyrrolidine-2-carboxylic acid}$ (**100**).

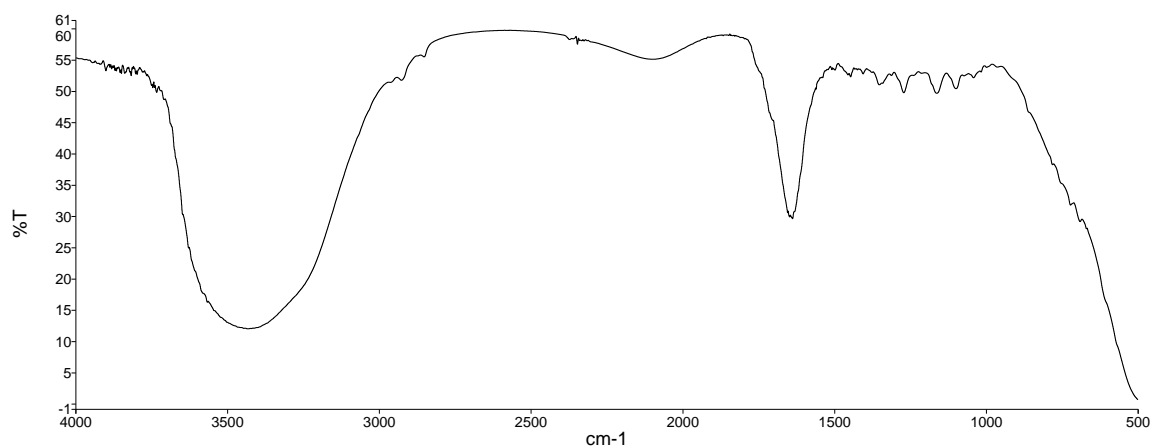


Figure 103: FTIR spectrum of (2R,4R)-1-(phenylsulfonyl)-4-((4-vinylbenzoyl)oxy)pyrrolidine-2-carboxylate (**108**)

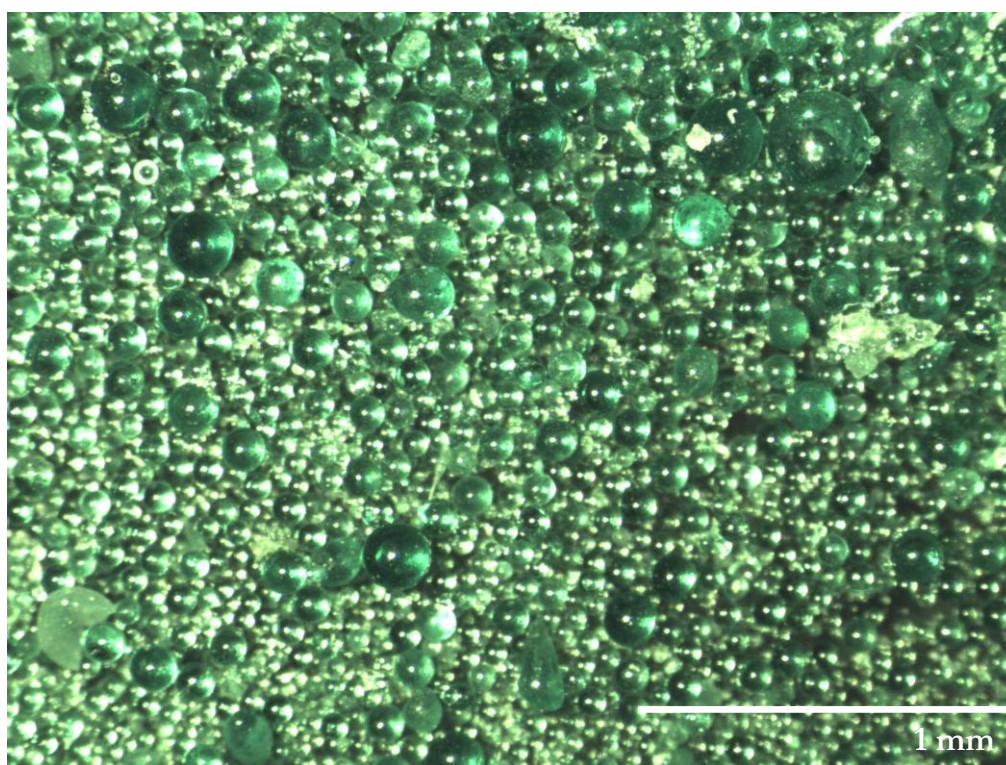


Figure 104: Microscopic picture of $\text{pol(T)-Rh}_2(4\text{VBA})_4$ (**84**).

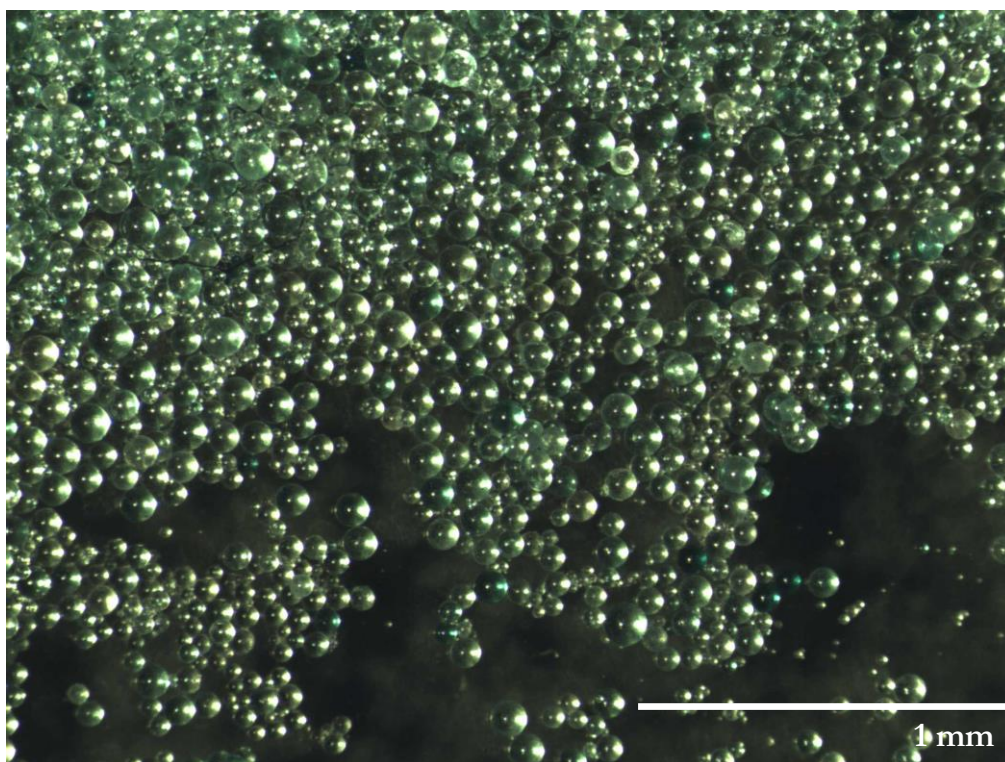


Figure 105: Microscopic picture of $\text{pol(I)-Rh}_2(\text{MCES})_4$ (**85**).

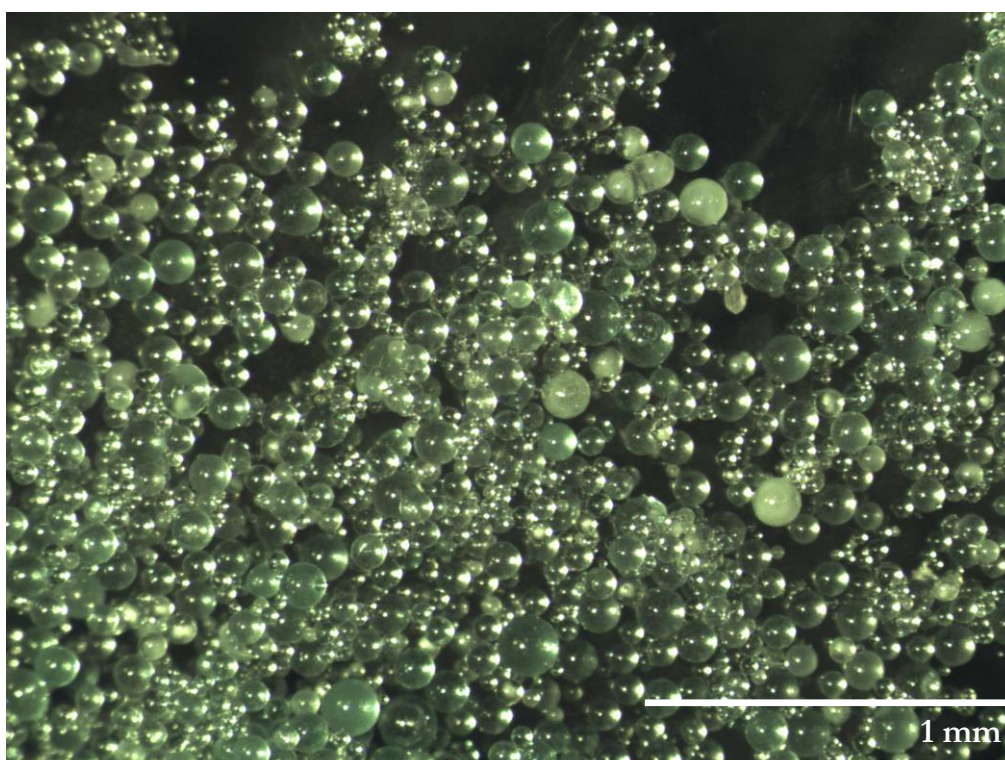


Figure 106: Microscopic picture of $\text{pol(I)-Rh}_2(\text{MCES})_2(\text{OAc}^{\text{F}})_2$ (**86**).

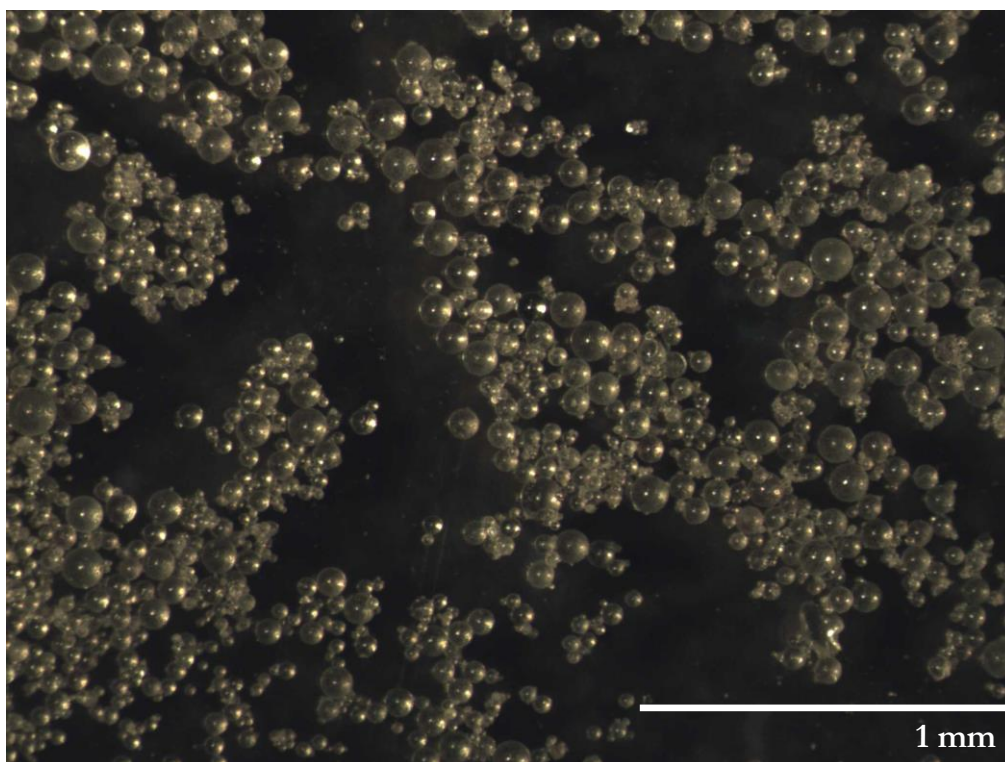


Figure 107: Microscopic picture of $\text{pol(I)-Rh}_2(4\text{VBA})_2(\text{OAc}^{\text{F}})_2$ (**83**).

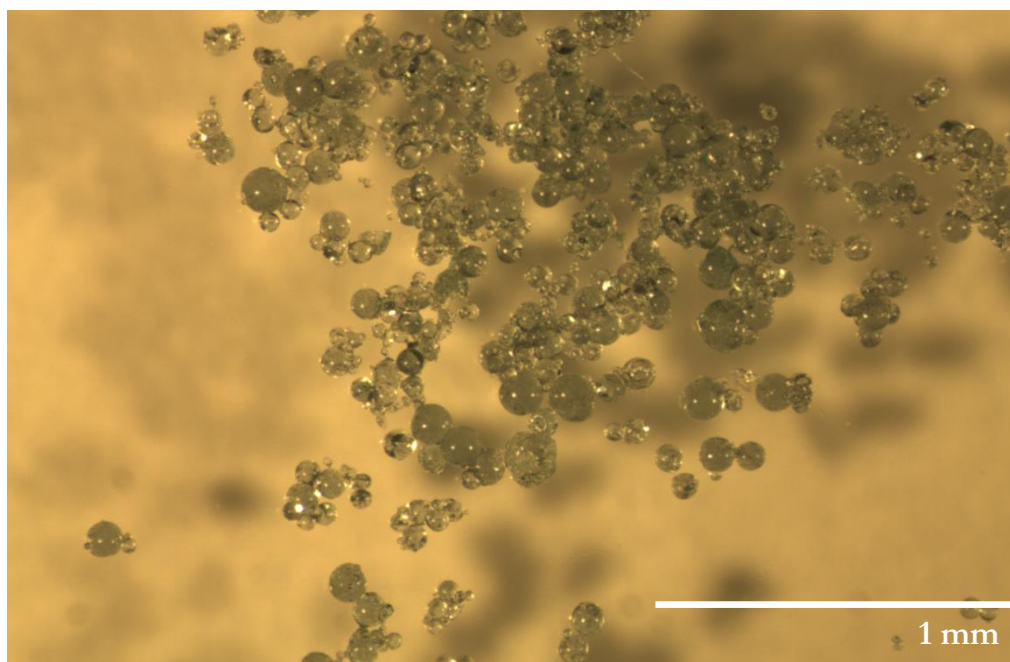


Figure 108: Microscopic picture of $\text{pol(II)-Rh}_2(\text{MCES})_4$ (**87**).

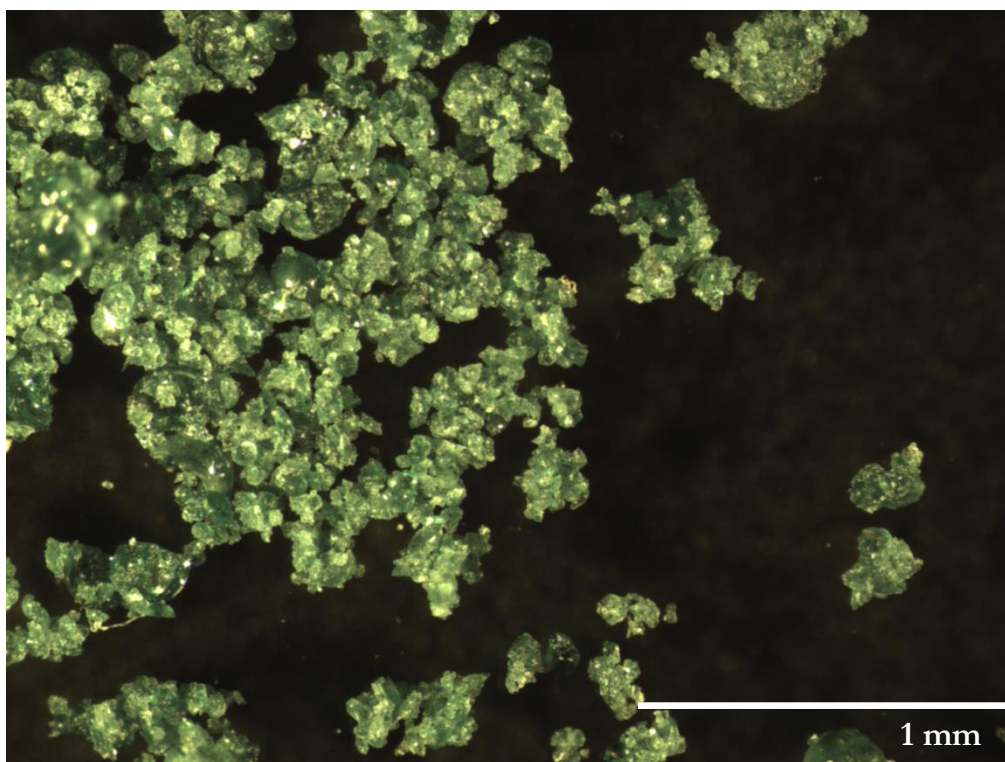


Figure 109: Microscopic picture of $\text{pol(II)-Rh}_2(4\text{VBA})_4$ (**88**).

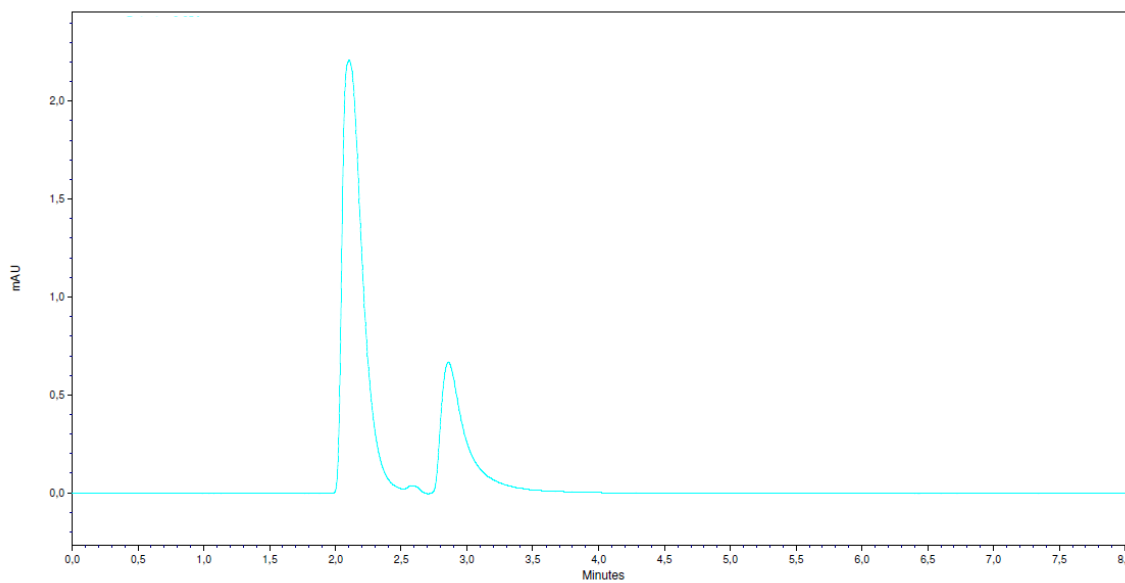


Figure 110: HPLC spectrum of $\text{Rh}_2(\text{MEPP})_4$ (**102**). Presumably, the two peaks represent two diastereomers of the complex **102**.

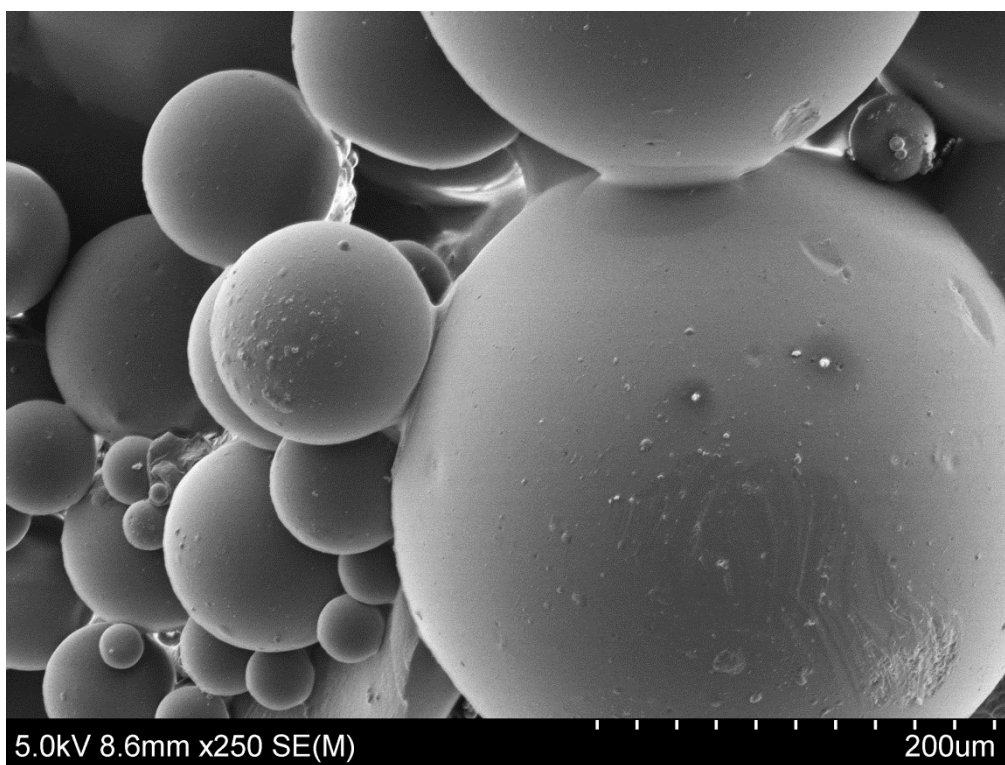


Figure 111: SEM picture of $\text{pol(I)-Rh}_2(4\text{VBA})_4$ (**84**).

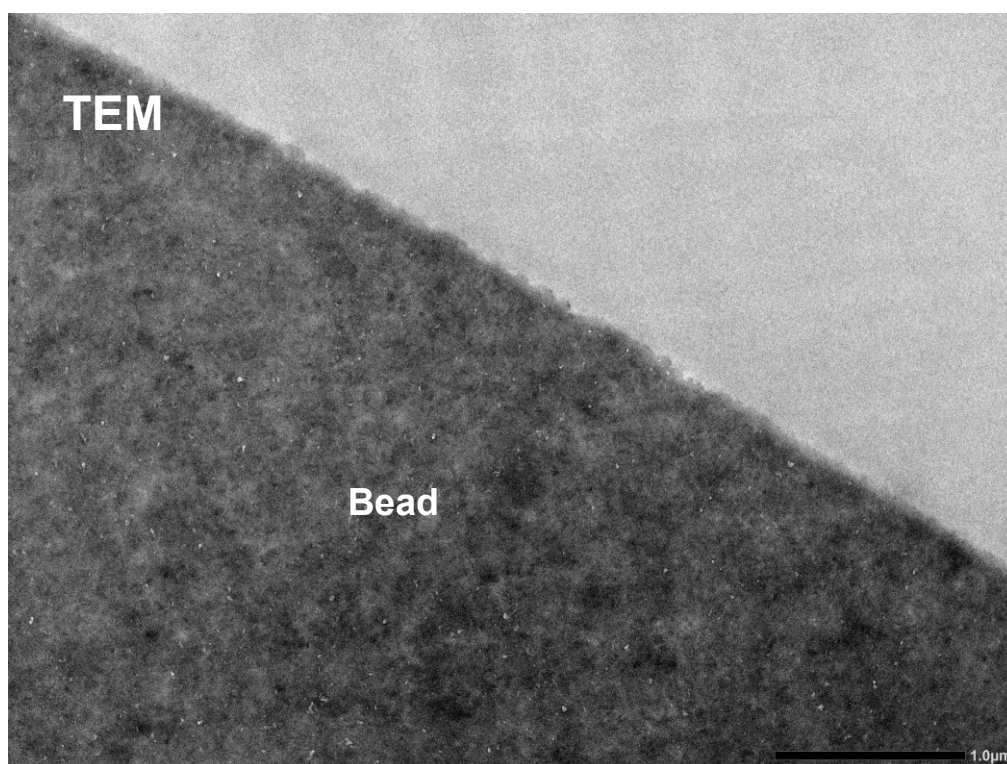


Figure 112: TEM picture of $\text{pol(I)-Rh}_2(4\text{VBA})_4$ (**84**).

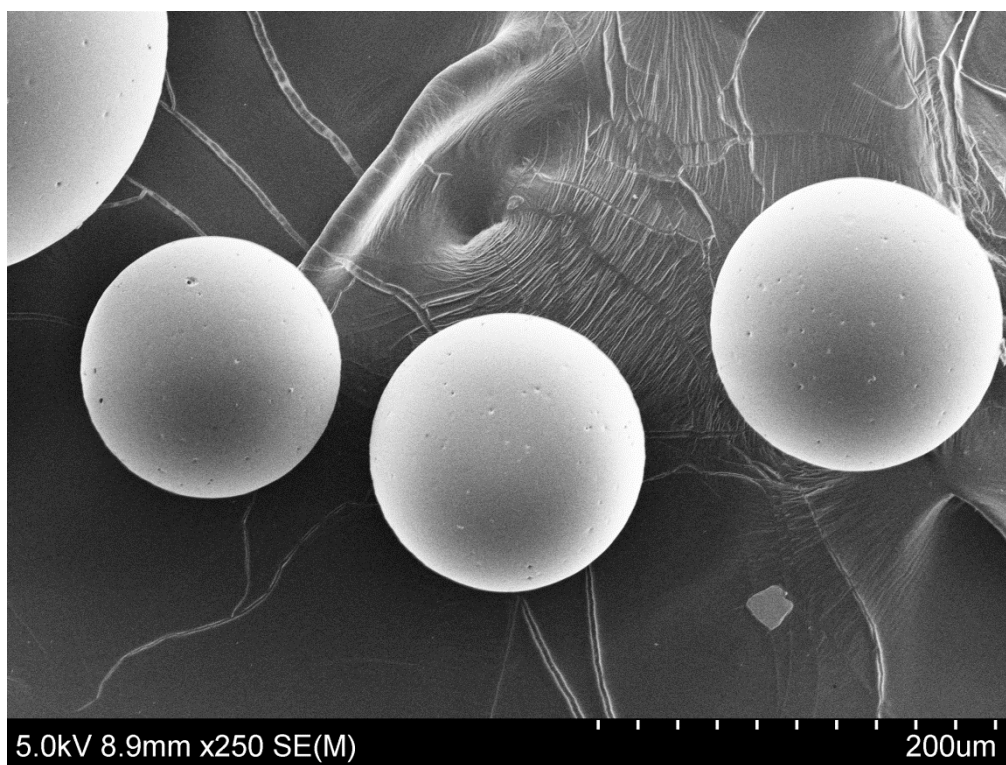


Figure 113: SEM picture of $\text{pol(I)-Rh}_2(\text{MCES})_4$ (85).

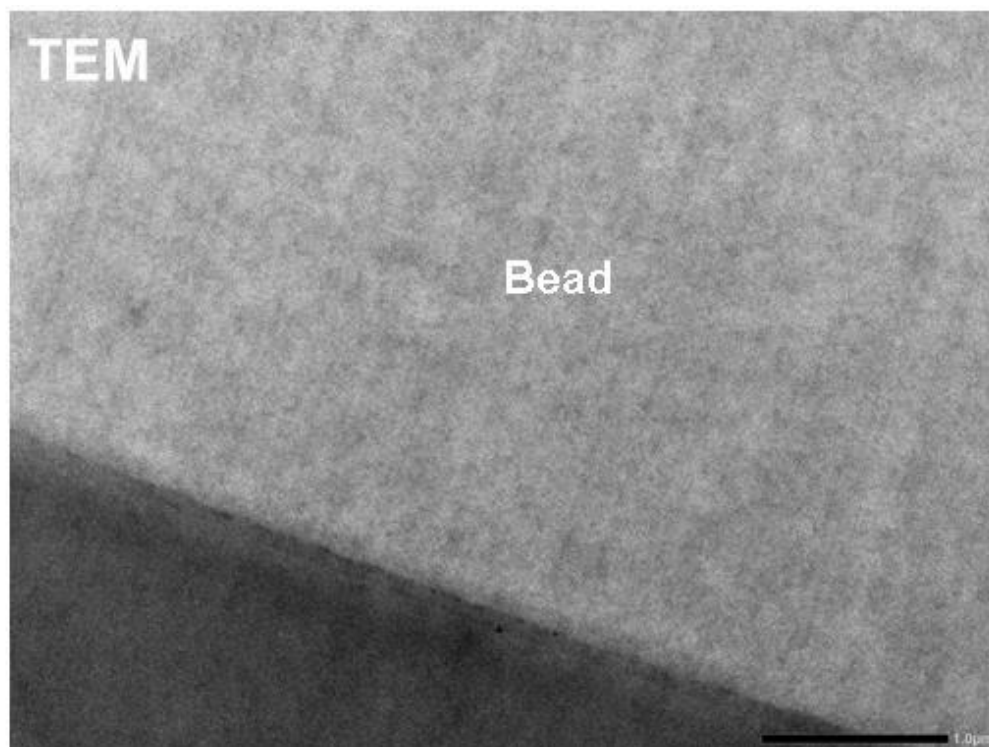


Figure 114: TEM picture of $\text{pol(I)-Rh}_2(\text{MCES})_4$ (85).

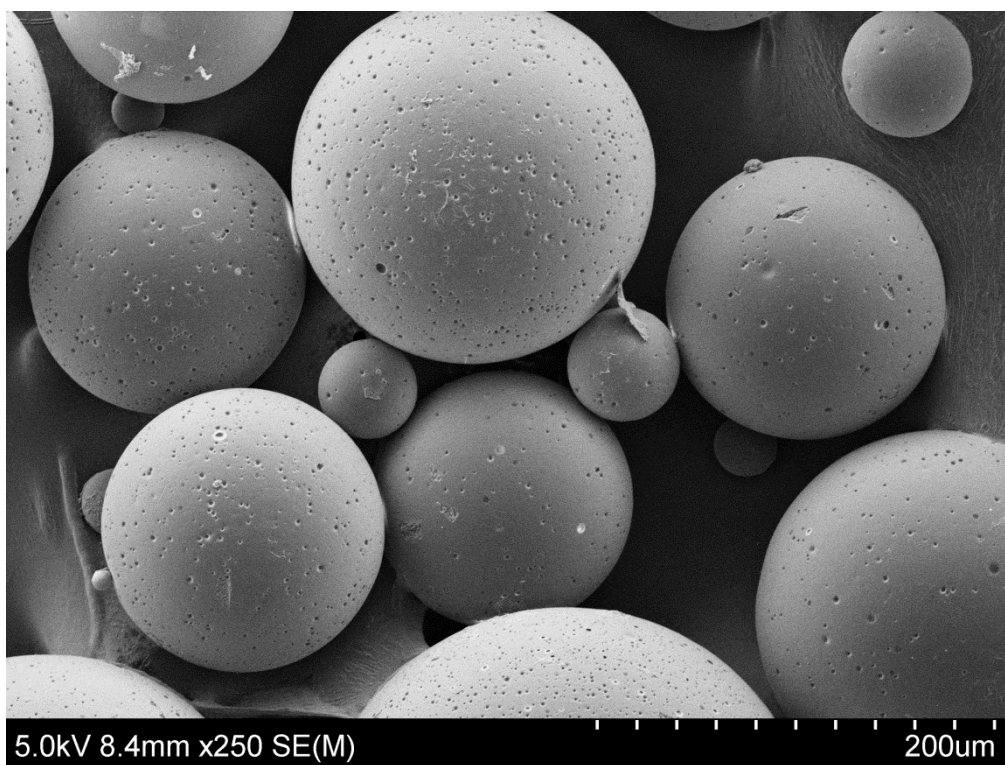


Figure 115: SEM picture of $\text{pol(I)-Rh}_2(\text{MCES})_2(\text{OAc}^{\text{F}})_2$ (**86**).

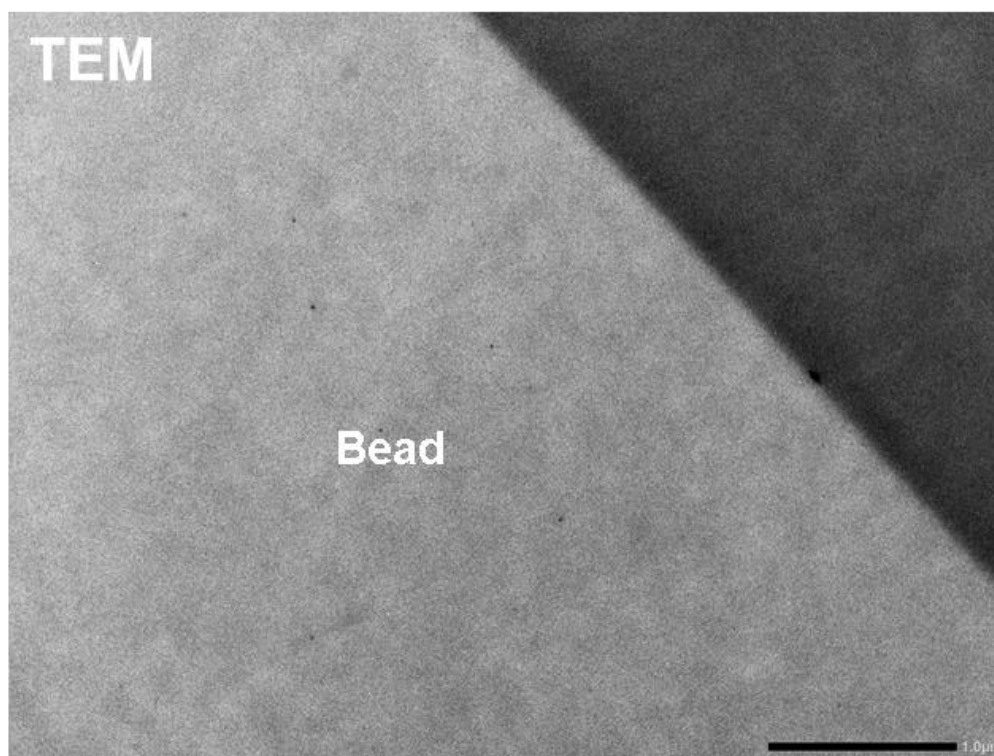


Figure 116: TEM picture of $\text{pol(I)-Rh}_2(\text{MCES})_2(\text{OAc}^{\text{F}})_2$ (**86**).

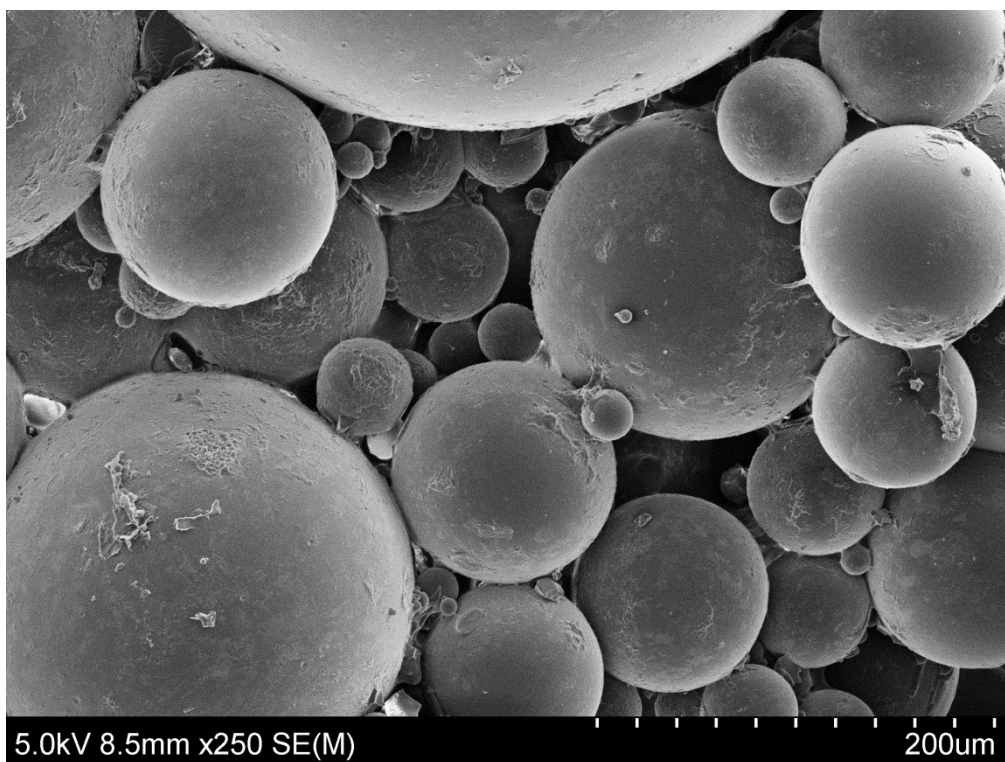


Figure 117: SEM picture of $\text{pol(I)-Rh}_2(4\text{VBA})_2(\text{OAc}^{\text{F}})_2$ (**83**).

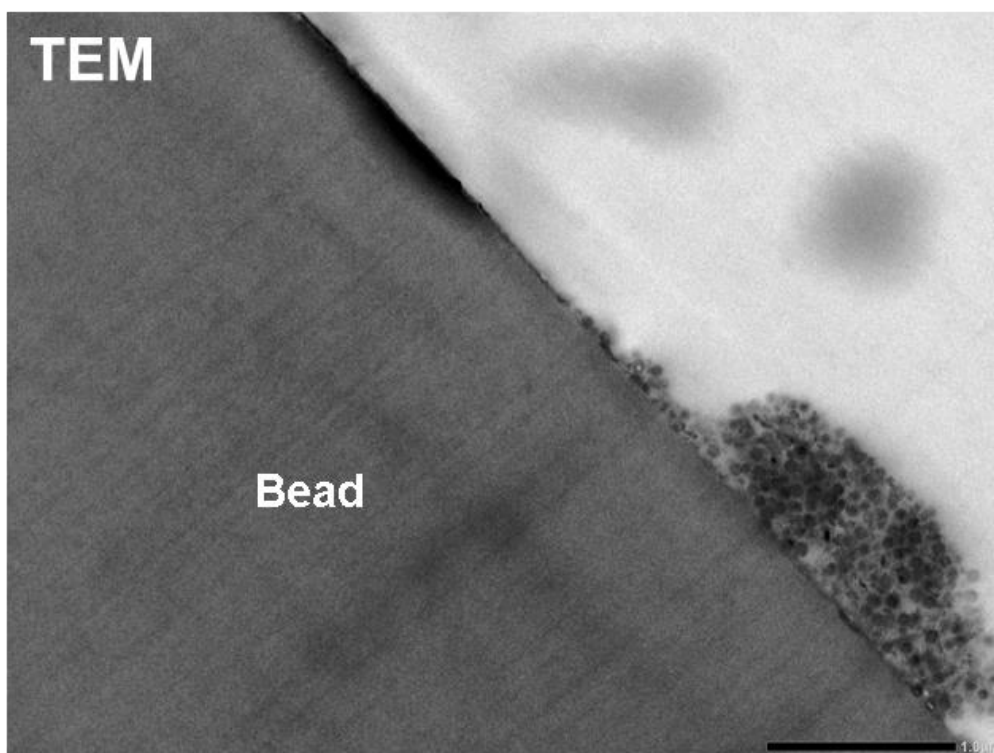


Figure 118: TEM picture of $\text{pol(I)-Rh}_2(4\text{VBA})_2(\text{OAc}^{\text{F}})_2$ (**83**).

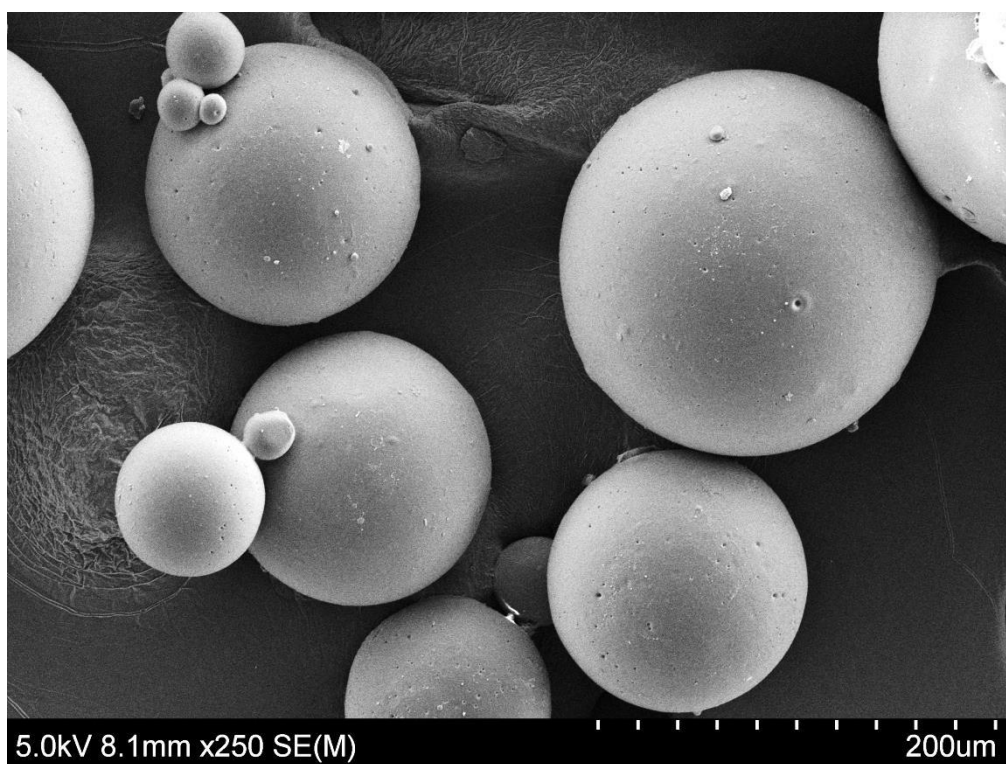


Figure 119: SEM picture of $\text{pol(II)-Rh}_2(\text{MCES})_4$ (**87**).

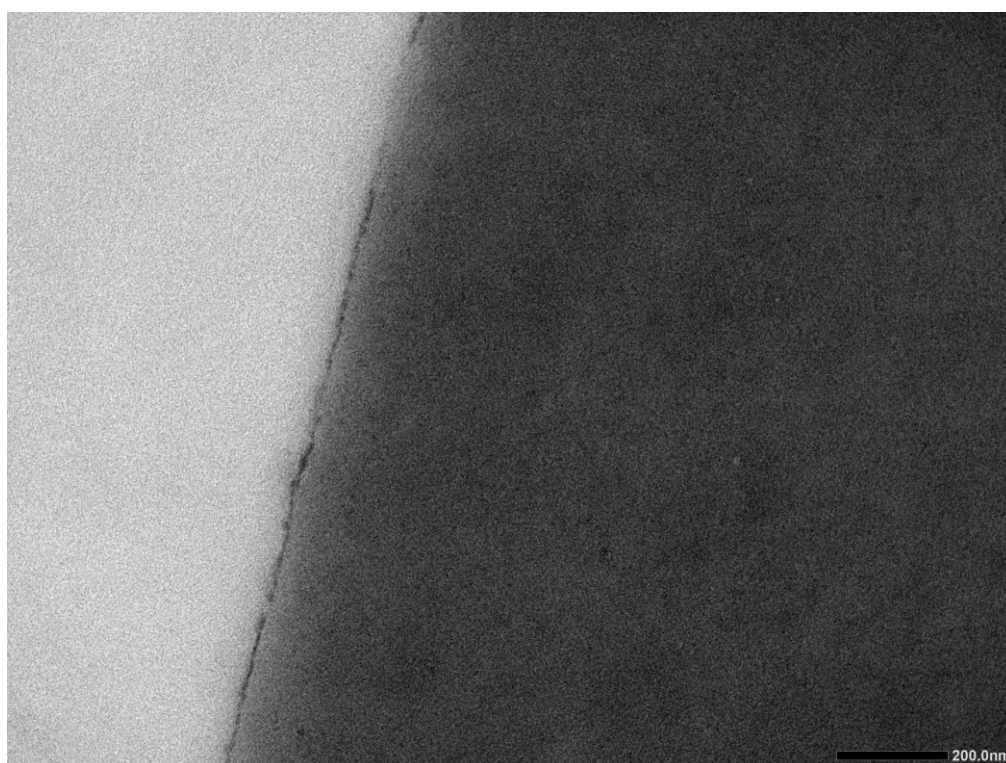


Figure 120: TEM picture of $\text{pol(II)-Rh}_2(\text{MCES})_4$ (**87**) in non-swollen state.

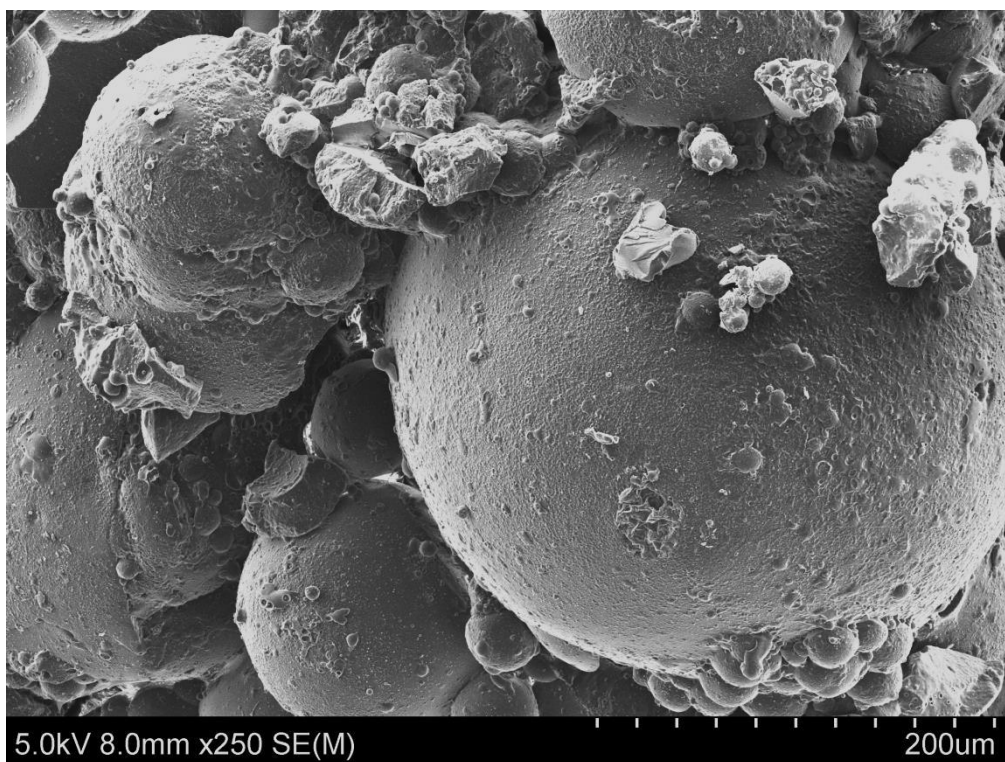


Figure 121: SEM picture of pol(II)-Rh₂(4VBA)₄ (88).

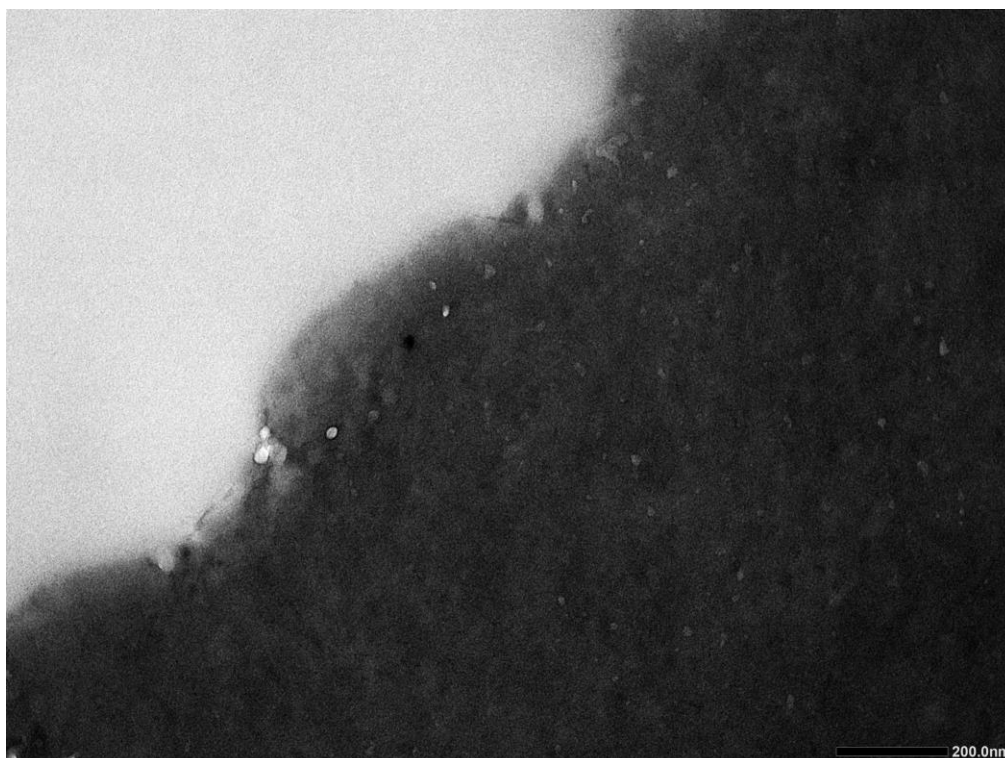


Figure 122: TEM picture of pol(II)-Rh₂(4VBA)₄ (88) in non-swollen state.

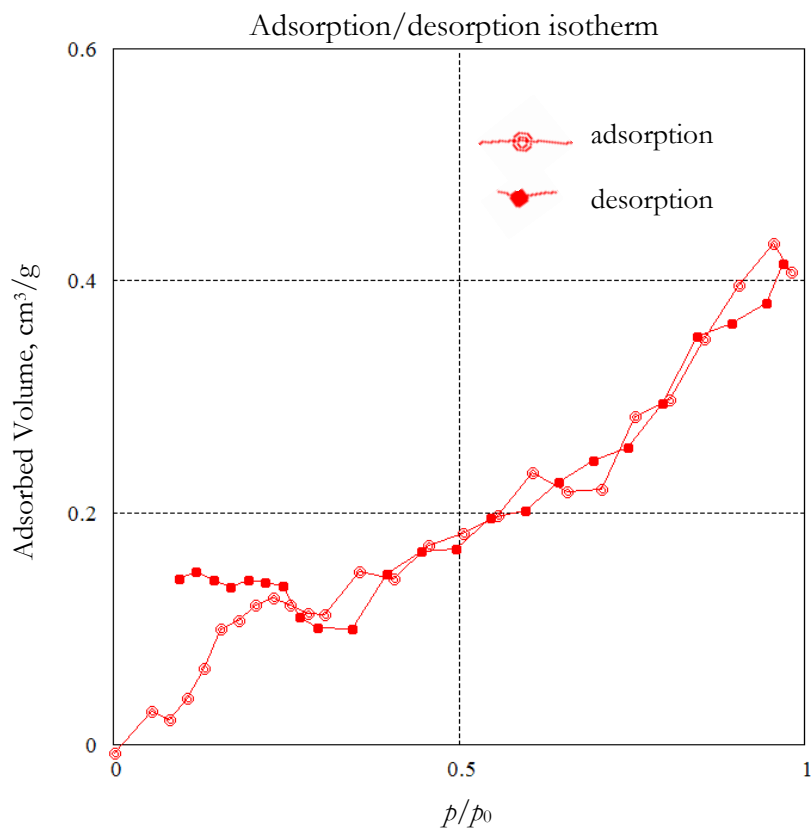


Figure 123: Isotherm of adsorption/desorption for the selected polymer catalyst of acrylic system, measured by BET method.

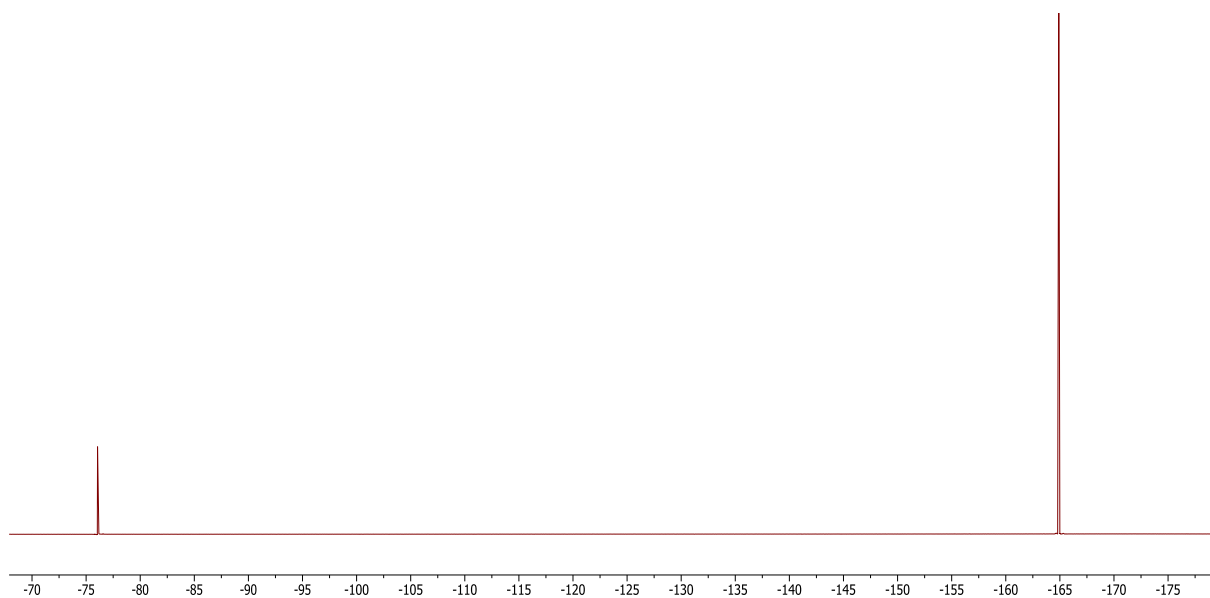


Figure 124: ¹⁹F NMR (376 MHz, Benzene-*d*₆) spectrum of Rh₂(OAc^F)₄ (7). Signal at -164.9 ppm belongs to C₆F₆.

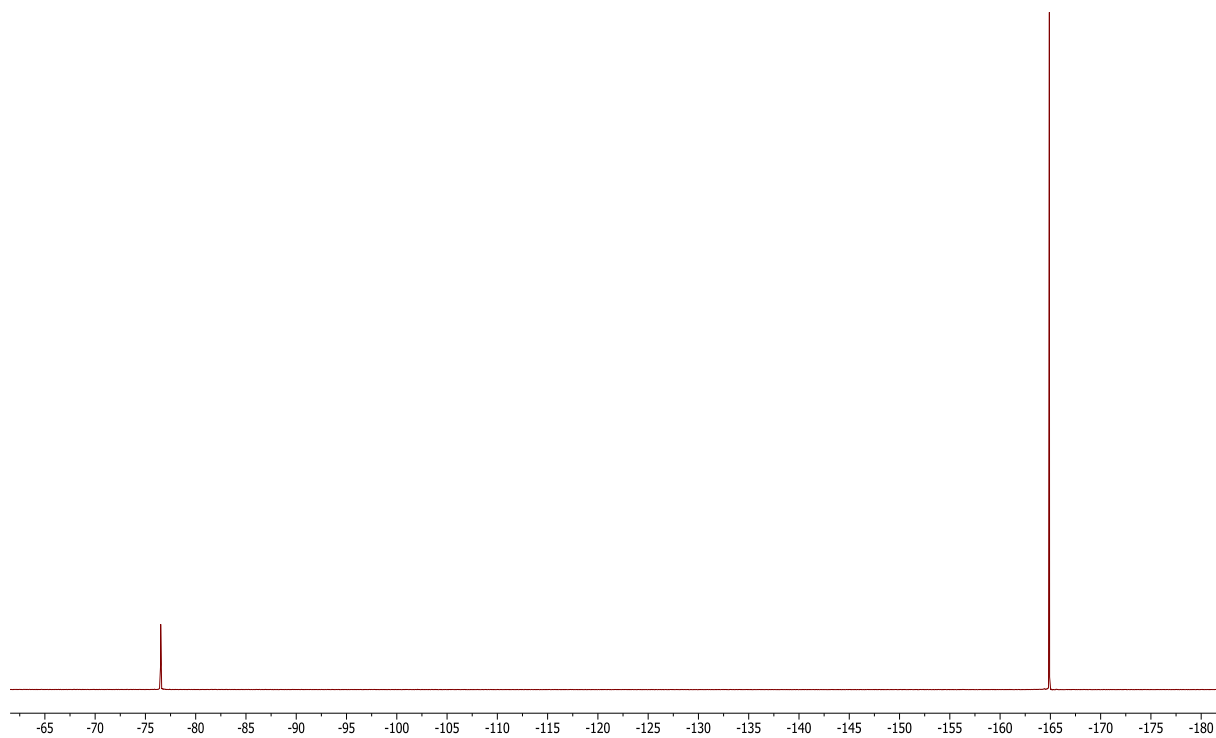


Figure 125: ^{19}F NMR (376 MHz, Benzene- d_6) spectrum of $\text{Rh}_2(\text{MCES})_2(\text{OAc}^{\text{F}})_2$ (**78**). Signal at -164.9 ppm belongs to C_6F_6 .

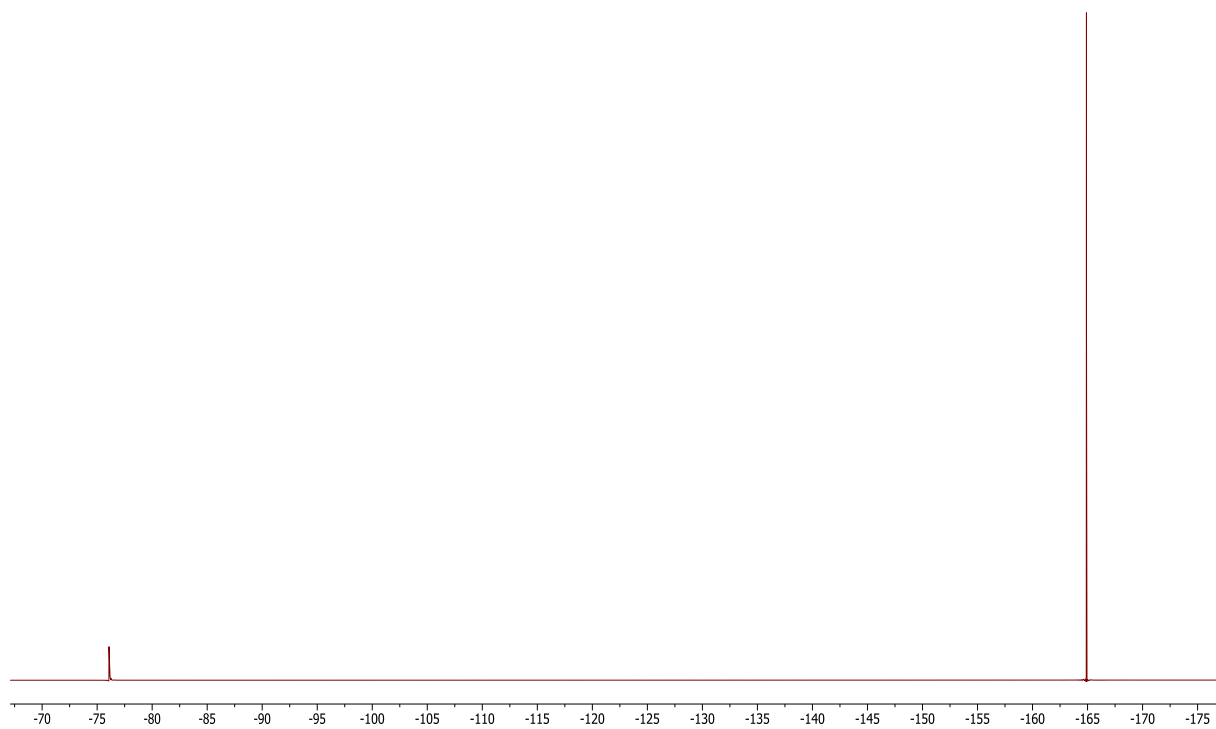


Figure 126: ^{19}F NMR (376 MHz, Benzene- d_6) spectrum of $\text{Rh}_2(4\text{VBA})_2(\text{OAc}^{\text{F}})_2$ (**77**). Signal at -164.9 ppm belongs to C_6F_6 .

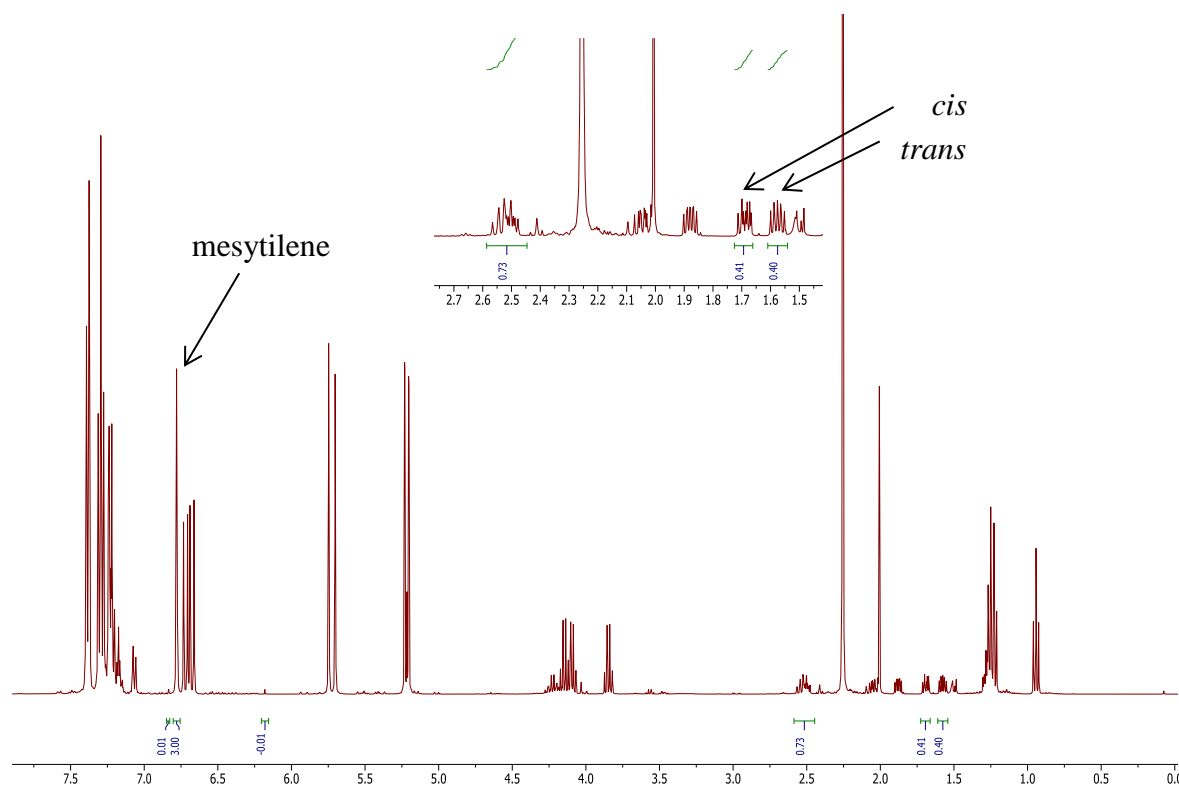


Figure 127: ^1H NMR analysis of the crude cyclopropanation reaction catalyzed by $\text{pol}(\text{I})\text{-Rh}_2(4\text{VBA})_4$ (**84**). Yield has been calculated adding the integrals for *cis*- and *trans*- diastereomers.

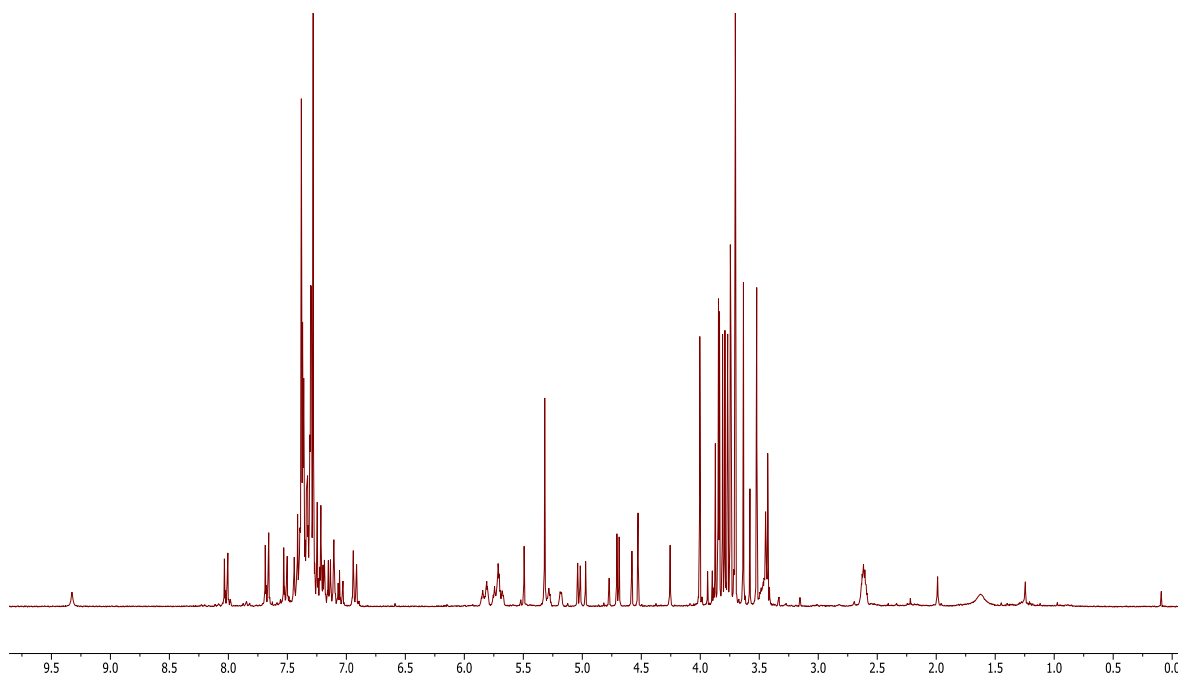


Figure 128: The crude ^1H NMR spectrum of the C-H insertion reaction displaying a complicated reaction mixture.

Table 19: Crystal data and structure refinement for Rh₂(4VBA)₂(OAc^F)₂ (**77**).

Chemical formula	C ₂₈ H ₂₆ F ₆ O ₁₀ Rh ₂
M_r	842.31
Crystal system, space group	Triclinic, $P\bar{1}$
Temperature (K)	100
a, b, c (Å)	9.0612 (4), 10.1992 (4), 10.3607 (4)
α, β, γ (°)	114.171 (2), 94.209 (2), 114.705 (2)
V (Å ³)	758.28 (6)
Z	1
Radiation type	Mo $K\alpha$
μ (mm ⁻¹)	1.18
Crystal size (mm)	0.23 × 0.11 × 0.05
T_{\min}, T_{\max}	0.668, 0.747
No. of measured, independent and observed [$I > 2s(I)$] reflections	10054, 3845, 3443
R_{int}	0.026
$(\sin \theta / \lambda)_{\text{max}}$ (Å ⁻¹)	0.676
$R[F^2 > 2s(F^2)], wR(F^2), S$	0.024, 0.054, 1.06
No. of reflections	3845
No. of parameters	260
H-atom treatment	All H-atom parameters refined
$D_{\text{Qmax}}, D_{\text{Qmin}}$ (e Å ⁻³)	0.97, -0.97

Table 20: Crystal data and structure refinement for Rh₂(MCES)₂(OAc^F)₂ (**78**).

Chemical formula	C ₃₀ H ₃₈ F ₆ O ₁₈ Rh ₂
M_r	1006.42
Crystal system, space group	Triclinic, $P\bar{1}$
Temperature (K)	100
a, b, c (Å)	8.3164 (8), 8.9446 (9), 13.3951 (13)
α, β, γ (°)	97.117 (2), 95.461 (2), 109.003 (2)
V (Å ³)	925.05 (16)
Z	1
Radiation type	Mo $K\alpha$
m (mm ⁻¹)	1.00
Crystal size (mm)	0.14 × 0.13 × 0.09
T_{\min}, T_{\max}	0.585, 0.746
No. of measured, independent and observed [$I > 2s(I)$] reflections	13632, 5578, 5084
R_{int}	0.029
$(\sin \theta/\lambda)_{\text{max}}$ (Å ⁻¹)	0.714
$R[F^2 > 2s(F^2)], wR(F^2), S$	0.024, 0.060, 1.06
No. of reflections	5578
No. of parameters	256
H-atom treatment	H-atom parameters constrained
$D_{\text{Qmax}}, D_{\text{Qmin}}$ (e Å ⁻³)	0.74, -0.93

Table 21: Crystal data and structure refinement for Rh₂(4VBA)₄ (75).

Chemical formula	C ₄₂ H ₄₀ O ₁₀ Rh ₂ ·C ₃ H ₆ O
M_r	968.64
Crystal system, space group	Monoclinic, $P2_1/n$
Temperature (K)	100
a, b, c (Å)	10.1957 (9), 15.6277 (11), 27.077 (2)
β (°)	100.461 (4)
V (Å ³)	4242.6 (6)
Z	4
Radiation type	Mo $K\alpha$
m (mm ⁻¹)	0.84
Crystal size (mm)	0.52 × 0.13 × 0.03
T_{\min}, T_{\max}	0.502, 0.746
No. of measured, independent and observed [$I > 2s(I)$] reflections	32224, 11011, 8843
R_{int}	0.056
$(\sin \theta/\lambda)_{\text{max}}$ (Å ⁻¹)	0.681
$R[F^2 > 2s(F^2)], wR(F^2), S$	0.112, 0.326, 1.11
No. of reflections	11011
No. of parameters	529
H-atom treatment	H-atom parameters constrained $w = 1/[s^2(F_o^2) + (0.0824P)^2 + 189.6551P]$ where $P = (F_o^2 + 2F_c^2)/3$
$D_{\text{Q}_{\max}}, D_{\text{Q}_{\min}}$ (e Å ⁻³)	4.29, -2.38

Bibliography

- (1) Goldsmith, D. *Journal of Chemical Education* **1999**, 76, 1191.
- (2) Grasse, P. B.; Brauer, B. E.; Zupancic, J. J.; Kaufmann, K. J.; Schuster, G. B. *Journal of the American Chemical Society* **1983**, 105, 6833.
- (3) de Frémont, P.; Marion, N.; Nolan, S. P. *Coordination Chemistry Reviews* **2009**, 253, 862.
- (4) Iwamoto, E.; Hirai, K.; Tomioka, H. *Journal of the American Chemical Society* **2003**, 125, 14664.
- (5) Furukawa, J.; Kawabata, N.; Fujita, T. *Tetrahedron* **1970**, 26, 243.
- (6) Hodgson, D. M.; Chung, Y. K.; Paris, J.-M. *Journal of the American Chemical Society* **2004**, 126, 8664.
- (7) Kovacs, D.; Lee, M.-S.; Olson, D.; Jackson, J. E. *Journal of the American Chemical Society* **1996**, 118, 8144.
- (8) Shapiro, R. H. In *Organic Reactions*; John Wiley & Sons, Inc.: 2004.
- (9) Forstinger, K.; Metz, H. J. In *Ullmann's Encyclopedia of Industrial Chemistry*; Wiley-VCH Verlag GmbH & Co. KGaA: 2000.
- (10) Cain, J. C.; Nicoll, F. *Journal of the Society of Dyers and Colourists* **1903**, 19, 102.
- (11) T. J. de Boer, H. J. B. *Organic Syntheses* **1963**, 4.
- (12) Saalfrank, R. W. *Angewandte Chemie* **1987**, 99, 1335.
- (13) Silberrad, O.; Roy, C. S. *Journal of the Chemical Society, Transactions* **1906**, 89, 179.
- (14) Anciaux, A. J.; Hubert, A. J.; Noels, A. F.; Petiniot, N.; Teyssie, P. *The Journal of Organic Chemistry* **1980**, 45, 695.
- (15) Paulissen, R.; Reimlinger, H.; Hayez, E.; Hubert, A. J.; Teyssié, P. *Tetrahedron Letters* **1973**, 14, 2233.
- (16) Cotton, F. A.; Dikarev, E. V.; Feng, X. *Inorganica Chimica Acta* **1995**, 237, 19.
- (17) Pirrung, M. C.; Morehead, A. T. *Journal of the American Chemical Society* **1996**, 118, 8162.
- (18) Drago, R. S.; Long, J. R.; Cosmano, R. *Inorganic Chemistry* **1981**, 20, 2920.
- (19) Telsler, J.; Drago, R. S. *Inorg. Chem.* **1984**, 23, 2599.
- (20) Doyle, M. P.; Colman, M. R.; Chinn, M. S. *Inorganic Chemistry* **1984**, 23, 3684.
- (21) Sargent, L. A.; Rollog, E. M.; Eagle, T. C. *Theoretical Chemistry Accounts*, 97, 283.
- (22) Yates, P.; Hambly, G. F. *Canadian Journal of Chemistry* **1979**, 57, 1668.
- (23) Doyle, M. P.; Winchester, W. R.; Simonsen, S. H.; Ghosh, R. *Inorganica Chimica Acta* **1994**, 220, 193.
- (24) Snyder, J. P.; Padwa, A.; Stengel, T.; Arduengo, A. J.; Jockisch, A.; Kim, H.-J. *Journal of the American Chemical Society* **2001**, 123, 11318.
- (25) Padwa, A.; Snyder, J. P.; Curtis, E. A.; Sheehan, S. M.; Worsencroft, K. J.; Kappe, C. O. *Journal of the American Chemical Society* **2000**, 122, 8155.
- (26) Werlé, C.; Goddard, R.; Philipps, P.; Farès, C.; Fürstner, A. *Journal of the American Chemical Society* **2016**, 138, 3797.
- (27) Doyle, M. P.; Forbes, D. C. *Chemical Reviews* **1998**, 98, 911.
- (28) Internet In <http://www.infomine.com/investment/metal-prices/rhodium/> 2016.
- (29) Doyle, M. P.; Duffy, R.; Ratnikov, M.; Zhou, L. *Chemical Reviews* **2010**, 110, 704.
- (30) Padwa, A.; Zhang, Z. J.; Zhi, L. *The Journal of Organic Chemistry* **2000**, 65, 5223.
- (31) Doyle, M. P.; Bagheri, V.; Wandless, T. J.; Harn, N. K.; Brinker, D. A.; Eagle, C. T.; Loh, K. L. *Journal of the American Chemical Society* **1990**, 112, 1906.

- (32) Davies, H. M. L.; Morton, D. *Chemical Society Reviews* **2011**, *40*, 1857.
- (33) Callot, H. J.; Metz, F. *Tetrahedron* **1985**, *41*, 4495.
- (34) Roos, G. H. P.; McKervey, M. A. *Synthetic Communications* **1992**, *22*, 1751.
- (35) Doyle, M. P.; Van Oeveren, A.; Westrum, L. J.; Protopopova, M. N.; Clayton, T. W. *Journal of the American Chemical Society* **1991**, *113*, 8982.
- (36) Doyle, M. P.; Zhou, Q.-L.; Charnsangavej, C.; Longoria, M. A.; McKervey, M. A.; García, C. F. *Tetrahedron Letters* **1996**, *37*, 4129.
- (37) Davies, H. M. L.; Bruzinski, P. R.; Lake, D. H.; Kong, N.; Fall, M. J. *Journal of the American Chemical Society* **1996**, *118*, 6897.
- (38) Davies, H. M. L.; Panaro, S. A. *Tetrahedron Letters* **1999**, *40*, 5287.
- (39) Lindsay, V. N. G.; Lin, W.; Charette, A. B. *Journal of the American Chemical Society* **2009**, *131*, 16383.
- (40) Crabtree, R. H. *Journal of Organometallic Chemistry* **2004**, *689*, 4083.
- (41) Davies, H. M. L.; Gregg, T. M. *Tetrahedron Letters* **2002**, *43*, 4951.
- (42) Davies, H. M. L.; Walji, A. M.; Townsend, R. J. *Tetrahedron Letters* **2002**, *43*, 4981.
- (43) Pellissier, H. *Tetrahedron* **2008**, *64*, 7041.
- (44) Davies, H. M. L.; Hansen, T.; Churchill, M. R. *Journal of the American Chemical Society* **2000**, *122*, 3063.
- (45) Lebel, H.; Marcoux, J.-F.; Molinaro, C.; Charette, A. B. *Chemical Reviews* **2003**, *103*, 977.
- (46) Doyle, M. P.; Westrum, L. J.; Wolthuis, W. N. E.; See, M. M.; Boone, W. P.; Bagheri, V.; Pearson, M. M. *Journal of the American Chemical Society* **1993**, *115*, 958.
- (47) Nakamura, E.; Yoshikai, N.; Yamanaka, M. *Journal of the American Chemical Society* **2002**, *124*, 7181.
- (48) Davies, H. M. L.; Coleman, M. G.; Ventura, D. L. *Organic Letters* **2007**, *9*, 4971.
- (49) Ventura, D. L.; Li, Z.; Coleman, M. G.; Davies, H. M. L. *Tetrahedron* **2009**, *65*, 3052.
- (50) Candeias, N. R.; Afonso, C. A. M.; Gois, P. M. P. *Organic & Biomolecular Chemistry* **2012**, *10*, 3357.
- (51) Baiker, A. In *Chiral Catalyst Immobilization and Recycling*; Wiley-VCH Verlag GmbH: 2007, p 155.
- (52) Bergbreiter, D. E. In *Chiral Catalyst Immobilization and Recycling*; Wiley-VCH Verlag GmbH: 2007, p 43.
- (53) Salvadori, P.; Pini, D.; Petri, A.; Mandoli, A. In *Chiral Catalyst Immobilization and Recycling*; Wiley-VCH Verlag GmbH: 2007, p 235.
- (54) Vankelecom, I. F. J.; Jacobs, P. A. In *Chiral Catalyst Immobilization and Recycling*; Wiley-VCH Verlag GmbH: 2007, p 19.
- (55) Bergbreiter, D. E.; Morvant, M.; Chen, B. *Tetrahedron Letters* **1991**, *32*, 2731.
- (56) Guenther, J.; Reibenspies, J.; Blümel, J. *Advanced Synthesis & Catalysis* **2011**, *353*, 443.
- (57) Doyle, M. P.; Timmons, D. J.; Tumonis, J. S.; Gau, H.-M.; Blossey, E. C. *Organometallics* **2002**, *21*, 1747.
- (58) Hultman, H. M.; de Lang, M.; Arends, I. W. C. E.; Hanefeld, U.; Sheldon, R. A.; Maschmeyer, T. *Journal of Catalysis* **2003**, *217*, 275.
- (59) Lively, R. P.; Chance, R. R.; Kelley, B. T.; Deckman, H. W.; Drese, J. H.; Jones, C. W.; Koros, W. J. *Industrial & Engineering Chemistry Research* **2009**, *48*, 7314.
- (60) Moschetta, E. G.; Negretti, S.; Chepiga, K. M.; Brunelli, N. A.; Labreche, Y.; Feng, Y.; Rezaei, F.; Lively, R. P.; Koros, W. J.; Davies, H. M. L.; Jones, C. W. *Angewandte Chemie International Edition* **2015**, *54*, 6470.
- (61) Chepiga, K. M.; Feng, Y.; Brunelli, N. A.; Jones, C. W.; Davies, H. M. L. *Organic Letters* **2013**, *15*, 6136.

- (62) Candeias, N. R.; Afonso, C. A. M.; Gois, P. M. P. *Org. Biomol. Chem.* **2012**, *10*, 3357.
- (63) Nagashima, T.; Davies, H. M. L. *Organic Letters* **2002**, *4*, 1989.
- (64) Wang, S.-S. *Journal of the American Chemical Society* **1973**, *95*, 1328.
- (65) Davies, H. M. L.; Walji, A. M. *Organic Letters* **2005**, *7*, 2941.
- (66) Davies, H. M. L.; Walji, A. M.; Nagashima, T. *Journal of the American Chemical Society* **2004**, *126*, 4271.
- (67) Dikarev, E. V.; Kumar, D. K.; Filatov, A. S.; Anan, A.; Xie, Y.; Asefa, T.; Petrukhina, M. A. *ChemCatChem* **2010**, *2*, 1461.
- (68) Kumar, D. K.; Filatov, A. S.; Napier, M.; Sun, J.; Dikarev, E. V.; Petrukhina, M. A. *Inorganic Chemistry* **2012**, *51*, 4855.
- (69) C. Sherrington, D. *Chemical Communications* **1998**, 2275.
- (70) Takeda, K.; Oohara, T.; Anada, M.; Nambu, H.; Hashimoto, S. *Angewandte Chemie International Edition* **2010**, *49*, 6979.
- (71) Saito, H.; Oishi, H.; Kitagaki, S.; Nakamura, S.; Anada, M.; Hashimoto, S. *Organic Letters* **2002**, *4*, 3887.
- (72) Oohara, T.; Nambu, H.; Anada, M.; Takeda, K.; Hashimoto, S. *Advanced Synthesis & Catalysis* **2012**, *354*, 2331.
- (73) Islam, R. U.; Taher, A.; Choudhary, M.; Siwal, S.; Mallick, K. *Scientific Reports* **2015**, *5*, 9632.
- (74) Kristensen, T. E.; Hansen, T. In *Catalytic Methods in Asymmetric Synthesis*; John Wiley & Sons, Inc.: 2011, p 209.
- (75) Kristensen, T. E.; Hansen, F. K.; Hansen, T. *European Journal of Organic Chemistry* **2009**, *2009*, 387.
- (76) Kristensen, T. E.; Hansen, T. *European Journal of Organic Chemistry* **2010**, *2010*, 3179.
- (77) Lou, Y.; Remarchuk, T. P.; Corey, E. J. *Journal of the American Chemical Society* **2005**, *127*, 14223.
- (78) Bear, J. L.; Kitchens, J.; Willcott Iii, M. R. *Journal of Inorganic and Nuclear Chemistry* **1971**, *33*, 3479.
- (79) Nandi, S.; Winter, H. H. *Macromolecules* **2005**, *38*, 4447.
- (80) Wang, H.; Guptill, D. M.; Alvarez, A. V.; Musaev, D. G.; Davies, H. M. L. *Chemical science (Royal Society of Chemistry : 2010)* **2013**, *4*, 2844.
- (81) Wren, S. P.; Nguyen, T. H.; Gascoine, P.; Lacey, R.; Sun, T.; Grattan, K. T. V. *Sensors and Actuators B: Chemical* **2014**, *193*, 35.
- (82) Dyker, G. *Angewandte Chemie International Edition* **2000**, *39*, 4237.
- (83) Bond, G. C.; Sermon, P. A. *Gold Bulletin*, *6*, 102.
- (84) Haruta, M. *Nature* **2005**, *437*, 1098.
- (85) Hutchings, G. J. *Journal of Catalysis* **1985**, *96*, 292.
- (86) Hashmi, A. S. K.; Yang, W.; Rominger, F. *Advanced Synthesis & Catalysis* **2012**, *354*, 1273.
- (87) Couper, A.; Eley, D. D. *Discussions of the Faraday Society* **1950**, *8*, 172.
- (88) Bond, G. C.; Sermon, P. A.; Webb, G.; Buchanan, D. A.; Wells, P. B. *Journal of the Chemical Society, Chemical Communications* **1973**, 444b.
- (89) Ito, Y.; Sawamura, M.; Hayashi, T. *Journal of the American Chemical Society* **1986**, *108*, 6405.
- (90) Hashmi, A. S. K.; Schwarz, L.; Choi, J.-H.; Frost, T. M. *Angewandte Chemie International Edition* **2000**, *39*, 2285.
- (91) Yang, C.-G.; He, C. *Journal of the American Chemical Society* **2005**, *127*, 6966.
- (92) Shi, Z.; He, C. *Journal of the American Chemical Society* **2004**, *126*, 13596.
- (93) Dreaden, E. C.; Alkilany, A. M.; Huang, X.; Murphy, C. J.; El-Sayed, M. A. *Chemical Society Reviews* **2012**, *41*, 2740.

- (94) Anker, J. N.; Hall, W. P.; Lyandres, O.; Shah, N. C.; Zhao, J.; Van Duyne, R. P. *Nat Mater* **2008**, *7*, 442.
- (95) Dreaden, E. C.; Mackey, M. A.; Huang, X.; Kang, B.; El-Sayed, M. A. *Chemical Society Reviews* **2011**, *40*, 3391.
- (96) Ding, Y.; Jiang, Z.; Saha, K.; Kim, C. S.; Kim, S. T.; Landis, R. F.; Rotello, V. M. *Mol Ther* **2014**, *22*, 1075.
- (97) Lal, S.; Clare, S. E.; Halas, N. J. *Accounts of Chemical Research* **2008**, *41*, 1842.
- (98) de Frémont, P.; Scott, N. M.; Stevens, E. D.; Nolan, S. P. *Organometallics* **2005**, *24*, 2411.
- (99) Pérez, P. J.; Díaz-Requejo, M. M.; Rivilla, I. *Beilstein Journal of Organic Chemistry* **2011**, *7*, 653.
- (100) Xu, G.; Zhu, C.; Gu, W.; Li, J.; Sun, J. *Angewandte Chemie International Edition* **2015**, *54*, 883.
- (101) Fructos, M. R.; Belderrain, T. R.; de Frémont, P.; Scott, N. M.; Nolan, S. P.; Díaz-Requejo, M. M.; Pérez, P. J. *Angewandte Chemie* **2005**, *117*, 5418.
- (102) Corma, A.; Leyva-Pérez, A.; Sabater, M. J. *Chemical Reviews* **2011**, *111*, 1657.
- (103) Fürstner, A.; Davies, P. W. *Angewandte Chemie International Edition* **2007**, *46*, 3410.
- (104) Antoniotti, S.; Genin, E.; Michelet, V.; Genêt, J.-P. *Journal of the American Chemical Society* **2005**, *127*, 9976.
- (105) Asao, N.; Takahashi, K.; Lee, S.; Kasahara, T.; Yamamoto, Y. *Journal of the American Chemical Society* **2002**, *124*, 12650.
- (106) Hashmi, A. S. K.; Bührle, M.; Salathé, R.; Bats, J. W. *Advanced Synthesis & Catalysis* **2008**, *350*, 2059.
- (107) Hashmi, A. S. K.; Frost, T. M.; Bats, J. W. *Journal of the American Chemical Society* **2000**, *122*, 11553.
- (108) Xu, Q.; Imamura, Y.; Fujiwara, M.; Souma, Y. *The Journal of Organic Chemistry* **1997**, *62*, 1594.
- (109) Qian, D.; Zhang, J. *Beilstein Journal of Organic Chemistry* **2011**, *7*, 808.
- (110) Hashmi, A. S. K.; Hutchings, G. J. *Angewandte Chemie International Edition* **2006**, *45*, 7896.
- (111) Kharasch, M. S.; Isbell, H. S. *Journal of the American Chemical Society* **1931**, *53*, 3053.
- (112) Hao, W.; Liu, Y. *Beilstein Journal of Organic Chemistry* **2015**, *11*, 2132.
- (113) Wei, C.; Li, C.-J. *Journal of the American Chemical Society* **2003**, *125*, 9584.
- (114) Li, Z.; Shi, Z.; He, C. *Journal of Organometallic Chemistry* **2005**, *690*, 5049.
- (115) Trofimenko, S. *Inorganic Chemistry* **1973**, *12*, 1215.
- (116) Bonnardel, P. A.; Parish, R. V.; Pritchard, R. G. *Journal of the Chemical Society, Dalton Transactions* **1996**, 3185.
- (117) Henderson, W.; Nicholson, B. K.; Faville, S. J.; Fan, D.; Ranford, J. D. *Journal of Organometallic Chemistry* **2001**, *631*, 41.
- (118) Xu, X.; Kim, S. H.; Zhang, X.; Das, A. K.; Hirao, H.; Hong, S. H. *Organometallics* **2013**, *32*, 164.
- (119) Biasiolo, L.; Del Zotto, A.; Zuccaccia, D. *Organometallics* **2015**, *34*, 1759.
- (120) Obradors, C.; Echavarren, A. M. *Chemical Communications* **2014**, *50*, 16.
- (121) Xia, Y.; Dudnik, A. S.; Gevorgyan, V.; Li, Y. *Journal of the American Chemical Society* **2008**, *130*, 6940.
- (122) Shaw, A. P.; Tilset, M.; Heyn, R. H.; Jakobsen, S. *Journal of Coordination Chemistry* **2011**, *64*, 38.
- (123) Langseth, E.; Görbitz, C. H.; Heyn, R. H.; Tilset, M. *Organometallics* **2012**, *31*, 6567.
- (124) Langseth, E.; Nova, A.; Traaseth, E. A.; Rise, F.; Oeien, S.; Heyn, R. H.; Tilset, M. *J. Am. Chem. Soc.* **2014**, *136*, 10104.

- (125) Langseth, E.; Nova, A.; Tråseth, E. A.; Rise, F.; Øien, S.; Heyn, R. H.; Tilstet, M. *Journal of the American Chemical Society* **2014**, *136*, 10104.
- (126) Bratsch, S. G. *Journal of Physical and Chemical Reference Data* **1989**, *18*, 1.
- (127) Pflasterer, D.; Hashmi, A. S. K. *Chemical Society Reviews* **2016**, *45*, 1331.
- (128) Boorman, T. C.; Larrosa, I. *Chemical Society Reviews* **2011**, *40*, 1910.
- (129) Haro, T. d.; Nevado, C. *Journal of the American Chemical Society* **2010**, *132*, 1512.
- (130) Peshkov, V. A.; Pereshivko, O. P.; Van der Eycken, E. V. *Chemical Society Reviews* **2012**, *41*, 3790.
- (131) Zeng, J.; Bai, Y.; Cai, S.; Ma, J.; Liu, X.-W. *Chemical Communications* **2011**, *47*, 12855.
- (132) Chernyak, N.; Gevorgyan, V. *Angewandte Chemie International Edition* **2010**, *49*, 2743.
- (133) Wachenfeldt, H. v.; Röse, P.; Paulsen, F.; Loganathan, N.; Strand, D. *Chemistry – A European Journal* **2013**, *19*, 7982.
- (134) von Wachenfeldt, H.; Polukeev, A. V.; Loganathan, N.; Paulsen, F.; Rose, P.; Garreau, M.; Wendt, O. F.; Strand, D. *Dalton Transactions* **2015**, *44*, 5347.
- (135) Yan, B.; Liu, Y. *Organic Letters* **2007**, *9*, 4323.
- (136) Mackay, W. D.; Johnson, J. S. *Organic Letters* **2016**, *18*, 536.
- (137) Liang, Y.; Harrell, M. L.; Bergbreiter, D. E. *Angewandte Chemie International Edition* **2014**, *53*, 8084.
- (138) Chen, G.; Song, J.; Yu, Y.; Luo, X.; Li, C.; Huang, X. *Chemical Science* **2016**, *7*, 1786.
- (139) Kristensen, T. E.; Vestli, K.; Fredriksen, K. A.; Hansen, F. K.; Hansen, T. *Organic Letters* **2009**, *11*, 2968.
- (140) Shaw, A. P.; Tilstet, M.; Heyn, R. H.; Jakobsen, S. J. *Coord. Chem.* **2011**, *64*, 38.
- (141) Montanel-Perez, S.; Herrera, R. P.; Laguna, A.; Villacampa, M. D.; Gimeno, M. C. *Dalton Transactions* **2015**, *44*, 9052.
- (142) Rajesh, U. C.; Purohit, G.; Rawat, D. S. *ACS Sustainable Chemistry & Engineering* **2015**, *3*, 2397.